

DISSERTATION

N,N-DIARYL DIHYDROPHENAZINE PHOTOREDOX CATALYSIS FOR
ORGANOCATALYZED ATOM TRANSFER RADICAL POLYMERIZATION

Submitted by

Matthew David Ryan

Department of Chemistry

In partial fulfillment of the requirements

For the Degree of Doctor of Philosophy

Colorado State University

Fort Collins, Colorado

Summer 2019

Doctoral Committee:

Advisor: Garret Miyake

Eugene Chen

Arun Kota

Christopher Snow

Copyright by Matthew David Ryan 2019

All Rights Reserved

ABSTRACT

N,N-DIARYL DIHYDROPHENAZINE PHOTOREDOX CATALYSIS FOR ORGANOCATALYZED ATOM TRANSFER RADICAL POLYMERIZATION

The synthesis, application, and mechanistic investigation of the 5,10-diaryldihydrophenazine catalyst family as applied to organocatalyzed atom transfer radical polymerization is presented in this dissertation. The *N,N*-Diaryl Dihydrophenazine catalyst family, which will be referred to in this dissertation as the phenazines, are an appealing class of molecules due to their strongly reducing excited states, accessed through modular syntheses enabling a wide range of photophysical and electrochemical properties. This class of molecules represented the first example of organic catalysts capable of operating a controlled, visible light driven, organocatalyzed atom transfer radical polymerization for the precision syntheses of (meth)acrylic polymers. Phenazine catalysts were shown to polymerize (meth)acrylic monomers to polymers of very low dispersities (< 1.10) in a process with quantitative initiator efficiency; both features crucial to produce precision polymeric materials poised for myriad applications. Supported by computational efforts, mechanistic understanding and structure-property-catalyst activity relationships were identified and harnessed to design optimal polymerization conditions, which have laid the groundwork for new research efforts into highly reducing, visible light absorbing, organic photocatalysts.

ACKNOWLEDGEMENTS

I would like to thank my thesis committee - Prof. Garret Miyake, Prof. Eugene Chen, Prof. Arun Kota, and Prof. Christopher Snow - for their guidance through, and defense of this dissertation.

I am indebted to Professor Garret Miyake for his mentorship and unwavering dedication to my scientific training and personal growth during my graduate studies. The culture of excellence and the relentless pursuit of perfection in all aspects of the Miyake laboratory will remain with me in my independent career, and the value of these guiding principles you have instilled is impossible to overstate.

Many thanks to the undergraduate researchers who have worked and learned alongside me over the years: Nathaniel Garrison, Laura Hansman, and Joseph Collins. You each provided me valuable lessons as mentees, and I hope your struggles and triumphs in academic research will prove valuable in all aspects of life. Thank you for your dedication to the science and trust in me as a mentor.

To my fellow graduate students (and post-docs), thank you for great collaborations, illuminating discussions, and all of the non-academic adventures.

None of the work described in this dissertation would have been possible without the support of my family and friends, in particular my father David Ryan, sister Stephanie Ryan, and partner Elizabeth Nakahama. To David and Stephanie, thank you for always raising the bar and being the best role models I could ever hope for. To Elizabeth, thank you for your never-ending support, love, and encouragement.

Chapter 2: This dissertation chapter contains the manuscript of an article [Theriot, J. C.; Lim, C.-H.; Yang, H.; Ryan, M. D.; Musgrave, C. B.; Miyake, G. M. *Science* **2016**, *352*, 1082-1086]. J.C.T. performed all polymerizations using catalysts 1-4. C.-H.L. performed all density functional theory calculations under the advisement of C.B.M. H.Y. synthesized catalysts 1-4. M.D.R synthesized catalysts 5-6 and performed all polymerizations using catalysts 5-6.

G.M.M. was supported by the University of Colorado Boulder and Advanced Research Projects Agency - Energy. C.B.M. and C.-H.L. were supported by NSF grant CHE-1214131. J.C.T. was supported by a NSF Graduate Research Fellowship Program fellowship. M.D.R. was supported by a Graduate Assistance in Areas of National Need fellowship. The authors acknowledge use of Extreme science and Engineering Development Environment supercomputing resources (NSF ACI-1053575). The authors thank L. Hansman, A. Lockwood, S. Fatur, and N. Damrauer for technical assistance and enlightening discussions. A provisional patent was filed on the work described in *Science* **2016**, *352*, 1082-1086.

Chapter 3: This dissertation chapter contains the manuscript of an article [Lim, C.-H.;* Ryan, M. D.;* McCarthy, B. G.; Theriot, J. C.; Sartor, S. M.; Damrauer, N. H.; Musgrave, C. B.; Miyake, G. M. *J. Am. Chem. Soc.* **2017**, *139*, 348-355. *These authors contributed equally.]. C.-H.L. performed all density functional theory calculations under the advisement of C.B.M. J.C.T. performed spectroscopic measurements with assistance from M.D.R. and S.M.S. M.D.R synthesized catalysts 2 and 3 and performed polymerizations with assistance from B.G.M. J.C.T. synthesized catalyst 1.

This work was supported by the University of Colorado Boulder and the Advanced Research Projects Agency-Energy (DE-AR0000683). Acknowledgement is made to the donors of The American Chemical Society Petroleum Research Fund for partial support of this research.

Research reported in this publication was supported by the National Institute of General Medical Sciences of the National Institutes of Health under Award Number R35GM119702. The content is solely the responsibility of the authors and does not necessarily represent the official views of the National Institutes of Health. MDR, BGM, and SMS are grateful for support from the U.S. Department of Education's Graduate Assistance in Areas of National Need Program. BGM appreciates support from the Marian Sharrah Fellowship from the CU Boulder Department of Chemistry and Biochemistry. JCT was supported by a National Science Foundation Graduate Research Fellowship. CBM was supported by NSF grant CHE-1214131. We gratefully acknowledge the use of XSEDE supercomputing resources (NSF ACI-1053575). We also gratefully acknowledge the use of photophysical equipment purchased in support of the NSF/EPA funded Catalysis Collaboratory for Light-Activated Earth Abundant Reagents (C-CLEAR) (CHE-1339674).

Chapter 4: This dissertation chapter contains the manuscript of an article [Ryan, M. D.; Theriot, J. C.; Lim, C.-H.; Yang, H.; Lockwood, A. G.; Garrison, N. G.; Lincoln, S. R.; Musgrave, C. B.; Miyake, G. M. *J. Poly. Sci., Part A: Polym. Chem.* **2017**, *55*, 3017-3027. Special Issue: Special Issue in Honor of Professor Robert H. Grubbs]. C.-H.L. performed all density functional theory calculations under the advisement of C.B.M. J.C.T. performed spectroscopic measurements with assistance from M.D.R. and S.R.L. J.C.T., M.D.R. and H.Y. synthesized catalysts with assistance from A.G.L. and N.G.G. M.D.R. and J.C.T. performed polymerizations with assistance from N.G.G.

This work was supported by the University of Colorado Boulder and the Advanced Research Projects Agency-Energy (DE-AR0000683). Acknowledgement is made to the donors of the American Chemical Society Petroleum Research Fund for partial support of this research

(56501-DNI7). Research reported in this publication was supported by the National Institutes of Health under Award Number R35GM119702. The content in this manuscript is solely the responsibility of the authors and does not necessarily represent the official views of the National Institutes of Health. M.D.R is grateful for support from the U.S. Department of Education's Graduate Assistance in Areas of National Need Program. J.C.T acknowledges support from a National Science Foundation Graduate Research Fellowship. S.R.L thanks support from the University of Colorado Undergraduate Research Opportunities Program. C.B.M was supported by NSF grant CHE-1214131. We gratefully acknowledge the use of XSEDE supercomputing resources (NSF ACI-1053575).

Chapter 5: This dissertation chapter contains the manuscript of an article [Ryan, M. D.; Pearson; R. M.; French, T. A.; Miyake, G. M. *Macromolecules* **2017**, *50*, 4616-4622.]. M.D.R. and R.M.P. performed all polymerizations with assistance from T.A.F. R.M.P. synthesized PC 2.

This work was supported by the University of Colorado Boulder and the Advanced Research Projects Agency-Energy (DE-AR0000683). Acknowledgement is made to the donors of The American Chemical Society Petroleum Research Fund for partial support of this research. Research reported in this publication was supported by the National Institutes of Health under Award Number R35GM119702. The content is solely the responsibility of the authors and does not necessarily represent the official views of the National Institutes of Health. M.D.R. is grateful for support from the U.S. Department of Education's Graduate Assistance in Areas of National Need Program. We thank Dr. Chern-Hooi Lim for the computed reduction potential of perylene. We thank Steven Sartor for spectral measurements.

DEDICATION

This dissertation is dedicated to the memory of my mother, Susan C. Ryan.

TABLE OF CONTENTS

ABSTRACT	ii
ACKNOWLEDGEMENTS	iii
DEDICATION	vii
Chapter 1	1
Introduction.....	1
Chapter 2	4
Overview.....	4
Introduction.....	4
Results and Discussion	7
Conclusion	17
Experimental.....	17
References	79
Chapter 3	83
Overview.....	83
Introduction.....	84
Results and Discussion	88
Conclusions.....	99
Experimental.....	100
References	128
Chapter 4	134
Overview.....	134
Introduction.....	134
Results and Discussion	138
Conclusions.....	149
Experimental.....	150
References	184
Chapter 5	189
Overview.....	189
Introduction.....	190
Results and Discussion	194

Conclusions.....	204
Experimental.....	205
References.....	214
Chapter 6.....	218
Summary.....	218
References.....	220
Appendix I.....	221

Chapter 1

Introduction

This dissertation is written to follow the Journals Format as accepted by the Graduate School at Colorado State University and is based on four peer-reviewed publications that have appeared in *Science*, the *Journal of the American Chemical Society*, the *Journal of Polymer Science Part A: Polymer Chemistry*, and *Macromolecules*. The chapters discussed in this dissertation are primarily modeled off of first-author or co-first author publications and supported by contributions as a supporting author where appropriate. The central theme of this dissertation is to develop, understand, optimize, and employ phenazine photoredox catalysis in organocatalyzed atom transfer radical polymerization. The following topics are discussed in detail in the proceeding chapters:

2. Organocatalyzed Atom Transfer Radical Polymerization Driven by Visible Light
3. Intramolecular Charge Transfer and Ion Pairing in *N,N*-Diaryl Dihydrophenazine Photoredox Catalysts for Efficient Organocatalyzed Atom Transfer Radical Polymerization
4. Solvent Effects on the Intramolecular Charge Transfer Character of *N,N*-Diaryl Dihydrophenazine Catalysts for Organocatalyzed Atom Transfer Radical Polymerization
5. Impact of Light Intensity on Control in Photoinduced Organocatalyzed Atom Transfer Radical Polymerization

In Chapter 2, the initial development and first example of controlled organocatalyzed atom transfer radical polymerization (O-ATRP) driven by low energy visible light is presented. The development of this powerful method for precision polymer synthesis was enabled by the

discovery of the highly reducing *N,N*-Diaryl Dihydrophenazine (phenazines) catalyst family. An initial mechanism was proposed, where crucial photophysical and electrochemical properties of the phenazine photocatalyst were posited to control the catalytic cycle through iterative reductions and oxidations of bromide terminated polymer chains. This work represented the first example of a visible light absorbing organic molecule capable of operating a highly controlled oxidative quenching mechanistic cycle as applied to atom transfer radical polymerization, offering an alternative to precious metal Iridium photocatalysts.

In Chapter 3, the phenomenon of intramolecular charge transfer (CT) was explored as an enabling feature of phenazine photoredox catalysis. These CT states are reminiscent of ligand to metal charge transfer in ruthenium and iridium polypyridyl complexes. A combined approach of experimental studies and density functional theory calculations illuminated the role of excited state electronic distributions as applied to O-ATRP, where it was found that the highly performing phenazine catalysts access CT states and exhibit substantial solvatochromism in their emission. Additionally, the solvent polarity was found to drastically effect the dispersity of the resulting polymers, which was rationalized by a proposed increase in the strength of ion pairing during deactivation in O-ATRP.

In Chapter 4, a wide variety of phenazine photocatalysts with differing chemical functionality and abilities of excited states to exhibit intramolecular CT character were employed in O-ATRP under varied solvent polarity conditions, ranging from non-polar hexanes to highly polar *N,N*-dimethylacetamide. A clear distinction between the phenazine catalysts capable of accessing intramolecular CT states, and those that cannot, was observed by their drastically different performance in O-ATRP under non-polar conditions. It was observed that phenazines with excited states not possessing CT character could not operate a controlled O-ATRP in non-

polar solvents, but catalysts with excited states exhibiting CT character could operate controlled O-ATRP in solvents with a wide range of polarity.

In Chapter 5, the influence of irradiation intensity on the control over O-ATRP is explored using two photocatalysts: perylene and *N*-Aryl phenoxazine. It was found that the perylene catalyst was able to control O-ATRP when the polymerization vessel was supplied with sufficient irradiation intensity, and that the degree of control quickly decreased as intensity was lowered. However, the phenoxazine catalyst was able to maintain a high degree of control over the polymerization under diminishing irradiation intensity, showcasing the importance of tailored catalyst photophysical and electrochemical properties to maintain a precision polymerization under non-ideal experimental conditions.

Chapter 6 contains a wholistic summary of the work presented in this dissertation. The majority of the work conducted by the author during graduate studies has been included in this dissertation, but work that has been published, yet not directly related to the main theme of the dissertation, have not been included in the chapters. All work that has resulted in publication during the course of this dissertation appear in Appendix I.

Chapter 2

Organocatalyzed Atom Transfer Radical Polymerization Driven by Visible Light

Overview

The development of atom transfer radical polymerization (ATRP) is among the most significant technological advancements of polymer science. However, contamination of the polymer by the metal catalyst remains a major limitation. Organic ATRP photoredox catalysts have been sought to address this difficult challenge but have not achieved the precision performance of metal catalysts. Here, we introduce *N,N*-diaryl dihydrophenazines, identified through computationally directed discovery, as a new class of strongly reducing photoredox catalysts. These catalysts achieve high initiator efficiencies to synthesize polymers with tunable molecular weights and low dispersities using visible light, including sunlight.

Introduction

Over the last two decades, atom transfer radical polymerization (ATRP)^{1,2,3,4} has matured into one of the most powerful methodologies for precision polymer synthesis⁵ and is considered to be the most important advancement in polymer synthesis in the last 50 years.⁶ Strict control over the equilibrium between a dormant alkyl halide and active propagating radical dictates a low concentration of radicals and minimizes bimolecular termination to achieve controlled polymerization.⁷ ATRP has historically relied on transition metal catalysts to mediate this equilibrium and polymerize monomers with diverse functionality into macromolecules with controlled molecular weight (MW), low MW dispersity (*D*), defined chemical composition, and complex architecture.⁸

The caveat of traditional ATRP has been that the transition metal catalysts present purification challenges for the polymer product and impede their use in biomedical and electronic applications.⁹ Despite significant strides to enable lower catalyst loading^{10,11} and improve purification techniques,¹² organocatalyzed methods remain highly desirable. Organocatalyzed variants of ATRP using alkyl iodide initiators have been established, although they are not a broadly applicable replacement for metal-catalyzed ATRP.^{13,14,15} In sum, considerable motivation exists for developing catalysts that mediate organocatalyzed ATRP (O-ATRP).

Our interest in this field originated in 2013 with the discovery that perylene could serve as a visible-light organic photoredox catalyst (PC) to mediate an ATRP mechanism with alkyl bromide initiators, albeit with less control over the polymerization than has become the benchmark for traditional metal catalyzed ATRP.^{16,17,18} Our ongoing work has striven to establish O-ATRP for the synthesis of polymers with the precision of traditional ATRP, using visible light PCs to realize energy efficient, “greener” polymerization methods to eliminate a major limitation of ATRP. Although photoredox catalysis has been established for decades, visible-light photoredox catalysis has drawn increasing attention by presenting the opportunity to harness solar energy to mediate chemical transformations under mild conditions.^{19,20} Phenyl phenothiazine derivatives have since also been shown to perform as PCs for the ATRP of methacrylates²¹ and acrylonitrile,²² but require irradiation by UV light and leave much room for improvement for generating polymers possessing higher molecular weights and lower dispersities with increased initiator efficiency.

Our proposed mechanism of a photoredox O-ATRP (Figure 2.1 C) relies on the ability of a photoexcited PC to reversibly activate an alkyl bromide initiator by electron transfer (ET). In addition to the requirement that the excited triplet state $^3\text{PC}^*$ possess a sufficiently strong excited-

state reduction potential (E^{0*}) to reduce the initiator, a delicate interplay must be balanced between the stability of the radical cation $^2\text{PC}^{+\bullet}$ and its oxidation potential relative to the propagating radical to yield a controlled radical polymerization.

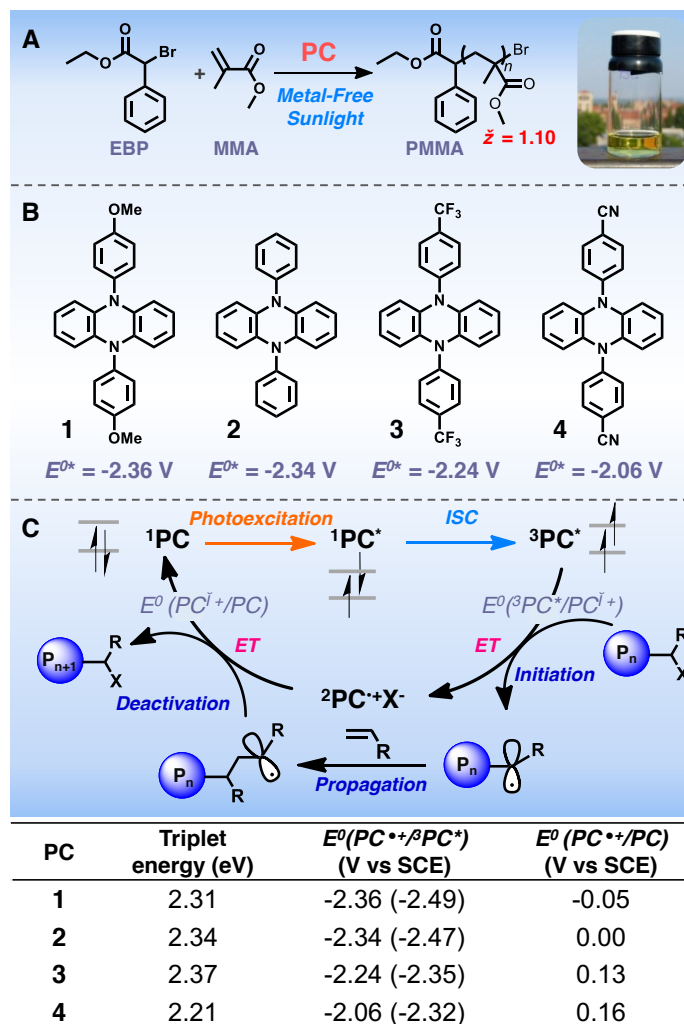


Fig. 2.1. **A.** Polymerization of methyl methacrylate to well-defined polymers using photoredox O-ATRP driven by sunlight. **B.** Structures of the diphenyl dihydrophenazine PCs **1-4** used in this study. **C.** A proposed mechanism for ATRP mediated by a PC *via* photoexcitation to

$^1\text{PC}^*$, intersystem crossing to the triplet state $^3\text{PC}^*$, ET to form the radical cation doublet $^2\text{PC}^{*\cdot}$ and back ET to regenerate PC and terminate polymerization. (Bottom) A table of the computed redox properties of the diphenyl dihydrophenazine PCs (experimentally measured E^{0*} in parentheses).

Results and Discussion

Computationally directed discovery^{23,24} inspired us to focus on 5,10-diphenyl-5,10-dihydrophenazines as a potential class of PCs for O-ATRP (Fig. 2.1 B).²⁵ Interestingly, the phenazine core is shared by several biologically relevant molecules that serve as redox-active antibiotics,^{26,27} while synthetic derivatives have drawn interest in organic photovoltaics^{28,29,30} and organic ferromagnets.^{31,32} We hypothesized that an appropriate union between the excited-state reduction potential (E^{0*}) and the stability of the radical cation $\text{PC}^{*\cdot}$ resulting from ET to the initiator is required for the production of polymers with controlled MW and low D . As such, we investigated electron donating (OMe, **1**), neutral (H, **2**), and withdrawing (CF_3 , **3** and CN, **4**) moieties on the *N*-phenyl substituents.

Density Functional Theory (DFT) was used to calculate the reduction potentials of the triplet excited state PCs, initiator, and propagating radicals.³³ We found that **2** possesses a triplet excited-state reduction potential of $E^0(\text{PC}^{*\cdot}/^3\text{PC}^*) = -2.34$ V vs. SCE. Functionalization of the phenyl substituents with an electron donating group OMe (**1**) strengthened the E^{0*} to -2.36 V, while introduction of CF_3 or CN electron withdrawing groups (EWGs) weakened the E^{0*} to -2.24 and -2.06 V for **3** and **4**, respectively, all of which is corroborated by the measured values within experimental error.³⁴ The triplet excited states of these PCs are all strongly reducing with respect to $1e^-$ transfer to the ethyl α -bromophenylacetate (EBP) initiator; we calculated that $E^0(\text{EBP}/\text{EBP}^{\cdot-}) = -0.74$ V vs. SCE for an adiabatic ET, consistent with our cyclic voltammetry results, which

show that the onset of EBP reduction occurs at ~ -0.8 V vs. SCE (Fig. 2.32). Impressively, these reduction potentials are significantly more reducing than classic metal PCs,¹⁹ including polypyridyl iridium complexes (E^{0*} as negative as -1.73 V vs. SCE) that have been used in photomediated ATRP.^{35,36} However, iridium PCs are expensive, do not address the problem of metal contamination, and have only been demonstrated to produce polymers with D as low as 1.19.

The remarkable reducing power of these dihydrophenazine based PCs, quantified by their very negative $E^0(\text{PC}^{*\beta}/\text{PC}^*)$ s, arises from a distinct combination of their high triplet state energies ($\sim 2.2 - 2.4$ eV) and the formation of relatively stable radical cations [$E^0(\text{PC}^{*\beta}/\text{PC}) = \sim -0.1 - 0.2$ V] upon their oxidation. Significantly, these radical cations are also sufficiently oxidizing to deactivate the propagating chains. We computed E^0 s for propagating radicals with n monomer repeat unit(s) bound to ethyl phenylacetate (EPA) of $E^0([\text{EPA-MMA}_n]/[\text{EPA-MMA}_n]^{\cdot+}) = -0.74, -0.86,$ and -0.71 V for $n = 0, 1$ and 2 , respectively. These E^0 s are sufficiently negative with respect to oxidization by the radical cations to drive radical deactivation and regeneration of the PC to complete the photocatalytic cycle.

An initial series of target PCs (**1-4**) were synthesized in two steps from commercial reagents in good yields.³⁴ Under otherwise identical conditions, all of the PCs were tested in the polymerization of methyl methacrylate (MMA), using EBP as the initiator, and white LEDs for irradiation in dimethylacetamide (Table 2.1, run 1 and Table 2.3, runs 1 – 3). All four PCs proved effective in polymerization after 8 hours of irradiation, with the PCs bearing EWGs exhibiting the best catalytic performance. PC **3** proved superior in producing polymers with a combination of not only the lowest dispersity ($D = 1.17$), but also the highest initiator efficiency ($I^* = 65.9\%$)³⁷ (Table 2.1, run 1). Using methyl α -bromoisobutyrate as the initiator was also efficient but did not achieve the same level of control of the polymerization as achieved with EBP (Table 2.3, run 5).

Remarkably, polymerization could even be driven by sunlight to produce poly(methyl methacrylate) (PMMA) with a low dispersity of $\mathcal{D} = 1.10$ (run 2).

Table 2.1 Results^a for the Organocatalyzed Atom Transfer Radical Polymerization of Methyl Methacrylate Catalyzed by **3** Using White LEDs or Sunlight^b.

Run No.	[MMA]:[EBP]:[3]	Time (h)	Conv. (%)	M_w (kDa)	\mathcal{D} (M_w/M_n)	I^* ($M_{n(\text{theo})}/M_{n(\text{exp})}$)
1	[1000]:[10]:[1]	8	98.4	17.9	1.17	65.9
2 ^b	[1000]:[10]:[1]	7	33.8	7.54	1.10	52.9
3	[1000]:[20]:[1]	8	78.9	7.12	1.18	69.5
4	[1000]:[15]:[1]	8	67.8	8.74	1.18	64.3
5	[1000]:[5]:[1]	8	86.9	37.3	1.26	59.6
6	[1000]:[2]:[1]	8	95.2	85.5	1.54	86.3
7	[5000]:[10]:[1]	8	74.7	77.4	1.32	64.2
8	[2500]:[10]:[1]	8	96.3	61.3	1.31	52.0
9	[750]:[10]:[1]	6.5	53.2	7.75	1.30	71.1
10	[500]:[10]:[1]	6.5	64.0	4.83	1.12	79.9

^aSee experimental section for details.

To examine the polymerization in detail, time-point aliquots were taken during polymerization to monitor the MW and \mathcal{D} progression as a function of monomer conversion (Figs. 2.2 A and B). The control provided by **3** was evidenced by the linear increase in polymer MW and low \mathcal{D} throughout the course of polymerization. However, the y-intercept of the M_n vs. conversion plot was 3.46 kDa, suggesting an uncontrolled chain-growth period adding ~32 MMA equivalents during the onset of polymerization before precise control is attained; whereas, an ideal polymerization would have a y-intercept equal to the mass of the initiator (MW of EBP = 243 Da).

Investigating the potential for modulation of the polymer MW, the effect of adjusting the initiator ratio was examined (runs 3 – 6). The M_w of the resulting PMMA could be modulated from 7.12 to 85.5 kDa. High EBP ratios resulted in controlled polymerizations and low dispersities ($\bar{D} = 1.26 - 1.17$), and despite the moderate loss of precise control over the polymerization at low EBP ratios ($\bar{D} = 1.54$), high MW polymer was produced with high initiator efficiency ($M_w = 85.5$ kDa, $I^* = 86.3\%$). Alternatively, adjusting the monomer ratio regulated polymer MW while also maintaining low \bar{D} (runs 7 - 10).

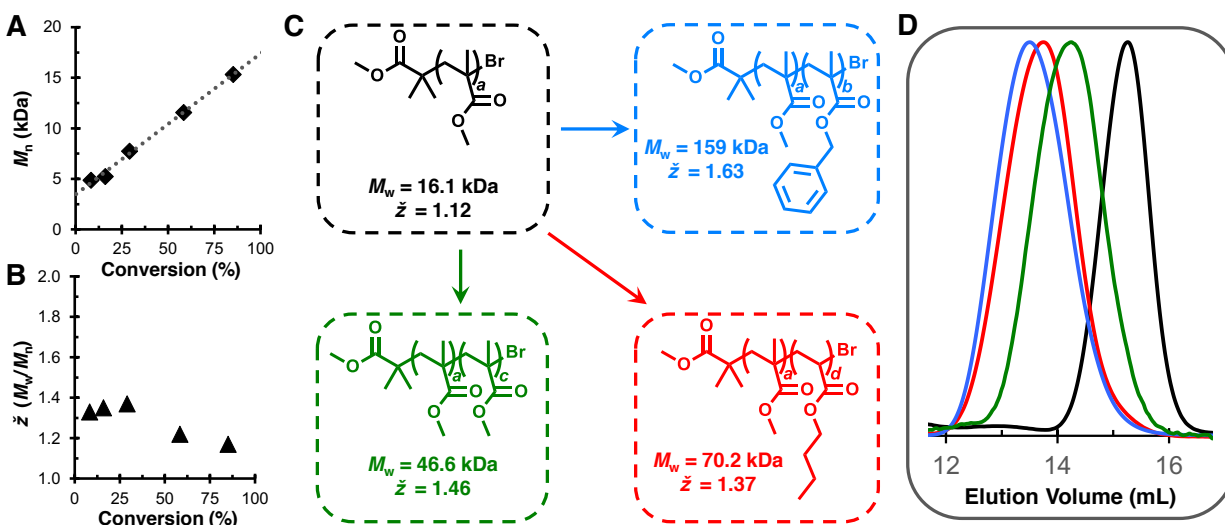


Fig. 2.2. **A.** Plot of molecular weight as a function of monomer conversion and **B.** Plot of dispersity as a function of monomer conversion for the polymerization of MMA mediated by **3**. **C.** Chain-extension from a PMMA macro-initiator (black) to produce block copolymers with MMA (green), benzyl methacrylate (blue), and butyl acrylate (red). **D.** GPC traces of each polymer depicted in **C** (color coded).

One of the greatest strengths of traditional ATRP is its ability to synthesize advanced polymeric architectures, including block copolymers. The reversible-deactivation mechanism enforced in ATRP repeatedly reinstalls the Br chain-end group onto the polymer and thus, isolated

polymers can be used to reinitiate polymerization. A combination of nuclear magnetic resonance spectroscopy and matrix-assisted laser desorption ionization mass spectroscopy were used to confirm the expected EBP derived polymer chain-end groups for a polymer produced through the proposed photoredox O-ATRP mechanism (Figs. 2.16 and 2.17). Additionally, to further support that this polymerization operates *via* an O-ATRP mechanism, a series of block polymerizations were performed to probe the Br chain-end group fidelity.

First, after initial polymerization of MMA proceeded for 12 h, additional MMA was added to the reaction mixture. GPC analysis revealed that the MW of the resulting polymer quantitatively increased (Fig. 2.26). Second, after polymerization of MMA was allowed to proceed for 8 h, the reaction mixture was placed in the dark for 8 h and subsequently additional MMA, benzyl methacrylate (BMA), or butyl acrylate (BA) was added. This resulted in no polymerization during the dark period, while the subsequent addition of monomer and further illumination resulted in continued and controlled polymer chain growth (Figs. 2.27, 2.28, and 2.30). Third, an isolated polymer was reintroduced to polymerization conditions by adding monomer, catalyst, solvent, and light, and served as a macro-initiator for the synthesis of block polymers. This chain-extension proved successful with MMA, BMA, and BA (Figs. 2.2C and 2.2D). The chain-extension polymerization from an isolated polymer produced from this polymerization method firmly supports that this methodology proceeds through the O-ATRP mechanism, while all of these experiments revealed base-line resolved peaks in the GPC traces, demonstrating high chain-end group fidelity.

DFT calculations were performed to gain insight into the differences in the performances of the PCs, all of which possess similar $E^0(\text{PC}^{+\bullet}/\text{PC}^*)$ s and $E^0(\text{PC}^{+\bullet}/\text{PC})$ s that are sufficiently reducing and oxidizing, respectively, to drive the photocatalytic cycle of Fig. 2.1 C. As such, we

reasoned that the superior performances of **4** and, in particular, **3** must be qualitatively different from that of **1** and **2** and result from a more complex effect.

Inspection of the triplet state ($^3\text{PC}^*$) frontier orbitals reveals qualitative differences in these PCs (Fig. 2.3). The low-lying singly occupied molecular orbital (SOMO) of all the PCs are similar, with the electron localized over the phenazine π system. Similarly, for PCs **1** (OMe) and **2** (H), the high-lying SOMO is also localized on the phenazine rings; in contrast, for **3** (CF_3) and **4** (CN) the high-lying SOMO, occupied by the reducing e^- , resides on the phenyl ring(s). We contend that the CF_3 and CN EWGs of **3** and **4** stabilize their π^* orbitals localized on the phenyl rings relative to the phenazine localized π^* orbital that is the high-lying SOMO of **1** and **2**. This reorders the energies of the π^* orbitals such that a π^* orbital localized on the phenyls becomes the high-lying SOMO of **3** and **4**, although the low-lying SOMO localized on the phenazine moiety remains singly occupied. Thus, **3** and **4** differ qualitatively from **1** and **2** in that their two triplet electrons reside on either the phenazine or the phenyl substituent and are thus spatially separated.

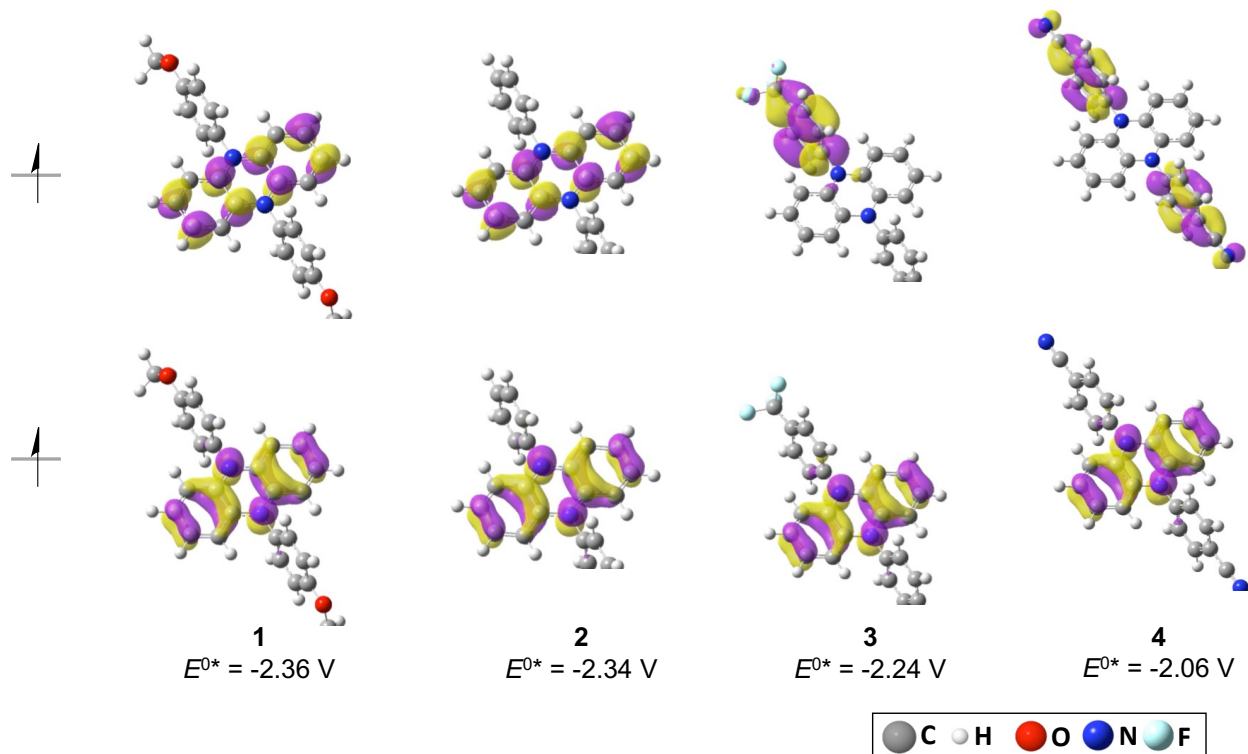


Fig. 2.3. Triplet state ($^3\text{PC}^*$) frontier orbitals and excited-state reduction potentials E^{0*} of diphenyl dihydrophenazine PCs **1-4**. Top figures show the higher-lying singly occupied molecular orbital (SOMO) and bottom figures the low-lying SOMO. Note that phenyl functionalization with electron withdrawing groups (CF_3 and CN) localizes the high-lying SOMO on the phenyl.

Furthermore, a comparison of **3** to **4** elucidates another significant distinction. For **3**, the high-lying SOMO is localized on one of the phenyl rings, while in **4** the reducing e^- is delocalized over both phenyl rings. Surprisingly, we note that one of the C-F bonds of the CF_3 functionalized phenyl possessing the high-lying SOMO of **3**, is lengthened from 1.35 Å to 1.40 Å, indicating partial localization of electron density on the C-F antibond. This symmetry breaking effect in the triplet state of **3** creates a more localized, higher electron density of the reducing electron of **3**

relative to **4** while also maintaining the spatial separation between the two SOMO electrons that preserves the reducing potential of the triplet.

With the above observations in mind, we attempted to discover even more efficient PCs to mediate O-ATRP using computational chemistry to design diaryl dihydrophenazines that possess sufficiently strong E^{0*} s and spatially separated excited state SOMOs with the higher energy SOMO localized over only one of the aromatic substituents off the dihydrophenazine core. Using these principles, we designed and synthesized 2-naphthyl (**5**) and 1-naphthyl (**6**) derivatives, with strong E^{0*} s of -2.20 and -2.12 V, respectively, and SOMOs with the targeted desirable geometric features (Fig. 2.4). Using EBP as the initiator, both PCs proved successful in the polymerization of MMA (Table 2.4, runs 8 and 9). Although **5** produced PMMA with an impressively low \mathcal{D} of 1.03 ($M_w = 9.35$ kDa, $I^* = 46.1$ %) – rivaling metal ATRP catalysts – **6** produced PMMA with a slightly higher I^* (47.5 %), faster polymerization rates, and an also impressively low \mathcal{D} of 1.08 ($M_w = 12.3$ kDa). Excitingly, the plot of M_n vs. monomer conversion exhibits a y-intercept of 850 Da, demonstrating the attainment of control over polymerization after the addition of only ~6 MMA units and therefore the much more efficient control in the O-ATRP mediated by **6** than achieved with **3** (Fig. 2.4C). Thus, we investigated **6** in more detail as the PC in the polymerization of MMA.

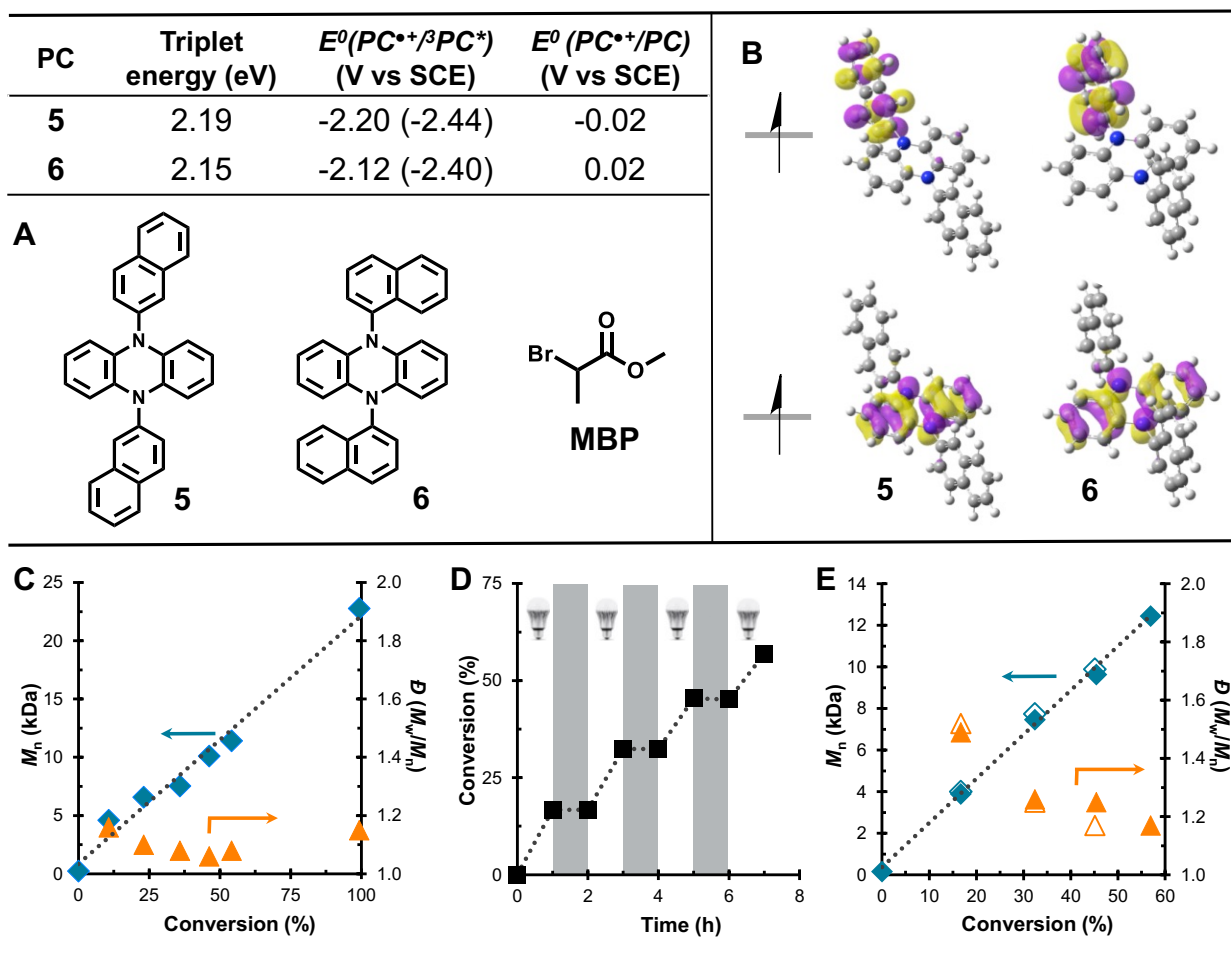


Fig. 2.4. **A.** (Top) Computed and experimentally measured properties of **5** and **6**. (Bottom) Structures of **5**, **6**, and MBP (methyl 2-bromopropionate). **B.** Triplet state frontier orbitals of **5** and **6**. Top figures show the higher-lying SOMO and bottom figures the low-lying SOMO. **C.** Plot of M_n and D vs. monomer conversion for the polymerization of MMA. **D.** Plot of monomer conversion vs. time, and **E.** Plot of M_n and D (filled symbols from after irradiation and empty symbols from after dark period) vs. monomer conversion using **6** as the PC during pulsed light irradiation with white LEDs. See experimental section for details.

A survey of initiators commonly employed in traditional metal-catalyzed ATRP in conjunction with **6** (Table 2.2, run 11 and Table 2.4, runs 9 – 12) revealed that methyl 2-

bromopropionate (MBP) provided the best overall results for the polymerization of MMA ($M_w = 10.6$ kDa; $\mathcal{D} = 1.28$; $I^* = 88.1$ %). Furthermore, temporal control was realized by employing a pulsed-irradiation sequence (Figs. 2.4D and E). Polymerization was only observed during irradiation, paused during dark periods, and the MW steadily increased with continued irradiation while producing a polymer with a low \mathcal{D} of 1.17. Finally, efficient control over the polymerization by **6** is highlighted by the consistently high I^* achieved over broad reaction conditions to produce polymers with tunable MWs through varying initiator (Runs 11 – 14) or monomer (Runs 15 – 17) ratios.

Table 2.2. Results for the Organocatalyzed Atom Transfer Radical Polymerization of Methyl Methacrylate Catalyzed by **6** Using White LEDs.^a

Run No.	[MMA]:[MBP]:[6]	Time (h)	Conv. (%)	M_w (kDa)	\mathcal{D} (M_w/M_n)	I^* ($M_{n(\text{theo})}/M_{n(\text{exp})}$)
11	[1000]:[10]:[1]	8	71.7	10.6	1.28	88.1
12	[1000]:[20]:[1]	8	73.1	5.24	1.29	94.5
13	[1000]:[15]:[1]	8	70.8	7.52	1.36	88.5
14	[5000]:[10]:[1]	8	69.5	46.9	1.32	98.7
15	[2500]:[10]:[1]	8	64.5	21.9	1.34	99.3
16	[750]:[10]:[1]	8	69.0	6.93	1.23	94.7
17	[500]:[10]:[1]	8	76.4	5.74	1.39	95.7

^aSee experimental section for details.

Conclusion

In conclusion, a series of computationally designed *N,N*-diaryl dihydrophenazines were synthesized and investigated as organic PCs in O-ATRP to efficiently polymerize MMA and other monomers to well-defined polymers, synthesizing polymers with dispersity as low as 1.03 and demonstrating quantitative initiator efficiency. Overall, we report organic PCs in O-ATRP rivaling metal ATRP catalysts in polymerization performance, able to polymerize a variety of methacrylates and acrylates (Table S3). First principles calculations inspired the discovery of these PCs, provided insight into why **3** proved a highly efficient PC, and ultimately led to the design of **6**, which proved to be the superior PC discovered in this study. Future reports will describe investigations of how subtle differences between these PCs produce different levels of success in mediating O-ATRP and will provide a more detailed fundamental description of the O-ATRP mechanism. We envision that this O-ATRP catalyst platform will significantly expand the application scope for polymers beyond those synthesized by metal-catalyzed ATRP, while their impressively strong reducing power presents great promise for their application toward other challenging chemical transformations.

Experimental

Materials and Methods

General Information

All reagents were purchased from Sigma-Aldrich. Those chemicals used in polymerizations, including methyl methacrylate (MMA), benzyl methacrylate (BnMA), *n*-butyl acrylate (BA), styrene (St), trimethylsilylhydroxyethyl methacrylate (TMSHEMA), 2,2,2-trifluoroethyl methacrylate (TFEMA), di(ethylene glycol) methacrylate (DEGMA), vinyl acetate (VA), acrylonitrile (AN), ethyl α -bromophenylacetate (EBP), ethyl α -chlorophenylacetate (ECIP), methyl α -bromoisobutyrate (MBriB), methyl bromopropionate (MBP), 2-bromopropionitrile

(BrPN), dimethylformamide (DMF), and dimethylacetamide (DMA) were purified by vacuum distillation followed by three freeze-pump-thaw cycles and stored under a nitrogen atmosphere before use. 2-Dicyclohexylphosphino-2,6-diisopropoxybiphenyl (RuPhos) and Chloro-(2-Dicyclohexylphosphino-2,6-diisopropoxy-1,1-biphenyl) [2-(2-aminoethyl)phenyl] palladium(II) - methyl-t-butyl ether adduct (RuPhos precatalyst) were stored under nitrogen atmosphere. All other reagents were used as received. The visible light source was a 16-inch strip of double-density white LEDs, purchased from Creative Lighting Solutions (item no. CL-FRS1210-5M-12V-WH), wrapped inside a 400 mL beaker (Figure 2.5).

^1H , ^{13}C , and ^{19}F NMR spectroscopy were performed in a Varian INOVA 300 MHz, 400 MHz, or 500 MHz spectrometer, as specified. Chemical shifts are referenced to the internal solvent resonance and reported as parts-per-million relative to tetramethylsilane. Analysis of polymer molecular weights was performed *via* gel permeation chromatography (GPC) coupled with multi-angle light scattering (MALS), using an Agilent HPLC fitted with one guard column and two PLgel 5 μm MIXED-C gel permeation columns, a Wyatt Technology TrEX differential refractometer, and a Wyatt Technology miniDAWN TREOS light scattering detector, using THF as the eluent at a flow rate of 1.0 mL/min. Ultraviolet-visible spectroscopy was performed on an Agilent spectrophotometer using DMF as the solvent. Emission spectroscopy was performed on a SLM 8000C spectrofluorimeter using DMF as the solvent. Samples were sparged with argon for 15 minutes prior to analysis. Cyclic voltammetry was performed with a CH Instruments electrochemical analyzer with a Ag/AgNO₃ (0.01 M in MeCN) reference electrode using MeCN as the solvent. Samples were sparged with argon for 5 minutes prior to analysis. ESI mass spectrometry analysis was performed at the University of Colorado Boulder mass spectrometry facility on a Waters Synapt G2 HDMS Qtof using acetonitrile as the solvent. MALDI-TOF mass

spectrometry analysis was performed at the Colorado State University mass spectrometry facility on a Bruker Microflex-LRF mass spectrometer in positive ion, reflector mode using THF as the solvent.

Polymerization Procedures

General Polymerization Procedure

A 20 mL vial was charged with a small stirbar and catalyst and transferred into a nitrogen-atmosphere glovebox. Solvent, monomer, and initiator were then added sequentially via pipette. The vial was then sealed, placed inside a beaker illuminated by white LED light, and stirred (Figure S1). To analyze the progress of a polymerization at a given time point, a 0.1 mL aliquot of the reaction media was removed *via* syringe and injected into a vial containing 0.7 mL CDCl_3 with 250 ppm butylated hydroxytoluene (BHT). This aliquot was then analyzed by ^1H NMR for conversion, dried under reduced pressure, and then re-dissolved in THF for analysis of M_w and M_n by gel permeation chromatography coupled with multi-angle light scattering.

Isolation

For copolymers specified as isolated, isolation was performed by pouring the reaction mixture into a 50-fold excess of CH_3OH , causing the polymer to precipitate. After 1 hour of stirring, the precipitate was collected *via* vacuum filtration and dried under reduced pressure. NMR analysis of poly(DEGMA) and poly(TFEMA) was performed by pouring their respective reaction mixtures into 50 mL water, stirring for 1 hour, and collecting the precipitate *via* vacuum filtration. NMR analysis of poly(TMSHEMA) was performed by pouring the reaction mixture into 50 mL CH_2Cl_2 , stirring for 1 hour, and collecting the precipitate *via* vacuum filtration.

Control Experiments

Control polymerizations revealed no polymerization occurred in the absence of any single component (*i.e.* light, PC, or initiator), or in the presence of oxygen or TEMPO, (supporting a radical polymerization mechanism).



Figure 2.5. Photograph of the general reaction setup for polymerizations using LED irradiation.

Polymerizations in Tables 1 and 2

Ratios given in table 1 are based on 1 mL of MMA for runs 1 – 6, 2.5 mL of MMA for runs 7 and 8, 0.75 mL MMA for run 9, and 0.5 mL MMA for run 10. The amount of DMA used was 1 mL, except for run 7 (3.5 mL), run 8 (2.5 mL), run 9 (1.25 mL), and run 10 (1.5 mL). See below for additional information on run 2.

Ratios given in table 2 are based on 1 mL of MMA for runs 11 – 15, 5 mL of MMA for run 16, 2.5 mL of MMA for run 17, 0.75 mL of MMA for run 18, and 0.5 mL of MMA for run 19. The amount of DMA used was 2 mL, except for runs 16 and 17 (5 mL), and run 19 (1 mL).



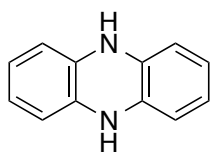
Figure 2.6 Photograph of the reaction run in sunlight.

Procedure for Polymerization Performed in Sunlight

A 20 mL vial was charged with a small stirbar and catalyst (9.35 μmol , 1.00 eq.) and transferred into a nitrogen-atmosphere glovebox. DMA (1.00 mL), MMA (1.00 mL, 9.35 mmol, 1000 eq.) and EBP (16.4 μL , 93.5 μmol , 10.0 eq.) were added sequentially via pipette. The vial was then removed from the glovebox, sealed with electrical tape, and placed on the roof of the University Memorial Center at the University of Colorado, Boulder from 9 AM to 4 PM on August 20th, 2015 (Figure 2, Results and Discussion section).

Catalyst Synthesis

5,10-dihydrophenazine



5,10-dihydrophenazine was synthesized according to a modified literature procedure (29). A 500 mL round bottom flask was charged with a mixture of H₂O (200 mL), EtOH (50 mL), and a stir bar. The mixture was sparged with nitrogen for 30 minutes and then phenazine (2.00 g, 11.1 mmol, 1.00 eq.) and Na₂S₂O₄ (23.3 g, 111 mmol, 10.0 eq.) were then added. This mixture was subsequently heated at reflux under nitrogen atmosphere for 3h. After cooling to RT, the product was isolated as a precipitate via cannula filtration, washed with excess deoxygenated H₂O, and dried under reduced pressure to yield a light green powder (1.35 g, 7.42 mmol, 67%). The product was stored under nitrogen until further use.

5,10-di(4-methoxyphenyl)-5,10-dihydrophenazine (1)

1 was synthesized using a modified literature procedure (21). An oven-dried vacuum tube was charged with 5,10-dihydrophenazine (1.00 g, 5.50 mmol, 1.00 eq.), NaOtBu (2.11 g, 22.00 mmol, 4.00 eq.), RuPhos (103 mg, 0.22 mmol, 0.04 eq.), RuPhos precatalyst (180 mg, 0.22 mmol, 0.04 eq.), 4-bromoanisole (4.05 g, 22.0 mmol, 4.00 eq), and 8.00 mL dioxane. This flask was sealed under nitrogen and heated at 110 °C for 10 h. After cooling to room temperature, 200 mL CH₂Cl₂ was added to the reaction mixture and this was extracted three times with 200 mL H₂O. The organic layer was dried with MgSO₄, filtered, and the volatiles were removed under reduced pressure to reveal a brown solid. Purification by column chromatography (1:3 mixture of CH₂Cl₂ and hexanes) afforded the product **1** as a light yellow solid (1.00 g, 2.53 mmol, 46%). ¹H NMR (C₆D₆, 500 MHz): δ 7.11 – 7.02 (m, 4H), 6.78 – 6.67 (m, 4H), 6.33 (dd, J = 5.9, 3.4 Hz, 4H), 5.89 (dd, J = 5.8, 3.5 Hz, 4H), 3.23 (s, 6H). ¹³C NMR (C₆D₆, 100 MHz): δ 54.53, 112.60, 116.33, 120.94, 127.52, 132.18, 137.24, 159.05. HRMS (ESI): calc'd for M⁺ C₂₆H₂₂N₂O₂, 394.1681; found 394.1675. UV/Vis: λ_{max} 373 nm.

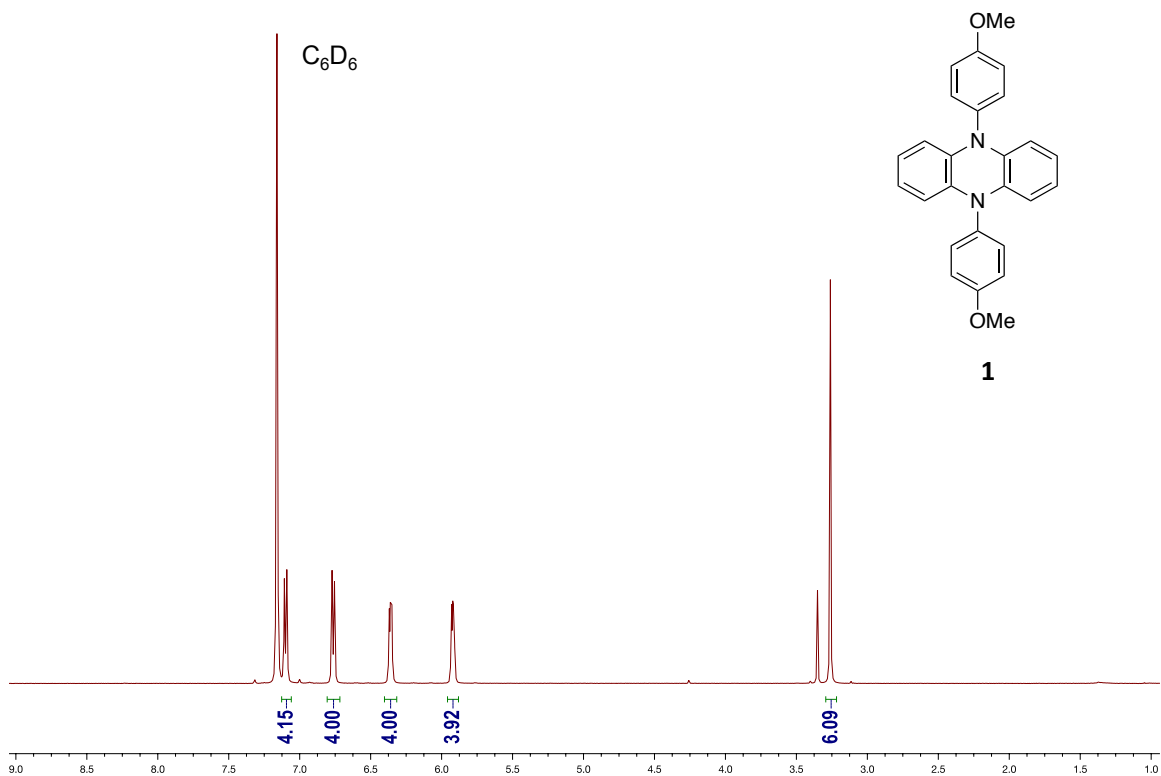


Figure 2.7 ^1H NMR spectrum of **1**

5,10-diphenyl-5,10-dihydrophenazine (2)

2 was synthesized using a modified literature procedure (21). An oven-dried vacuum tube was charged with 5,10-dihydrophenazine (1.00 g, 5.50 mmol, 1.00 eq.), NaOtBu (2.11 g, 22.00 mmol, 4.00 eq.), RuPhos (103 mg, 0.22 mmol, 0.04 eq.), RuPhos precatalyst (180 mg, 0.22 mmol, 0.04 eq.), iodobenzene (4.49 g, 22.0 mmol, 4.00 eq.), and 8.00 mL dioxane. This flask was sealed under nitrogen and heated at 110 °C for 10 h. After cooling to room temperature, 200 mL CH_2Cl_2 was added to the reaction mixture and this was extracted three times with 200 mL H_2O . The organic layer was dried with MgSO_4 , filtered, and the volatiles were removed under reduced pressure to reveal a red-brown solid. Purification by column chromatography (1:3 mixture of CH_2Cl_2 and

hexanes) afforded the product **2** as a light yellow solid (1.27 g, 3.80 mmol, 69%). Further purification by layering a solution of the product in CH₂Cl₂ with hexanes gave **2** as yellow needles. ¹H NMR (C₆D₆, 400 MHz): δ 7.16 (could not be resolved from NMR solvent peak), 7.07 – 7.00 (m, 2H), 6.31 – 6.25 (m, 4H), 5.85 – 5.79 (m, 4H). ¹³C NMR (C₆D₆, 100 MHz): δ 112.69, 121.03, 127.69, 131.03, 131.22, 136.75, 140.38. HRMS (ESI): calc'd for M+ C₂₄H₁₈N₂, 334.1470; found 334.1482. UV/Vis: λ_{max} 370 nm.

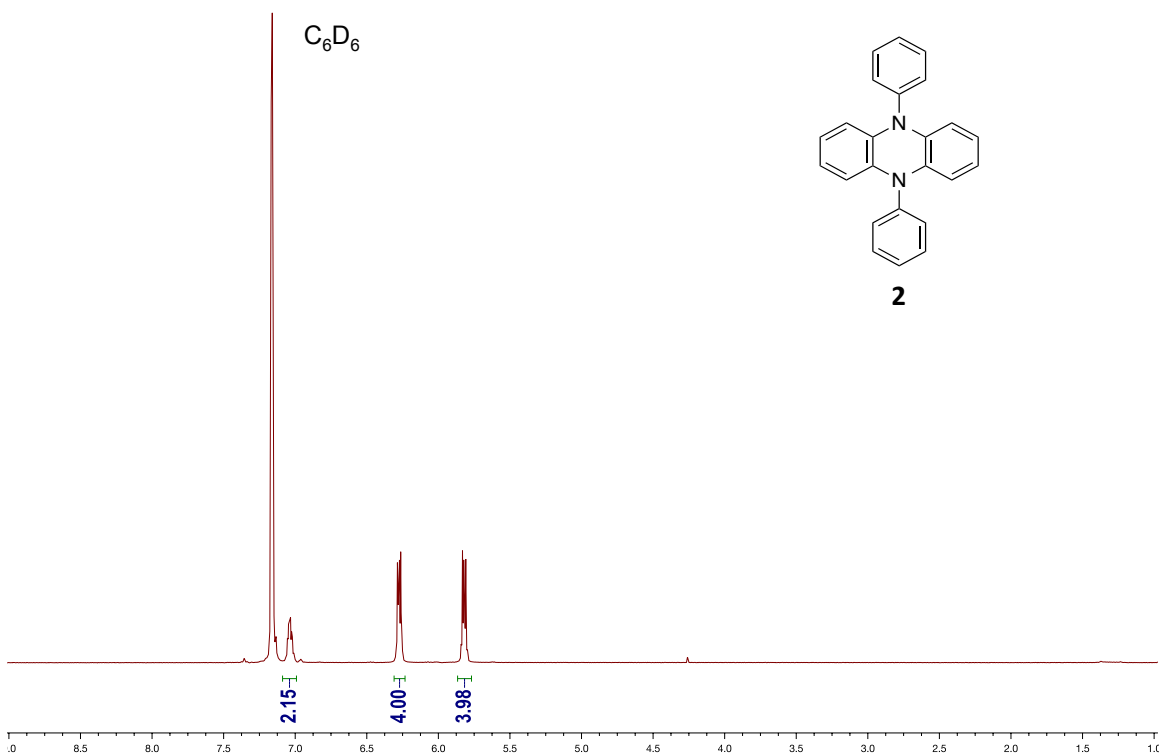


Figure 2.8 ¹H NMR spectrum of **2**.

5,10-di(4-trifluoromethylphenyl)-5,10-dihydrophenazine (3)

3 was synthesized using a modified literature procedure (21). An oven-dried vacuum tube was charged with 5,10-dihydrophenazine (1.01 mg, 5.55 mmol, 1.00 eq.), NaOtBu (2.13 g, 22.22 mmol, 4.00 eq.), RuPhos (102 mg, 0.22 mmol, 0.04 eq.), RuPhos precatalyst (180 mg, 0.22 mmol, 0.04 eq.), 4-bromobenzotrifluoride (5.00 g, 22.22 mmol, 4.00 eq), and 8.00 mL dioxane. This flask was sealed under nitrogen and heated at 110 °C for 10 h. After cooling to room temperature, 200 mL CH₂Cl₂ and 200 mL H₂O was added to the reaction flask, causing the product to precipitate. Filtration and washing with CH₂Cl₂ afforded **3** as a light yellow powder (1.65 g, 3.52 mmol, 63%). Further purification by layering a solution of the product in CH₂Cl₂ with hexanes gave **3** as light yellow needles. ¹H NMR (C₆D₆, 400 MHz) δ 7.25 (d, J = 8.1 Hz, 4H), 6.90 (d, J = 8.0 Hz, 4H), 6.36 – 6.30 (m, 4H), 5.69 - 5.63 (m, 4H). ¹³C NMR (C₆D₆, 100 MHz): δ 113.26, 121.65, 128.17, 127.52, 128.21, 131.32, 135.91, 143.54. ¹⁹F NMR (C₆D₆, 376 MHz): δ -62.23. HRMS (ESI): calc'd for M+ C₂₆H₁₆F₆N₂, 470.1218; found 470.1216. UV/Vis: λ_{max} 367 nm.

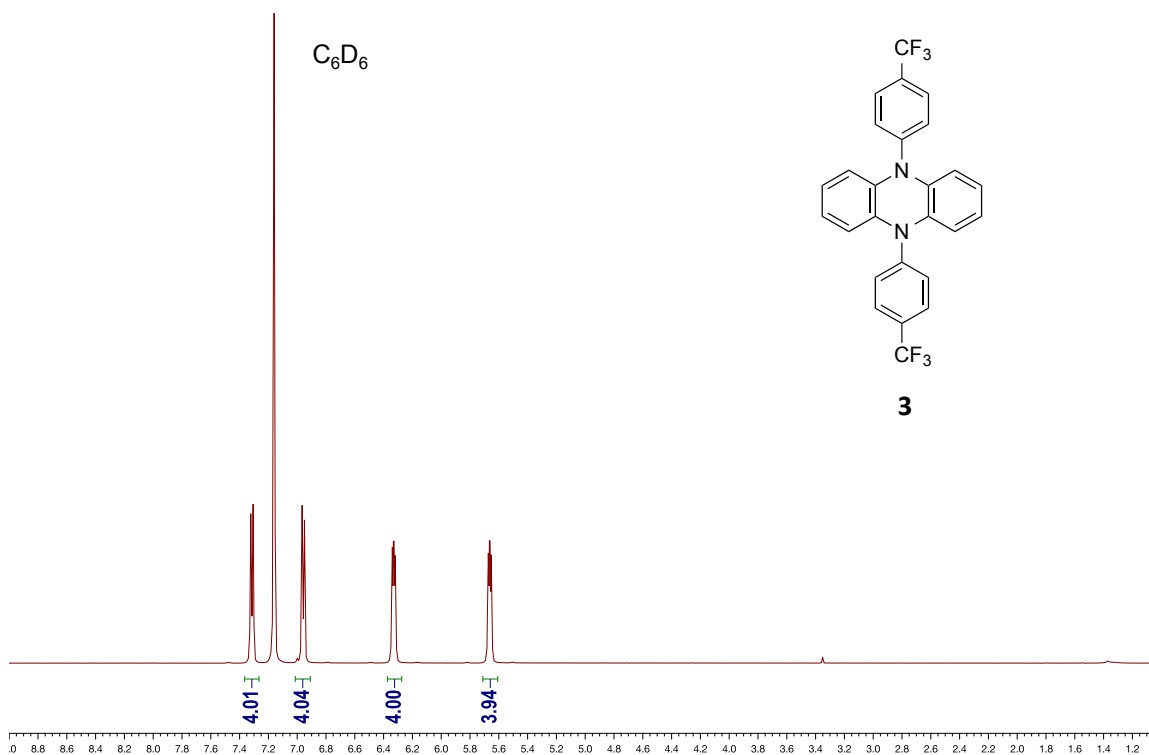


Figure 2.9 ^1H NMR spectrum of **3**.

5,10-di(4-cyanophenyl)-5,10-dihydrophenazine (4)

4 was synthesized using a modified literature procedure (21). An oven-dried vacuum tube was charged with 5,10-dihydrophenazine (500 mg, 2.75 mmol, 1.00 eq.), NaOtBu (1.06 g, 11.00 mmol, 4.00 eq.), RuPhos (51 mg, 0.11 mmol, 0.04 eq.), RuPhos precatalyst (90 mg, 0.11 mmol, 0.04 eq.), 4-bromobenzonitrile (2.00 g, 11.0 mmol, 4.00 eq), and 3.00 mL dioxane. This flask was sealed under nitrogen and heated at 110 °C for 10 h. After cooling to room temperature, 200 mL CH_2Cl_2 was added to the reaction mixture and this was extracted three times with 200 mL H_2O . The organic layer was dried with MgSO_4 , filtered, and the volatiles were removed under reduced pressure to reveal a brown solid. Purification by column chromatography (1:1 mixture of CH_2Cl_2 and hexanes) produced the product **4** as a brown powder (718 mg, 1.87 mmol, 68%). Further purification by layering a solution of the product in CH_2Cl_2 with hexanes gave **4** as dark gold needles. ^1H NMR (C_6D_6 , 400 MHz) δ 6.98 – 6.89 (m, 4H), 6.73 – 6.64 (m, 4H), 6.42 - 6.36 (m, 4H), 5.72 - 5.66 (m, 4H). ^{13}C NMR (C_6D_6 , 100 MHz): δ 111.56, 114.16, 117.82, 121.96, 130.35, 134.52, 135.69, 144.12. HRMS (ESI): calc'd for M^+ $\text{C}_{26}\text{H}_{16}\text{N}_4$, 384.1375; found 384.1370. UV/Vis: λ_{max} 322 nm.

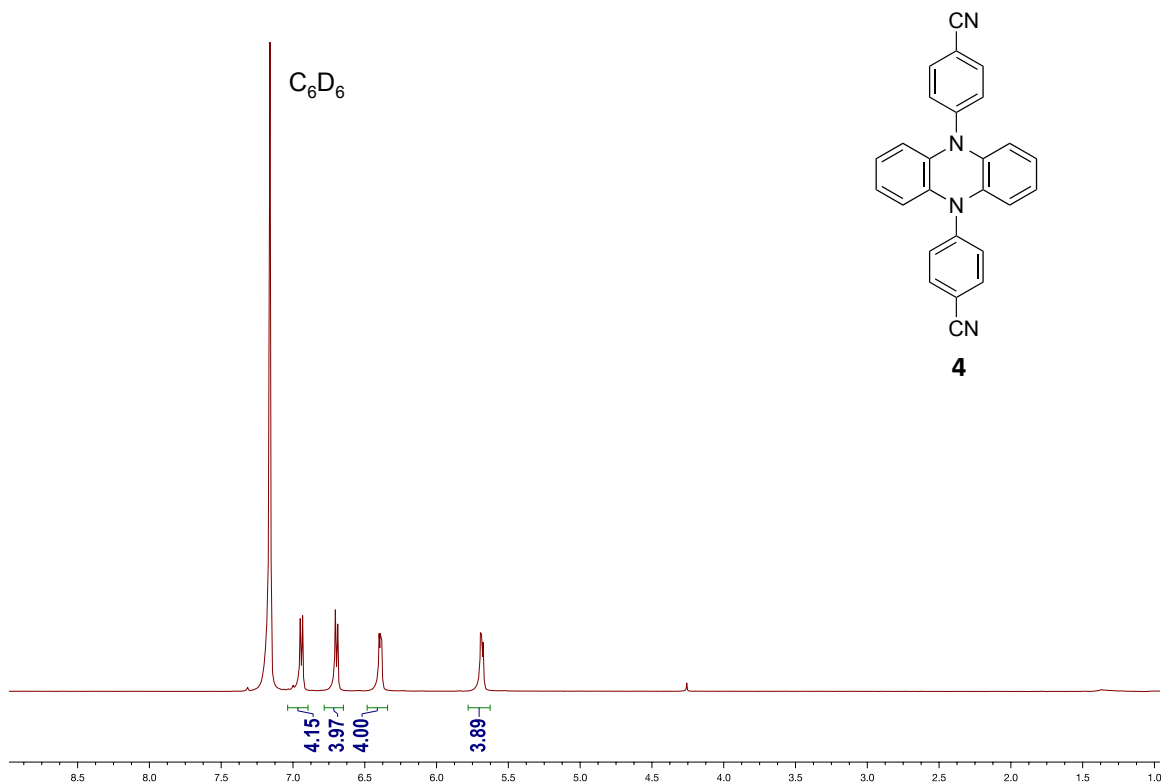


Figure 2.10 ^1H NMR spectrum of **4**.

5,10-di(2-naphthyl)-5,10-dihydrophenazine (5)

5 was synthesized using a modified literature procedure (21). An oven-dried vacuum tube was charged with 5,10-dihydrophenazine (911 mg, 5.00 mmol, 1.00 eq.), NaOtBu (1.92 g, 20.0 mmol, 4.00 eq.), RuPhos (46.7 mg, 0.10 mmol, 0.04 eq.), RuPhos precatalyst (81.7 mg, 0.10 mmol, 0.04 eq.), 2-bromonaphthalene (4.14 g, 20.0 mmol, 4.00 eq.), and 10.0 mL dioxane. This flask was sealed under nitrogen and heated at 110 °C for 10 h. After cooling to room temperature, 250 mL CH_2Cl_2 and 250 mL H_2O was added to the reaction flask, causing the product to precipitate. Filtration and washing with CH_2Cl_2 afforded **6** as a light yellow-green powder (1.95 g, 4.50 mmol, 90%). ^1H NMR (C_6D_6 , 300 MHz) δ 7.67 (dd, 4H), 7.63 – 7.47 (m, 4H), 7.36 – 7.16 (m, 8H), 6.33 – 6.21 (dd, 4H), 5.91 – 5.79 (dd, 4H). ^{13}C NMR (C_6D_6 , 75 MHz): δ 137.77, 136.91, 135.29, 132.99,

131.63, 130.54, 128.80, 127.83, 127.61, 126.53, 126.16, 121.30, 113.09. HRMS (ESI): calc'd for M+ C₃₂H₂₂N₂ 434.1783; found 434.1777. UV/Vis: λ_{max} 340 nm.

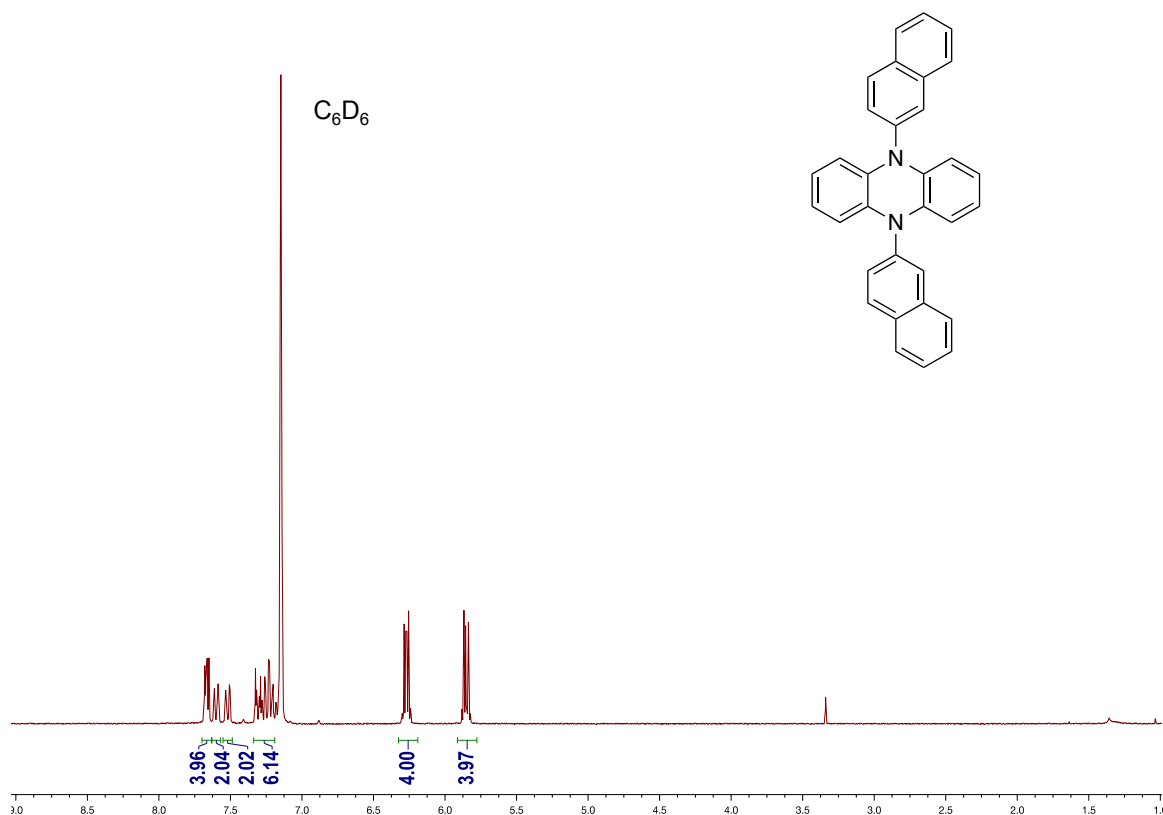


Figure 2.11 ¹H NMR spectrum of **5**.

5,10-di(1-naphthyl)-5,10-dihydrophenazine (6)

6 was synthesized using a modified literature procedure (21). An oven-dried vacuum tube was charged with 5,10-dihydrophenazine (911 mg, 5.00 mmol, 1.00 eq.), NaO^tBu (1.92 g, 20.0 mmol, 4.00 eq.), RuPhos (46.7 mg, 0.10 mmol, 0.04 eq.), RuPhos precatalyst (81.7 mg, 0.10 mmol, 0.04 eq.), 1-bromonaphthalene (4.14 g, 20.0 mmol, 4.00 eq.), and 10.0 mL dioxane. This flask was sealed under nitrogen and heated at 110 °C for 48 h. After cooling to room temperature, 250 mL CH₂Cl₂ and 250 mL H₂O was added to the reaction flask, causing the product to precipitate.

Filtration and washing with CH_2Cl_2 afforded **7** as a yellow powder (0.06 g, 0.15 mmol, 3%). ^1H NMR (C_6D_6 , 400 MHz) δ 8.64 – 8.54 (m, 2H), 7.73 – 7.63 (m, 4H), 7.47 (m, 2H), 7.33 – 7.22 (m, 6H), 6.12 – 6.03 (dd, 4H), 5.70 – 5.63 (dd, 4H). ^{13}C NMR (C_6D_6 , 100 MHz): δ 136.65, 135.98, 129.27, 128.61, 128.41, 127.69, 127.46, 127.04, 126.94, 126.51, 123.89, 121.23, 112.97. HRMS (ESI): calc'd for M^+ $\text{C}_{32}\text{H}_{22}\text{N}_2$, 434.1783; found 434.1771. UV/Vis: λ_{max} 362 nm.

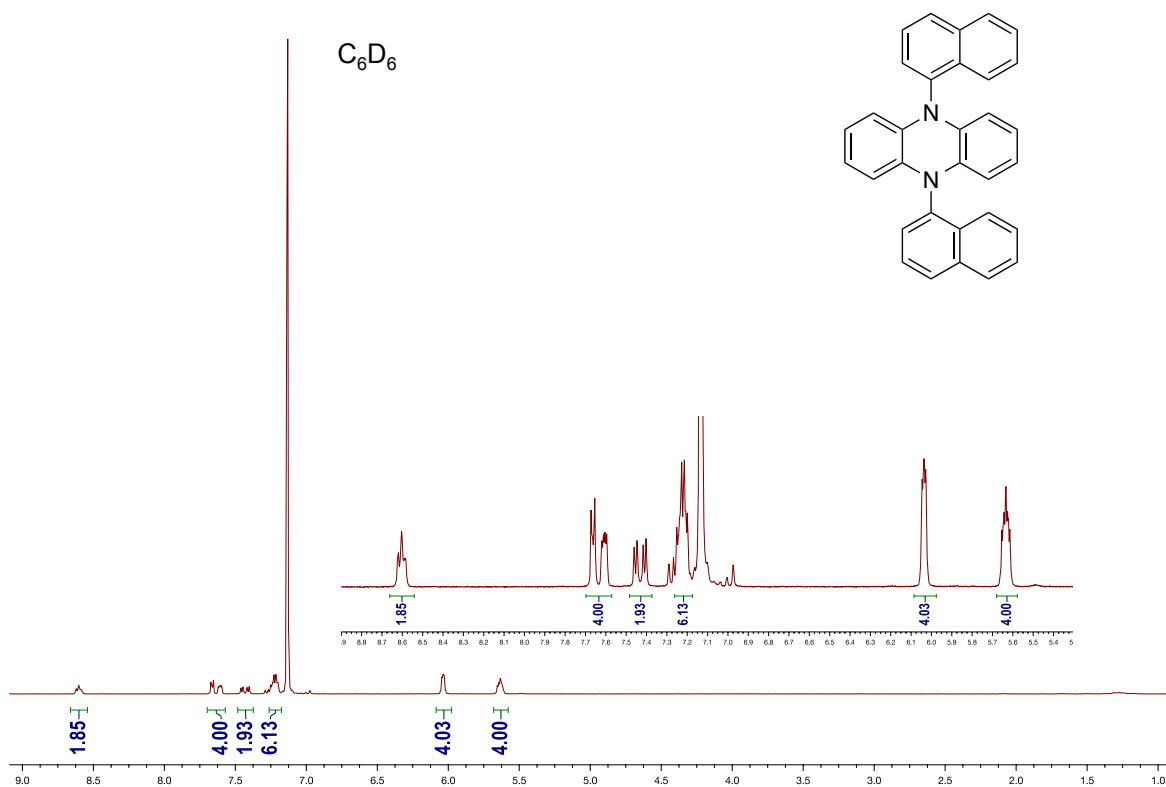


Figure 2.12 ^1H NMR spectrum of **6** with zoomed inset.

Photophysical Characterization of Catalysts

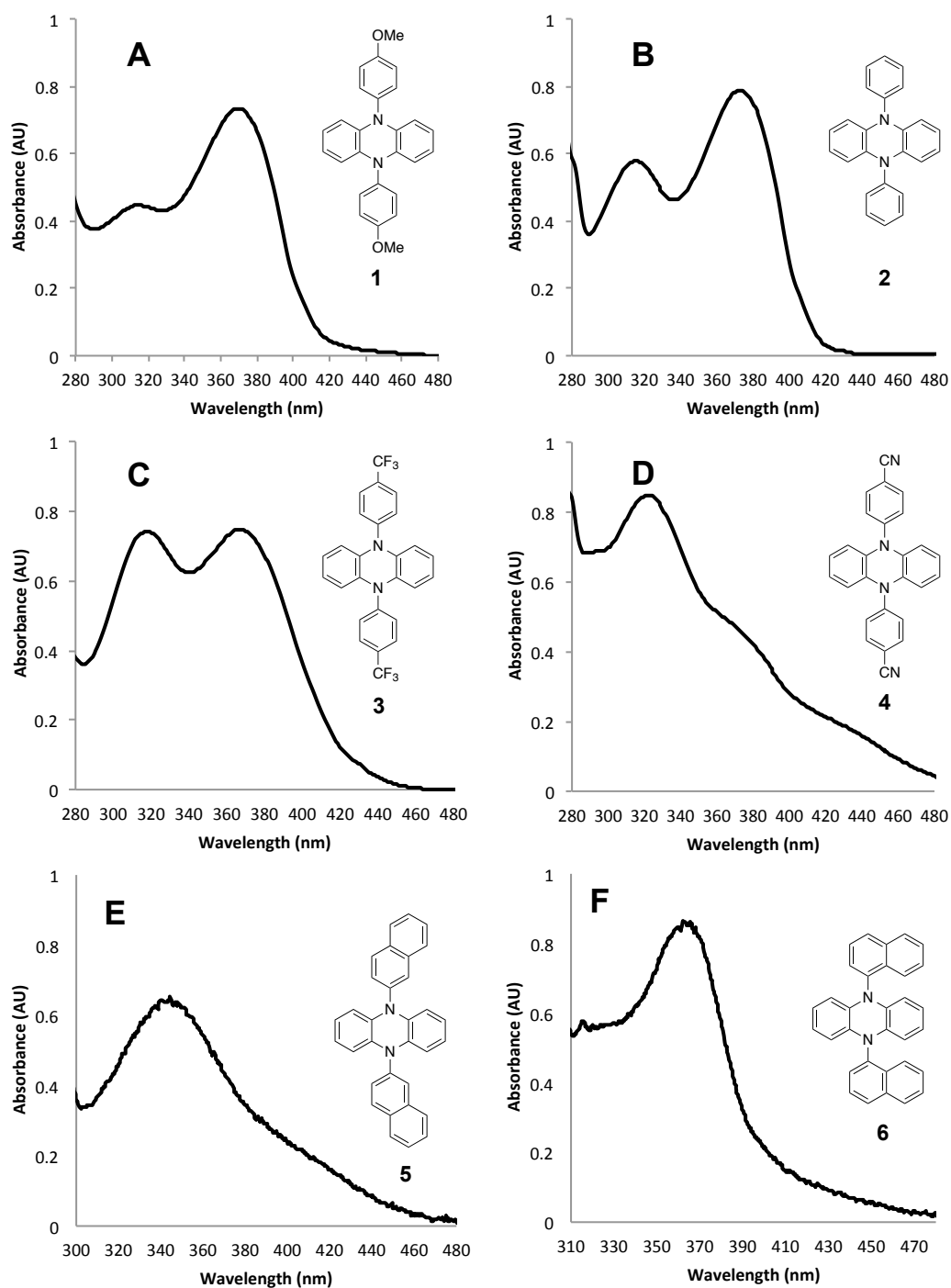


Figure 2.13 UV-Vis spectra of catalysts **1** (A), **2** (B), **3** (C), **4** (D), **5** (E), and **6** (F) at 0.15 mM in DMF.

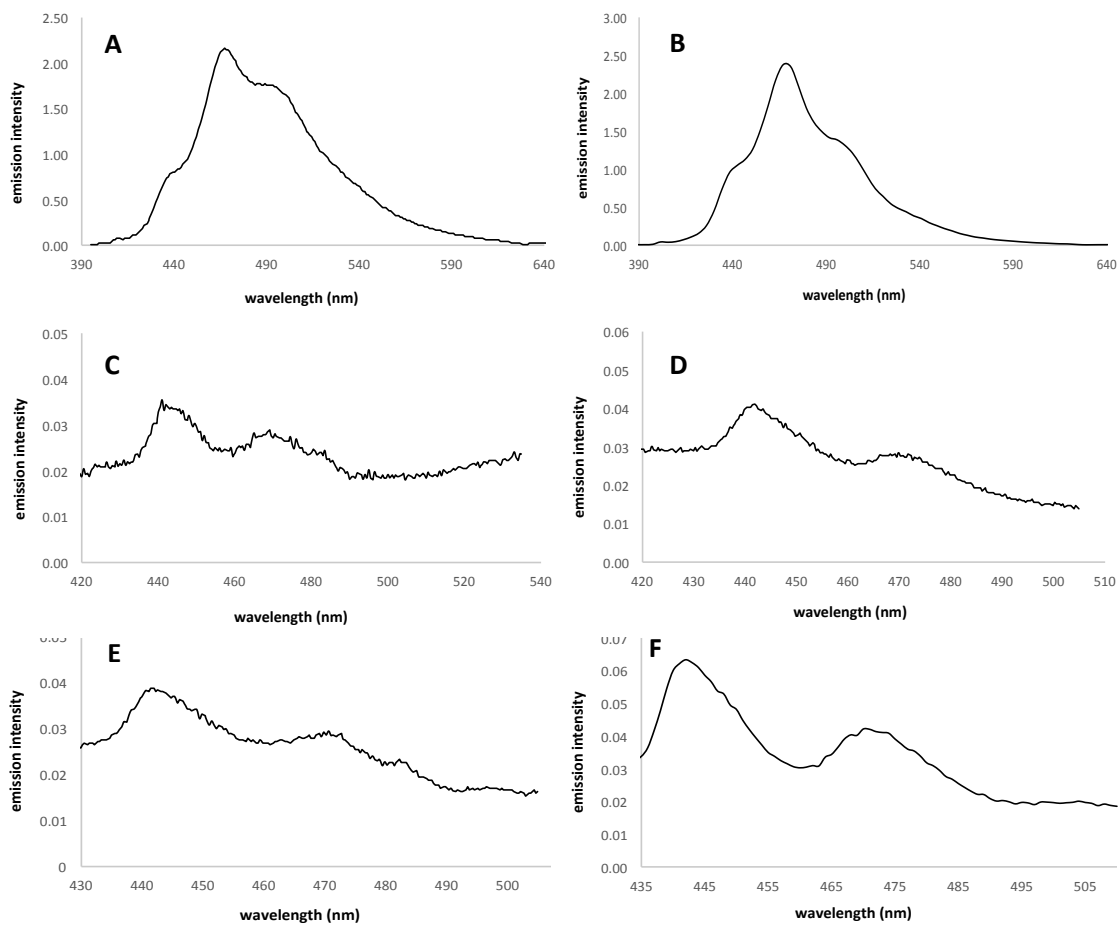


Figure 2.14 Emission spectra of catalysts **1** (A), **2** (B), **3** (C), **4** (D), **5** (E), and **6** (F) in DMF.

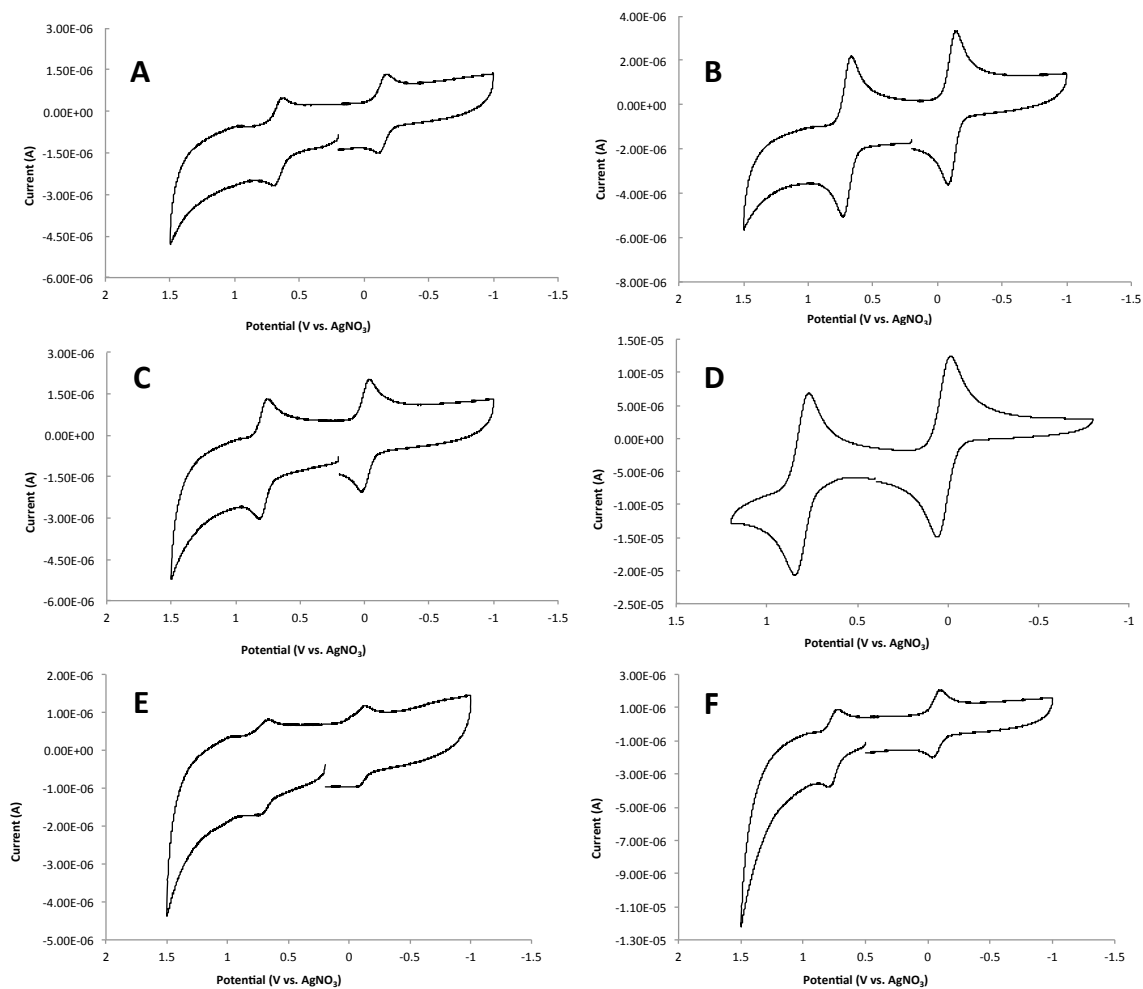


Figure 2.15 Cyclic voltammograms (vs. Ag/AgNO₃) of catalysts **1** (A), **2** (B), **3** (C), **4** (D), **5** (E), and **6** (F) in MeCN.

Table 2.3 Calculation of excited state reduction potentials of photocatalysts **1** – **6**. ^a L/mol*cm ^b V vs. SCE

PC	abs λ_{\max} (nm)	$\epsilon_{\lambda_{\max}}$ ^a	em λ_{\max} (nm)	E(em λ_{\max}) (V)	$E_{1/2}$ ^b	E^{*b} (calc'd)	E^{*b} (theo.)
1	373	5200	467	2.66	0.16	-2.50	-2.36
2	370	4900	467	2.66	0.19	-2.47	-2.34
3	367	4700	469	2.64	0.29	-2.35	-2.24
4	322	5600	469	2.64	0.32	-2.32	-2.06
5	340	6300	471	2.63	0.19	-2.44	-2.20
6	366	5500	471	2.63	0.23	-2.40	-2.12

End-Group Analysis of PMMA Synthesized Using O-ATRP

Analysis by ¹H NMR

MMA (4.00 mL, 37.4 mmol, 250 eq.), EBP (262 μ L, 1.50 mmol, 10 eq.), and **3** (10.4 mg, 0.025 mmol, 1 eq.) were dissolved in 6.00 mL DMA and reacted according to the above general polymerization procedure for 3.5 hours. At this time, the reaction was removed from the glovebox, poured into 200 mL of a mixture of 50% methanol and 50% water and stirred overnight. The resulting precipitate was then isolated by vacuum filtration and washed with excess methanol. The polymer was then re-dissolved in a minimal amount of THF and again poured into 200 mL of a mixture of 50% methanol and 50% water and stirred overnight. The product was again collected by vacuum filtration and dried under reduced pressure to reveal a white powder ($M_w = 8.83$ kDa, $D = 1.17$).

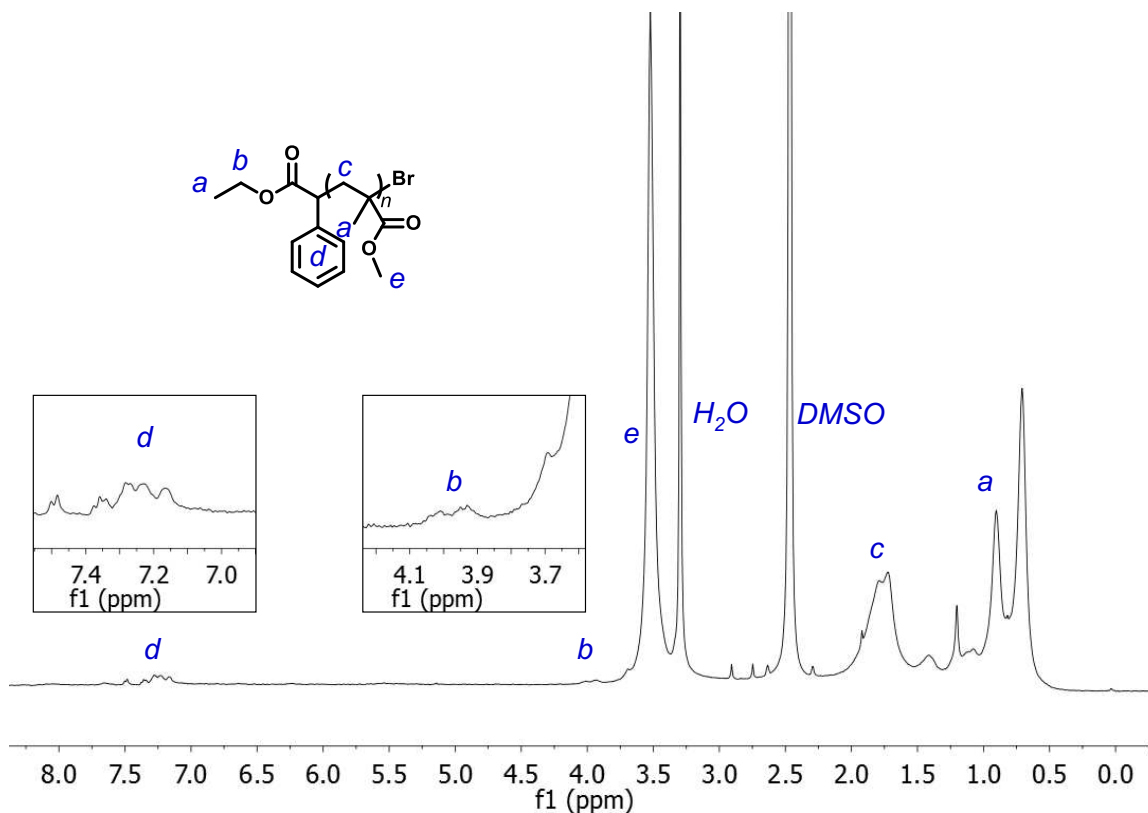


Figure 2.16 ¹H NMR spectrum of isolated poly(methyl methacrylate) (DMSO-*d*₆).

Analysis by MALDI-TOF

MMA (1.00 mL, 9.35 mmol, 1000 eq.), EBP (16.4 μ L, 93.5 μ mol, 10 eq.), and **3** (4.4 mg, 9.35 μ mol, 1 eq.) were dissolved in 1.00 mL DMA and reacted according to the above general polymerization procedure for 8 hours. At this time, the reaction was removed from the glovebox, poured into 50 mL methanol and stirred for 1 hour. The resulting precipitate was then isolated by vacuum filtration and washed with excess methanol. The polymer was then re-dissolved in a minimal amount of THF and the above precipitation and isolation process repeated twice to reveal a white powder ($M_w = 10.26$ kDa, $\bar{D} = 1.22$).

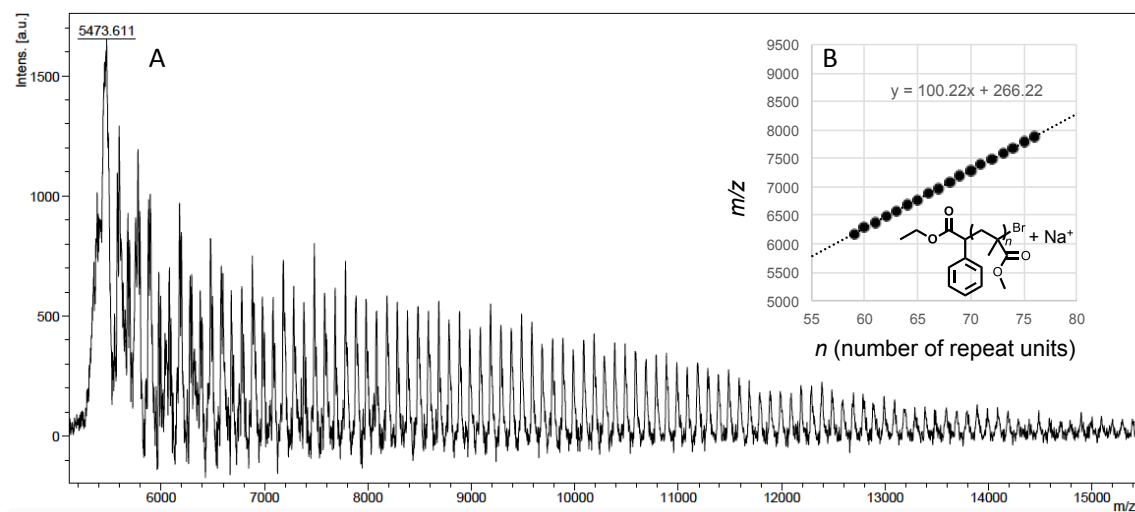
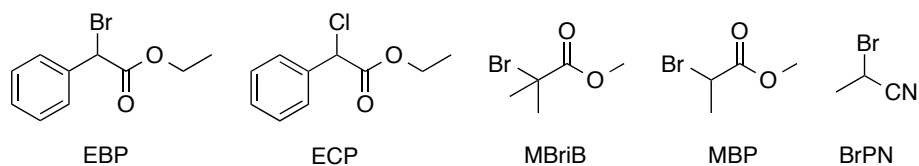


Figure 2.17 **A.** MALDI-TOF mass spectrum of a poly(methyl methacrylate) sample. **B.** Plot of m/z vs number of MMA repeat units revealing a slope equal to the mass of MMA and a y-intercept equal to the mass of the EBP chain-end group plus Na.

Supplemental Polymerization Data

Table 2.4 Supplemental polymerization data, including information for PCs **1**, **2**, **4**, and **5**, and an initiator screen for PCs **3** and **6**. Polymerizations were performed according to the above general polymerization procedure using 9.35 mmol (1000 eq.) monomer, 9.35 μmol (1 eq.) catalyst, and 93.5 μmol initiator.



Run No.	PC	Initiator	DMA	Time (h)	Conv. (%)	M_w	M_n	\bar{D} (M_n/M_w)	I^*
S1	1	EBP	1 mL	8	69.6	36.3	24.7	1.47	29.2
S2	2	EBP	1 mL	8	85.9	18.4	11.9	1.55	74.5
S3	4	EBP	1 mL	8	73.5	21.4	16.1	1.33	47.2
S4	4	EBP	1 mL	7	36.7	9.63	7.47	1.29	52.5
S5	3	MBriB	1 mL	8	94.0	18.8	15.0	1.25	63.5
S6	3	MBP	1 mL	8	86.0	9.80	7.37	1.33	118
S7	3	ECIP	1 mL	4	96.0	21.9	8.62	2.54	111
S8	5	EBP	1 mL	5	39.4	9.35	9.08	1.03	46.1
S9	6	EBP	1 mL	5	54.1	12.3	11.4	1.08	47.5
S10	6	BrPN	2 mL	8	73.3	15.8	12.8	1.24	58.1
S11	6	ECIP	2 mL	8	93.7	24.3	18.0	1.35	53.2
S12	6	MBriB	2 mL	8	90.2	14.4	10.7	1.35	85.9

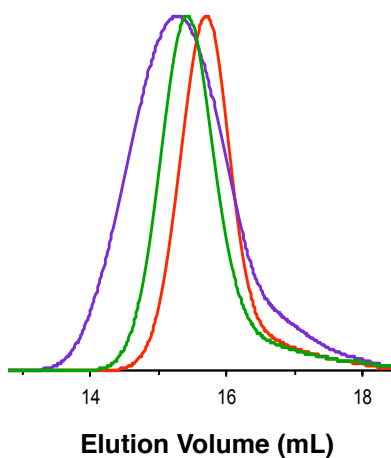
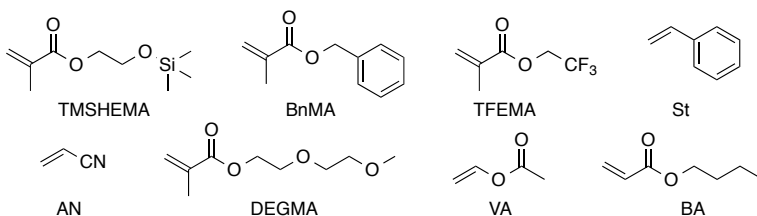


Figure 2.18 GPC traces of runs S10 (red), S11 (purple), and S12 (green).

Table 2.5 Monomer scope of catalysts **3** and **6**. Polymerizations were performed according to the above general polymerization procedure using 9.35 mmol (1000 eq.) monomer, 9.35 μ mol (1 eq.) catalyst, 93.5 μ mol initiator, and 1.00 mL DMA. ^aDetermined using PMMA standards



Run No.	PC	Monomer	Initiator	Conv. (%)	M_w	M_n	\bar{D} (M_n/M_w)	I^*
S13	3	TMSHEMA	EBP	83.3	25.3	20.0	1.26	85.5
S14	3	TFEMA	EBP	77.4	58.2	54.7	1.06	24.2
S15	3	DEGMA	EBP	94.7	30.1	21.3	1.41	84.6
S16	3	BA	EBP	98.5	26.6	16.4	1.62	60.0
S17	3	St	EBP	0.0	n/a	n/a	n/a	n/a
S18	3	VA	EBP	0.0	n/a	n/a	n/a	n/a
S19	3	AN	EBP	71.3	40.3 ^a	23.7 ^a	1.70	15.6
S20	6	TMSHEMA	MBP	90.8	18.7	16.0	1.17	116
S21	6	TFEMA	MBP	79.4	53.9	32.9	1.64	41.3
S22	6	DEGMA	MBP	92.6	22.8	18.4	1.24	96.0
S23	6	BA	MBP	99.9	30.1	21.2	1.42	60.3
S24	6	BnMA	MBP	96.6	53.4	43.1	1.24	79.0

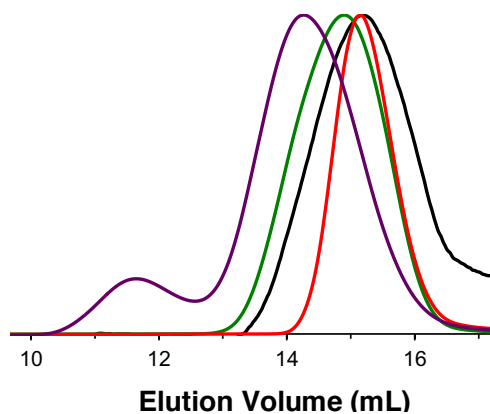


Figure 2.19 GPC traces of runs S13 (blue), S14 (red), S15 (purple), and S16 (orange).

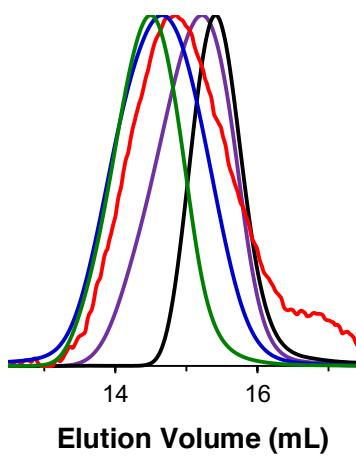


Figure 2.20 GPC traces of runs S20 (blue), S21 (red), S22 (purple), S23 (orange), and S24 (green).

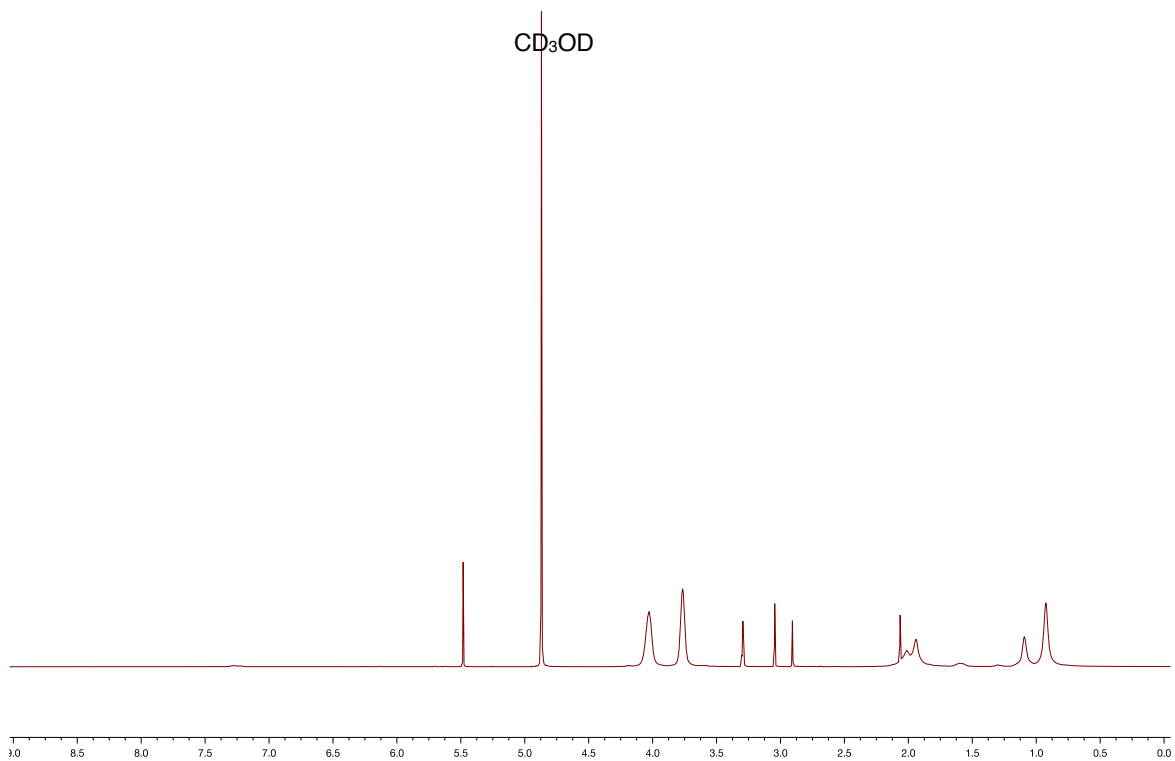


Figure 2.21 ^1H NMR spectrum of isolated poly(TMS-HEMA) made using 3 as the catalyst. It was found that the isolation method (described in the above general procedures section) resulted in loss of the TMS groups to give poly(HEMA), whereas the TMS groups remained intact in the ^1H NMR of the aliquot used to determine the values found in Table S3.

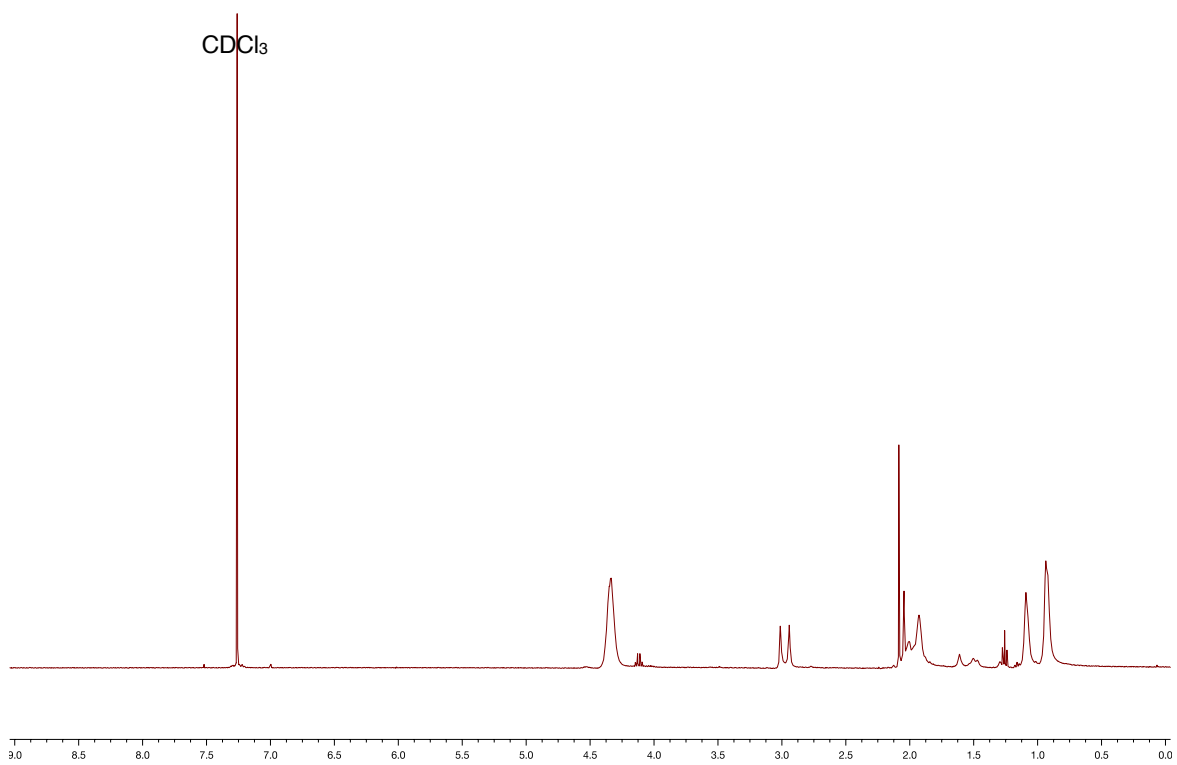


Figure 2.22 ^1H NMR spectrum of isolated poly(TFEMA) made using 3 as the catalyst.

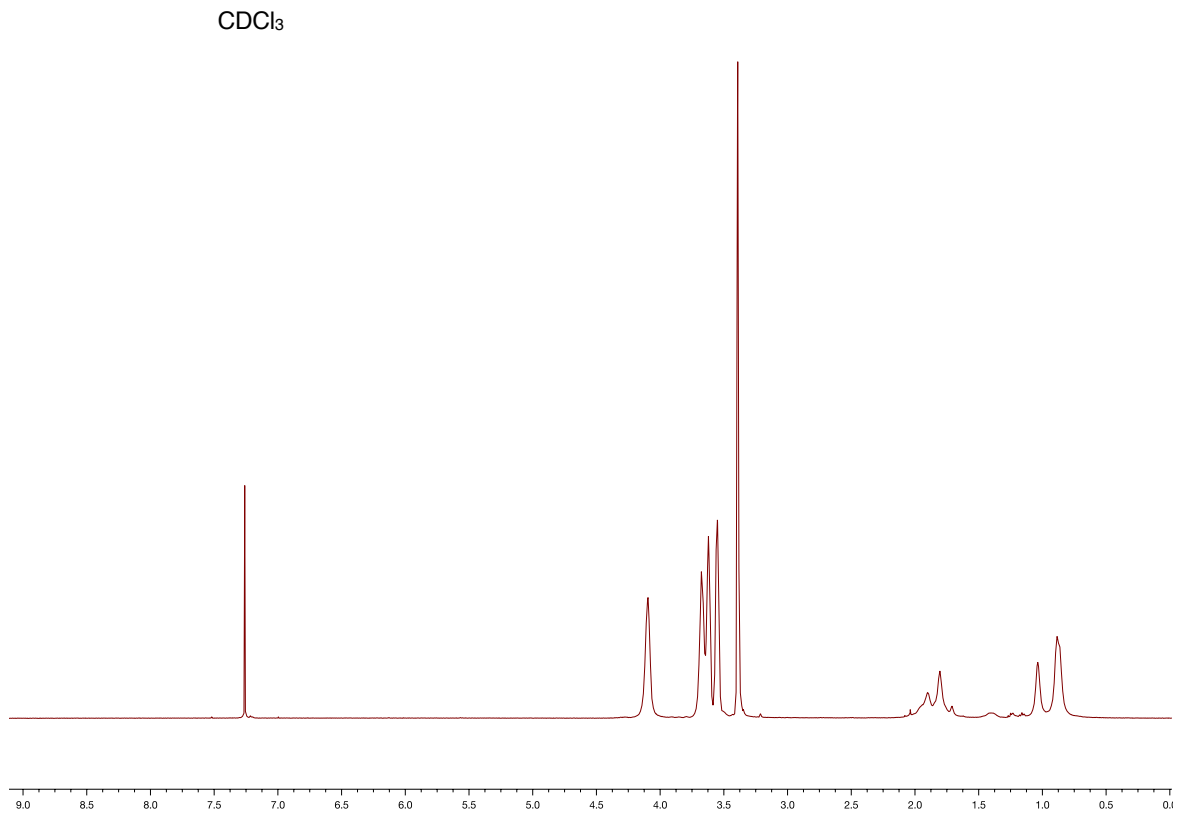


Figure 2.23 ¹H NMR spectrum of isolated poly(DEGMA) made using 3 as the catalyst.

GPC Traces of Various Runs in Tables 1 and 2

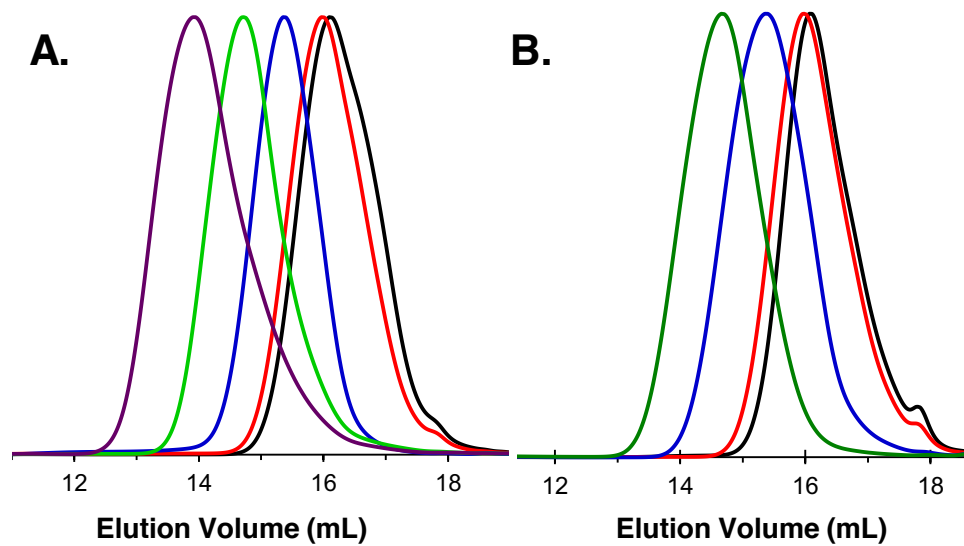


Figure 2.24 A. GPC trace of runs 6 (purple), 5 (green), 1 (blue), 4 (red), and 3 (black), Table 1, main text. B.GPC trace of runs 10 (green), 9 (blue), 8 (red), and 7 (black), Table 1, main text.

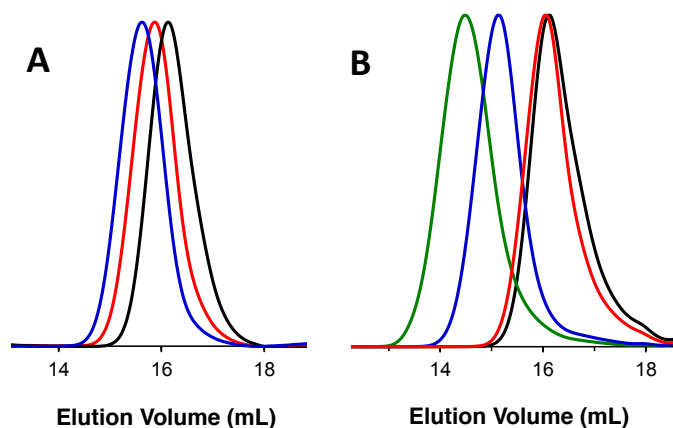


Figure 2.25 A. GPC trace of runs 11 (blue), 12 (red), and 13 (black), Table 2, main text. B. GPC trace of runs 14 (green), 15 (blue), 16 (red), and 17 (black), Table 2, main text.

Block Copolymerizations

Synthesis of PMMA Macroinitiator

MMA (3.00 mL, 28.1 mmol, 1000 eq.), methyl α -bromoisobutyrate (54.5 μ L, 0.42 mmol, 15 eq.), and **3** (13.2 mg, 0.03 mmol, 1 eq.) were dissolved in 3.00 mL DMA and reacted according to the above general polymerization procedure for 5 hours. At this time, the reaction was removed from the glovebox, poured into 100 mL of methanol, stirred for approximately 1 hour, and the product polymer was then isolated by vacuum filtration and washed with excess methanol. The polymer was then re-dissolved in a minimal amount of THF and the process repeated a total of three times to ensure complete removal of any unreacted monomer, initiator, or catalyst ($M_w = 16.1$ kDa, $\bar{D} = 1.12$) (GPC trace in Figure 2D, Main Text).

Synthesis of PMMA-*b*-PMMA

MMA (1.00 mL, 9.35 mmol, 1000 eq.), EBP (16.4 μ L, 93.5 μ mol, 10 eq.), and **3** (4.4 mg, 9.35 μ mol, 1 eq.) were dissolved in 1.00 mL DMA and reacted according to the above general polymerization procedure for 12 hours. At this time, an aliquot was taken for analysis (conv. = 76.2%, M_w = 14.3 kDa, D = 1.21) and an additional 1.00 mL MMA and 1.00 mL DMA were added to the reaction mixture. After an additional 6 h, the resulting polymer was isolated according to the above general polymerization procedure and analyzed (isol. yield = 72%, %, M_w = 40.7 kDa, D = 1.16).

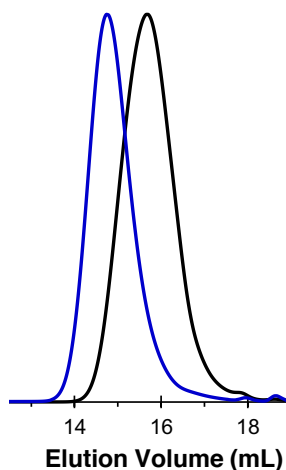


Figure 2.26 GPC trace showing the results of the synthesis of PMMA-*b*-PMMA. The polymer produced after 12 hours (black) and the polymer produced after additional monomer and 6 hours of irradiation (blue).

*Synthesis of PMMA-*b*-PMMA with a dark resting period*

MMA (1.00 mL, 9.35 mmol, 1000 eq.), EBP (16.4 μ L, 93.5 μ mol, 10.0 eq.), and **3** (4.4 mg, 9.35 μ mol, 1.00 eq.) were dissolved in 1.00 mL DMA and reacted according to the above general polymerization procedure for 8 h. At this time, an aliquot was taken for analysis (conv. = 61.2%, M_w = 12.0 kDa, \bar{D} = 1.25). The reaction was then covered and left in the dark for 8 h. At this time, an aliquot was taken for analysis (conv. = 61.0%, M_w = 12.0 kDa, \bar{D} = 1.26) and an additional 1.00 mL MMA and 1.00 mL DMA were added to the reaction mixture and irradiated. After 8 h, the resulting polymer was isolated according to the above general polymerization procedure and analyzed (isol. yield = 70%, M_w = 40.7 kDa, \bar{D} = 1.16).

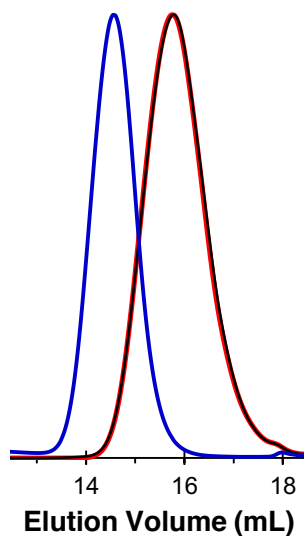


Figure 2.27 GPC trace showing the results of the synthesis of PMMA-*b*-PMMA with a dark resting period. The polymer produced after 8 hours (red), the polymer produced after the dark period (black), and the polymer produced after additional monomer and irradiation 8 hours of (blue).

*Synthesis of PMMA-*b*-PMMA from isolated macroinitiator*

PMMA macroinitiator (*vide supra*) (100 mg, 6.25 μmol , 10.0 eq.), MMA (200 μL , 1.88 mmol, 3000 eq.), and **3** (0.3 mg, 0.63 μmol , 1.0 eq.) were dissolved in 2.00 mL DMA and reacted according to the above general polymerization procedure for 8 h. The resulting polymer was isolated according to the above general polymerization procedure and analyzed (isol. yield = 62%, $M_w = 46.6$ kDa, $\text{Đ} = 1.46$) (GPC trace in Figure 3, Main Text).

*Synthesis of PMMA-*b*-PBA with a dark resting period*

MMA (1.00 mL, 9.35 mmol, 1000 eq.), EBP (16.4 μL , 93.5 μmol , 10.0 eq.), and **3** (4.4 mg, 9.35 μmol , 1.00 eq.) were dissolved in 1.00 mL DMA and reacted according to the above general polymerization procedure for 8 h. At this time, an aliquot was taken for analysis (conv. = 72.0%, $M_w = 13.7$ kDa, $\text{Đ} = 1.24$). The reaction was then covered and left in the dark for 8 h. At this time, an aliquot was taken for analysis (conv. = 71.4%, $M_w = 13.3$ kDa, $\text{Đ} = 1.32$) and an additional 1.30 mL BA and 1.00 mL DMA were added to the reaction mixture. After 8 h, the resulting polymer was isolated according to the above general polymerization procedure and analyzed (isol. yield = 27%, $M_w = 84.5$ kDa, $\text{Đ} = 1.33$).

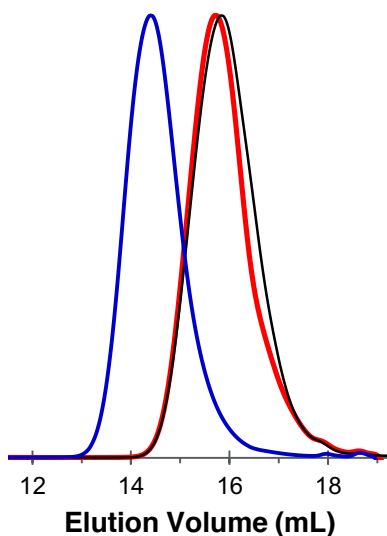


Figure 2.28 GPC trace showing the results of the synthesis of PMMA-*b*-PBA with a dark resting period. The polymer produced after 8 hours (red), the polymer produced after the dark period (black), and the polymer produced after additional monomer and 8 hours of irradiation (blue).

*Synthesis of PMMA-*b*-PBA from isolated macroinitiator*

PMMA macroinitiator (*vide supra*) (100 mg, 6.25 μmol , 10.0 eq.), BA (448 μL , 3.13 mmol, 5000 eq.), and 3 (0.3 mg, 0.63 μmol , 1.00 eq.) were dissolved in 2.00 mL DMA and reacted according to the above general polymerization procedure for 8 h. The resulting polymer was isolated according to the general polymerization procedure described above and analyzed (isol. yield = 47%, $M_w = 70.2$ kDa, $\bar{D} = 1.37$) (GPC trace in Figure 2C, Main Text).

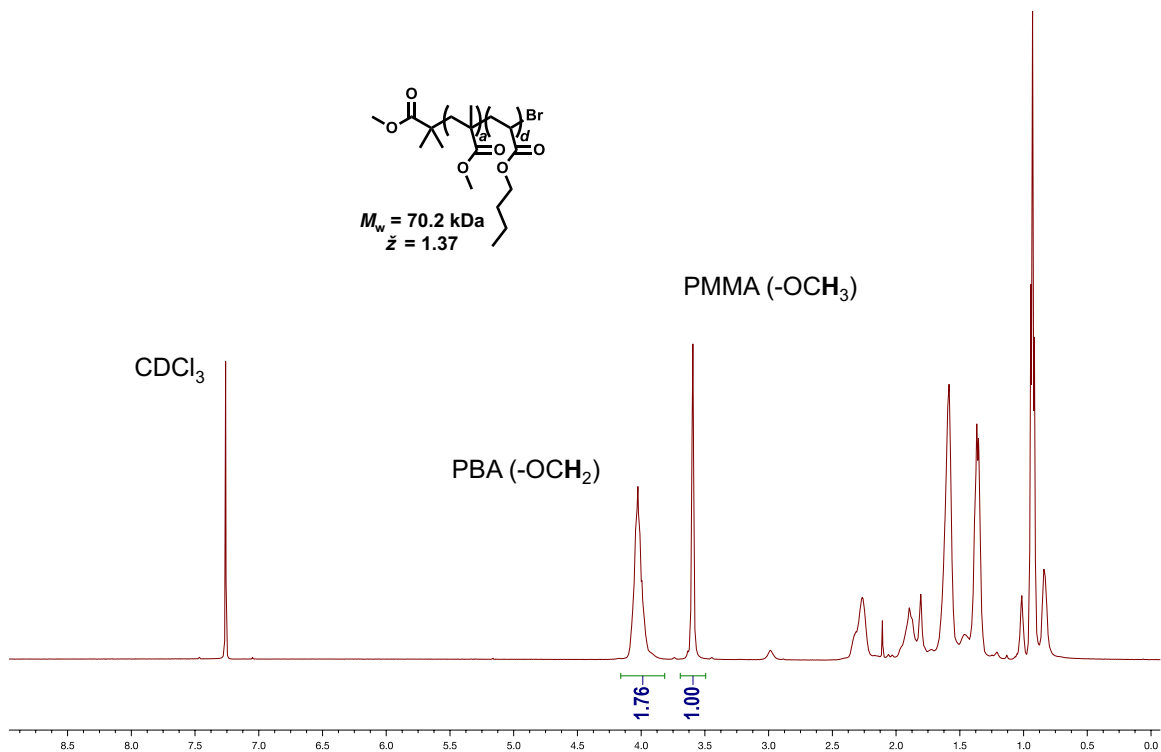


Figure 2.29 ^1H NMR of PMMA-*b*-PBA (CDCl_3).

*Synthesis of PMMA-*b*-PBnMA with a dark resting period*

MMA (1.00 mL, 9.35 mmol, 1000 eq.), EBP (16.4 μL , 93.5 μmol , 10.0 eq.), and **3** (4.4 mg, 9.35 μmol , 1.00 eq.) were dissolved in 1.00 mL DMA and reacted according to the above general polymerization procedure for 8 h. At this time, an aliquot was taken for analysis (conv. = 66.0%, M_w = 11.2 kDa, \bar{D} = 1.34). The reaction was then covered and left in the dark for 8 h. At this time, an aliquot was taken for analysis (conv. = 66.0%, M_w = 11.1 kDa, \bar{D} = 1.34) and an additional 1.50 mL BnMA and 1.00 mL DMA were added to the reaction mixture. After 8 h, the resulting polymer was isolated according to the above general polymerization procedure and analyzed (isol. yield = 69%, M_w = 62.5 kDa, \bar{D} = 1.32).

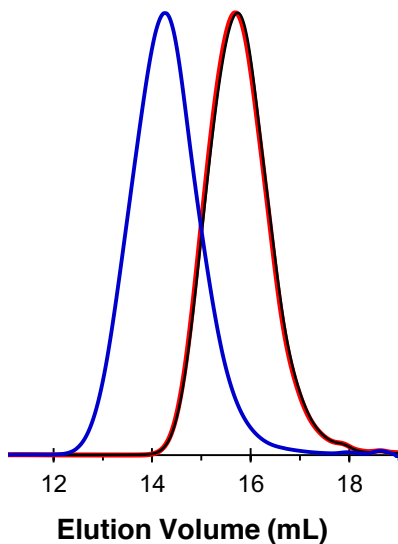


Figure 2.30 GPC trace showing the results of the synthesis of PMMA-*b*-PBnMA with a dark resting period. The polymer produced after 8 hours (red), the polymer produced after the dark period (black), and the polymer produced after additional monomer 8 hours of irradiation (blue).

*Synthesis of PMMA-*b*-PBnMA from isolated macroinitiator*

PMMA macroinitiator (*vide supra*) (100 mg, 6.25 μ mol, 10.0 eq.), BnMA (529 μ L, 3.13 mmol, 5000 eq.), and 3 (0.3 mg, 0.63 μ mol, 1.00 eq.) were dissolved in 2.00 mL DMA and reacted according to the above general polymerization procedure for 8 h. The resulting polymer was isolated according to the above general polymerization procedure and analyzed (isol. yield = 79%, M_w = 158.8 kDa, \bar{D} = 1.63) (GPC trace in Figure 2C, Main Text).

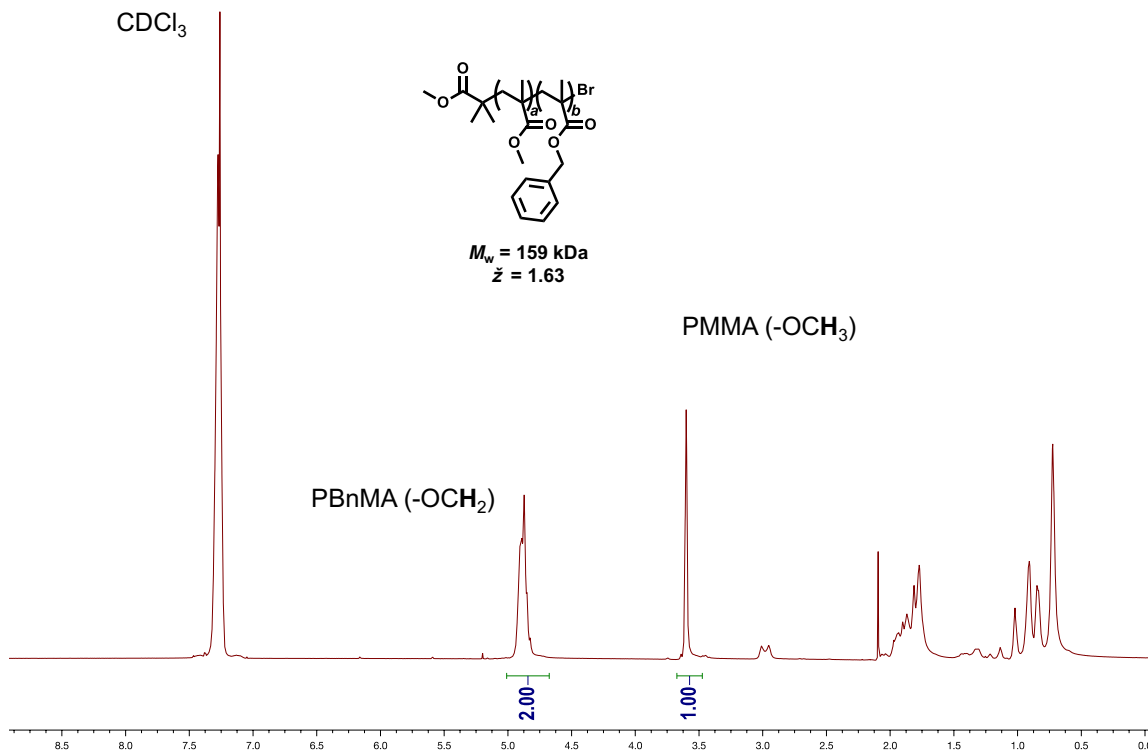


Figure 2.31 ^1H NMR of PMMA-*b*-PBnMA (CDCl_3).

Computational Details: Performed by C.-H.L. and C.B.M.

Standard reduction potentials (E^0) were calculated following previously reported procedures. (39 – 42) A value of -100.5 kcal/mol was assumed for the reduction free energy of the standard hydrogen electrode (SHE) as described in Ref. 39. Thus, $E^0 = (-100.5 - \Delta G_{\text{red}})/23.06$ (V vs. SHE); for $E^0(\text{PC}^{*+}/{}^3\text{PC}^*)$, $\Delta G_{\text{red}} = G({}^3\text{PC}^*) - G(\text{PC}^{*+})$ while for $E^0(\text{PC}^{*+}/\text{PC})$, $\Delta G_{\text{red}} = G(\text{PC}) - G(\text{PC}^{*+})$. The Gibbs free energies of ${}^3\text{PC}^*$, PC^{*+} , and PC were calculated at the unrestricted M06/6-31+G** level of theory in CPCM- H_2O solvent. (40) To reference to the Saturated Calomel Electrode (SCE), E^0 (vs. SHE) is converted to E^0 (vs. SCE) using E^0 (vs. SCE) = E^0 (vs. SHE) - 0.24 V. Triplet energies (in eV) of PCs were obtained by $[G({}^3\text{PC}^*) - G(\text{PC})]$, in kcal/mol/23.06.

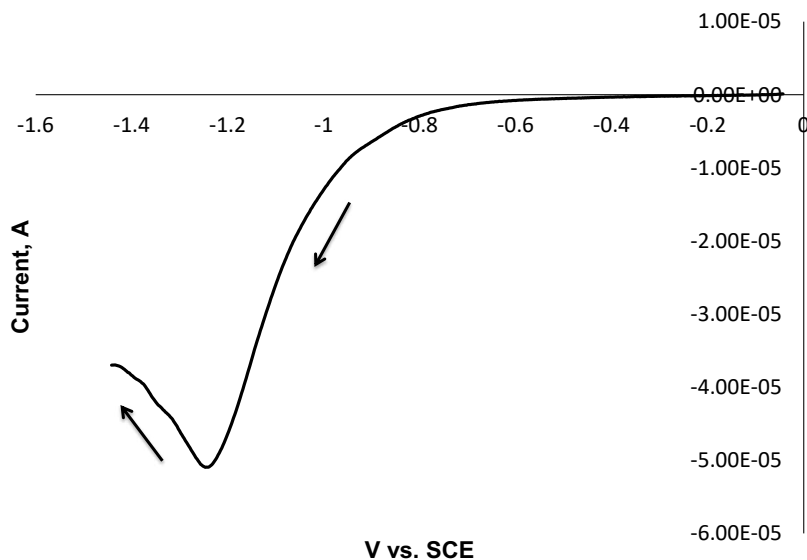


Figure 2.32 Cyclic voltammetry (CV) of EBP on glassy carbon electrode in acetonitrile (0.10 M Bu_4NClO_4 electrolyte). Scan rate = 100 mV/s. Onset of EBP reduction at ~ -0.8 V vs. SCE. CV was performed using saturated Ag/AgCl reference electrode, and was converted to vs. SCE by subtracting 0.043 V. Although the onset of reduction measured here is consistent with our calculated $E^0(\text{EBP}/\text{EBP}^{\cdot-})$ of -0.74 V vs. SCE, we note that an actual E^0 would be determined using saturated solute and standard conditions that produce a reversible CV.

Coordinates of Molecular Structures

All coordinates are reported as XYZ Cartesian coordinates. In parentheses are uM06/6-31+G**/CPCM- H_2O energies. Energies reported here are computed at 0 K (not ZPE and thermally corrected) and are stated in Hartrees units. All energies reported were calculated using the GAUSSIAN 09 computational chemistry package

5,10-di(4-methoxyphenyl)-5,10-dihydrophenazine (1)

Ground state (-1263.12336902)

C	-0.69230	3.64841	-0.27940
C	-1.38528	2.43592	-0.20652
C	-0.70621	1.22231	-0.12662
C	0.70616	1.22233	-0.12664
C	1.38523	2.43593	-0.20658
C	0.69224	3.64843	-0.27944
C	0.70620	-1.22230	-0.12661
C	-0.70616	-1.22232	-0.12661
C	-1.38523	-2.43592	-0.20649
H	-2.47193	-2.43741	-0.20220
C	-0.69224	-3.64842	-0.27935
C	0.69230	-3.64840	-0.27939
C	1.38528	-2.43590	-0.20654
H	-1.24996	4.57994	-0.33423
H	-2.47197	2.43741	-0.20224
H	2.47192	2.43740	-0.20233
H	1.24988	4.57996	-0.33433
H	-1.24987	-4.57995	-0.33417
H	1.24996	-4.57992	-0.33425
H	2.47198	-2.43737	-0.20230
N	1.39197	0.00002	-0.01551
N	-1.39198	-0.00002	-0.01563
C	2.81939	0.00002	-0.02326
C	3.51898	-0.00006	1.17615
C	3.52041	0.00007	-1.23215
C	4.91362	-0.00008	1.18882
H	2.96492	-0.00009	2.11309
C	4.90520	0.00005	-1.23473
H	2.96639	0.00013	-2.16960
C	5.60890	-0.00003	-0.02264
H	5.43706	-0.00015	2.13963
H	5.46814	0.00010	-2.16492
C	-2.81940	-0.00004	-0.02332
C	-3.52044	-0.00021	-1.23220
C	-3.51896	0.00013	1.17611
C	-4.90523	-0.00018	-1.23474
H	-2.96643	-0.00037	-2.16965
C	-4.91359	0.00019	1.18881
H	-2.96488	0.00024	2.11303
C	-5.60890	0.00004	-0.02265
H	-5.46820	-0.00032	-2.16492
H	-5.43702	0.00033	2.13962
O	6.96007	-0.00008	-0.12668
O	-6.96008	0.00011	-0.12665
C	7.72209	0.00010	1.06889

H	8.76924	0.00019	0.76460
H	7.51803	0.89605	1.66844
H	7.51824	-0.89581	1.66858
C	-7.72207	-0.00010	1.06894
H	-8.76922	-0.00032	0.76467
H	-7.51789	-0.89602	1.66851
H	-7.51829	0.89584	1.66860

Triplet excited state (-1263.03344183)

C	-0.71693	-3.63964	0.10068
C	-1.40509	-2.44792	0.09883
C	-0.72614	-1.21086	0.09699
C	0.72597	-1.21091	0.09734
C	1.40483	-2.44802	0.09957
C	0.71659	-3.63970	0.10110
C	0.72613	1.21111	0.09717
C	-0.72596	1.21116	0.09750
C	-1.40482	2.44827	0.09919
H	-2.49198	2.45362	0.09939
C	-0.71659	3.63996	0.10050
C	0.71693	3.63989	0.10015
C	1.40508	2.44817	0.09855
H	-1.26450	-4.57828	0.10197
H	-2.49225	-2.45321	0.09865
H	2.49199	-2.45341	0.09997
H	1.26407	-4.57839	0.10285
H	-1.26406	4.57865	0.10192
H	1.26449	4.57854	0.10119
H	2.49225	2.45341	0.09829
N	1.38935	0.00004	0.09562
N	-1.38935	0.00023	0.09564
C	2.82435	-0.00001	0.09552
C	3.51071	-0.00066	-1.10915
C	3.51438	0.00055	1.30599
C	4.90545	-0.00068	-1.12141
H	2.95275	-0.00113	-2.04366
C	4.90062	0.00049	1.30460
H	2.95817	0.00101	2.24145
C	5.60112	-0.00009	0.09078
H	5.42805	-0.00117	-2.07242
H	5.46506	0.00091	2.23354
C	-2.82436	0.00025	0.09552
C	-3.51438	0.00033	1.30598
C	-3.51070	0.00009	-1.10918
C	-4.90063	0.00014	1.30462
H	-2.95811	0.00056	2.24141

C	-4.90542	-0.00014	-1.12140
H	-2.95276	0.00015	-2.04369
C	-5.60110	-0.00016	0.09079
H	-5.46504	0.00026	2.23357
H	-5.42810	-0.00017	-2.07237
O	6.95154	-0.00010	0.19235
O	-6.95153	-0.00037	0.19235
C	7.71310	-0.00058	-1.00399
H	8.76021	-0.00047	-0.69982
H	7.50880	-0.89689	-1.60276
H	7.50882	0.89526	-1.60346
C	-7.71313	-0.00038	-1.00397
H	-8.76023	-0.00044	-0.69975
H	-7.50891	0.89572	-1.60309
H	-7.50884	-0.89643	-1.60312

Cation Radical (-1262.95864356)

C	0.70130	-3.62042	-0.10945
C	1.39918	-2.43001	-0.10648
C	0.70950	-1.20682	-0.10361
C	-0.70940	-1.20683	-0.10360
C	-1.39909	-2.43003	-0.10640
C	-0.70122	-3.62044	-0.10940
C	-0.70950	1.20706	-0.10359
C	0.70940	1.20707	-0.10354
C	1.39909	2.43026	-0.10586
H	2.48427	2.43148	-0.10524
C	0.70122	3.62067	-0.10862
C	-0.70130	3.62066	-0.10875
C	-1.39918	2.43024	-0.10610
H	1.24664	-4.55944	-0.11183
H	2.48437	-2.43124	-0.10617
H	-2.48427	-2.43126	-0.10596
H	-1.24655	-4.55946	-0.11172
H	1.24655	4.55969	-0.11057
H	-1.24663	4.55968	-0.11084
H	-2.48437	2.43147	-0.10570
N	-1.38695	0.00009	-0.09998
N	1.38694	0.00015	-0.09990
C	-2.82769	0.00008	-0.09558
C	-3.50768	-0.00021	1.11339
C	-3.51761	0.00037	-1.30699
C	-4.89992	-0.00022	1.12701
H	-2.94951	-0.00047	2.04744
C	-4.90144	0.00031	-1.29988
H	-2.96598	0.00050	-2.24481

C	-5.59945	0.00001	-0.08385
H	-5.41965	-0.00039	2.07934
H	-5.46777	0.00046	-2.22730
C	2.82769	0.00014	-0.09552
C	3.51759	0.00086	-1.30695
C	3.50769	-0.00073	1.11344
C	4.90140	0.00075	-1.29988
H	2.96590	0.00166	-2.24474
C	4.89993	-0.00091	1.12702
H	2.94956	-0.00118	2.04751
C	5.59944	-0.00018	-0.08385
H	5.46772	0.00141	-2.22730
H	5.41972	-0.00158	2.07931
O	-6.94584	0.00019	-0.18176
O	6.94583	-0.00067	-0.18180
C	-7.70815	-0.00092	1.01612
H	-8.75461	-0.00118	0.71070
H	-7.50282	-0.89778	1.61303
H	-7.50360	0.89538	1.61416
C	7.70819	-0.00007	1.01605
H	8.75464	0.00066	0.71057
H	7.50260	0.89640	1.61346
H	7.50391	-0.89676	1.61356

5,10-diphenyl-5,10-dihydrophenazine (2)

Ground state (-1034.18152904)

C	-0.69208	3.65413	-0.09070
C	-1.38523	2.44000	-0.05085
C	-0.70622	1.22465	-0.00668
C	0.70623	1.22463	-0.00667
C	1.38527	2.43998	-0.05081
C	0.69214	3.65412	-0.09068
C	0.70621	-1.22464	-0.00668
C	-0.70623	-1.22463	-0.00668
C	-1.38527	-2.43997	-0.05082
H	-2.47196	-2.44325	-0.04892
C	-0.69214	-3.65411	-0.09066
C	0.69208	-3.65412	-0.09067
C	1.38523	-2.43999	-0.05083
H	-1.25002	4.58654	-0.12072
H	-2.47192	2.44329	-0.04898

H	2.47196	2.44326	-0.04891
H	1.25009	4.58652	-0.12068
H	-1.25009	-4.58651	-0.12066
H	1.25002	-4.58653	-0.12067
H	2.47192	-2.44328	-0.04893
N	1.39212	-0.00001	0.05550
N	-1.39212	0.00001	0.05549
C	2.82034	-0.00002	0.04679
C	3.51517	0.00001	1.25367
C	3.50840	-0.00005	-1.16517
C	4.90809	0.00001	1.24829
H	2.95547	0.00003	2.18730
C	4.90058	-0.00004	-1.16780
H	2.94373	-0.00007	-2.09614
C	5.60036	-0.00001	0.03845
H	5.45319	0.00004	2.18898
H	5.44027	-0.00007	-2.11163
H	6.68745	-0.00001	0.03501
C	-2.82034	0.00002	0.04679
C	-3.50840	-0.00000	-1.16517
C	-3.51517	0.00003	1.25367
C	-4.90059	-0.00001	-1.16780
H	-2.94374	-0.00001	-2.09614
C	-4.90809	0.00002	1.24830
H	-2.95546	0.00004	2.18730
C	-5.60036	0.00000	0.03845
H	-5.44027	-0.00002	-2.11163
H	-5.45318	0.00002	2.18898
H	-6.68745	-0.00001	0.03502

Triplet excited state (-1034.09147796)

C	0.71758	-3.63997	0.00030
C	1.40576	-2.44835	0.00009
C	0.72638	-1.21153	-0.00007
C	-0.72584	-1.21185	0.00003
C	-1.40466	-2.44894	0.00050
C	-0.71595	-3.64026	0.00056
C	-0.72638	1.21153	0.00009
C	0.72584	1.21186	-0.00007
C	1.40466	2.44894	-0.00059
H	2.49180	2.45620	-0.00080
C	0.71595	3.64026	-0.00061
C	-0.71758	3.63997	-0.00024
C	-1.40576	2.44836	-0.00000

H	1.26517	-4.57853	0.00011
H	2.49292	-2.45521	-0.00018
H	-2.49180	-2.45620	0.00064
H	-1.26319	-4.57904	0.00077
H	1.26319	4.57904	-0.00088
H	-1.26517	4.57854	-0.00000
H	-2.49292	2.45521	0.00034
N	-1.38774	-0.00031	0.00009
N	1.38774	0.00032	-0.00010
C	-2.82393	-0.00047	-0.00003
C	-3.50337	0.00028	1.21264
C	-3.50331	-0.00109	-1.21279
C	-4.89681	0.00044	1.20912
H	-2.93825	0.00067	2.14275
C	-4.89671	-0.00100	-1.20923
H	-2.93821	-0.00173	-2.14290
C	-5.59084	-0.00018	-0.00007
H	-5.43965	0.00093	2.15078
H	-5.43955	-0.00153	-2.15090
H	-6.67784	-0.00003	-0.00012
C	2.82393	0.00047	0.00003
C	3.50338	-0.00034	-1.21264
C	3.50330	0.00116	1.21279
C	4.89682	-0.00051	-1.20910
H	2.93827	-0.00078	-2.14276
C	4.89670	0.00105	1.20925
H	2.93819	0.00185	2.14290
C	5.59084	0.00017	0.00009
H	5.43966	-0.00104	-2.15076
H	5.43953	0.00164	2.15092
H	6.67784	0.00003	0.00015

Cation Radical (-1034.01562908)

C	0.70128	3.62088	-0.00006
C	1.39938	2.43059	-0.00005
C	0.70941	1.20769	-0.00003
C	-0.70937	1.20771	-0.00001
C	-1.39930	2.43062	-0.00001
C	-0.70116	3.62090	-0.00004
C	-0.70941	-1.20769	0.00001
C	0.70937	-1.20771	-0.00003
C	1.39930	-2.43062	-0.00003
H	2.48445	-2.43365	-0.00005
C	0.70116	-3.62090	0.00003

C	-0.70128	-3.62088	0.00008
C	-1.39938	-2.43059	0.00008
H	1.24656	4.55988	-0.00007
H	2.48455	2.43357	-0.00005
H	-2.48445	2.43365	-0.00002
H	-1.24644	4.55990	-0.00006
H	1.24644	-4.55990	0.00004
H	-1.24656	-4.55988	0.00015
H	-2.48455	-2.43357	0.00011
N	-1.38499	0.00000	0.00001
N	1.38499	0.00000	-0.00005
C	-2.82766	-0.00001	0.00000
C	-3.50277	-0.00012	-1.21525
C	-3.50278	0.00009	1.21525
C	-4.89470	-0.00009	-1.20928
H	-2.93993	-0.00012	-2.14633
C	-4.89470	0.00014	1.20928
H	-2.93993	0.00020	2.14632
C	-5.58785	0.00004	-0.00001
H	-5.43716	-0.00012	-2.15071
H	-5.43717	0.00031	2.15070
H	-6.67450	0.00010	-0.00002
C	2.82766	0.00001	-0.00001
C	3.50274	0.00008	1.21524
C	3.50281	-0.00005	-1.21525
C	4.89467	0.00005	1.20931
H	2.93989	0.00006	2.14631
C	4.89473	-0.00011	-1.20925
H	2.93998	-0.00014	-2.14633
C	5.58785	-0.00004	0.00005
H	5.43712	0.00005	2.15075
H	5.43722	-0.00025	-2.15066
H	6.67450	-0.00010	0.00008

5,10-di(4-trifluoromethylphenyl)-5,10-dihydrophenazine (3)

Ground state (-1708.09865654)

C	-0.67470	-3.65796	0.09802
C	-1.37370	-2.44764	0.05879
C	-0.69995	-1.22973	0.01690
C	0.71145	-1.22321	0.01734
C	1.39684	-2.43450	0.06083

C	0.70941	-3.65150	0.09928
C	0.69994	1.22985	0.01693
C	-0.71145	1.22333	0.01729
C	-1.39685	2.43463	0.06068
H	-2.48351	2.43526	0.05978
C	-0.70942	3.65163	0.09914
C	0.67470	3.65809	0.09798
C	1.37370	2.44777	0.05884
H	-1.22816	-4.59290	0.12662
H	-2.46024	-2.45938	0.05614
H	2.48350	-2.43513	0.06003
H	1.27173	-4.58109	0.12900
H	-1.27173	4.58122	0.12877
H	1.22814	4.59303	0.12661
H	2.46023	2.45950	0.05625
N	1.39062	0.00664	-0.04391
N	-1.39062	-0.00653	-0.04394
C	2.81571	0.01266	-0.02644
C	3.51751	0.00798	-1.23095
C	3.49514	0.02180	1.18858
C	4.90560	0.00996	-1.21873
H	2.96625	0.00178	-2.16850
C	4.88599	0.02416	1.20539
H	2.92777	0.02623	2.11682
C	5.58401	0.01822	0.00100
H	5.46170	0.00532	-2.15349
H	5.41940	0.03046	2.15090
C	-2.81572	-0.01258	-0.02646
C	-3.49512	-0.02162	1.18857
C	-3.51753	-0.00807	-1.23097
C	-4.88597	-0.02402	1.20540
H	-2.92773	-0.02593	2.11681
C	-4.90561	-0.01013	-1.21872
H	-2.96626	-0.00195	-2.16851
C	-5.58400	-0.01828	0.00101
H	-5.41939	-0.03024	2.15091
H	-5.46177	-0.00566	-2.15346
C	7.08029	0.00011	-0.02804
C	-7.08028	-0.00026	-0.02802
F	7.57904	1.01353	-0.76214
F	7.55129	-1.13190	-0.58910
F	7.63181	0.08991	1.18892
F	-7.55138	1.13170	-0.58904
F	-7.57894	-1.01368	-0.76219
F	-7.63181	-0.09017	1.18894

Triplet excited state (-1708.00895503)

C	-0.71278	-3.57919	0.00664
C	-1.39868	-2.38240	0.00615
C	-0.69877	-1.16342	0.00599
C	0.72036	-1.17790	0.00696
C	1.39958	-2.40584	0.00705
C	0.68976	-3.59073	0.00680
C	0.73255	1.23962	0.00603
C	-0.68658	1.23883	0.00617
C	-1.37388	2.46488	0.00756
H	-2.45943	2.44863	0.00869
C	-0.67602	3.65467	0.00742
C	0.72663	3.65244	0.00534
C	1.42440	2.46036	0.00488
H	-1.26509	-4.51430	0.00689
H	-2.48401	-2.35624	0.00587
H	2.48475	-2.42448	0.00730
H	1.22784	-4.53416	0.00674
H	-1.21886	4.59533	0.00878
H	1.27414	4.59042	0.00439
H	2.50978	2.46664	0.00390
N	1.40405	0.02748	0.00740
N	-1.38089	0.04122	0.00423
C	2.84225	0.01873	0.01292
C	3.52446	0.00773	-1.19996
C	3.51308	0.01665	1.22880
C	4.91200	-0.00894	-1.19019
H	2.96881	0.01044	-2.13453
C	4.90406	0.00008	1.23551
H	2.94943	0.02596	2.15853
C	5.59388	-0.01276	0.02738
H	5.46366	-0.01887	-2.12706
H	5.44181	-0.00323	2.17816
C	-2.81591	0.04937	0.00622
C	-3.52311	0.02666	1.24385
C	-3.52846	0.04188	-1.22356
C	-4.89529	0.03291	1.24748
H	-2.96463	0.00659	2.17969
C	-4.90023	0.04966	-1.22094
H	-2.97437	0.03159	-2.16249
C	-5.63281	0.08427	0.01837
H	-5.42697	0.01341	2.19677
H	-5.44194	0.04210	-2.16551
C	7.09160	-0.05279	-0.00837
C	-7.07451	-0.03435	-0.00434

F	7.59729	0.95038	-0.74895
F	7.53923	-1.19401	-0.56639
F	7.64715	0.03420	1.20574
F	-7.67340	0.69180	-0.99424
F	-7.56560	-1.32142	-0.24598
F	-7.67716	0.32312	1.15443

Cation Radical (-1707.92843021)

C	0.68577	3.62468	0.00091
C	1.38911	2.43759	0.00207
C	0.70418	1.21243	0.00398
C	-0.71433	1.20664	0.00449
C	-1.40975	2.42583	0.00392
C	-0.71655	3.61889	0.00204
C	-0.70417	-1.21213	0.00400
C	0.71434	-1.20634	0.00440
C	1.40976	-2.42552	0.00369
H	2.49485	-2.42674	0.00474
C	0.71656	-3.61859	0.00182
C	-0.68575	-3.62438	0.00081
C	-1.38910	-2.43728	0.00208
H	1.22704	4.56586	-0.00075
H	2.47409	2.44890	0.00168
H	-2.49484	2.42703	0.00509
H	-1.26583	4.55541	0.00143
H	1.26585	-4.55510	0.00109
H	-1.22704	-4.56555	-0.00085
H	-2.47407	-2.44860	0.00176
N	-1.38318	-0.00567	0.00625
N	1.38319	0.00599	0.00614
C	-2.82377	-0.01125	0.01279
C	-3.50453	-0.00986	-1.20054
C	-3.49145	-0.01731	1.23000
C	-4.89210	-0.01247	-1.18914
H	-2.94958	-0.00620	-2.13544
C	-4.88251	-0.02000	1.23684
H	-2.92724	-0.01914	2.15934
C	-5.57274	-0.01757	0.02902
H	-5.44440	-0.01117	-2.12561
H	-5.41968	-0.02404	2.17975
C	2.82379	0.01154	0.01271
C	3.49142	0.01724	1.22995
C	3.50458	0.01043	-1.20060
C	4.88247	0.01977	1.23686

H	2.92716	0.01890	2.15927
C	4.89215	0.01289	-1.18915
H	2.94964	0.00703	-2.13551
C	5.57273	0.01756	0.02905
H	5.41962	0.02346	2.17978
H	5.44457	0.01184	-2.12554
C	-7.07142	-0.00031	-0.00586
C	7.07140	-0.00013	-0.00582
F	-7.56144	-1.01281	-0.74378
F	-7.53538	1.13276	-0.56613
F	-7.62414	-0.09301	1.20880
F	7.53499	-1.13384	-0.56523
F	7.56173	1.01160	-0.74452
F	7.62417	0.09328	1.20875

5,10-di(4-cyanophenyl)-5,10-dihydrophenazine (4)

Ground state (-1218.56819144)

C	0.69216	3.65183	-0.14089
C	1.38552	2.43936	-0.08041
C	0.70544	1.22623	-0.01411
C	-0.70542	1.22625	-0.01406
C	-1.38548	2.43940	-0.08029
C	-0.69209	3.65185	-0.14082
C	-0.70543	-1.22621	-0.01404
C	0.70542	-1.22623	-0.01410
C	1.38548	-2.43938	-0.08040
H	2.47212	-2.44595	-0.07707
C	0.69210	-3.65183	-0.14086
C	-0.69216	-3.65182	-0.14077
C	-1.38552	-2.43935	-0.08024
H	1.24976	4.58357	-0.18638
H	2.47216	2.44592	-0.07707
H	-2.47212	2.44599	-0.07686
H	-1.24967	4.58361	-0.18623
H	1.24967	-4.58359	-0.18633
H	-1.24975	-4.58357	-0.18616
H	-2.47216	-2.44592	-0.07679
N	-1.38893	0.00002	0.07984
N	1.38893	-0.00000	0.07986
C	-2.81339	0.00002	0.06514
C	-3.49646	-0.00007	-1.15108

C	-3.50889	0.00009	1.27237
C	-4.88351	-0.00007	-1.16427
H	-2.93087	-0.00013	-2.08031
C	-4.89706	0.00009	1.27085
H	-2.95238	0.00015	2.20655
C	-5.58289	0.00000	0.04995
H	-5.42816	-0.00014	-2.10427
H	-5.45149	0.00014	2.20506
C	2.81339	-0.00001	0.06515
C	3.50889	0.00000	1.27238
C	3.49647	-0.00002	-1.15107
C	4.89705	0.00000	1.27087
H	2.95236	0.00001	2.20656
C	4.88351	-0.00002	-1.16425
H	2.93089	-0.00002	-2.08031
C	5.58289	-0.00002	0.04997
H	5.45148	0.00001	2.20508
H	5.42816	-0.00003	-2.10425
C	-7.01418	-0.00001	0.04221
C	7.01418	-0.00002	0.04223
N	-8.17776	-0.00003	0.03600
N	8.17776	-0.00005	0.03603

Triplet excited state (-1218.48676941)

C	-0.70185	-3.61950	-0.00015
C	-1.40059	-2.42930	-0.00015
C	-0.71048	-1.20572	-0.00009
C	0.71018	-1.20592	-0.00003
C	1.39996	-2.42968	-0.00002
C	0.70090	-3.61970	-0.00009
C	0.71048	1.20572	0.00008
C	-0.71019	1.20592	0.00003
C	-1.39996	2.42968	0.00002
H	-2.48534	2.42933	-0.00002
C	-0.70090	3.61970	0.00009
C	0.70185	3.61950	0.00015
C	1.40059	2.42930	0.00015
H	-1.24665	-4.55897	-0.00020
H	-2.48598	-2.42870	-0.00016
H	2.48534	-2.42932	0.00002
H	1.24547	-4.55930	-0.00009
H	-1.24547	4.55931	0.00009
H	1.24665	4.55897	0.00020
H	2.48598	2.42870	0.00016

N	1.38912	-0.00015	0.00006
N	-1.38912	0.00015	-0.00006
C	2.82595	-0.00020	0.00004
C	3.51603	0.00015	-1.22286
C	3.51609	-0.00031	1.22290
C	4.89546	0.00021	-1.22671
H	2.95683	0.00021	-2.15660
C	4.89552	-0.00026	1.22669
H	2.95694	-0.00054	2.15667
C	5.61206	-0.00003	-0.00003
H	5.43994	0.00030	-2.16746
H	5.44004	-0.00050	2.16741
C	-2.82595	0.00020	-0.00004
C	-3.51603	-0.00015	1.22286
C	-3.51609	0.00031	-1.22290
C	-4.89546	-0.00021	1.22671
H	-2.95683	-0.00021	2.15660
C	-4.89552	0.00026	-1.22668
H	-2.95694	0.00054	-2.15667
C	-5.61205	0.00003	0.00003
H	-5.43994	-0.00030	2.16745
H	-5.44004	0.00050	-2.16740
C	7.02424	-0.00014	-0.00008
C	-7.02424	0.00014	0.00008
N	8.19685	-0.00023	-0.00001
N	-8.19684	0.00023	0.00001

Cation Radical (-1218.39658509)

C	-0.70074	-3.62196	-0.00005
C	-1.39928	-2.43204	-0.00005
C	-0.70909	-1.20999	0.00001
C	0.70934	-1.20982	0.00006
C	1.39982	-2.43168	0.00006
C	0.70159	-3.62178	0.00001
C	0.70909	1.20999	-0.00002
C	-0.70934	1.20982	-0.00006
C	-1.39982	2.43168	-0.00006
H	-2.48488	2.43863	-0.00004
C	-0.70159	3.62178	-0.00001
C	0.70074	3.62196	0.00005
C	1.39928	2.43204	0.00005
H	-1.24583	-4.56090	-0.00012
H	-2.48435	-2.43926	-0.00012
H	2.48488	-2.43864	0.00004

H	1.24693	-4.56056	-0.00002
H	-1.24693	4.56056	0.00002
H	1.24583	4.56090	0.00012
H	2.48435	2.43926	0.00012
N	1.38268	0.00017	0.00004
N	-1.38268	-0.00017	-0.00004
C	2.82280	0.00030	0.00002
C	3.49575	0.00031	-1.21688
C	3.49578	0.00025	1.21691
C	4.88344	0.00026	-1.21832
H	2.93480	0.00020	-2.14806
C	4.88346	0.00019	1.21833
H	2.93482	0.00016	2.14809
C	5.57335	0.00019	0.00000
H	5.43230	0.00016	-2.15525
H	5.43232	0.00007	2.15527
C	-2.82280	-0.00030	-0.00003
C	-3.49575	-0.00031	1.21688
C	-3.49579	-0.00025	-1.21691
C	-4.88344	-0.00026	1.21832
H	-2.93480	-0.00019	2.14806
C	-4.88346	-0.00019	-1.21833
H	-2.93482	-0.00016	-2.14809
C	-5.57335	-0.00019	0.00000
H	-5.43230	-0.00016	2.15525
H	-5.43233	-0.00007	-2.15527
C	7.00580	0.00001	-0.00009
C	-7.00580	-0.00001	0.00009
N	8.16870	-0.00023	-0.00001
N	-8.16870	0.00023	0.00002

5,10-di(2-naphthyl)-5,10-dihydrophenazine (5)

Ground state (-1341.25092633)

C	-0.69252	-3.63498	-0.64518
C	-1.38604	-2.42738	-0.52259
C	-0.70556	-1.21933	-0.39142
C	0.70556	-1.21935	-0.39145
C	1.38602	-2.42740	-0.52267
C	0.69248	-3.63500	-0.64522
C	0.70557	1.21971	-0.39135
C	-0.70555	1.21972	-0.39133

C	-1.38602	2.42780	-0.52230
H	-2.47271	2.43021	-0.51415
C	-0.69249	3.63543	-0.64464
C	0.69251	3.63542	-0.64461
C	1.38603	2.42780	-0.52229
H	-1.24927	-4.56401	-0.73723
H	-2.47273	-2.42978	-0.51445
H	2.47272	-2.42981	-0.51459
H	1.24921	-4.56404	-0.73732
H	-1.24924	4.56448	-0.73653
H	1.24927	4.56447	-0.73644
H	2.47273	2.43020	-0.51413
N	1.38547	0.00019	-0.21212
N	-1.38545	0.00019	-0.21198
C	2.81397	0.00016	-0.23192
C	3.49875	0.00026	-1.47242
C	3.50820	-0.00005	0.95085
C	4.87026	0.00010	-1.49825
H	2.91747	0.00043	-2.39314
C	4.92580	-0.00017	0.95369
C	5.61984	-0.00013	-0.29295
H	5.40369	0.00014	-2.44733
C	-2.81395	0.00014	-0.23185
C	-3.50822	0.00000	0.95090
C	-3.49870	0.00014	-1.47236
C	-4.92582	-0.00014	0.95369
C	-4.87021	0.00000	-1.49824
C	-5.61983	-0.00015	-0.29296
H	-2.96411	-0.00003	1.89483
C	7.03701	-0.00028	-0.28870
C	7.73499	-0.00044	0.89527
H	8.82210	-0.00056	0.88642
C	5.67203	-0.00034	2.15844
H	5.13608	-0.00036	3.10617
C	7.04587	-0.00046	2.13053
H	7.60983	-0.00055	3.06007
H	2.96407	-0.00014	1.89476
H	7.56305	-0.00027	-1.24211
H	-2.91740	0.00024	-2.39308
H	-5.40361	-0.00000	-2.44734
C	-7.03699	-0.00030	-0.28876
C	-7.73501	-0.00042	0.89519
H	-8.82212	-0.00054	0.88631
C	-7.04593	-0.00039	2.13047
H	-7.60991	-0.00047	3.06000
C	-5.67209	-0.00026	2.15842

H	-5.13617	-0.00026	3.10618
H	-7.56300	-0.00032	-1.24218

Triplet excited state (-1341.16553097)

C	0.70278	3.61834	-0.33257
C	1.39589	2.42528	-0.33395
C	0.70121	1.20315	-0.34238
C	-0.71792	1.20826	-0.34109
C	-1.40467	2.43475	-0.34836
C	-0.70167	3.62205	-0.34522
C	-0.71802	-1.20743	-0.34172
C	0.70111	-1.20241	-0.34295
C	1.39570	-2.42463	-0.33557
H	2.48112	-2.40650	-0.33022
C	0.70249	-3.61763	-0.33519
C	-0.70195	-3.62122	-0.34783
C	-1.40487	-2.43388	-0.35003
H	1.24985	4.55650	-0.32313
H	2.48131	2.40710	-0.32854
H	-2.48997	2.44270	-0.35584
H	-1.24415	4.56304	-0.35108
H	1.24949	-4.55584	-0.32665
H	-1.24451	-4.56217	-0.35459
H	-2.49017	-2.44172	-0.35764
N	-1.39500	0.00045	-0.33522
N	1.38027	0.00034	-0.36434
C	-2.83536	0.00048	-0.33893
C	-3.50959	0.00103	-1.57976
C	-3.51005	-0.00019	0.85372
C	-4.88182	0.00082	-1.59442
H	-2.93085	0.00154	-2.50099
C	-4.92613	-0.00042	0.85993
C	-5.62357	0.00006	-0.38543
H	-5.41948	0.00123	-2.54048
C	2.82379	0.00022	-0.38572
C	3.50433	-0.00086	0.84503
C	3.48675	0.00140	-1.60226
C	4.92639	-0.00082	0.86094
C	4.88816	0.00136	-1.61353
C	5.63626	0.00022	-0.39691
H	2.94380	-0.00178	1.78008
C	-7.04078	-0.00027	-0.37644
C	-7.73301	-0.00102	0.81020
H	-8.81998	-0.00128	0.80577

C	-5.66666	-0.00118	2.06821
H	-5.12743	-0.00153	3.01370
C	-7.03988	-0.00148	2.04351
H	-7.60117	-0.00207	2.97443
H	-2.96014	-0.00057	1.79409
H	-7.57018	0.00010	-1.32763
H	2.91469	0.00230	-2.52966
H	5.42649	0.00215	-2.56062
C	7.04636	0.00011	-0.37284
C	7.76221	-0.00092	0.83437
H	8.85087	-0.00097	0.81881
C	7.07684	-0.00188	2.04571
H	7.62601	-0.00271	2.98614
C	5.67555	-0.00184	2.05926
H	5.13793	-0.00265	3.00816
H	7.58057	0.00091	-1.32388

Cation radical (-1341.08431706)

C	0.70102	3.62065	-0.37295
C	1.39926	2.43055	-0.35936
C	0.70931	1.20778	-0.34738
C	-0.70940	1.20771	-0.34739
C	-1.39955	2.43036	-0.35952
C	-0.70149	3.62056	-0.37309
C	-0.70929	-1.20761	-0.34734
C	0.70941	-1.20753	-0.34750
C	1.39956	-2.43020	-0.35987
H	2.48472	-2.43275	-0.35848
C	0.70151	-3.62040	-0.37347
C	-0.70102	-3.62049	-0.37314
C	-1.39925	-2.43040	-0.35935
H	1.24620	4.55965	-0.38323
H	2.48441	2.43335	-0.35766
H	-2.48470	2.43294	-0.35794
H	-1.24679	4.55949	-0.38352
H	1.24678	-4.55933	-0.38412
H	-1.24617	-4.55950	-0.38344
H	-2.48440	-2.43316	-0.35757
N	-1.38499	0.00001	-0.33355
N	1.38501	0.00014	-0.33368
C	-2.82713	0.00001	-0.33514
C	-3.50057	-0.00009	-1.57622
C	-3.49885	0.00011	0.85901
C	-4.87269	-0.00017	-1.58892

H	-2.92275	-0.00014	-2.49794
C	-4.91490	-0.00002	0.86586
C	-5.61308	-0.00016	-0.37913
H	-5.41119	-0.00029	-2.53442
C	2.82715	0.00017	-0.33520
C	3.49881	-0.00007	0.85898
C	3.50063	0.00035	-1.57626
C	4.91486	-0.00008	0.86586
C	4.87275	0.00029	-1.58892
C	5.61309	0.00008	-0.37910
H	2.94799	-0.00024	1.79871
C	-7.03019	-0.00028	-0.36936
C	-7.72136	-0.00027	0.81786
H	-8.80830	-0.00037	0.81427
C	-5.65426	-0.00001	2.07476
H	-5.11445	0.00010	3.01985
C	-7.02745	-0.00014	2.05070
H	-7.58822	-0.00015	2.98190
H	-2.94806	0.00020	1.79877
H	-7.56022	-0.00038	-1.32013
H	2.92284	0.00051	-2.49800
H	5.41129	0.00041	-2.53440
C	7.03020	0.00002	-0.36928
C	7.72133	-0.00019	0.81795
H	8.80827	-0.00021	0.81441
C	7.02738	-0.00034	2.05077
H	7.58811	-0.00052	2.98199
C	5.65419	-0.00029	2.07479
H	5.11434	-0.00044	3.01986
H	7.56026	0.00015	-1.32003

5,10-di(1-naphthyl)-5,10-dihydrophenazine (6)

Ground state (-1341.25409703)

C	-6.78762	-0.25351	0.09658
C	-5.40871	-0.21155	0.32069
C	-4.76701	0.98252	0.64129
C	-5.52704	2.16751	0.73682
C	-6.90010	2.11448	0.50646
C	-7.53361	0.90999	0.18881
C	-3.48588	3.44223	1.18272
C	-2.72549	2.25739	1.08770
C	-1.33931	2.32906	1.21065
H	-0.75184	1.41705	1.14165

C	-0.69485	3.54990	1.42775
C	-1.44139	4.71301	1.51815
C	-2.83205	4.65419	1.39328
H	-7.26034	-1.20103	-0.14891
H	-4.82297	-1.12477	0.24983
H	-7.48603	3.02720	0.57973
H	-8.60675	0.89929	0.01690
H	0.38767	3.57355	1.52167
H	-0.96032	5.67346	1.68445
H	-3.41846	5.56672	1.46491
N	-4.88694	3.37303	1.07670
N	-3.38205	1.02886	0.88568
C	-5.64422	4.58300	1.08355
C	-6.18013	5.04090	2.26218
C	-5.83185	5.29775	-0.13376
C	-6.93102	6.23700	2.29115
H	-6.01555	4.46696	3.17203
C	-6.59103	6.50544	-0.09779
C	-7.13054	6.95150	1.13560
H	-7.34818	6.58599	3.23211
C	-2.59455	-0.13950	0.65746
C	-2.13191	-0.42606	-0.65888
C	-2.27863	-0.96067	1.71185
C	-1.32893	-1.58913	-0.85423
C	-1.48265	-2.11045	1.51195
H	-2.64805	-0.70672	2.70352
C	-1.01849	-2.41513	0.25608
H	-1.23934	-2.74801	2.35779
H	-0.40247	-3.29778	0.09278
H	-7.71002	7.87311	1.14847
C	-6.78711	7.22746	-1.30269
C	-6.25818	6.77553	-2.48690
H	-6.41619	7.33628	-3.40481
C	-5.50641	5.57833	-2.51930
H	-5.09236	5.22902	-3.46204
C	-5.29677	4.85556	-1.36956
H	-4.71580	3.93478	-1.39598
H	-7.36870	8.14737	-1.27066
C	-2.43521	0.39652	-1.77265
H	-3.04708	1.28509	-1.62622
C	-0.85929	-1.88774	-2.15865
C	-1.16977	-1.07410	-3.22069
H	-0.80434	-1.31223	-4.21655
C	-1.96535	0.07824	-3.02409
H	-2.20581	0.71581	-3.87134
H	-0.24637	-2.77632	-2.30067

Triplet excited state (-1341.17037718)

C	-6.76626	-0.25860	0.18202
C	-5.39876	-0.22117	0.35657
C	-4.75246	0.99495	0.63678
C	-5.52147	2.18266	0.73855
C	-6.91162	2.12450	0.55251
C	-7.52485	0.91809	0.27859
C	-3.50735	3.43545	1.19151
C	-2.74899	2.24110	1.08418
C	-1.35445	2.29493	1.25593
H	-0.78638	1.37356	1.17120
C	-0.73158	3.49538	1.52552
C	-1.48351	4.67548	1.62850
C	-2.85412	4.64770	1.46272
H	-7.25443	-1.20500	-0.03180
H	-4.79374	-1.12023	0.28418
H	-7.50065	3.03354	0.62655
H	-8.60133	0.88584	0.13855
H	0.34618	3.52373	1.65589
H	-0.99064	5.62045	1.83790
H	-3.43414	5.56216	1.54119
N	-4.88009	3.38078	1.00917
N	-3.38076	1.04340	0.80319
C	-5.64496	4.60018	1.03658
C	-6.16997	5.03469	2.22671
C	-5.82710	5.31283	-0.17833
C	-6.91943	6.23002	2.26649
H	-6.00139	4.45153	3.12959
C	-6.58673	6.51968	-0.12400
C	-7.12054	6.95247	1.11603
H	-7.33324	6.57090	3.21119
C	-2.58939	-0.14435	0.60203
C	-2.13861	-0.42385	-0.71564
C	-2.26321	-0.93968	1.72131
C	-1.31095	-1.59502	-0.88573
C	-1.46772	-2.05931	1.53373
H	-2.63950	-0.65915	2.70433
C	-0.99461	-2.38935	0.25250
H	-1.20757	-2.68585	2.38534
H	-0.36668	-3.26900	0.11122
H	-7.69958	7.87379	1.13892
C	-6.78886	7.25351	-1.32002
C	-6.26588	6.81320	-2.51091

H	-6.42877	7.38258	-3.42228
C	-5.51425	5.61702	-2.55948
H	-5.10519	5.27705	-3.50744
C	-5.29704	4.88124	-1.41965
H	-4.71499	3.96180	-1.46706
H	-7.37036	8.17253	-1.27537
C	-2.44673	0.36901	-1.84407
H	-3.07204	1.25487	-1.72493
C	-0.84449	-1.89917	-2.18436
C	-1.16685	-1.09557	-3.28898
H	-0.79022	-1.35766	-4.27654
C	-1.96238	0.03090	-3.12020
H	-2.21569	0.65758	-3.97385
H	-0.21714	-2.78176	-2.31395

Cation radical (-1341.08567245)

C	-6.76889	-0.25832	0.18757
C	-5.40024	-0.22519	0.35835
C	-4.75362	0.98907	0.63763
C	-5.51853	2.17922	0.74079
C	-6.90982	2.12311	0.55990
C	-7.52549	0.91899	0.28773
C	-3.50338	3.43713	1.17912
C	-2.73837	2.24720	1.07573
C	-1.34495	2.30688	1.23978
H	-0.75699	1.39783	1.16318
C	-0.72798	3.51300	1.49987
C	-1.48471	4.68992	1.60049
C	-2.85468	4.65418	1.44199
H	-7.25799	-1.20398	-0.02592
H	-4.81415	-1.13576	0.28115
H	-7.49616	3.03336	0.63592
H	-8.60210	0.88771	0.15098
H	0.34996	3.54599	1.62515
H	-0.99495	5.63769	1.80281
H	-3.44020	5.56495	1.51927
N	-4.87575	3.37660	1.00485
N	-3.38017	1.05116	0.80113
C	-5.64329	4.59672	1.03620
C	-6.16052	5.02858	2.23057
C	-5.83092	5.30847	-0.17806
C	-6.90947	6.22381	2.27522
H	-5.98631	4.44495	3.13201
C	-6.58963	6.51561	-0.11726

C	-7.11622	6.94703	1.12625
H	-7.31792	6.56398	3.22237
C	-2.58809	-0.13659	0.60191
C	-2.12114	-0.42335	-0.70833
C	-2.29639	-0.93446	1.67838
C	-1.31950	-1.59180	-0.87526
C	-1.50270	-2.08745	1.49790
H	-2.67698	-0.66635	2.66174
C	-1.02646	-2.40388	0.24928
H	-1.27112	-2.71609	2.35275
H	-0.41121	-3.28962	0.10342
H	-7.69451	7.86865	1.15319
C	-6.79801	7.25173	-1.31068
C	-6.28185	6.81330	-2.50517
H	-6.44924	7.38439	-3.41458
C	-5.53146	5.61675	-2.55995
H	-5.12787	5.27822	-3.51072
C	-5.30815	4.87837	-1.42293
H	-4.72684	3.95892	-1.47749
H	-7.37859	8.17098	-1.26093
C	-2.41065	0.38696	-1.83428
H	-3.02336	1.27958	-1.71758
C	-0.83416	-1.90837	-2.16893
C	-1.12937	-1.10748	-3.24452
H	-0.75231	-1.35915	-4.23232
C	-1.92449	0.04863	-3.07393
H	-2.15336	0.67470	-3.93243
H	-0.22215	-2.80006	-2.29076

EBP-MMA_n (for n=0)

Ground state (-3109.39759236)

C	0.08282	1.52944	0.39144
H	0.54345	2.23554	1.08554
C	-1.34443	1.32937	0.86437
O	-1.69546	1.62122	1.98865
O	-2.12477	0.78461	-0.05474
C	-3.49422	0.51131	0.32735
H	-3.95166	1.45159	0.65397
H	-3.47908	-0.17535	1.18113
C	-4.18128	-0.07615	-0.87343
H	-5.22258	-0.30496	-0.62735

H	-4.17385	0.62837	-1.71138
H	-3.69179	-1.00269	-1.19061
Br	0.96236	-0.19112	0.81909
C	0.32581	1.92321	-1.02713
C	0.90201	3.17052	-1.27605
C	-0.02532	1.10755	-2.10818
C	1.10315	3.61212	-2.58235
H	1.18443	3.80742	-0.43933
C	0.18057	1.54278	-3.41058
H	-0.45711	0.12599	-1.92808
C	0.74807	2.79535	-3.65104
H	1.54830	4.58775	-2.76017
H	-0.09519	0.90085	-4.24349
H	0.90973	3.13238	-4.67208

Anion radical (-3109.53159713)

C	-0.61107	2.55547	0.16829
H	-0.08829	3.15386	0.91346
C	-1.76993	1.87848	0.72466
O	-2.09087	1.99776	1.90377
O	-2.47721	1.14905	-0.14751
C	-3.50160	0.29923	0.39270
H	-4.31880	0.92133	0.77756
H	-3.07430	-0.26359	1.23216
C	-3.94521	-0.60872	-0.72316
H	-4.71732	-1.29762	-0.36666
H	-4.35560	-0.03401	-1.56058
H	-3.09753	-1.19920	-1.09074
Br	0.30809	-0.76214	0.92769
C	-0.02023	2.47278	-1.11995
C	1.21810	3.14429	-1.30313
C	-0.56992	1.79969	-2.24319
C	1.86554	3.15147	-2.52624
H	1.65975	3.66391	-0.45403
C	0.08643	1.81236	-3.46324
H	-1.51412	1.27540	-2.14225
C	1.30319	2.48339	-3.61778
H	2.81270	3.67427	-2.63455
H	-0.35504	1.29277	-4.31058
H	1.80717	2.48687	-4.58114

EBP-MMA_n (for n=1)

Ground state (-3455.03151979)

C	0.68124	1.88048	-0.35529
H	1.30238	2.70246	0.02620
C	-0.59810	1.95053	0.45873
O	-0.96905	2.95311	1.03736
O	-1.27905	0.80774	0.44189
C	-2.48306	0.74721	1.23926
H	-3.20212	1.47126	0.84019
H	-2.22778	1.04882	2.26278
C	-2.98771	-0.66767	1.17331
H	-3.89935	-0.76370	1.77075
H	-3.22069	-0.95437	0.14271
H	-2.24226	-1.36546	1.57020
C	0.33222	2.21361	-1.79449
C	0.54190	3.50994	-2.27006
C	-0.22092	1.25753	-2.65130
C	0.21121	3.84780	-3.58029
H	0.97051	4.25967	-1.60611
C	-0.55027	1.59399	-3.96148
H	-0.40051	0.24411	-2.29696
C	-0.33391	2.88873	-4.43015
H	0.38443	4.86014	-3.93742
H	-0.97716	0.84084	-4.61951
H	-0.59012	3.14803	-5.45456
C	1.44616	0.55640	-0.23405
C	2.16149	0.38232	1.09922
C	3.31372	1.37535	1.23557
O	3.57826	1.66563	2.50399
C	1.25590	0.29064	2.30763
H	2.18741	0.51745	-1.03931
H	0.76513	-0.29096	-0.37081
C	4.67974	2.55761	2.73013
H	0.46657	-0.44596	2.12477
H	1.81258	-0.00107	3.20040
H	0.79250	1.26468	2.51471
O	3.92314	1.82918	0.29017
H	4.48706	3.52261	2.25506
H	5.60018	2.12714	2.32750
H	4.75063	2.67108	3.81077
Br	3.14129	-1.35048	0.98058

Anion radical (-3455.1615723)

C	0.71221	2.09566	-0.55281
H	1.32374	2.97095	-0.29945
C	-0.47469	2.17558	0.38683
O	-0.75635	3.16137	1.04135
O	-1.17950	1.04521	0.41654
C	-2.31138	1.00320	1.31243
H	-3.04525	1.74462	0.97609
H	-1.97170	1.29494	2.31343
C	-2.85591	-0.39800	1.28255
H	-3.72340	-0.47180	1.94554
H	-3.17187	-0.67591	0.27180
H	-2.10304	-1.11724	1.62318
C	0.24676	2.25540	-1.98593
C	0.33816	3.51211	-2.59143
C	-0.30012	1.19601	-2.71699
C	-0.10542	3.71051	-3.89661
H	0.76340	4.34379	-2.03084
C	-0.74346	1.39208	-4.02256
H	-0.39167	0.20911	-2.26819
C	-0.64873	2.64925	-4.61647
H	-0.02343	4.69503	-4.35131
H	-1.16641	0.55760	-4.57713
H	-0.99592	2.79968	-5.63592
C	1.56169	0.83560	-0.29756
C	2.02344	0.74609	1.11880
C	3.13020	1.59509	1.50631
O	3.41432	1.52477	2.82660
C	1.28949	-0.06794	2.12300
H	2.42749	0.88177	-0.97066
H	0.99026	-0.06655	-0.54636
C	4.56834	2.24522	3.24811
H	0.76372	-0.89531	1.63338
H	1.97075	-0.47686	2.87469
H	0.53294	0.52729	2.66274
O	3.76327	2.31677	0.73961
H	4.45583	3.31608	3.05342
H	5.45982	1.87855	2.72756
H	4.66163	2.06600	4.31967
Br	4.17435	-1.42928	0.69867

EBP-MMA_n (for n=2)

Ground state (-3800.65685811)

C	0.62161	1.83922	-0.37919
H	1.12618	2.66524	0.14255
C	-0.72855	1.71630	0.30683
O	-1.30165	2.65428	0.82570
O	-1.22693	0.48098	0.25646
C	-2.46382	0.23967	0.96381
H	-3.27401	0.75187	0.43262
H	-2.37759	0.68386	1.96293
C	-2.66020	-1.25085	1.01954
H	-3.60230	-1.48231	1.52583
H	-2.69646	-1.68194	0.01334
H	-1.84776	-1.73443	1.57712
C	0.36968	2.30157	-1.80265
C	0.62832	3.62671	-2.15879
C	-0.13668	1.42715	-2.76950
C	0.39293	4.07190	-3.45800
H	1.02143	4.31436	-1.41101
C	-0.37266	1.87089	-4.06798
H	-0.35047	0.39095	-2.51152
C	-0.10802	3.19449	-4.41625
H	0.60423	5.10590	-3.72047
H	-0.76569	1.17939	-4.80959
H	-0.29171	3.53971	-5.43082
C	1.48648	0.57720	-0.32199
C	2.17658	0.30898	1.02735
C	3.31472	1.32748	1.17597
O	3.64479	1.54101	2.44980
C	1.22481	0.40148	2.22388
H	2.26808	0.66658	-1.08572
H	0.87712	-0.28248	-0.60367
C	4.76809	2.40143	2.67928
H	0.36802	-0.27083	2.10063
H	1.73446	0.15036	3.15658
H	0.83051	1.41758	2.34240
O	3.89826	1.84483	0.24487
H	4.58303	3.39121	2.25444
H	5.66869	1.97350	2.23097
H	4.87594	2.46585	3.76128
C	2.93643	-1.05166	0.97808
C	1.68819	-2.52836	2.59838
O	0.44177	-2.98189	2.68208
C	1.07251	-2.63970	0.11411
H	3.70142	-1.05141	1.76473
H	3.46299	-1.10963	0.01530
C	-0.09629	-3.09504	4.00752
H	1.49151	-2.51608	-0.88999

H	0.70212	-3.66306	0.21251
H	0.21534	-1.96603	0.22812
O	2.38547	-2.27466	3.55689
H	-0.15949	-2.10226	4.46392
H	0.53219	-3.74424	4.62139
H	-1.09051	-3.52379	3.88702
C	2.13704	-2.34847	1.14957
Br	3.48812	-3.81231	0.96406

Anion radical (-3800.79096325)

C	0.63968	1.98330	-0.39700
H	1.19497	2.81955	0.05133
C	-0.70594	1.98349	0.30968
O	-1.19603	2.96589	0.83228
O	-1.30068	0.79281	0.26555
C	-2.52888	0.62490	1.00285
H	-3.32570	1.17398	0.48812
H	-2.39538	1.06956	1.99668
C	-2.79416	-0.85479	1.07049
H	-3.71342	-1.04749	1.63183
H	-2.90718	-1.28009	0.06750
H	-1.96809	-1.37310	1.57414
C	0.38705	2.33970	-1.85079
C	0.61495	3.64507	-2.29279
C	-0.09363	1.39184	-2.76023
C	0.37557	3.99913	-3.61876
H	0.98886	4.38833	-1.58944
C	-0.33422	1.74458	-4.08538
H	-0.28538	0.37078	-2.43430
C	-0.09942	3.04859	-4.51885
H	0.56377	5.01831	-3.94818
H	-0.70696	0.99759	-4.78240
H	-0.28623	3.32124	-5.55479
C	1.42588	0.67878	-0.23628
C	2.12274	0.48295	1.11709
C	3.32428	1.41882	1.18744
O	3.70160	1.67553	2.44291
C	1.18780	0.69432	2.30798
H	2.19045	0.63826	-1.02201
H	0.74885	-0.16198	-0.40758
C	4.87645	2.47981	2.59922
H	0.30400	0.05133	2.21102
H	1.68795	0.43809	3.24525
H	0.85269	1.73580	2.38567

O	3.92246	1.84922	0.22020
H	4.72961	3.46145	2.14103
H	5.73779	1.98839	2.13886
H	5.02642	2.58133	3.67357
C	2.73753	-0.95522	1.16926
C	1.45159	-2.57278	2.61372
O	0.48241	-3.51694	2.60175
C	1.03137	-2.60777	0.10086
H	3.42075	-1.00334	2.02616
H	3.33197	-1.10465	0.25525
C	0.21996	-4.14459	3.85290
H	1.55211	-2.33659	-0.82438
H	0.96977	-3.69946	0.15805
H	-0.00339	-2.23119	0.02574
O	1.99646	-2.21573	3.65352
H	-0.13725	-3.41771	4.58879
H	1.12563	-4.62684	4.23650
H	-0.54956	-4.89300	3.66083
C	1.74072	-2.05679	1.28761
Br	3.85568	-4.34223	1.21226

References

- 1) Patten, T. E.; Xia, J.; Abernathy, T.; Matyjaszewski, K. *Science* **272**, 866-868 (1996).
- 2) Matyjaszewski, K.; Xia, J. *Chem. Rev.* **101**, 2921-2990 (2001).
- 3) Sawamoto, M. *Chem. Rev.* **109**, 4963-5050 (2009).
- 4) Matyjaszewski, K.; Tsarevsky, N. V. *Nature Chem.* **1**, 276-288 (2009).
- 5) Hawker, C. J.; Wooley, K. L. *Science* **309**, 1200-1205 (2005).
- 6) www.dreyfus.org/Prize/prize.shtml. Accessed January 19, 2016.
- 7) Matyjaszewski, K. *ACS Symposium Series*. **1187**, 1-17 (2015).

-
- 8) Matyjaszewski, K.; Tsarevsky, N. V. *J. Am. Chem. Soc.* **136**, 6513-6533 (2014).
 - 9) Tsarevsky, N. V.; Matyjaszewski, K. *Chem. Rev.* **107**, 2270-2299 (2007).
 - 10) Magenau, A. J. D.; Strandwitz, N. C.; Gennaro, A.; Matyjaszewski, K. *Science*, **332**, 81-84 (2011).
 - 11) Matyjaszewski, K.; Jakubowski, W.; Min, K.; Tang, W.; Huang, J.; Braunecker, W. A.; Tsarevsky, N. V. *Proc. Natl. Acad. Sci. U.S.A.* **103**, 15309-15314 (2006).
 - 12) Pintauer, T.; Matyjaszewski, K. *Chem. Soc. Rev.* **37**, 1087-1097 (2008).
 - 13) Ohtsuki, A.; Lei, L.; Tanishima, M.; Goto, A.; Kaji, H. *J. Am. Chem. Soc.* **137**, 5610-5617 (2015).
 - 14) Goto, A.; Ohtsuki, A.; Ohfuji, H.; Tanishima, M.; Kaji, H. *J. Am. Chem. Soc.* **135**, 11131-11139 (2013).
 - 15) Goto, A. *et. al. J. Am. Chem. Soc.* **129**, 13347-13354 (2007).
 - 16) Miyake, G. M. *U.S. Application. No. 61/846,212.* (2013).
 - 17) Miyake, G. M. *U.S. Patent Application Publication. No. US20150018446 A1.* (2015)
 - 18) Miyake, G. M.; Theriot, J. C. *Macromolecules.* **47**, 8255-8261 (2014).
 - 19) Prier, C. K.; Rankic, D. A.; MacMillan, D. W. C. *Chem. Rev.* **113**, 5322-5363 (2013).
 - 20) Yoon, T. P.; Ischay, M. A.; Du, J. *Nature Chem.* **2**, 527-532 (2010).
 - 21) Treat, N. J. *et. al. J. Am. Chem. Soc.* **136**, 16096-16101 (2014).
 - 22) Pan, X.; Lamson, M.; Yan, J.; Matyjaszewski, K. *ACS Macro Lett.* **4**, 192-196 (2015).
 - 23) Aguirre-Soto, A.; Lim, C.-H.; Hwang, A. T.; Musgrave, C. B.; Stansbury, J. W. *J. Am. Chem. Soc.* **136**, 7418-7427 (2014).
 - 24) Lim, C.-H.; Holder, A. M.; Hynes, J. T.; Musgrave, C. B. *J. Am. Chem. Soc.* **136**, 16081-16095 (2014).

-
- 25) *A full account of this work will be the focus of a future manuscript.*
- 26) Dietrich, L. E. P.; Teal, T. K.; Price-Whelan, A.; Newman, D. K. *Science*. **321**, 1203-1206 (2008).
- 27) Lauresn, J. B.; Nielsen, J. *Chem. Rev.* **104**, 1663-1685 (2004).
- 28) Zhang, Z. *et. Al. J. Am. Chem. Soc.* **137**, 8509-8520 (2015).
- 29) Zheng, Z.; Dong, Q.; Gou, L.; Su, J.-H.; Huang, J. *J. Mater. Chem. C*, **2**, 9858- 9865 (2014).
- 30) Okamoto, T.; Terada, E.; Kozaki, M.; Uchida, M. *Org. Lett.* **5**, 373-376 (2003).
- 31) Terada, E. *et. al. J. Org. Chem.* **70**, 10073-10081 (2005).
- 32) Hiraoka, S. *et. al. J. Am. Chem. Soc.* **126**, 58-59 (2004).
- 33) Recently, it was suggested that the singlet excited state of phenyl phenothiazines may be responsible for dehalogenations as described by E. H. Disceki, *et. al. Chem. Commun.* **51**, 11705-11708 (2015). Due to the oxygen intolerance of this polymerization system and the well-known phenomenon that the triplet state possesses a significantly longer lifetime sufficient for photocatalysis we have based our computational interpretations on this polymer mechanism proceeding *via* the triplet state of the diphenyl dihydrophenazines.
- 34) *See Supporting Information.*
- 35) Fors, B. P.; Hawker, C. J. *Angew. Chem. Int. Ed.* **51**, 8850-8853 (2012).
- 36) Treat, N. J. *et. al. ACS Macro Lett.* **3**, 580-584 (2014).
- 37) The ratio between the theoretical and experimentally measured number average molecular weight.
- 38) Theriot, J. C.; Ryan, M. D.; French, T. A.; Pearson, R. M.; Miyake, G. M. *J. Vis. Exp.* In Press.
- 39) Tossell, J. A. *Comput. Theor. Chem.* **977**, 123-127 (2011).

-
- 40) Winget, P.; Cramer, C. J.; Truhlar, D. G. *Theor. Chem. Acc.* **112**, 217-227 (2004).
- 41) He, H.; Zapol, P.; Curtiss, L. A. *J. Phys. Chem. C.* **114**, 21474-21481 (2010).
- 42) Zhao, Y.; Truhlar, D. *Theor. Chem. Acc.* **120**, 215-241 (2008).

Chapter 3

Intramolecular Charge Transfer and Ion Pairing in *N,N*-Diaryl Dihydrophenazine

Photoredox Catalysts for Efficient Organocatalyzed Atom Transfer Radical

Polymerization

Overview

Photoexcited intramolecular charge transfer (CT) states in *N,N*-diaryl dihydrophenazine photoredox catalysts are accessed through catalyst design and investigated through combined experimental studies and density functional theory (DFT) calculations. These CT states are reminiscent of the metal to ligand charge transfer (MLCT) states of ruthenium and iridium polypyridyl complexes. For cases where the polar CT state is the lowest energy excited state, we observe its population through significant solvatochromic shifts in emission wavelength across the visible spectrum by varying solvent polarity. We propose the importance of accessing CT states for photoredox catalysis of atom transfer radical polymerization lies in their ability to minimize fluorescence while enhancing electron transfer rates between the photoexcited photoredox catalyst and the substrate. Additionally, solvent polarity influences the deactivation pathway, greatly affecting the strength of ion pairing between the oxidized photocatalyst and the bromide anion and thus the ability to realize a controlled radical polymerization. Greater understanding of these photoredox catalysts with respect to CT and ion pairing enables their application toward the polymerization of methyl methacrylate for the synthesis of polymers with precisely tunable molecular weights and dispersities typically lower than 1.10

Introduction

Visible light photoredox catalysis presents a platform for greener chemistries through the use of solar energy to drive chemical transformations under mild conditions.¹ Photoredox catalysis has been successfully applied in polymer synthesis for the production of well-defined polymers through controlled radical polymerization (CRP) mechanisms, including reversible addition fragmentation transfer (RAFT),² reversible complexation mediated living radical polymerization (RCMP),³ and atom transfer radical polymerization (ATRP)⁴. CRPs have greatly impacted polymer synthesis, providing methodologies to produce well-defined polymers under experimentally accessible and versatile reaction conditions.⁵ Amongst all CRPs, ATRP has become the most studied method.⁶ In ATRP, the catalyst's control over the equilibrium between a dormant alkyl halide and the active propagating radical maintains a low concentration of radicals in solution to minimize bimolecular termination pathways and enable the synthesis of well-defined polymers with low dispersity (D).

Ruthenium,⁷ copper,⁸ iron,⁹ and iridium¹⁰ complexes have been used as photoredox catalysts (PCs) in ATRP; however, most PCs do not possess a sufficiently negative reducing potential to directly reduce an alkyl bromide (e.g. ~ -0.8 V vs SCE for ethyl α -bromophenylacetate)¹¹ ATRP initiator through an outer sphere electron transfer mechanism, necessitating the addition of a sacrificial electron donor for the polymerization to proceed through a reductive quenching pathway; such sacrificial electron donors introduce undesirable reaction pathways¹² that make the synthesis of polymers with low D challenging.¹³ Photoexcited states of certain strongly reducing iridium¹⁰ and copper⁸ PCs can directly reduce an alkyl bromide via the oxidative quenching pathway, eliminating the need for sacrificial electron donors and enabling the synthesis of well-defined polymers. However, concerns are raised regarding sustainability of

precious metals¹⁴ and trace metal contamination that can impede use of the resulting materials, for example in electronic applications. Although extensive efforts to develop purification techniques and catalyst strategies have succeeded in reducing transition metal contamination,¹⁵ a more direct route to eliminate this issue is the development of organocatalyzed-ATRP (O-ATRP) (Figure 3.1).

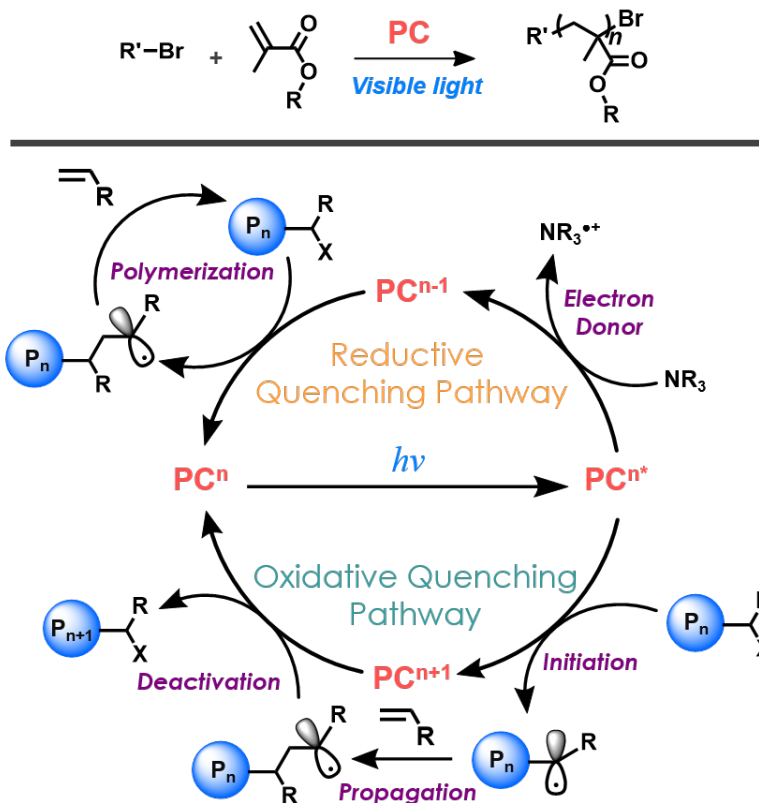


Figure 3.1. The photoredox mediated O-ATRP of polar vinyl monomers with an alkyl bromide initiator can proceed through either a reductive (top) or oxidative quenching pathway (bottom).

Similar to metal complexes, organic PCs¹⁶ that directly reduce alkyl bromide bonds are less common. However, perylene,¹⁷ *N*-arylphenothiazines,¹⁸ *N,N*-diaryl dihydrophenazines,¹⁹ and *N*-arylphenoxazines²⁰ (Figure 3.2) have all been reported as organic PCs for ATRP proceeding

through an oxidative quenching pathway. Our recent work in this field has involved using computational quantum chemical catalyst design and analysis to understand the intricacies of the polymerization mechanism to enable further advancements toward the realization of more efficient organic PCs. Furthermore, we have striven to design PCs that operate in the visible spectrum in order to minimize UV light-induced side reactions and develop energy efficient polymerization methodologies. For example, theoretical insight lead to the discovery of a core substituted *N*-aryl phenoxazine as an efficient visible light organic PC for the O-ATRP for the synthesis of poly(methyl methacrylate) (PMMA) with tailored molecular weights (MWs) and low \bar{D} while achieving high initiator efficiencies (I^*s).²⁰

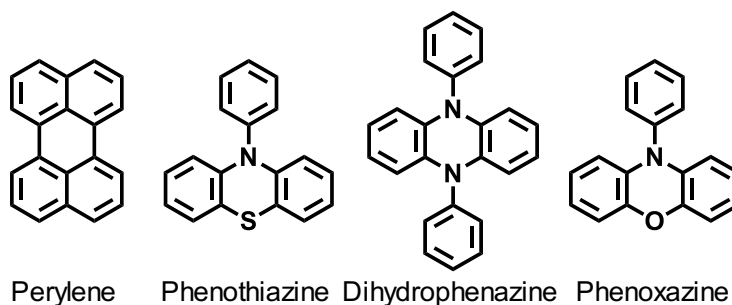


Figure 3.2. Structures of strongly reducing organic photoredox catalysts used in O-ATRP.

Our previous studies using *N,N*-diaryl dihydrophenazines and *N*-aryl phenoxazines revealed that PCs with lowest energy excited states possessing quantum chemically-predicted charge separated singly occupied molecular orbitals (SOMOs) exhibited superior performance in O-ATRP compared to those possessing SOMOs that are both localized on either the dihydrophenazine or phenoxazine core. The predicted charge separated SOMOs suggest the occurrence of intramolecular CT in their lowest triplet excited state. The CT nature of

dihydrophenazines and phenoxazines has also been recognized as an important feature in the design of organic light emitting diodes.²¹ Here, we substantiate the CT nature of diaryl dihydrophenazines with experimental and computational data and hypothesize on the necessity of the CT state for efficient O-ATRP.

DFT calculations predict that for dihydrophenazines with *N*-aryl substituents possessing extended conjugation (e.g. naphthalene) or phenyl substituents functionalized with electron withdrawing groups, the *N*-aryl substituents' lowest energy π^* orbital becomes the lowest unoccupied molecular orbital (LUMO) of the dihydrophenazine molecule, suggesting that the lowest energy excited state possesses CT character. These predictions are supported by the experimental observation that these types of molecules exhibit significant solvatochromic shifts in emission (*vide infra*), spanning wavelengths from blue (in non-polar 1-hexene) to red (in polar dimethylformamide, DMF). In contrast, the dihydrophenazine possessing the less conjugated and unfunctionalized phenyl *N*-aryl substituent, possesses a LUMO that is localized on the dihydrophenazine core. Dihydrophenazines of this nature possess non-polar lowest energy excited states that are localized excitations and do not display solvatochromism, emitting blue light regardless of solvent polarity.

These results corroborate DFT predictions that charge separated SOMOs correspond to intramolecular CT in the lowest excited state and that the observed increasing solvatochromic red-shift in emission with increasing solvent polarity is due to stabilization of the polar CT state. The direction of the intramolecular CT is from the electron rich dihydrophenazine core to the lowest lying π^* orbital of the *N*-aryl substituent, which is reminiscent of the metal to ligand charge transfer (MLCT) states of polypyridyl ruthenium and iridium PCs²² and the proposed CT state of 9-mesityl-10-methylacridinium.²³

We posit that intramolecular CT in the lowest lying excited state of *N,N*-diaryl dihydrophenazine PCs minimizes fluorescence and enables fast electron transfer. Herein, we further investigate the formation of dihydrophenazine CT states in solvents of varying polarity and elucidate their importance for O-ATRP performance using a combined computational and experimental approach. Holistic consideration of the O-ATRP mechanism and the influences imparted by solvent polarity are shown to affect the interplay between the nature of the PC's CT character as well as the free energy of ion pair binding between the PC radical cation and bromide anion, which is crucial in the deactivation step and thus obtaining desirable O-ATRP results. This insight into the effects of solvent polarity and subsequent optimization of reaction conditions to encourage efficient activation and deactivation allow for the synthesis of PMMA with \bar{D} typically below 1.10 and quantitative initiator efficiencies (I^* s).

Results and Discussion

Three representative diaryl dihydrophenazine based PCs possessing phenyl (**1**), 2-naphthalene (**2**), and 1-naphthalene (**3**) *N*-aryl substituents were investigated for their ability to form CT states and their associated potential influences on their O-ATRP performance (Figure 3.3). Our proposed mechanism of O-ATRP hinges on the ability of the photoexcited PC to access the triplet excited state ($^3\text{PC}^*$) via intersystem crossing (ISC), which may be of local excitation (LE) or of CT character, depending on the relative energies of the π^* orbitals of the dihydrophenazine core and the *N*-aryl substituents. Thereafter, $^3\text{PC}^*$ can reduce an alkyl halide to generate the active propagating radical and the ion pair between the oxidized PC ($^2\text{PC}^{\bullet+}$) and bromide (Br^-). Finally, the propagating radical must be efficiently deactivated by the $^2\text{PC}^{\bullet+}\text{Br}^-$ ion pair to complete the catalytic cycle. A Jablonski diagram for PCs that possess lowest energy

excited states with LE or CT character are schematically represented in Figures 3A and 3B. Time-dependent DFT (TD-DFT) calculations and ultraviolet-visible (UV-vis) spectroscopy were used to evaluate the nature of the initial photoexcitation event (Figure 3.4).²⁴ Interestingly, TD-DFT calculations reveal that the initial photoexcitation of PC **1** involves mixed CT and LE characters, although the dark, fully relaxed, lowest singlet and triplet excited states are exclusively of LE character (Figure 3.5).

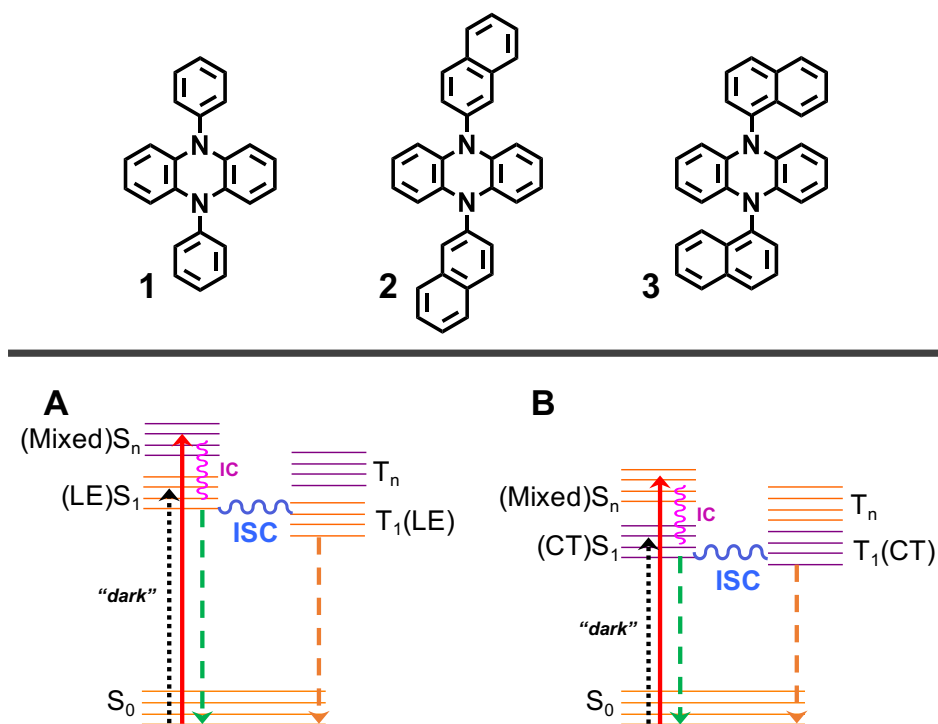


Figure 3.3. Structures of diaryl dihydrophenazines studied in this work (top). Jablonski diagrams representing dihydrophenazines possessing electron neutral or rich (A) and electron poor or highly conjugated (B) *N*-aryl substituents used to explain the formation of local excitation (LE) or charge transfer (CT) in their lowest photoexcited states. The black dotted arrow indicates transition from S_0 to S_1 is a dark state with approximately zero oscillator strength; green and orange dashed arrows

indicate radiative and/or non-radiative decay from the S₁ and T₁ states, respectively; the red arrow indicates bright optical absorption from S₀ to S_n, where S_n has a mixed LE and CT character.

TD-DFT calculations of PC **1** predict that the lower energy S₀ → S₁ excitation dominantly possesses π_{HOMO}-π_{LUMO} character and is dark with zero oscillator strength (f) value. However, the S₀ → S₂ excitation is predicted to be bright with a maximum wavelength (λ_{max,abs}) of 369 nm, a f = 0.229 and contributions of 82% from the π_{HOMO}-π_{LUMO+1} and 12% from the π_{HOMO}-π_{LUMO+7} transitions (Figure 3.4A). The π_{HOMO}-π_{LUMO+1} transition is of CT character, where an electron occupying PC **1**'s HOMO, which is a π orbital localized on the phenazine core (π_{core} = π_{HOMO}), is promoted into the spatially separated *N*-substituent's π*_{phenyl} LUMO+1 orbital (π_{LUMO+1}). On the other hand, the π_{HOMO}-π_{LUMO+7} transition is of LE character involving only π_{core} (π_{HOMO}) and π*_{core} (π_{LUMO+7}). In the absence of π*_{phenyl} such as in the case of 5,10-dimethyl-5,10-dihydrophenazine, only one peak of exclusively LE character is observed at a blue-shifted λ_{max,abs} of 337 nm.²⁵

After initial photon absorption, fast relaxation via internal conversion (IC) results in thermalization of the excited electron from S₂ (π_{LUMO+1} and π_{LUMO+7}) to the lowest singlet excited state S₁ (π_{LUMO}), followed by ISC to the lowest triplet excited state (T₁) comprised of exclusively LE character (Figure 3.5A). The triplet quantum yield of PC **1** has been reported to be 0.26 at 77 K in 3-methylpentane.²⁵ Further, the electrostatic potential (ESP)-mapped electron density reveals minimal dipole moment (μ) change for PC **1** as it transitions from the ground state (¹PC) to ³PC*, despite the slight increase in electron density on the core from δ = -0.68e to -0.80e (Figure 3.5A).

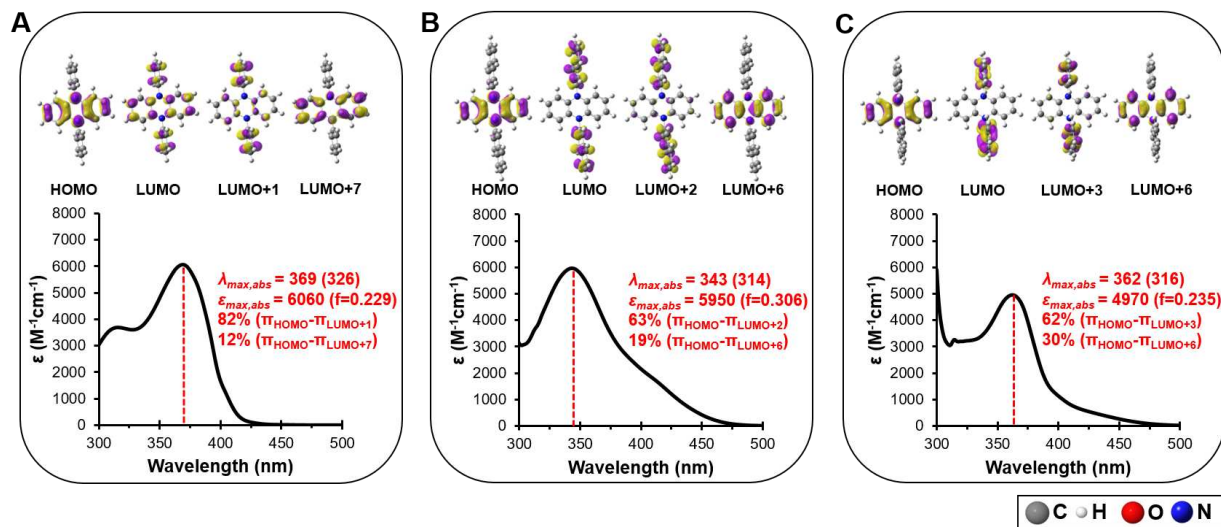


Figure 3.4. Ultraviolet-visible (UV-vis) spectrum of *N,N*-diaryl dihydrophenazines **1** (A), **2** (B), and **3** (C) along with theoretically assigned percentage contributions (> 10%) of various orbitals to the observed absorption peaks. $\lambda_{\max, \text{abs}}$ is the absorption maximum wavelength in unit of nm and $\epsilon_{\max, \text{abs}}$ is the molar absorptivity at $\lambda_{\max, \text{abs}}$ in unit of $\text{M}^{-1}\text{cm}^{-1}$; both are measured in dimethylacetamide (DMA) solvent. $\lambda_{\max, \text{abs}}$ and oscillator strength (*f*) values predicted at TD-DFT CAM-B3LYP/6-31+G(d,p)/CPCM-DMA level of theory are enclosed in parenthesis for comparison.

Similar to PC **1**, the initial photon absorption by PCs **2** and **3** consists of a combination of CT and LE character (Figures 3.4B and C). For PC **2**, the $\lambda_{\max, \text{abs}}$ at 343 nm is assigned to be the $S_0 \rightarrow S_4$ excitation with $f = 0.306$ and consists of 63% of the $\pi_{\text{HOMO}}-\pi_{\text{LUMO}+2}$ (CT character) and 19% of the $\pi_{\text{HOMO}}-\pi_{\text{LUMO}+6}$ (LE character) transitions (Figure 3.4B). While for PC **3**, the $\lambda_{\max, \text{abs}}$ at 362 nm is similarly assigned to be the $S_0 \rightarrow S_4$ excitation with $f = 0.235$ and composed of 62% of the $\pi_{\text{HOMO}}-\pi_{\text{LUMO}+3}$ (CT character) and 30% of the $\pi_{\text{HOMO}}-\pi_{\text{LUMO}+6}$ (LE character) transitions

(Figure 3.4C). Following photon absorption, fast IC from S₄ (high-lying π*) to S₁ (π_{LUMO}) occurs for both PC **2** and **3**.

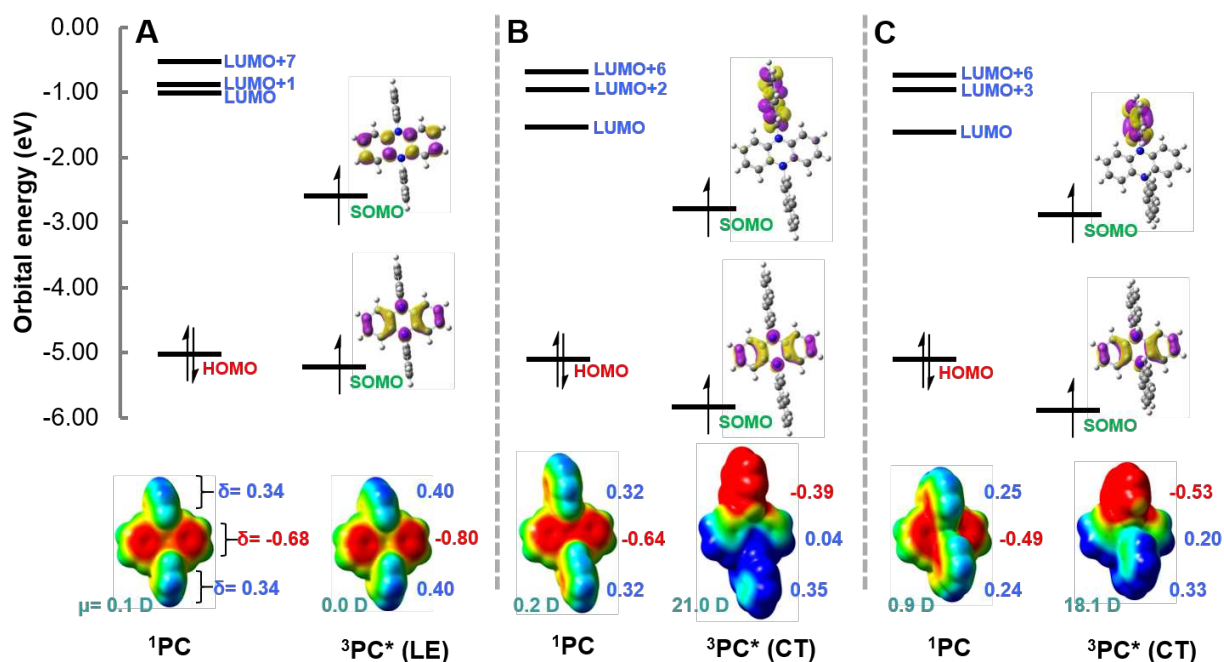


Figure 3.5. Orbital energy (in eV) of ¹PC (HOMO and LUMOs) and ³PC* (SOMOs) of *N,N*-diaryl dihydrophenazines **1** (A), **2** (B), and **3** (C); HOMO = highest occupied molecular orbital, LUMO = lowest unoccupied molecular orbital, SOMO = singly occupied molecular orbital, ¹PC = photocatalyst's ground state, ³PC* = photocatalyst's lowest triplet state. Computed partial charge (δ, in units of e) using the electrostatic potential (ESP) CHELPG formalism. ESP-mapped electron density (displayed at the bottom): “red” indicates electron rich regions while “blue” indicates electron poor regions. Computed dipole moment (μ) in units of Debye (D).

In contrast to PC **1**, the LUMOs of PCs **2** and **3** are exclusively π* orbitals of the *N*-naphthalene substituent (Figure 3.4) and are lower in energy relative to the LUMO of PC **1** by 0.57 eV and 0.66 eV, respectively (Figure 3.5). As such, during IC to the S₁ state, PCs **2** and **3**'s π*_{naphthyl}

LUMO will be populated to first form the CT S₁ state, which upon ISC results in the CT T₁ state composed of the charge separated SOMOs (Figures 3.5B and 3.5C). The electrostatic potential (ESP)-mapped electron density highlights the CT character and large dipole moments of 21.0 D and 18.1 D for PCs **2** and **3**'s ³PC* state, respectively (Figures 3.5B and C). For extended details of Figure 4, see Figure 3.9.

The LE nature of PC **1**'s and the CT nature of PC **2** and **3**'s lowest excited states are further supported through examination of their absorption and emission spectra (Figure 3.6). In PC **1**, the thermal relaxation of the excited electron from S₂ to S₁ results in a Stokes shift of 98 nm with emission spectra possessing rather sharp features. In contrast, for PCs **2** and **3**, much broader and featureless peaks and larger Stokes shifts of 311 nm and 301 nm, respectively, are observed due to the relaxation of the excited electron from S₄ into the much lower energy LUMO (relative to PC **1**'s LUMO) of S₁ stabilized by electron delocalization of the extended π^* _{naphthalene} orbital. We suggest that the observed emission spectra in Figure 6 are predominantly due to direct fluorescence from the lowest singlet excited state. This assignment is made because introduction of oxygen to such samples results in a minimal quenching of the emission (Figure 3.17). It is worth noting that the fluorescence wavelength from the CT singlet state can be used to estimate the energy of the CT lowest triplet state as the energy of the CT lowest singlet and triplet states are expected to be nearly degenerate.^{21,26}

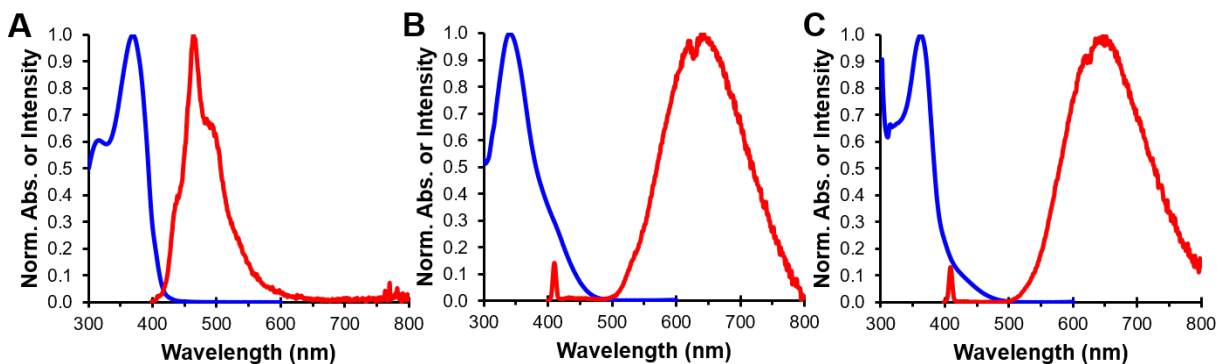


Figure 3.6. Overlaid absorption (blue) and emission (red) spectra of PCs **1** (A), **2** (B) and **3** (C) in DMA.

Due to the large differences in computed LE or CT characters, dipole moments, and observed emission spectra for PCs **1** versus **2** or **3**, we reasoned that increased solvent polarity would significantly stabilize the polar $S_1(\text{CT})$ state of **2** and **3** (and thus red-shift the emission wavelength) and minimally stabilize the non-polar $S_1(\text{LE})$ state of **1**. To test this hypothesis, the emission profiles of these dihydrophenazines were investigated in solvents possessing a range of polarities. These experiments validate the predicted striking contrast in the dihydrophenazine derivatives. Emission remains essentially unchanged for PC **1**, whereas for PCs **2** and **3** a large solvatochromic effect in emission is observed, with the maximum wavelength ($\lambda_{\text{max,em}}$) spanning nearly the entire visible spectrum (Figure 3.7). This solvatochromic response is attributed to emission from polar $S_1(\text{CT})$ states of PCs **2** and **3**, which are stabilized in more polar solvents, resulting in increasingly larger Stokes shifts and therefore red-shifted emission (see Figure 3.15 for further details).

Using the observed Stokes shifts in various solvents and the Lippert equation,²⁷ the change in dipole moment ($\Delta\mu$) from $S_1(\text{CT})$ to S_0 of PCs **2** and **3** was estimated to be 22.1 D and 16.0 D,

respectively (Figures 3.11 and 3.12). These experimentally derived $\Delta\mu$ values corroborate the DFT-predicted $\Delta\mu$ values (estimated from the T_1 state possessing similar CT character). For PCs **2** and **3**, the predicted $\Delta\mu$ values are 20.8 D [e.g. 20.8 D = 21.0 D ($^3PC^*$) - 0.2 D (1PC)] and 17.2 D, respectively (Figures 3.5B and C). The large $\Delta\mu$ values for PCs **2** and **3** between the ground state and the lowest excited state, along with their broad and featureless emission profiles, strongly suggest that PC **2** and **3**'s lowest excited states are CT in character.²⁸ Combined, these data indicate that PC **1**'s lowest excited state is of LE character while for PCs **2** and **3**, which possess low-lying π^* _{naphthalene} LUMOs, the lowest excited state has CT character with extraordinary sensitivity to solvent polarity.

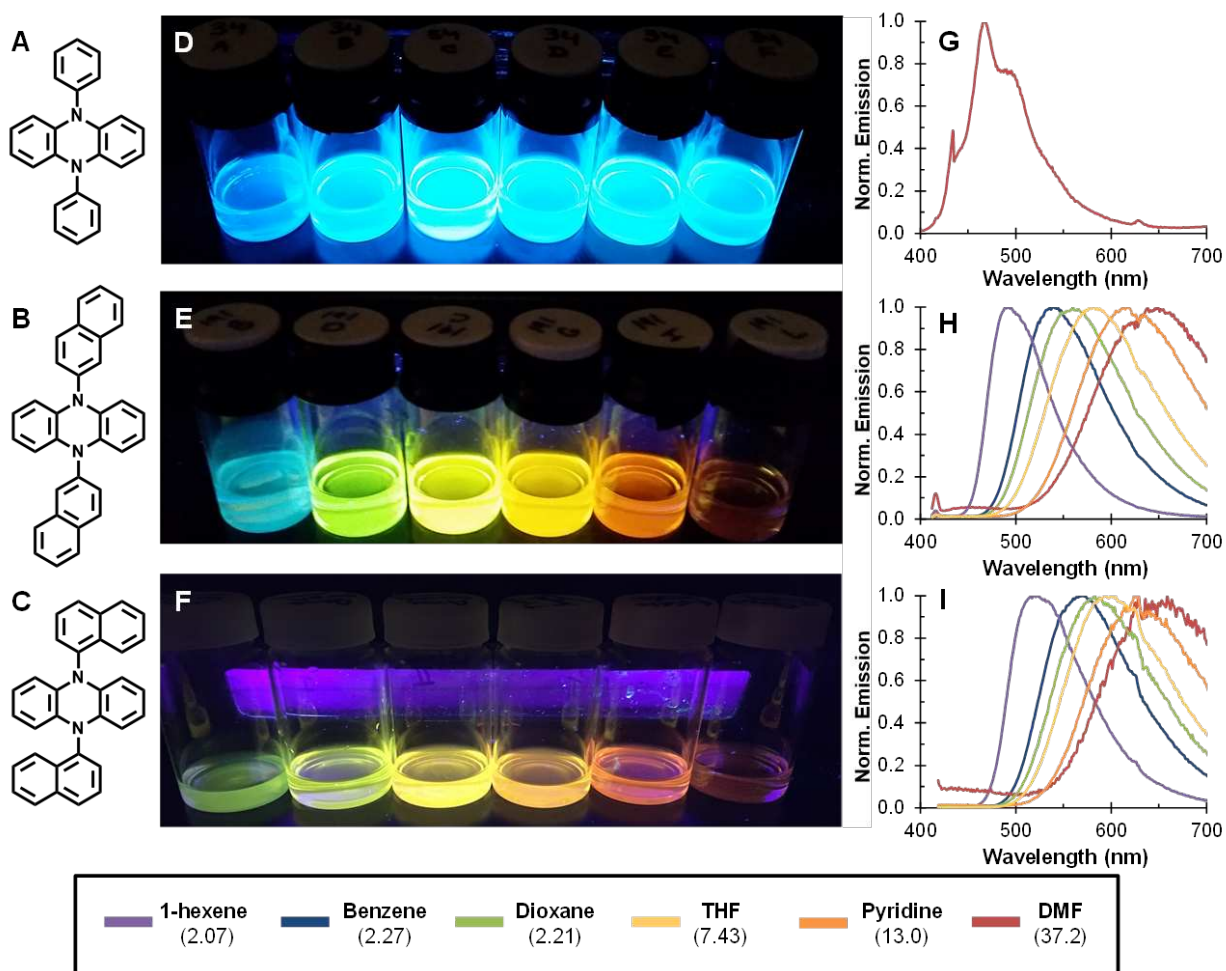


Figure 3.7. Structures of diaryl dihydrophenazines with LE (**A**) or CT (**B** and **C**) natures. Photographs of solutions of the diaryl dihydrophenazines upon excitation with 365 nm light (**D**, **E**, and **F**) and their emission spectra (**G**, **H**, and **I**) in solvents with varying polarity. For **D** - **F**, the order of solvents from left to right (dielectric constant, ϵ): 1-hexene ($\epsilon = 2.07$), benzene ($\epsilon = 2.27$), dioxane ($\epsilon = 2.21$), THF ($\epsilon = 7.43$), pyridine ($\epsilon = 13.0$), and DMF ($\epsilon = 37.2$).

In light of the strong influence of solvent polarity on the emission profiles of PCs **2** and **3**, we reasoned that solvent polarity would greatly influence catalyst performance in polymerization reactions from multiple perspectives. Performing polymerizations in polar solvents effectively stabilizes the $^3\text{PC}^*$ of CT complexes, which decreases the reducing power of the PC. Even more influential when considering the entire O-ATRP mechanism, the polarity of the solvent would be expected to significantly influence the ion pairing of $^2\text{PC}^{\bullet+}\text{Br}^-$, and thus affect its formation, binding energy, lifetime and thus ability to deactivate the propagating radical efficiently (*vide infra*).²⁹ In short, the appropriate polarity of the reaction medium is required to balance all of these properties to achieve an optimal polymerization synthesis through O-ATRP.

Efficient deactivation minimizes bimolecular termination of active propagating radicals (P_n^\bullet) and is critical for controlled O-ATRP. Deactivation of O-ATRP requires oxidation of P_n^\bullet by $^2\text{PC}^{\bullet+}\text{Br}^-$ to reinstall the bromine chain-end group to regenerate ^1PC and $\text{P}_n\text{-Br}$ (Figure 3.16). This deactivation step is formally a three-body event requiring P_n^\bullet , $^2\text{PC}^{\bullet+}$ and Br^- to come together via random diffusion to produce a productive collision; however, such three-body events are entropically improbable, especially considering the low concentrations of these species. Therefore, we hypothesize that ion pairing of $^2\text{PC}^{\bullet+}$ and Br^- to form $^2\text{PC}^{\bullet+}\text{Br}^-$ is essential for effective

deactivation because it reduces a three-body collision to a more likely pseudo two-body collision event involving only ${}^2\text{PC}^{\bullet+}\text{Br}^-$ and P_n^\bullet .

We studied this ion pair using DFT (Figure 3.10) to calculate the standard complexation Gibbs free energy ($\Delta G^0_{\text{complex}}$) for ${}^2\text{PC}^{\bullet+}\text{Br}^-$ formation in DMA and the less polar THF, shown in Figure 3.8A. For PC **3**, the formation of ${}^2\text{PC}^{\bullet+}\text{Br}^-$ in DMA is predicted to be exergonic ($\Delta G^0_{\text{complex}} = -4.2$ kcal/mol). However, its formation is even more favorable in the less polar THF solvent ($\Delta G^0_{\text{complex}} = -11.1$ kcal/mol).²⁴ The optimized geometry of the ${}^2\text{PC}^{\bullet+}\text{Br}^-$ complex consists of the bromide anion residing on the center of the dihydrophenazine core (the positive charge of ${}^2\text{PC}^{\bullet+}$ localizes the anion) ~ 3.5 Å from each nitrogen (Figure 3.8B). In short, modulation of the strength of ion pairing between ${}^2\text{PC}^{\bullet+}$ and Br^- by conducting the polymerization in a medium with optimal polarities enhances the capability of these PCs to produce polymers with controlled MWs and low \bar{D} .

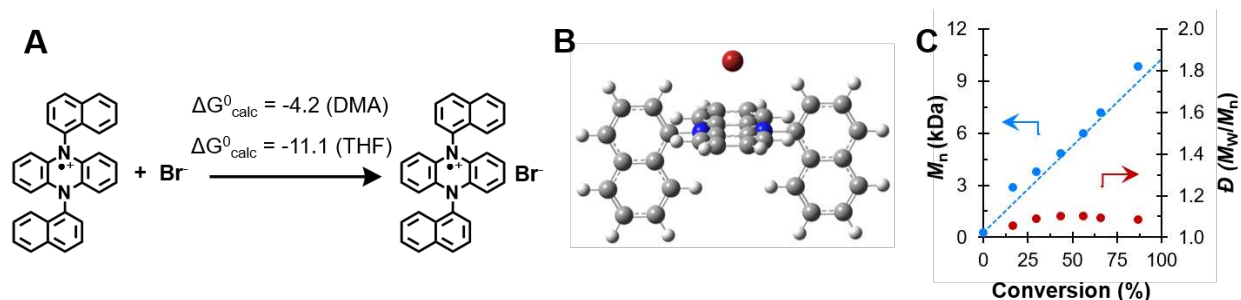


Figure 3.8. Solvent effects on the ion pairing of ${}^2\text{PC}^{\bullet+}$ and Br^- (A). Optimized geometry of the ${}^2\text{PC}^{\bullet+}\text{Br}^-$ pair (B). (C) Plot of M_n and \bar{D} as a function of monomer conversion for the polymerization of MMA in 3:1 DMA: THF. The dashed line represents the theoretical M_n growth.

To test the combined effects of solvent polarity on overall catalyst performance in polymerization, PC **3** was used to polymerize MMA in mixed solvent systems comprised of

various percentages of DMA ($\epsilon = 37.8$) and THF ($\epsilon = 7.58$) to systematically alter the overall dielectric constant (ϵ) of the overall reaction medium (Table 3.2, Figures 3.13 and 3.14). These experiments reveal that the best overall MMA polymerization performance is obtained using a 3:1 volume:volume ratio of DMA to THF, to produce polymers with the combination of lowest D and highest I^* . Using diethyl 2-bromo-2-methylmalonate (DBMM) as the initiator results in the production of PMMA with $D = 1.08$ and a nearly quantitative I^* of 91.2%, while exhibiting a highly linear increase in polymer MW as a function of monomer conversion (Figure 3.8C).

Using this mixed solvent system allows for the synthesis of polymers with target MWs and low D through modulation of either the initiator or monomer in the overall stoichiometry of the reaction (Table 3.1). In comparison, using only DMA as the solvent results in the production of PMMA with higher dispersity ($D = 1.16$) and decreased control over MW ($I^* = 79.7\%$). The enhanced control over the polymerization through manipulation of the solvent polarity further validates the proposed O-ATRP mechanism, although the improvements in polymerization performance could be attributed to influences in both the activation (i.e. nature of the CT states) and deactivation steps. Combined, these effects are macroscopically observed in that the rate of polymerization decreases with decreasing polarity of the reaction medium.

Table 3.1. Solvent Effects on the Ion Pairing of ${}^2\text{PC}^{\bullet+}\text{Br}^-$ and Results for the Polymerization of MMA in DMA: THF.^a

Run No.	[MMA]: [DBMM]:[3]	Conversion (%) ^b	M_w (kDa) ^c	M_n (kDa) ^c	\bar{D} (M_w/M_n) ^c	I^* (%) ^d
1	1000:5:1	81.7	18.9	16.2	1.16	102
2	1000:10:1	86.8	10.6	9.8	1.08	91.2
3	1000:15:1	83.2	5.55	5.15	1.08	113
4	1000:20:1	76.4	4.67	4.29	1.09	95.1
5	500:10:1	94.8	5.20	4.77	1.09	105
6	750:10:1	93.1	6.67	6.07	1.10	119

^aSee experimental section for details. ^bMeasured by ${}^1\text{H}$ NMR. ^cMeasured by GPC coupled with light scattering. ^d $I^* = \text{theoretical number average MW} / \text{experimentally measured number average MW} * 100$. DMA: THF = 3:1 (v:v).

Conclusions

Factors affecting how *N,N*-diaryl dihydrophenazine photoredox catalysts access photoexcited intramolecular charge transfer states have been studied through a combined experimental and computational approach, and the importance of this state in the proposed polymerization mechanism has been hypothesized. Solvent polarity has proven to be an influential parameter for polymerization, affecting both the degree of charge transfer in the excited states of the photoredox catalyst as well as the ion pairing between the catalyst radical cation and the bromide anion. These combined factors hone our understanding of the polymerization mechanism and this has enabled the synthesis of well-defined poly(methyl methacrylate) with dispersities typically less than 1.10 through organocatalyzed atom transfer radical polymerization. Increasing understanding of these organic photoredox catalysts has enabled the application of design

principles to accelerate the development of these catalysts with superior properties, which we envision will have the potential to broadly replace unsustainable precious metal photoredox catalysts.

Experimental

General Information

All reagents were purchased from Sigma-Aldrich. Monomers and solvents used in polymerizations: methyl methacrylate (MMA), dimethylacetamide (DMA), were dried over CaH_2 , purified by vacuum distillation, and degassed by 20 minutes of N_2 sparging before storage and subsequent use in a N_2 glovebox. Spectral grade tetrahydrofuran (THF) and dimethylformamide (DMF) were purified using a Mbraun solvent system and used without further treatment. 1-hexene, benzene, and dioxane were used as received. Monomers were stored at $-34\text{ }^\circ\text{C}$ in the glovebox freezer and allowed to warm to room temperature before use in polymerizations.

Alkyl halide initiators used in polymerizations: methyl 2-bromopropionate (M2BP) and diethyl 2-bromo-2-methylmalonate (DBMM) were purified by vacuum distillation and degassed by three freeze-pump-thaw cycles before storage and subsequent use in a N_2 glovebox. Initiators were stored at $-34\text{ }^\circ\text{C}$ in the glovebox freezer and allowed to warm to room temperature before use in polymerizations.

Reagents used in the synthesis of organic photocatalysts: 2-Dicyclohexylphosphino-2,6-diisopropoxybiphenyl (RuPhos) and Chloro-(2-Dicyclohexylphosphino-2,6-diisopropoxy-1,1-biphenyl) [2-(2-aminoethyl)phenyl] palladium(II) – methyl-t-butyl ether adduct (RuPhos precatalyst, 1st generation) were stored and used in N_2 glovebox. All other reagents were used as received without further treatment.

The visible light irradiation source was white LEDs (16-inch strip, double-density white LEDs), purchased from Creative Lighting Solutions (item no. CL-FRS1210-5M-12V-WH), wrapped inside of an aluminum foil lined 400mL beaker.

^1H , ^{13}C , and ^{19}F NMR spectroscopy were obtained from either a Varian INOVA 400 MHz, 500 MHz, or Bruker 300MHz spectrometer. Chemical shifts referenced to an internal solvent resonance as parts-per-million (ppm) relative to tetramethylsilane. Deuterated solvents were purchased from Cambridge Isotope Labs and used as received. Polymer molecular weights were obtained *via* gel permeation chromatography (GPC) coupled with multi-angle light scattering (MALS), using an Agilent HPLC fitted with one guard column and three PLgel 5 μm MIXED-C gel permeation columns, a Wyatt Technology TrEX differential refractometer, and a Wyatt Technology miniDAWN TREOS light scattering detector, using THF as the eluent at a flow rate of 1.0mL/min. Ultraviolet-visible spectroscopy (UV-Vis) was performed on an Agilent Cary 5000 spectrophotometer. Emission spectroscopy was performed on a SLM 8000C spectrofluorimeter; samples sparged with argon for 15 minutes prior to data acquisition. Electrospray Ionization Mass Spectrometry (ESI-MS) and was performed at the University of Colorado-Boulder Central Analytical Mass Spectrometry Facility on a Waters Synapt G2 HDMS Qtof with MeCN as the solvent.

General Polymerization Procedure

A 20 mL scintillation vial with a plastic-lined cap was charged with a small stirbar and photocatalyst (4.00 mg, 9.35 μmol , 1 eq), and transferred to a N_2 glovebox. DMA (1.50 mL), THF (0.50 mL), MMA (1.00 mL, 9.35 mmol, 1000 eq), and DBMM (17.9 μL , 93.5 μmol , 10 eq) were added sequentially *via* pipette. The vial was then quickly sealed and placed into the beaker with

white LEDs and stirred for 8 hours. To track the progression of the polymerization, 0.1 mL aliquots were removed *via* syringe at 1-hour increments and injected into a sealed HPLC vial containing 0.7 mL of CDCl_3 with 250 ppm butylated hydroxytoluene (BHT) additive. This aliquot was analyzed by ^1H NMR to analyze the monomer conversion and then dried to remove the volatiles. The dried sample was re-dissolved in spectral grade THF for analysis by GPC coupled with MALS.

Solvent System Optimization

The selected solvent systems were: 100/0, 75/25, 50/50, 25/75, 0/100 by volume (DMA/THF). The progression of all polymerizations was tracked in the same way as for those in the *General Polymerization Procedure*. An overall 2:1 solvent:monomer volume ratio (v:v) was maintained for the different solvent systems. The data for these experiments are presented in the *Supplementary Polymerization Data* section.

Computational Details

All calculations were performed using computational chemistry software package Gaussian 09 ver. D01.³⁰ We acknowledge the use of computational resource provided by XSEDE - Comet supercomputer.

Excited State Calculation

Ground state geometries of PC **1**, **2** and **3** were obtained from previous calculations³¹ computed at uM06/6-31+G(d,p)/CPCM- H_2O level of theory.³² Using these geometries, single point time dependent density functional theory (TD-DFT) calculations were performed using the rCAM-B3LYP/6-31+G(d,p)/CPCM-DMA level of theory.³³ rCAM-B3LYP was chosen because

it gave better λ_{\max} predictions that are closer to experimental values in comparison to ω B97xd level of theory; however, both of these methods gave similar results in terms of contributions of local excitation (LE) and charge transfer (CT) in the initial photoexcitation. The first 10 excited states of PC 1, 2, and 3 are reported below. Dominant UV-vis absorption peaks with significant and relevant oscillator strengths (f value) are highlighted.

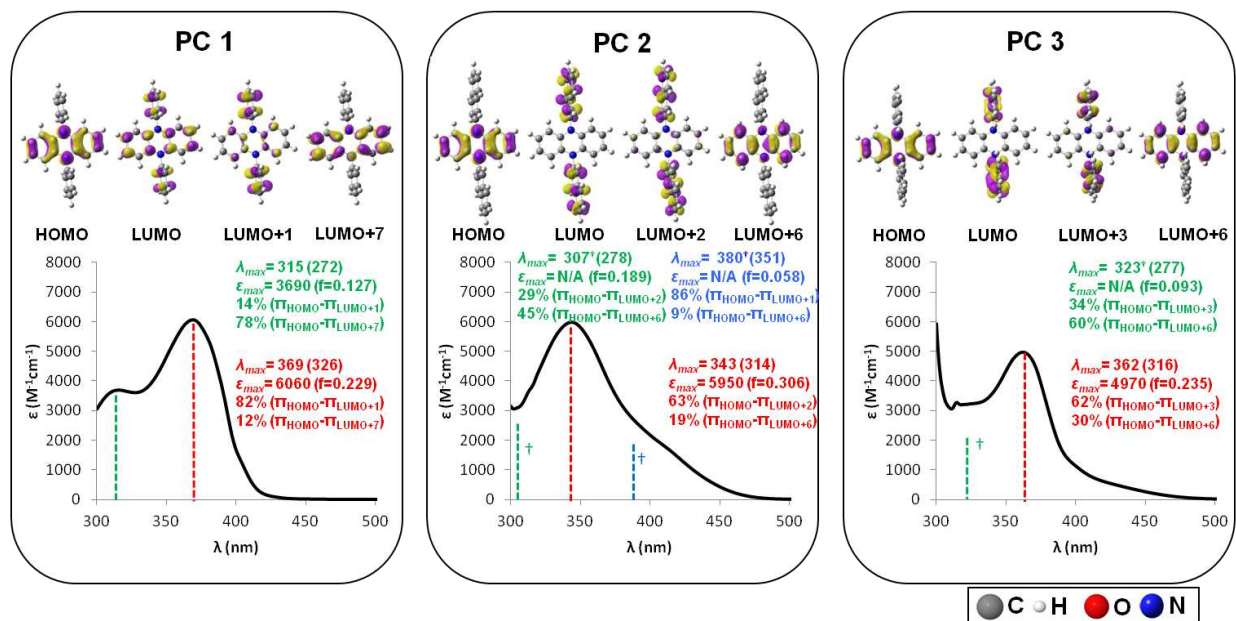


Figure 3.9 UV-vis spectrums of PC 1, 2, and 3 (in DMA) along with theoretically assigned orbital contributions to observed electronic transitions. \dagger Predicted wavelength of hidden peaks.

PC 1

Excited State 1: Singlet-A 3.4017 eV 364.47 nm f=0.0000 $\langle S^{*2} \rangle = 0.000$
 88 -> 89 0.62220
 88 -> 94 -0.31360

Excited State 2: Singlet-A 3.8009 eV 326.20 nm f=0.2292 $\langle S^{*2} \rangle = 0.000$
 87 -> 89 0.13082
 88 -> 90 0.63929 ($\pi_{\text{HOMO}}-\pi_{\text{LUMO}+1}$, $2 \times (0.63929)^2 \times 100 = 82\%$ contribution)
 88 -> 96 0.24989 ($\pi_{\text{HOMO}}-\pi_{\text{LUMO}+7}$, 12% contribution)

Excited State 3: Singlet-A 3.9447 eV 314.31 nm f=0.0000 $\langle S^{*2} \rangle = 0.000$
 87 -> 92 -0.12845
 88 -> 91 0.68214

Excited State 4: Singlet-A 3.9843 eV 311.18 nm f=0.0048 $\langle S^{*2} \rangle = 0.000$
 87 -> 91 -0.13516
 88 -> 92 0.67915

Excited State 5: Singlet-A 4.2367 eV 292.65 nm f=0.0008 $\langle S^{*2} \rangle = 0.000$

88 -> 93	0.46039				
88 -> 97	-0.45803				
88 ->100	0.13505				
88 ->101	0.15853				
Excited State 6:	Singlet-A	4.3213 eV	286.92 nm	f=0.0020	<S**2>=0.000
88 -> 93	0.41284				
88 -> 97	0.46387				
88 -> 99	0.13330				
88 ->101	0.24115				
Excited State 7:	Singlet-A	4.3981 eV	281.91 nm	f=0.0000	<S**2>=0.000
87 -> 90	0.13676				
88 -> 89	0.31306				
88 -> 94	0.61150				
Excited State 8:	Singlet-A	4.5616 eV	271.80 nm	f=0.1268	<S**2>=0.000
87 -> 94	-0.13898				
88 -> 90	-0.26664	$(\pi_{\text{HOMO}}-\pi_{\text{LUMO}+1}$, 14% contribution)			
88 -> 96	0.62461	$(\pi_{\text{HOMO}}-\pi_{\text{LUMO}+7}$, 78% contribution)			
Excited State 9:	Singlet-A	5.0577 eV	245.14 nm	f=0.0000	<S**2>=0.000
88 -> 97	0.16644				
88 -> 99	-0.43523				
88 ->100	0.45641				
88 ->107	0.22361				
Excited State 10:	Singlet-A	5.0803 eV	244.05 nm	f=0.0001	<S**2>=0.000
88 -> 98	0.67080				
88 ->113	-0.13676				

PC 2

Excited State 1:	Singlet-A	3.4371 eV	360.73 nm	f=0.0000	<S**2>=0.000
114 ->115	0.52456				
114 ->118	0.16236				
114 ->119	-0.42658				
Excited State 2:	Singlet-A	3.5334 eV	350.90 nm	f=0.0576	<S**2>=0.000
111 ->115	0.11053				
114 ->116	0.65605	$(\pi_{\text{HOMO}}-\pi_{\text{LUMO}+1}$, 86% contribution)			
114 ->121	-0.20734	$(\pi_{\text{HOMO}}-\pi_{\text{LUMO}+6}$, 9% contribution)			
Excited State 3:	Singlet-A	3.6890 eV	336.09 nm	f=0.0000	<S**2>=0.000
114 ->115	0.40605				
114 ->118	-0.38413				
114 ->119	0.36653				
114 ->125	0.15114				
Excited State 4:	Singlet-A	3.9476 eV	314.08 nm	f=0.3058	<S**2>=0.000
114 ->117	0.56126	$(\pi_{\text{HOMO}}-\pi_{\text{LUMO}+2}$, 63% contribution)			
114 ->121	0.30706	$(\pi_{\text{HOMO}}-\pi_{\text{LUMO}+6}$, 19% contribution)			
114 ->124	0.19584				
114 ->130	0.11703				
Excited State 5:	Singlet-A	4.2124 eV	294.33 nm	f=0.0033	<S**2>=0.000

114 ->120	0.44774				
114 ->123	-0.42924				
114 ->127	0.26363				
Excited State 6:	Singlet-A	4.3266 eV	286.56 nm	f=0.0000	<S**2>=0.000
111 ->117	-0.11704				
114 ->115	0.15221				
114 ->118	0.54188				
114 ->119	0.37951				
Excited State 7:	Singlet-A	4.4626 eV	277.83 nm	f=0.1894	<S**2>=0.000
114 ->116	0.16671				
114 ->117	-0.38403	($\pi_{\text{HOMO}}-\pi_{\text{LUMO}+2}$, 29% contribution)			
114 ->121	0.47616	($\pi_{\text{HOMO}}-\pi_{\text{LUMO}+6}$, 45% contribution)			
114 ->124	0.21307				
114 ->130	0.12695				
Excited State 8:	Singlet-A	4.4718 eV	277.26 nm	f=0.0348	<S**2>=0.000
114 ->120	0.42463				
114 ->123	0.30228				
114 ->126	-0.24083				
114 ->127	-0.29061				
114 ->129	-0.15481				
114 ->134	0.10264				
Excited State 9:	Singlet-A	4.5617 eV	271.79 nm	f=0.0732	<S**2>=0.000
112 ->115	0.47529				
113 ->116	0.47719				
Excited State 10:	Singlet-A	4.5646 eV	271.62 nm	f=0.2685	<S**2>=0.000
112 ->116	0.46511				
113 ->115	0.47435				

PC 3

Excited State 1:	Singlet-A	3.2951 eV	376.26 nm	f=0.0006	<S**2>=0.000
111 ->116	-0.11194				
114 ->115	0.68293				
Excited State 2:	Singlet-A	3.2994 eV	375.78 nm	f=0.0001	<S**2>=0.000
111 ->115	-0.11294				
114 ->116	0.68297				
Excited State 3:	Singlet-A	3.4583 eV	358.51 nm	f=0.0000	<S**2>=0.000
114 ->117	0.54297				
114 ->119	0.43295				
Excited State 4:	Singlet-A	3.9264 eV	315.77 nm	f=0.2348	<S**2>=0.000
111 ->117	0.12212				
114 ->118	0.55789	($\pi_{\text{HOMO}}-\pi_{\text{LUMO}+3}$, 62% contribution)			
114 ->121	0.38533	($\pi_{\text{HOMO}}-\pi_{\text{LUMO}+6}$, 30% contribution)			
Excited State 5:	Singlet-A	4.2086 eV	294.60 nm	f=0.0039	<S**2>=0.000
114 ->120	0.32888				
114 ->122	0.51724				
114 ->124	-0.23782				

Excited State 6: Singlet-A 4.3984 eV 281.89 nm f=0.0000 <S**2>=0.000
 111 ->118 -0.11515
 114 ->117 -0.43405
 114 ->119 0.53821

Excited State 7: Singlet-A 4.4798 eV 276.76 nm f=0.0928 <S**2>=0.000
 111 ->119 0.12675
 114 ->118 -0.40986 ($\pi_{\text{HOMO}}-\pi_{\text{LUMO}+3}$, 34% contribution)
 114 ->121 0.54780 ($\pi_{\text{HOMO}}-\pi_{\text{LUMO}+6}$, 60% contribution)

Excited State 8: Singlet-A 4.5164 eV 274.52 nm f=0.0007 <S**2>=0.000
 112 ->115 0.16157
 113 ->116 -0.16123
 114 ->120 0.49491
 114 ->122 -0.14153
 114 ->124 0.15330
 114 ->126 -0.25117
 114 ->127 -0.12869
 114 ->128 0.15964
 114 ->136 0.14175

Excited State 9: Singlet-A 4.5372 eV 273.26 nm f=0.4513 <S**2>=0.000
 112 ->116 -0.47673
 113 ->115 0.48817

Excited State 10: Singlet-A 4.5843 eV 270.45 nm f=0.0035 <S**2>=0.000
 112 ->115 -0.43341
 113 ->116 0.43520
 114 ->120 0.13311
 114 ->122 -0.13453

For PC **1**, the "red" peak was experimentally determined to have maximum absorption wavelength (λ_{max}) of 369 nm and molar absorptivity at λ_{max} (ϵ_{max}) of 6060 M⁻¹cm⁻¹ (Figure S1). TD-DFT predictions generally underestimated λ_{max} values of dihydrophenazine derivatives, where the "red" peak of PC **1** was predicted to be $\lambda_{\text{max,calc}} = 326$ nm with its oscillator strength (f) of 0.229. This peak was theoretically assigned to be contributed by 82% $\pi_{\text{HOMO}}-\pi_{\text{LUMO}+1}$ and 12% $\pi_{\text{HOMO}}-\pi_{\text{LUMO}+7}$ transitions. A second "green" peak of PC **1** at $\lambda_{\text{max}} = 315$ nm ($\epsilon_{\text{max}} = 3690$ M⁻¹cm⁻¹) was also identified, which was predicted to have $\lambda_{\text{max,calc}} = 272$ nm (f = 0.127) and contributed by 14% $\pi_{\text{HOMO}}-\pi_{\text{LUMO}+1}$ and 78% $\pi_{\text{HOMO}}-\pi_{\text{LUMO}+7}$ transitions.

For PC **2**, the main "red" peak was measured at $\lambda_{\max} = 343 \text{ nm}$ ($\epsilon_{\max} = 5950 \text{ M}^{-1}\text{cm}^{-1}$) and was predicted to be $\lambda_{\max,\text{calc}} = 314 \text{ nm}$ ($f = 0.306$). We theoretically identified two hidden peaks, "green" and "blue" peaks, with $\lambda_{\max,\text{calc}} = 278 \text{ nm}$ and $\lambda_{\max,\text{calc}} = 351 \text{ nm}$, respectively. These hidden peaks (with smaller molar absorptivity) were over signaled by the other peaks that they were not observed as distinctive peaks in the UV-vis spectrum. Using the relative shift between λ_{\max} and $\lambda_{\max,\text{calc}}$ of the "red" peak ($\Delta\lambda = 29 \text{ nm}$), the hidden "green" and "blue" peaks were predicted to reside at 307 nm and 380 nm, respectively. π_{HOMO} , $\pi_{\text{LUMO}+1}$, $\pi_{\text{LUMO}+2}$, and $\pi_{\text{LUMO}+6}$ orbitals with varying contributions were involved in PC **2**'s electronic transitions.

For PC **3**, the main "red" peak was measured at $\lambda_{\max} = 362 \text{ nm}$ ($\epsilon_{\max} = 4970 \text{ M}^{-1}\text{cm}^{-1}$) and was predicted to be $\lambda_{\max,\text{calc}} = 316 \text{ nm}$ ($f = 0.235$). This peak was contributed by 62% $\pi_{\text{HOMO}}-\pi_{\text{LUMO}+3}$ and 30% $\pi_{\text{HOMO}}-\pi_{\text{LUMO}+6}$ transitions. A hidden "green" peak was predicted to reside at 323 nm and was predicted to be contributed by 34% $\pi_{\text{HOMO}}-\pi_{\text{LUMO}+3}$ and 60% $\pi_{\text{HOMO}}-\pi_{\text{LUMO}+6}$ transitions.

Orbital Energy

Converged ^1PC and $^3\text{PC}^*$ geometries of PC **1**, **2** and **3** were obtained from previous calculations² computed at uM06/6-31+G(d,p)/CPCM-H₂O level of theory. Using these geometries, single point energy calculations were performed at uM06/6-311+G(d,p)/CPCM-DMA level of theory to obtain the orbital energies of PC **1**, **2**, and **3** (π_{HOMO} , π_{SOMO} , π_{LUMO} , and $\pi_{\text{LUMO}+n}$, where $n = 1 - 7$).

Electrostatic Potential (ESP) Calculation

Converged ^1PC and $^3\text{PC}^*$ geometries of PC **1**, **2** and **3** were obtained from previous calculations² computed at uM06/6-31+G(d,p)/CPCM-H₂O level of theory. Using these geometries, single point energy calculations with CHELPG³⁴ ESP population analysis were performed at uM06/6-31G(d,p)/CPCM-DMA level of theory. Total electron density of ^1PC and $^3\text{PC}^*$ were first plotted and then were mapped with ESP derived charges to show distribution of charges on the dihydrophenazine derivatives.

Complexation Free Energy of $^2\text{PC}^{\bullet+}$ and Br^-

Geometries of $^2\text{PC}^{\bullet+}$, Br^- , and ion pair $^2\text{PC}^{\bullet+}\text{Br}^-$ were optimized at uM06/6-31+G(d,p)/CPCM-DMA level of theory followed by frequency calculations to obtain zero point energy (ZPE) corrections, thermal corrections, and entropic TS terms using ideal gas approximations. The obtained Gibbs free energy, $G^{0*}(298\text{ K}, 1\text{ atm})$, by default has a standard reference state of 298.15K and 1 atm. However, a standard reference state of 298.15K and 1 mole/liter [$G^0(298\text{ K}, 1\text{ M})$] is more relevant to our examined systems as the O-ATRP reactions are carried out in the liquid phase in DMA or THF.

To obtain the Gibbs free energy with relevant standard state reference, $G^0(298\text{ K}, 1\text{ M}) = G^{0*}(298\text{ K}, 1\text{ atm}) + RT \ln(0.08206\text{ T})$, where R is the gas constant and T is the temperature. $\Delta G^0(298\text{ K}, 1\text{ M}) = \Delta G^{0*}(298\text{ K}, 1\text{ atm})$ when there is no mole change to the product from the reactant. However, the reaction of $^2\text{PC}^{\bullet+} + \text{Br}^- = ^2\text{PC}^{\bullet+}\text{Br}^-$ has one net mole change and $\Delta G^0(298\text{ K}, 1\text{ M}) = \Delta G^{0*}(298\text{ K}, 1\text{ atm}) - 1.89\text{ kcal/mol}$.

At the converged geometries, single point calculations at uM06/6-31+G(d,p)/CPCM-DMA were performed; the various corrections and entropic TS terms from uM06/6-31+G(d,p)

calculations will then be applied to the energy obtained with uM06/6-311+G(d,p). Similar procedures were performed using THF, described by CPCM solvent model.

The just-described computational methods were benchmarked against available experimental values for the complexation free energy between tetrabutylammonium cation (NBu_4^+) and Br^- in DMA and THF.³⁵ Our methods correctly predicted the trend of stronger complexation between NBu_4^+ and Br^- in THF versus DMA; in addition, our methods satisfactorily reproduced the experimental $\Delta G^0_{\text{complex}}$ values to within < 1.5 kcal/mol (Figure S2).

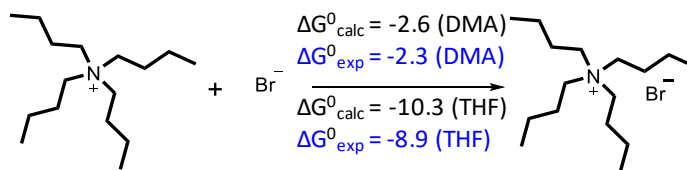


Figure 3.10 Experimental and predicted complexation free energy between NBu_4^+ and Br^- in THF and DMA.

Solvatochromic Determination of Dipole Moment

The sensitivity of the maximum wavelength of emission to changes in solvent polarity can be related to the change in dipole moment between the ground and excited state using the Lippert equation:³⁶

$$\Delta\nu = \frac{2}{hc} \frac{\Delta\mu^2}{a^3} \Delta f + c$$

Where $\Delta\nu$ is the observed Stokes shift in a given solvent, h is Planck's constant, c is the speed of light, $\Delta\mu$ is the change in dipole upon excitation, a is the radius of the solvent sphere surrounding the molecule, Δf is the solvent orientation polarizability, a value derived from both

the solvent's dielectric constant and refractive index, and c is a constant. A plot of $\Delta\nu$ versus Δf , referred to as a Lippert-Mataga plot, gives a slope from which $\Delta\mu$ can be extracted (Figure S3 and S4).

To estimate a , a spherical approximation, where a equals half the length of the molecule, was used for **3**. An ellipsoidal approximation, where a equals 0.4 times the length of the molecule, was used for the more elongated **2**. This gave a value for $\Delta\mu$ of 16.0 D for **3** and 22.1 D for **2**, which is in good agreement with the computationally-derived values of 17.2 D and 20.8 D, respectively.

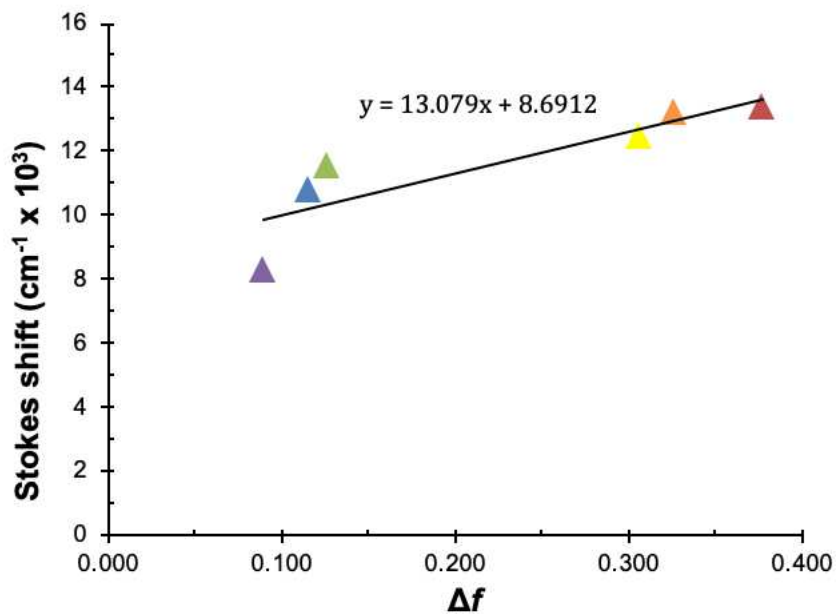


Figure 3.11 The Lippert-Mataga plot for PC **2**, where the stokes shift ($\Delta\nu$) is plotted as a function of solvent orientation polarizability (Δf) for 1-hexene (purple), benzene (blue), dioxane (green), THF (yellow), pyridine (orange), and DMF (red).

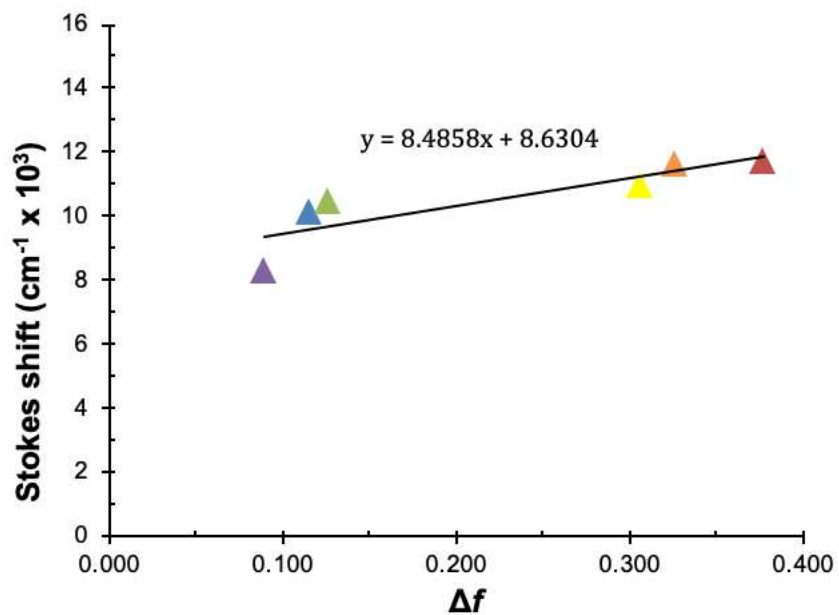


Figure 3.12 The Lippert-Mataga plot for PC **3**, where the stokes shift ($\Delta\nu$) is plotted as a function of solvent orientation polarizability (Δf) for 1-hexene (purple), benzene (blue), dioxane (green), THF (yellow), pyridine (orange), and DMF (red).

Supplementary Polymerization Data: M2BP Initiator

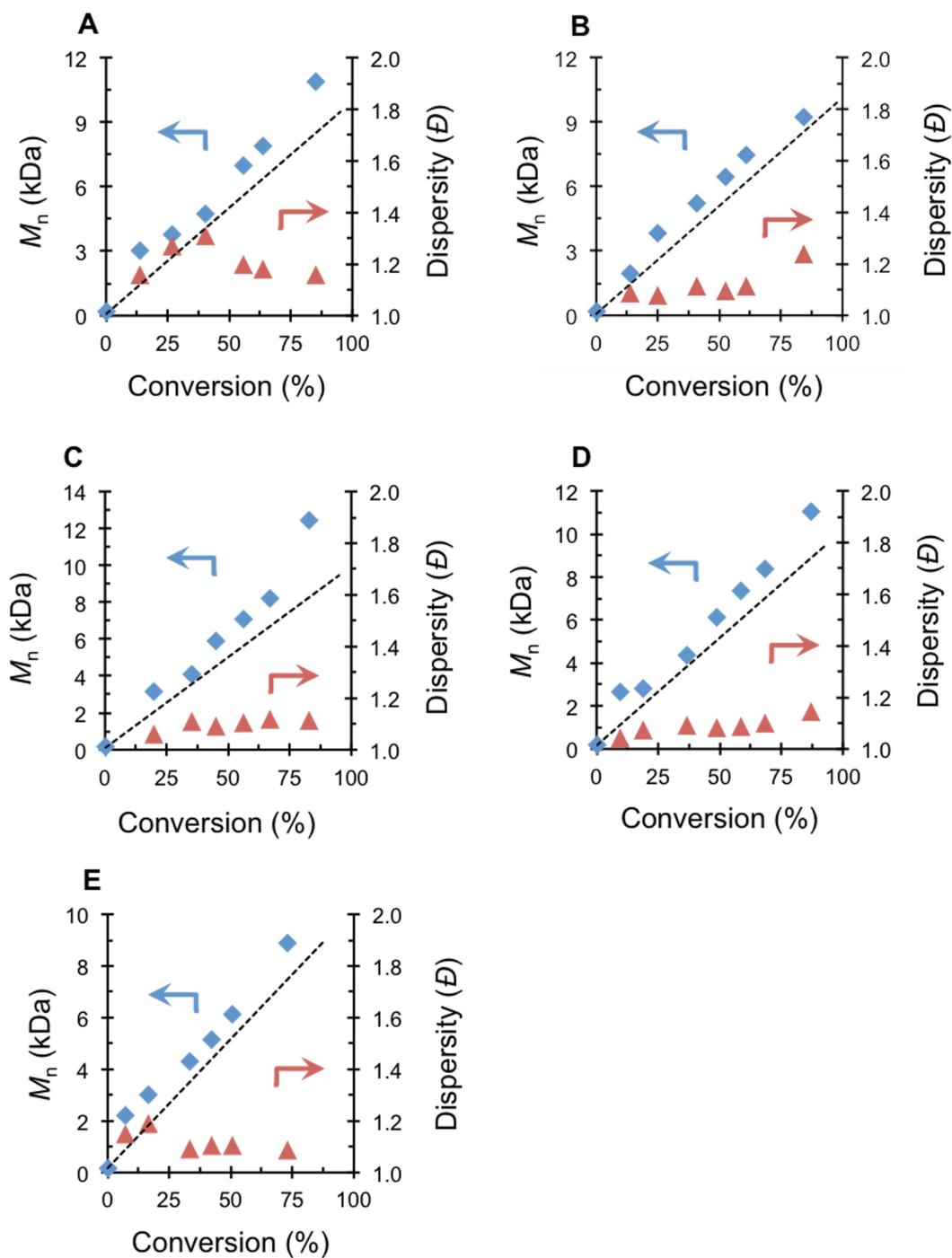


Figure 3.13 Plots of molecular weight (M_n , blue) and dispersity (\bar{D} , red) as a function of monomer conversion for the polymerization of MMA (1000 eq, 1.00 mL, 9.35 mmol) catalyzed by PC **3** (1 eq, 4.00 mg, 9.35 μ mol), using M2BP (10 eq, 10.00 μ L, 93.5 μ mol) initiator, and 100/0 (**A**), 75/25

(B), 50/50 (C), 25/75 (D), 0/100 (E) DMA/THF solvent systems (2/1, solvent/monomer volume ratio).

Supplementary Polymerization Data: DBMM Initiator

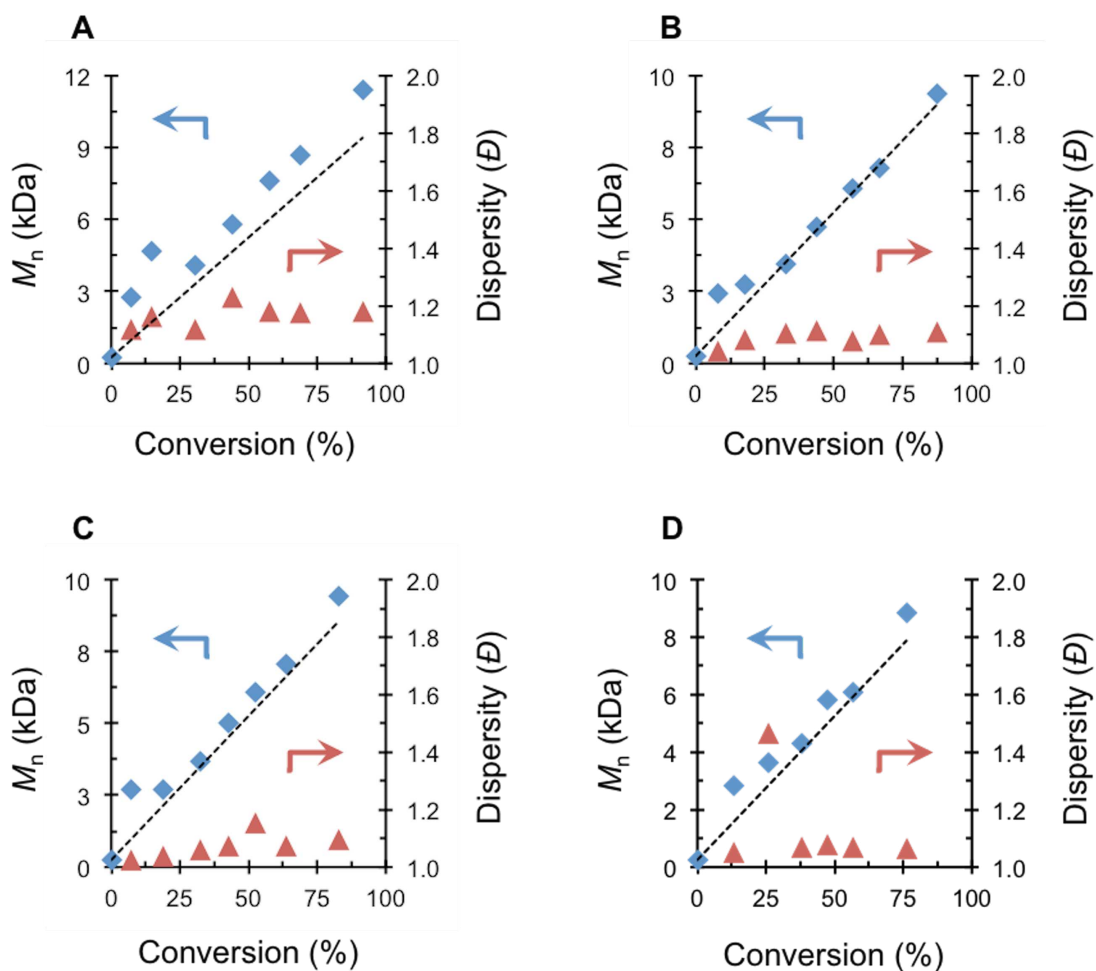


Figure 3.14 Plots of molecular weight (M_n , blue) and dispersity (D , red) as a function of monomer conversion for the polymerization of MMA (1000 eq, 1.00 mL, 9.35 mmol) catalyzed by PC **3** (1 eq, 4.00 mg, 9.35 μ mol), using DBMM initiator (10 eq, 18.0 μ L, 93.5 μ mol), and 100/0 (A), 75/25 (B), 50/50 (C), 25/75 (D), 0/100 (E) DMA/THF solvent systems (2/1, solvent/monomer volume ratio).

Table 3.2 Results of the O-ATRP of MMA Using PC **3** in Different Solvent Systems^a

Run No.	Initiator	Solvent Ratio (DMA/THF) ^a	Time (h)	Conversion (%) ^b	M_w (kDa) ^c	M_n (kDa) ^c	\bar{D} (M_w/M_n) ^c	I^* (%) ^d
1	M2BP	100/0	8	85.14	12.6	10.9	1.16	79.7
2	M2BP	75/25	8	84.19	11.4	9.2	1.24	93.4
3	M2BP	50/50	8	82.99	13.8	12.4	1.11	68.2
4	M2BP	25/75	8	87.02	12.6	11.0	1.14	80.6
5	M2BP	0/100	8	72.90	9.7	8.9	1.09	83.9
6	DBMM	100/0	8	91.51	13.4	11.4	1.18	81.9
7	DBMM	50/50	8	87.62	10.4	9.4	1.11	95.1
8	DBMM	25/75	8	82.95	10.3	9.4	1.10	90.9
9	DBMM	0/100	8	76.10	9.5	8.9	1.07	87.8

^aSee Supporting Information section 2a and 2b for details. ^bMeasured by ¹H NMR. ^cMeasured by GPC coupled with light scattering. ^d $I^* = \text{theoretical number average MW} / \text{experimentally measured number average MW} * 100$.

UV-Vis Spectrum of PC **2** in Solvents of Varying Polarity

To confirm that the solvatochromic response of PC **2** is not due to photoexcitation events, the UV-vis spectrum of PC **2** was acquired in solvents of different polarities. Regardless of the solvent, PC **2**'s absorption profile and λ_{max} are nearly identical (Figure S7).

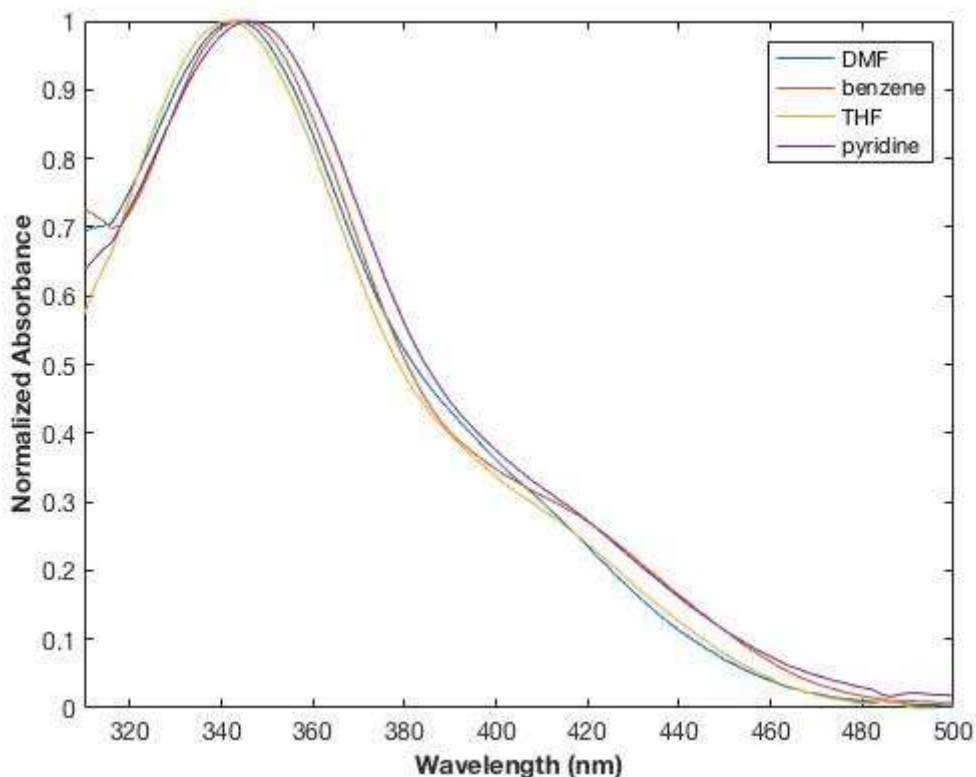


Figure 3.15 UV-vis spectrum of PC 2 in benzene ($\epsilon = 2.27$), THF ($\epsilon = 7.43$), pyridine ($\epsilon = 13.0$), and DMF ($\epsilon = 37.2$), where ϵ is the dielectric constant of the solvent.

Oxidation of P_n^\bullet by ${}^2PC^{\bullet+}Br^-$ Ion Pair

Deactivation of O-ATRP requires oxidation of P_n^\bullet by ${}^2PC^{\bullet+}$ and Br^- to reinstall the bromine chain-end group to regenerate 1PC and P_n-Br (Figure S8). We propose that ion pairing of ${}^2PC^{\bullet+}$ and Br^- to form ${}^2PC^{\bullet+}Br^-$ is essential for effective deactivation because it reduces a three-body collision to a more likely pseudo two-body collision event involving only two entities of ${}^2PC^{\bullet+}Br^-$ and P_n^\bullet .

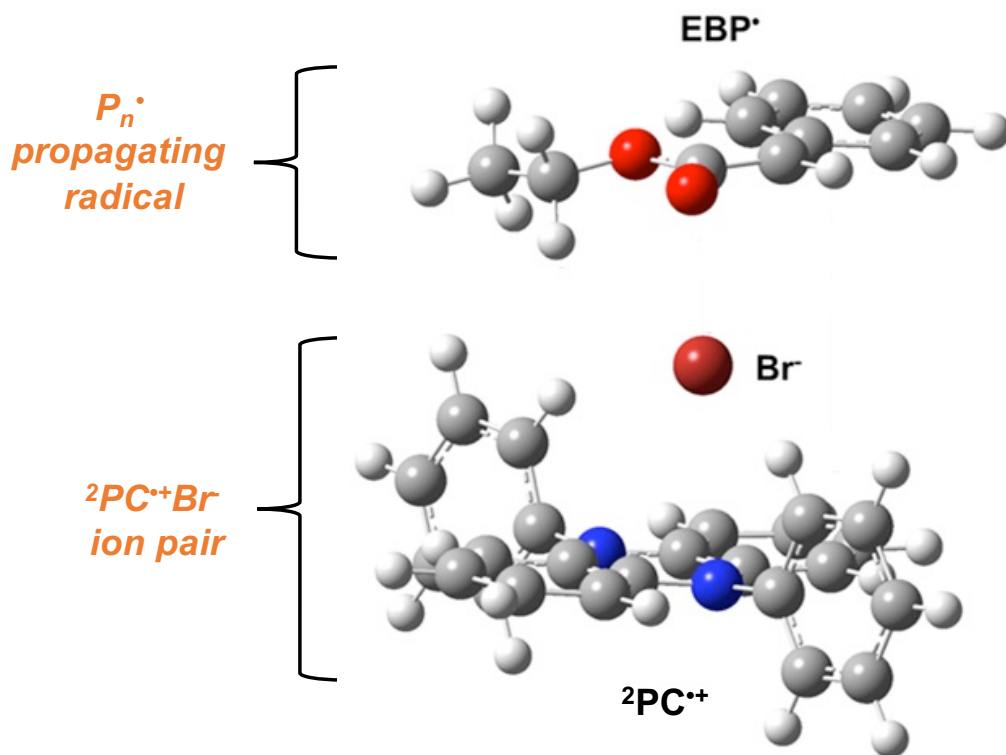


Figure 3.16 Proposed O-ATRP deactivation mechanism via oxidation of propagating radical (P_n^\bullet) by $^2PC^{\bullet+}Br^-$ ion pair. P_n^\bullet is exemplified by neutral radical of ethyl α -bromophenylacetate (EBP) and $^2PC^{\bullet+}$ is exemplified by radical cation of 5,10-diphenyl-5,10-dihydrophenazine.

Oxygen Quenching on PC 3's Emission Spectrum

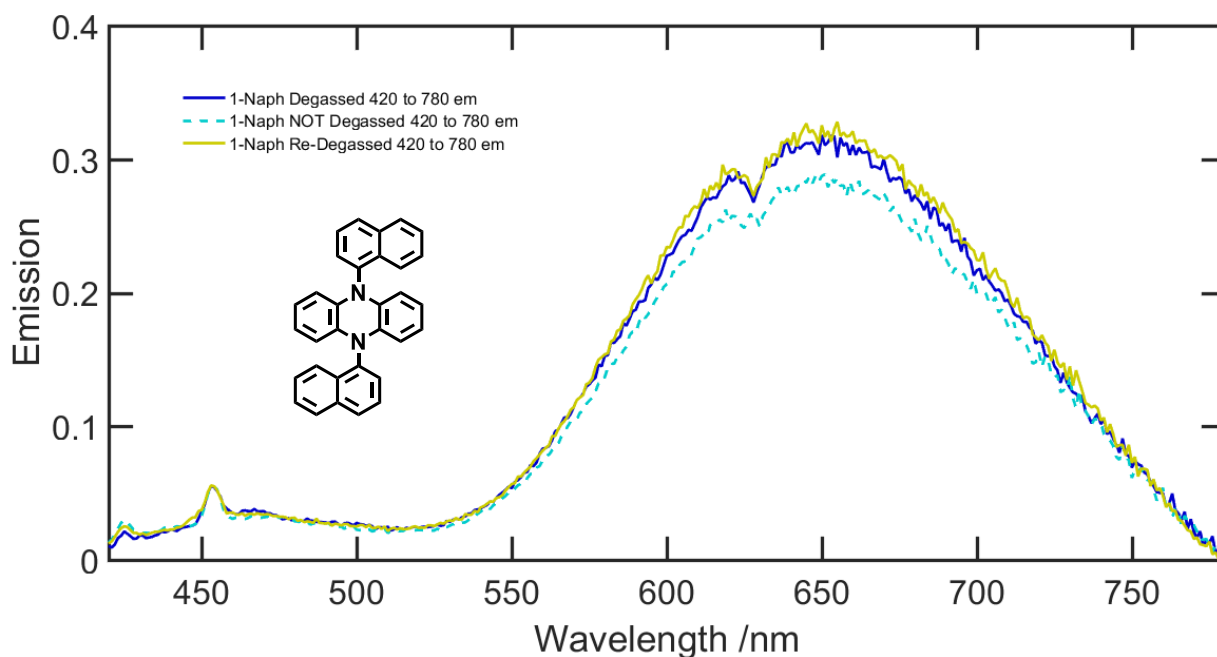


Figure 3.17 Introduction of oxygen minimally quenches the emission, which supports that the emission is due to fluorescence from the lowest singlet excited state.

Coordinates of Molecular Structures

All coordinates are reported as XYZ Cartesian coordinates. Converged geometries were obtained from uM06/6-31+G** level of theory in CPCM-described solvents (DMA or THF). Single point energies computed at uM06/6-311+G** level of theory (reported in parentheses) are arranged in the following order: E_{0K} (not ZPE and thermally corrected), H (298.15 K, 1atm), G^{0*} (298.15K, 1atm), and G^0 (298.15K, 1M). They are stated in Hartrees units. All energies reported were calculated using the GAUSSIAN 09 ver. D.01 computational chemistry package.

a) Br⁻

DMA solvent (-2574.199117, -2574.196756, -2574.215292, -2574.212274)

Br -3.89062 2.11056 3.84586

THF solvent (-2574.187588, -2574.185227, -2574.203763, -2574.200745)

Br -3.89062 2.11056 3.84586

b) ${}^2\text{PC}^{\bullet+}\text{Br}^-$ (PC 3)

DMA solvent (-3915.519316, -3915.044939, -3915.135648, -3915.13263)

C	-6.67223	-0.14732	-0.21807
C	-5.31022	-0.11830	0.00578
C	-4.67740	1.08346	0.35938
C	-5.44474	2.26991	0.46538
C	-6.82566	2.22160	0.21853
C	-7.43211	1.02608	-0.11138
C	-3.45576	3.50760	1.03045
C	-2.68724	2.32132	0.92097
C	-1.31578	2.35917	1.21744
H	-0.72824	1.44895	1.15123
C	-0.71859	3.54352	1.59703
C	-1.47854	4.71862	1.70103
C	-2.83069	4.69991	1.42795
H	-7.15042	-1.08472	-0.48636
H	-4.72046	-1.02546	-0.08414
H	-7.41551	3.12975	0.29293
H	-8.50190	1.00201	-0.29604
H	0.34291	3.55860	1.82547
H	-1.00747	5.64749	2.00872
H	-3.42138	5.60588	1.52229
N	-4.81077	3.45945	0.77394
N	-3.31204	1.14165	0.56838
Br	-4.32196	1.87850	3.87399
C	-5.60946	4.64279	0.96655
C	-5.85428	5.48939	-0.14453
C	-6.12087	4.89388	2.21473
C	-5.33333	5.24196	-1.43897
C	-6.67548	6.63563	0.07385
C	-6.92689	6.03471	2.41610
H	-5.89357	4.20068	3.02568
C	-5.61931	6.09822	-2.47463
H	-4.70687	4.36796	-1.60817
C	-6.94865	7.49630	-1.01889
C	-7.19790	6.88161	1.36869

H	-7.33318	6.23395	3.40381
C	-6.43386	7.23474	-2.26466
H	-5.21616	5.90263	-3.46502
H	-7.57643	8.36920	-0.84943
H	-7.82337	7.75980	1.51816
H	-6.65087	7.90110	-3.09548
C	-2.54906	-0.08052	0.57751
C	-1.91891	-0.50574	-0.61946
C	-2.45136	-0.77878	1.75486
C	-2.00979	0.20560	-1.84171
C	-1.15822	-1.71190	-0.56493
C	-1.69876	-1.97169	1.79113
H	-2.95215	-0.38782	2.64208
C	-1.37075	-0.26356	-2.96389
H	-2.59007	1.12559	-1.88559
C	-0.51116	-2.16340	-1.74265
C	-1.06760	-2.42387	0.65766
H	-1.61945	-2.52556	2.72240
C	-0.61394	-1.45680	-2.91549
H	-1.44521	0.28723	-3.89812
H	0.07033	-3.08248	-1.69794
H	-0.48202	-3.34118	0.68175
H	-0.11327	-1.81200	-3.81251

THF solvent (-3915.513707, -3915.039018, -3915.129317, -3915.126298)

C	-6.73237	-0.36441	0.67262
C	-5.35588	-0.28956	0.74173
C	-4.72923	0.93410	1.02134
C	-5.52020	2.09289	1.22218
C	-6.91751	1.99789	1.13536
C	-7.51520	0.78235	0.87030
C	-3.52689	3.38046	1.64381
C	-2.73639	2.22114	1.44459
C	-1.34434	2.30062	1.60261
H	-0.73688	1.41367	1.45372
C	-0.75241	3.49652	1.95517
C	-1.53518	4.64317	2.15411
C	-2.90548	4.58769	1.99737
H	-7.20652	-1.31882	0.46349
H	-4.74985	-1.17736	0.59003
H	-7.52473	2.88444	1.28842
H	-8.59779	0.71965	0.81329
H	0.32535	3.54396	2.07920
H	-1.06616	5.58209	2.43316

H	-3.51164	5.47428	2.15541
N	-4.89282	3.30069	1.45725
N	-3.35360	1.04356	1.07181
Br	-4.29672	1.44687	4.37403
C	-5.69375	4.48181	1.63174
C	-5.98253	5.27325	0.49125
C	-6.15013	4.79616	2.88637
C	-5.51570	4.95974	-0.81012
C	-6.78587	6.43544	0.68745
C	-6.94099	5.95109	3.06578
H	-5.89193	4.14483	3.72143
C	-5.83786	5.76964	-1.87216
H	-4.90054	4.07439	-0.96443
C	-7.09789	7.24613	-0.43269
C	-7.25000	6.74854	1.99025
H	-7.30293	6.20191	4.05888
C	-6.63588	6.92155	-1.68413
H	-5.47691	5.52429	-2.86780
H	-7.71229	8.13150	-0.27969
H	-7.86120	7.63940	2.12305
H	-6.88189	7.54930	-2.53672
C	-2.54825	-0.12641	0.84748
C	-2.11266	-0.39928	-0.47408
C	-2.22699	-0.92658	1.91434
C	-2.43762	0.42085	-1.58368
C	-1.31061	-1.56210	-0.67146
C	-1.43064	-2.07257	1.70342
H	-2.59376	-0.65596	2.90497
C	-1.98432	0.09437	-2.83871
H	-3.04963	1.30973	-1.43671
C	-0.86128	-1.86627	-1.98102
C	-0.98550	-2.37983	0.44036
H	-1.17349	-2.70689	2.54707
C	-1.19014	-1.05781	-3.04105
H	-2.23787	0.72597	-3.68638
H	-0.24999	-2.75477	-2.12859
H	-0.37119	-3.26266	0.27289
H	-0.84079	-1.30039	-4.04136

c) ²PC^{•+} (PC 3)

DMA solvent (-1341.308536, -1340.835929, -1340.916642, -1340.913624)

C	-6.76872	-0.25821	0.18681
---	----------	----------	---------

C	-5.40010	-0.22514	0.35792
C	-4.75350	0.98911	0.63736
C	-5.51841	2.17930	0.74036
C	-6.90966	2.12325	0.55908
C	-7.52529	0.91913	0.28676
C	-3.50326	3.43720	1.17888
C	-2.73825	2.24724	1.07559
C	-1.34482	2.30692	1.23967
H	-0.75687	1.39787	1.16304
C	-0.72787	3.51307	1.49970
C	-1.48460	4.69000	1.60024
C	-2.85457	4.65427	1.44170
H	-7.25781	-1.20384	-0.02683
H	-4.81398	-1.13569	0.28076
H	-7.49596	3.03355	0.63484
H	-8.60186	0.88789	0.14966
H	0.35008	3.54608	1.62497
H	-0.99482	5.63778	1.80249
H	-3.44010	5.56505	1.51882
N	-4.87566	3.37669	1.00461
N	-3.38005	1.05114	0.80112
C	-5.64325	4.59680	1.03618
C	-6.16036	5.02847	2.23070
C	-5.83108	5.30869	-0.17796
C	-6.90933	6.22368	2.27564
H	-5.98604	4.44473	3.13205
C	-6.58981	6.51581	-0.11686
C	-7.11622	6.94704	1.12678
H	-7.31768	6.56373	3.22289
C	-2.58796	-0.13667	0.60208
C	-2.12108	-0.42363	-0.70813
C	-2.29624	-0.93439	1.67868
C	-1.31942	-1.59209	-0.87488
C	-1.50255	-2.08740	1.49839
H	-2.67680	-0.66614	2.66202
C	-1.02635	-2.40399	0.24979
H	-1.27094	-2.71594	2.35331
H	-0.41110	-3.28975	0.10405
H	-7.69452	7.86864	1.15394
C	-6.79842	7.25208	-1.31015
C	-6.28249	6.81382	-2.50478
H	-6.45006	7.38503	-3.41407
C	-5.53211	5.61730	-2.55986
H	-5.12874	5.27893	-3.51077
C	-5.30856	4.87877	-1.42298
H	-4.72729	3.95932	-1.47777

H	-7.37901	8.17131	-1.26020
C	-2.41066	0.38645	-1.83422
H	-3.02342	1.27907	-1.71765
C	-0.83410	-1.90887	-2.16850
C	-1.12937	-1.10820	-3.24422
H	-0.75233	-1.36003	-4.23198
C	-1.92452	0.04791	-3.07382
H	-2.15343	0.67378	-3.93244
H	-0.22209	-2.80056	-2.29022

THF solvent (-1341.303108, -1340.830596, -1340.910828, -1340.90781)

C	-0.70150	-3.61988	-0.73835
C	-1.39945	-2.42997	-0.75063
C	-0.70918	-1.20729	-0.76396
C	0.70914	-1.20732	-0.76394
C	1.39937	-2.43001	-0.75058
C	0.70139	-3.61990	-0.73832
C	0.70918	1.20833	-0.76235
C	-0.70913	1.20835	-0.76236
C	-1.39937	2.43101	-0.74743
H	-2.48479	2.43210	-0.74713
C	-0.70138	3.62089	-0.73360
C	0.70151	3.62086	-0.73358
C	1.39945	2.43097	-0.74741
H	-1.24652	-4.55896	-0.72779
H	-2.48487	-2.43102	-0.75034
H	2.48479	-2.43110	-0.75025
H	1.24637	-4.55900	-0.72773
H	-1.24638	4.55996	-0.72179
H	1.24653	4.55992	-0.72177
H	2.48488	2.43202	-0.74709
N	1.38620	0.00050	-0.77113
N	-1.38619	0.00055	-0.77115
C	2.82766	0.00048	-0.74353
C	3.51480	0.00125	-1.93049
C	3.48281	-0.00034	0.51602
C	4.92567	0.00121	-1.92059
H	2.96391	0.00188	-2.86878
C	4.90956	-0.00037	0.51061
C	5.60306	0.00041	-0.72588
H	5.46721	0.00181	-2.86207
C	-2.82765	0.00061	-0.74353
C	-3.48281	-0.00035	0.51602
C	-3.51479	0.00160	-1.93049

C	-4.90956	-0.00031	0.51060
C	-4.92566	0.00163	-1.92060
H	-2.96389	0.00234	-2.86878
C	-5.60305	0.00069	-0.72589
H	-5.46719	0.00239	-2.86208
H	-6.69115	0.00070	-0.71044
H	6.69116	0.00037	-0.71043
C	5.59755	-0.00117	1.75003
C	4.90619	-0.00192	2.93611
H	5.44332	-0.00254	3.88090
C	3.49292	-0.00189	2.93601
H	2.95606	-0.00248	3.88111
C	2.79266	-0.00112	1.75387
H	1.70359	-0.00112	1.76778
H	6.68573	-0.00120	1.74099
C	-2.79268	-0.00139	1.75389
H	-1.70361	-0.00148	1.76783
C	-5.59756	-0.00128	1.75001
C	-4.90622	-0.00226	2.93610
H	-5.44337	-0.00300	3.88088
C	-3.49295	-0.00231	2.93602
H	-2.95610	-0.00310	3.88112
H	-6.68574	-0.00125	1.74096

d) NBu₄⁺Br⁻

DMA solvent (-3259.813448, -3259.285106, -3259.37108, -3259.368062)

C	-0.73729	-0.75440	-1.32447
H	-1.54996	-0.08898	-1.00438
C	1.52273	-1.40864	-0.59166
H	1.11143	-2.31084	-0.12634
C	0.92399	0.98608	-1.07203
H	0.00389	1.48334	-1.40190
H	1.50847	0.71714	-1.96140
C	0.04537	-0.08574	0.96584
H	-0.55241	0.83229	0.93198
H	0.96845	0.12224	1.51616
N	0.45880	-0.34268	-0.46935
Br	-2.45475	2.28525	-0.02012
H	1.61637	-1.60785	-1.66717
H	-0.46900	-0.47288	-2.35013
C	1.68275	1.95652	-0.18738
H	1.04591	2.29262	0.64158

H	2.58135	1.51261	0.25778
C	2.88660	-1.10696	-0.00801
H	3.36785	-0.28159	-0.54978
H	2.81547	-0.80821	1.04744
C	-1.16562	-2.21116	-1.32336
H	-0.46433	-2.82257	-1.90752
H	-1.20057	-2.64536	-0.31827
C	-0.74310	-1.15662	1.68611
H	-1.74088	-1.27028	1.23703
H	-0.24680	-2.13733	1.65118
C	-2.55684	-2.30992	-1.94391
H	-2.56006	-1.80472	-2.92125
H	-3.26813	-1.75588	-1.31176
C	2.07718	3.17345	-1.01879
H	1.17246	3.60784	-1.47093
H	2.71796	2.85719	-1.85502
C	2.79177	4.22180	-0.18301
H	3.06104	5.09851	-0.78135
H	2.15719	4.56299	0.64452
H	3.71456	3.81734	0.25154
C	-3.00892	-3.75135	-2.10261
H	-4.01481	-3.81386	-2.53072
H	-2.32977	-4.30708	-2.76111
H	-3.02475	-4.26605	-1.13361
C	3.76999	-2.34659	-0.11049
H	3.82471	-2.66948	-1.16041
H	3.29954	-3.17331	0.44130
C	5.16834	-2.09280	0.42699
H	5.79415	-2.98857	0.35783
H	5.66688	-1.29206	-0.13337
H	5.13535	-1.78840	1.48063
C	-0.90813	-0.73401	3.14297
H	-1.35047	0.27377	3.17395
H	0.08312	-0.64918	3.61151
C	-1.77577	-1.70245	3.92780
H	-1.88817	-1.38698	4.97032
H	-2.77883	-1.77503	3.48923
H	-1.34078	-2.70989	3.92802

THF solvent (-3259.808068, -3259.279549, -3259.364557, -3259.361538)

C	-0.75836	-0.72228	-1.32238
H	-1.54898	-0.03184	-0.99962
C	1.48181	-1.44500	-0.59478
H	1.04430	-2.33637	-0.13187

C	0.95348	0.96840	-1.06685
H	0.04675	1.49522	-1.38801
H	1.52627	0.68631	-1.96002
C	0.04832	-0.08383	0.96939
H	-0.51967	0.85313	0.93905
H	0.97871	0.09025	1.51939
N	0.45149	-0.34884	-0.46797
Br	-2.37667	2.31848	-0.03118
H	1.56889	-1.64456	-1.67100
H	-0.48252	-0.44556	-2.34748
C	1.74423	1.91132	-0.18014
H	1.12028	2.25975	0.65336
H	2.63317	1.44020	0.25763
C	2.85496	-1.18747	-0.01125
H	3.36025	-0.37454	-0.54982
H	2.79315	-0.88937	1.04499
C	-1.22978	-2.16545	-1.32330
H	-0.55129	-2.79701	-1.91365
H	-1.27066	-2.60073	-0.31885
C	-0.77897	-1.12785	1.68510
H	-1.77781	-1.20411	1.23074
H	-0.31817	-2.12606	1.65229
C	-2.62785	-2.21913	-1.93415
H	-2.62036	-1.71547	-2.91230
H	-3.31508	-1.63886	-1.29919
C	2.16500	3.12358	-1.00549
H	1.26836	3.58244	-1.44919
H	2.79396	2.79819	-1.84742
C	2.90817	4.14883	-0.16598
H	3.19336	5.02399	-0.75911
H	2.28538	4.49770	0.66710
H	3.82428	3.72107	0.26058
C	-3.13037	-3.64422	-2.08746
H	-4.13884	-3.67204	-2.51299
H	-2.47334	-4.22621	-2.74589
H	-3.16302	-4.15545	-1.11701
C	3.70334	-2.45099	-0.11789
H	3.75070	-2.77082	-1.16923
H	3.20971	-3.26724	0.42939
C	5.10735	-2.23805	0.42253
H	5.70951	-3.14937	0.34789
H	5.62744	-1.44698	-0.13190
H	5.08146	-1.93996	1.47812
C	-0.93575	-0.69937	3.14118
H	-1.33456	0.32620	3.16915
H	0.05511	-0.65761	3.61670

C	-1.84986	-1.62963	3.91940
H	-1.95001	-1.31396	4.96306
H	-2.85412	-1.65151	3.47841
H	-1.46389	-2.65696	3.91610

e) NBu_4^+

DMA solvent (-685.6036184, -685.0778359, -685.1547159, -685.1516974)

C	-1.20240	-1.53755	0.13688
H	-1.44939	-1.85606	-0.88367
C	0.13432	0.20819	1.25862
H	-0.78240	0.79846	1.34721
C	1.20129	-1.52983	-0.20323
H	0.82563	-2.38040	-0.78363
H	1.44061	-1.89797	0.80239
C	-0.13643	0.25697	-1.25559
H	-0.12917	-0.44803	-2.09632
H	0.77947	0.85169	-1.32123
N	-0.00061	-0.60211	-0.01469
H	0.12782	-0.52877	2.07124
H	-0.82364	-2.41569	0.67259
C	2.44022	-0.98887	-0.89450
H	2.25054	-0.84981	-1.96683
H	2.75739	-0.01698	-0.49966
C	1.33723	1.11771	1.38985
H	2.26720	0.53591	1.44189
H	1.42040	1.79783	0.52992
C	-2.43493	-1.02945	0.86307
H	-2.23600	-0.93929	1.93895
H	-2.75440	-0.04052	0.51596
C	-1.33979	1.17063	-1.35157
H	-2.27165	0.59308	-1.41585
H	-1.41646	1.82473	-0.47099
C	-3.57714	-2.01934	0.65106
H	-3.24796	-3.02725	0.94359
H	-3.81315	-2.07206	-0.42202
C	3.57851	-1.99014	-0.71740
H	3.24781	-2.98344	-1.05500
H	3.80636	-2.08968	0.35414
C	4.82530	-1.57247	-1.47813
H	5.63710	-2.29432	-1.34182
H	4.62339	-1.49465	-2.55353
H	5.18628	-0.59443	-1.13606

C	-4.81679	-1.62942	1.43796
H	-5.63301	-2.34116	1.27724
H	-4.60665	-1.59826	2.51415
H	-5.17528	-0.63606	1.14047
C	1.20695	1.94834	2.66350
H	1.09017	1.27606	3.52592
H	0.28680	2.54837	2.61359
C	2.40776	2.85545	2.87261
H	2.30863	3.44572	3.78932
H	3.33381	2.27217	2.94875
H	2.52368	3.55461	2.03514
C	-1.21551	2.03896	-2.60048
H	-1.11606	1.39263	-3.48457
H	-0.28865	2.62788	-2.54316
C	-2.40888	2.96466	-2.76687
H	-2.31448	3.58219	-3.66595
H	-3.34210	2.39379	-2.84961
H	-2.50671	3.63829	-1.90653

THF solvent (-685.596295, -685.0704783, -685.1473603, -685.1443418)

C	-1.20281	-1.53735	0.13718
H	-1.45003	-1.85588	-0.88345
C	0.13463	0.20837	1.25882
H	-0.78272	0.79763	1.34813
C	1.20149	-1.52978	-0.20343
H	0.82553	-2.38075	-0.78329
H	1.44120	-1.89782	0.80228
C	-0.13661	0.25737	-1.25540
H	-0.13029	-0.44768	-2.09625
H	0.78006	0.85089	-1.32174
N	-0.00064	-0.60212	-0.01457
H	0.12894	-0.52874	2.07150
H	-0.82391	-2.41583	0.67249
C	2.44071	-0.98987	-0.89504
H	2.25119	-0.85115	-1.96750
H	2.75814	-0.01779	-0.50078
C	1.33663	1.11915	1.38988
H	2.26758	0.53869	1.44023
H	1.41824	1.79998	0.53026
C	-2.43579	-1.03018	0.86333
H	-2.23713	-0.93986	1.93931
H	-2.75571	-0.04131	0.51631
C	-1.33889	1.17245	-1.35120
H	-2.27171	0.59617	-1.41369

H	-1.41396	1.82737	-0.47098
C	-3.57763	-2.02078	0.65133
H	-3.24803	-3.02867	0.94360
H	-3.81374	-2.07368	-0.42178
C	3.57896	-1.99141	-0.71767
H	3.24815	-2.98497	-1.05452
H	3.80714	-2.09056	0.35388
C	4.82567	-1.57452	-1.47891
H	5.63702	-2.29654	-1.34220
H	4.62412	-1.49764	-2.55436
H	5.18754	-0.59663	-1.13761
C	-4.81746	-1.63177	1.43830
H	-5.63294	-2.34403	1.27733
H	-4.60791	-1.60099	2.51453
H	-5.17719	-0.63885	1.14107
C	1.20690	1.94881	2.66441
H	1.09231	1.27585	3.52663
H	0.28572	2.54748	2.61644
C	2.40652	2.85764	2.87256
H	2.30752	3.44683	3.78978
H	3.33375	2.27619	2.94751
H	2.52034	3.55808	2.03597
C	-1.21508	2.03971	-2.60108
H	-1.11730	1.39263	-3.48486
H	-0.28743	2.62763	-2.54555
C	-2.40750	2.96664	-2.76701
H	-2.31308	3.58309	-3.66661
H	-3.34161	2.39723	-2.84884
H	-2.50387	3.64158	-1.90761

References

-
- 1) (a) Shaw, M. H.; Twilton, J.; MacMillan, D. W. C. *J. Org. Chem.* **2016**, *81*, 6898-6926. (b) Corrigan, N.; Shanmugam, S.; Xu, J.; Boyer, C. *Chem. Soc. Rev.* **2016**, *45*, 6165-6212. (c) Prier, C. K.; Rankic, D. A.; MacMillan, D. W. C. *Chem. Rev.* **2013**, *113*, 5322-5363. (d) Arias-Rotondo, D. M.; MuCusker, J. K. *Chem. Soc. Rev.* **2016**, *45*, 5803-5820. (e) Narayanam, J. M. R.; Stephenson, C. R. J. *Chem. Soc. Rev.* **2011**, *40*, 102-113 (f) Schultz, D. M.; Yoon, T. P. *Science* **2014**, *343*, 1239176-1-1239176-8.

-
- 2) (a) McKenzie, T. G.; Fu, Q.; Uchiyama, M.; Satoh, K.; Xu, J.; Boyer, C.; Kamigaito, M.; Qiao, G. G. *Adv. Sci.* **2016**, 1500394. (b) Shanmugam, S.; Xu, J.; Boyer, C. *Angew. Chem. Int. Ed.* **2016**, *55*, 1036-1040. (c) Shanmugam, S.; Xu, J.; Boyer, C. *J. Am. Chem. Soc.* **2015**, *137*, 9174-9185. (d) Chen, M.; MacLeod, M. J.; Johnson, J. J. *ACS Macro Lett.* **2015**, *4*, 566-569. (e) Xu, J.; Shanmugam, S.; Duong, H. T.; Boyer, C. *Polym. Chem.* **2015**, *6*, 5615-5624. (f) Xu, J.; Jung, K.; Atme, A.; Shanmugam, S.; Boyer, C. *J. Am. Chem. Soc.* **2014**, *136*, 5508-5519.
- 3) (a) Ohtsuki, A.; Lei, L.; Tanishima, M.; Goto, A.; Kaji, H. *J. Am. Chem. Soc.* **2015**, *137*, 5610-5617. (b) Ohtsuki, A.; Goto, A.; Kaji, H. *Macromolecules* **2013**, *46*, 96-102.
- 4) Zivic, N.; Bouzrati-Zerelli, M.; Kermagoret, A.; Dumur, F.; Fouassier, J.-P.; Gigmes, D.; Lalevée, J. *ChemCatChem* **2016**, *8*, 1617-1631.
- 5) (a) Matyjaszewski, K. *ACS Symposium Series* **2015**, *1187*, 1-17. (b) di Lena, F.; Matyjaszewski, K. *Prog. Polym. Sci.* **2010**, *35*, 959-1021. (c) Rosen, B. M.; Percec, V. *Chem. Rev.* **2009**, *109*, 5069-5119. (d) Moad, G.; Rizzardo, E.; Thang, S. H. *Acc. Chem. Res.* **2008**, *41*, 1133-1142. (e) Braunecker, W. A.; Matyjaszewski, K. *Prog. Polym. Sci.* **2007**, *32*, 93-146. (f) Kamigaito, M.; Ando, T.; Sawamoto, M. *Chem. Rev.* **2001**, *101*, 3689-3746. (g) Matyjaszewski, K. *ACS Symposium Series* **2000**, *768*, 2-26.
- 6) (a) Boyer, C.; Corrigan, N. A.; Jung, K.; Nguyen, D.; Nguyen, T.-K.; Adnan, N. N. M.; Oliver, S.; Shanmugam, S.; Yeow, J. *Chem. Rev.* **2016**, *116*, 1803-1949. (b) Matyjaszewski, K.; Tsarevsky, N. V. *J. Am. Chem. Soc.* **2013**, *136*, 6513-6533. (c) Matyjaszewski, K. *Macromolecules* **2012**, *45*, 4015-4039. (d) Ouchi, M.; Terashima, T.; Sawamoto, M. *Chem. Rev.* **2009**, *109*, 4963-5050. (e) Matyjaszewski, K.; Tsarevsky, N. V. *Nature Chem.* **2009**, *1*, 276-288. (f) Ouchi, M.; Terashima, T.; Sawamoto, M. *Acc. Chem. Res.* **2008**, *41*, 1120-1132. (g) Matyjaszewski, K.; Xia, J. *Chem. Rev.* **2001**, *101*, 2921-2990.

-
- 7) Zhang, G.; Song, I. Y.; Ahn, K. H.; Park, T.; Choi, W. *Macromolecules* **2011**, *44*, 7594-7599.
- 8) (a) Ma, W.; Chen, D.; Ma, Y.; Wang, L.; Zhao, C.; Yang, W. *Polym. Chem.* **2016**, *7*, 4226-4236. (b) Yang, Q.; Dumur, F.; Morlet-Savary, F.; Poly, J.; Lalevée, J. *Macromolecules* **2015**, *48*, 1972-1980. (c) Konkolewicz, D.; Schröder, K.; Buback, J.; Bernhard, S.; Matyjaszewski, K. *Macromolecules* **2012**, *1*, 1219-1223. (d) Tasdelen, M. A.; Uygun, M.; Yagci, Y. *Macromol. Rapid Commun.* **2011**, *32*, 58-62.
- 9) (a) Telitel, S.; Dumur, F.; Campolo, D.; Poly, J.; Gigmes, D.; Fouassier, J. P.; Lalevée, J. *J. Poly. Sci., Part A: Polym. Chem.* **2016**, *54*, 702-713. (b) Bansal, A.; Kumar, P.; Sharma, C. D.; Ray, S. S.; Jain, S.L.; *J. Poly. Sci., Part A: Polym. Chem.* **2015**, *53*, 2739-2746. (c) Pan, X.; Malhotra, N.; Zhang, J.; Matyjaszewski, K. *Macromolecules* **2015**, *48*, 6948-6954.
- 10) (a) Treat, N. J.; Fors, B. P.; Kramer, J. W.; Christianson, M.; Chiu, C.-Y.; Read de Alaniz, J.; Hawker, C. J. *ACS Macro Lett.* **2014**, *3*, 580-584. (b) Fors, B. P.; Hawker, C. J. *Angew. Chem. Int. Ed.* **2012**, *51*, 8850-8853.
- 11) Isse, A. A.; Lin, C. Y.; Coote, M. L.; Gennaro, A. *J. Phys. Chem.* **2011**, *115*, 678-684.
- 12) Furst, L.; Matsuura, B. S.; Narayanam, J. M. R.; Tucker, J. W. Stephenson, C. R. *J. Org. Lett.*, **2010**, *12*, 3104-3107.
- 13) Hu, J.; Wang, J.; Nguyen, T. H.; Zheng, N. *Beilstein J. Org. Chem.* **2013**, *9*, 1977-2001.
- 14) Volz, D.; Wallesch, M.; Flechon, C.; Danz, M.; Verma, A.; Navarro, J. M.; Zink, D. M.; Brase, S.; Baumann, T. *Green Chemistry* **2015**, *17*, 1988-2011
- 15) (a) Ding, M.; Jian, X.; Zhang, L.; Cheng, Z.; Zhu, X. *Macromol. Rapid. Commun.* **2015**, *36*, 1702-1721. (b) Magenau, A. J. D.; Strandwitz, N. C.; Gennaro, A.; Matyjaszewski, K. *Science* **2011**, *332*, 81-84. (c) Matyjaszewski, K.; Jakubowski, W.; Min, K.; Tang, W.; Huang, J.;

-
- Braunecker, W. A.; Tsarevsky, N. V. *Proc. Natl. Acad. Sci. U.S.A.* **2006**, *103*, 15309-15314. (d)
- Faucher, S.; Okrutny, P.; Zhu, S. *Macromolecules* **2006**, *39*, 3-5.
- 16) Romero, N. A.; Nicewicz, D. A. *Chem. Rev.* **2016**, *116*, 10075-10166.
- 17) Miyake, G. M.; Theriot, J. C. *Macromolecules* **2014**, *47*, 8255-8261.
- 18) (a) Treat, N. J.; Sprafke, H.; Kramer, J. W.; Clark, P. G.; Barton, B. E.; Read de Alaniz, J.; Fors, B. P.; Hawker, C. J. *J. Am. Chem. Soc.* **2014**, *136*, 16096. (b) Pan, X.; Lamson, M.; Yan, J.; Matyjaszewski, K. *ACS Macro Lett.* **2015**, *4*, 192-196. (c) Pan, X.; Fang, C.; Fantin, M.; Malhotra, N.; So, W. Y.; Peteanu, L. A.; Isse, A. A.; Gennaro, A.; Liu, P.; Matyjaszewski, K. *J. Am. Chem. Soc.* **2016**, *138*, 2411-2425.
- 19) Theriot, J. C.; Lim, C.-H.; Yang, H.; Ryan, M. D.; Musgrave, C. B.; Miyake, G. M. *Science* **2016**, *352*, 1082-1086.
- 20) Pearson, R. M.; Lim, C.-H.; McCarthy, B. G.; Musgrave, C. B.; Miyake, G. M. *J. Am. Chem. Soc.* **2016**, *138*, 11399-11407.
- 21) (a) Lee, J.; Shizu, K.; Tanaka, H.; Nakanotani, H.; Yasuda, T.; Kaji, H.; Adachi, C. *J. Mater. Chem. C* **2015**, *3*, 2175-2181. (b) Uoyama, H.; Goushi, K.; Shizu, K.; Nomura, H.; Adachi, C. *Nature* **2012**, *492*, 234-238. (c) Tanaka, H.; Shizu, K.; Nakanotani, H.; Adachi, C. *Chem. Mater.* **2013**, *25*, 3766-3771.
- 22) (a) Kalyanasundaram, K. *Coord. Chem. Rev.* **1982**, *46*, 159-244. (b) Flamigni, L.; Barbieri, A.; Sabatini, C.; Ventura, B.; Barigelletti, F. *Top. Curr. Chem.* **2007**, *281*, 143-203.
- 23) Fukuzumi, S.; Kotani, H.; Ohkubo, K.; Ogo, S.; Tkachenko, N. V.; Lemmetyinen, H. *J. Am. Chem. Soc.* **2004**, *126*, 1600-1601.
- 24) See *Experimental Section* for details.

-
- 25) Morris, J. V.; Brühlmann, U.; Serafimov, O.; Huber, J. R. *Ber. Bunsenges. Phys. Chem.* **1974**, *78* (12), 1348-1353.
- 26) Tao, Y.; Yuan, K.; Chen, T.; Xu, P.; Li, h.; Chen, R.; Zheng, C.; Zhange, L.; Huang, W. *Adv. Mater.* **2014**, *26*, 7931-7958.
- 27) Lakowicz, J. R. *Principles of Fluorescence Spectroscopy*. Springer Science: New York, 2006.
- 28) (a) Tanaka, H.; Shizu, K.; Nakanotani, H.; Adachi, C. *Chem. Mater.* **2013**, *25*, 3766-3771. (b) Grabowski, Z. R.; Rotkiewicz, K. *Chem. Rev.* **2003**, *103*, 3899-4032. (c) Borowicz, P.; Herbich, J.; Kapturkiewicz, A.; Opalło, M.; Nowacki, J. *Chem. Phys.* **1999**, *249*, 49-62.
- 29) Marcuz, Y.; Hefter, G.; *Chem. Rev.* **2006**, *106*, 4585-4621.
- 30) Gaussian 09, R. D., Frisch, M. J.; Trucks, G. W.; Schlegel, H. B.; Scuseria, G. E.; Robb, M. A.; Cheeseman, J. R.; Scalmani, G.; Barone, V.; Mennucci, B.; Petersson, G. A.; Nakatsuji, H.; Caricato, M.; Li, X.; Hratchian, H. P.; Izmaylov, A. F.; Bloino, J.; Zheng, G.; Sonnenberg, J. L.; Hada, M.; Ehara, M.; Toyota, K.; Fukuda, R.; Hasegawa, J.; Ishida, M.; Nakajima, T.; Honda, Y.; Kitao, O.; Nakai, H.; Vreven, T.; Montgomery, J. A., Jr.; Peralta, J. E.; Ogliaro, F.; Bearpark, M.; Heyd, J. J.; Brothers, E.; Kudin, K. N.; Staroverov, V. N.; Kobayashi, R.; Normand, J.; Raghavachari, K.; Rendell, A.; Burant, J. C.; Iyengar, S. S.; Tomasi, J.; Cossi, M.; Rega, N.; Millam, J. M.; Klene, M.; Knox, J. E.; Cross, J. B.; Bakken, V.; Adamo, C.; Jaramillo, J.; Gomperts, R.; Stratmann, R. E.; Yazyev, O.; Austin, A. J.; Cammi, R.; Pomelli, C.; Ochterski, J. W.; Martin, R. L.; Morokuma, K.; Zakrzewski, V. G.; Voth, G. A.; Salvador, P.; Dannenberg, J. J.; Dapprich, S.; Daniels, A. D.; Farkas, Ö.; Foresman, J. B.; Ortiz, J. V.; Cioslowski, J.; Fox, D. J. Gaussian, Inc., Wallingford CT, 2009.

-
- 31) Theriot, J. C.; Lim, C.-H.; Yang, H.; Ryan, M. D.; Musgrave, C. B.; Miyake, G. M. *Science* **2016**, 352, 1082-1086.
- 32) Zhao, Y.; Truhlar, D. *Theor. Chem. Acc.* **2008**, 120, 215-241.
- 33) Yanai, T.; Tew, D. P.; Handy, N. C. *Chemical Physics Letters* **2004**, 393, 51-57.
- 34) Spackman, M. A. *J. Comput. Chem.* **1996**, 17, 1-18.
- 35) Marcus, Y.; Hefter, G. *Chem. Rev.* **2006**, 106, 4585-4621.
- 36) Verhoeven, J. W. Sigma-coupled Charge-Transfer Probes of the Fluoroprobe and Fluorotrope Type. In *Advanced Concepts in Fluorescence Sensing Part A: Small Molecule Sensing*; Springer US, 2005.

Chapter 4

Solvent Effects on the Intramolecular Charge Transfer Character of *N,N*-Diaryl Dihydrophenazine Catalysts for Organocatalyzed Atom Transfer Radical Polymerization

Overview

The nature of intramolecular charge transfer of *N,N*-diaryl dihydrophenazine photocatalysts (PCs) in different solvents is explored in context of their performance in organocatalyzed atom transfer radical polymerization (O-ATRP). PCs having a computationally predicted lowest energy excited state exhibiting charge transfer (CT) character can operate a highly controlled O-ATRP in a wide range of solvent polarities, from non-polar hexanes to highly polar *N,N*-dimethylacetamide. For PCs having a computationally predicted lowest energy excited state not possessing CT character, their ability to operate a controlled O-ATRP is decreased. This study confirms the importance of CT character in the excited state for *N,N*-diaryl dihydrophenazine PCs, and a deeper understanding of the activity of CT PCs has enabled the synthesis of polymers of low dispersity (< 1.10) in a controlled fashion.

Introduction

The development of controlled radical polymerizations (CRPs) and photo-mediated CRPs have revolutionized the way in which precision polymeric materials are synthesized. Importantly, these methodologies allow facile access to polymers of tunable molecular weights and narrow molecular weight dispersities (\mathcal{D}).^{1,2} CRPs are capable of polymerizing a wide variety of monomers through various mechanisms, such as nitroxide mediated polymerization (NMP),^{3,4,5} reversible addition fragmentation chain transfer (RAFT) polymerization,^{6,7,8,9,10} iodine transfer

polymerization (ITP),^{11,12,13} and atom transfer radical polymerization (ATRP).¹⁴ The incorporation of photochemistry with CRPs¹⁵ has enabled these methodologies to add spatial and temporal control.¹⁶ Additionally, the development of photo-induced processes inspired by these mechanisms allow for facile modification of existing materials.^{17,18,19}

The discovery that the iridium complex, *fac*-[Ir(ppy)₃], could mediate a controlled ATRP with external regulation by visible light irradiation²⁰ was key to extending ATRP to other redox-active photocatalysts. Additionally, *fac*-[Ir(ppy)₃] and other transition metal complexes have found widespread use as photocatalysts (PCs) to operate photoredox-catalyzed small molecule transformations²¹ due to their ability to mediate single electron transfer processes.²² A key property of many of these successful transition metal complex PCs is their ability to access a long lived²³ metal-to-ligand charge transfer (MLCT) excited state.^{24,25} In addition to possessing key photophysical characteristics, the design of these complexes is highly modular, with synthetic alteration of the ligands or metals enabling access to a wide range of redox potentials.^{26,27} Although the chemistry accessed through these PCs is quite remarkable, contamination of the product with metal residue may raise concerns in some applications.²⁸ To circumvent this problem, organic PCs have emerged as promising alternatives to transition metal complexes with tunable photophysical properties.

Strongly reducing organic PCs, such as perylene^{29,30} *N*-aryl phenothiazines^{31,32,33,34} *N,N*-diaryl dihydrophenazines^{35,36} *N*-aryl phenoxazines³⁷, carbazoles,³⁸ and other polyaromatic hydrocarbons,³⁹ have been shown to mediate an organo-catalyzed ATRP (O-ATRP). A proposed mechanism for O-ATRP mediated by PCs occurs through four key events: 1) photoexcitation to a singlet excited state (¹PC*) and intersystem crossing (ISC) to the triplet state (³PC*); for high performing PCs, their ¹PC* and ³PC* possess charge transfer character (*vide infra*), 2) activation

of an alkyl halide initiator or halide-capped chain end group by electron transfer from $^3\text{PC}^*$, producing the carbon-centered radical and oxidized catalyst $^2\text{PC}^{++}/\text{X}^-$; 3) propagation for polymer MW growth via addition of the carbon-centered radical to a monomer, and 4) deactivation of the propagating radical by $^2\text{PC}^{++}/\text{X}^-$ (Figure 4.1).

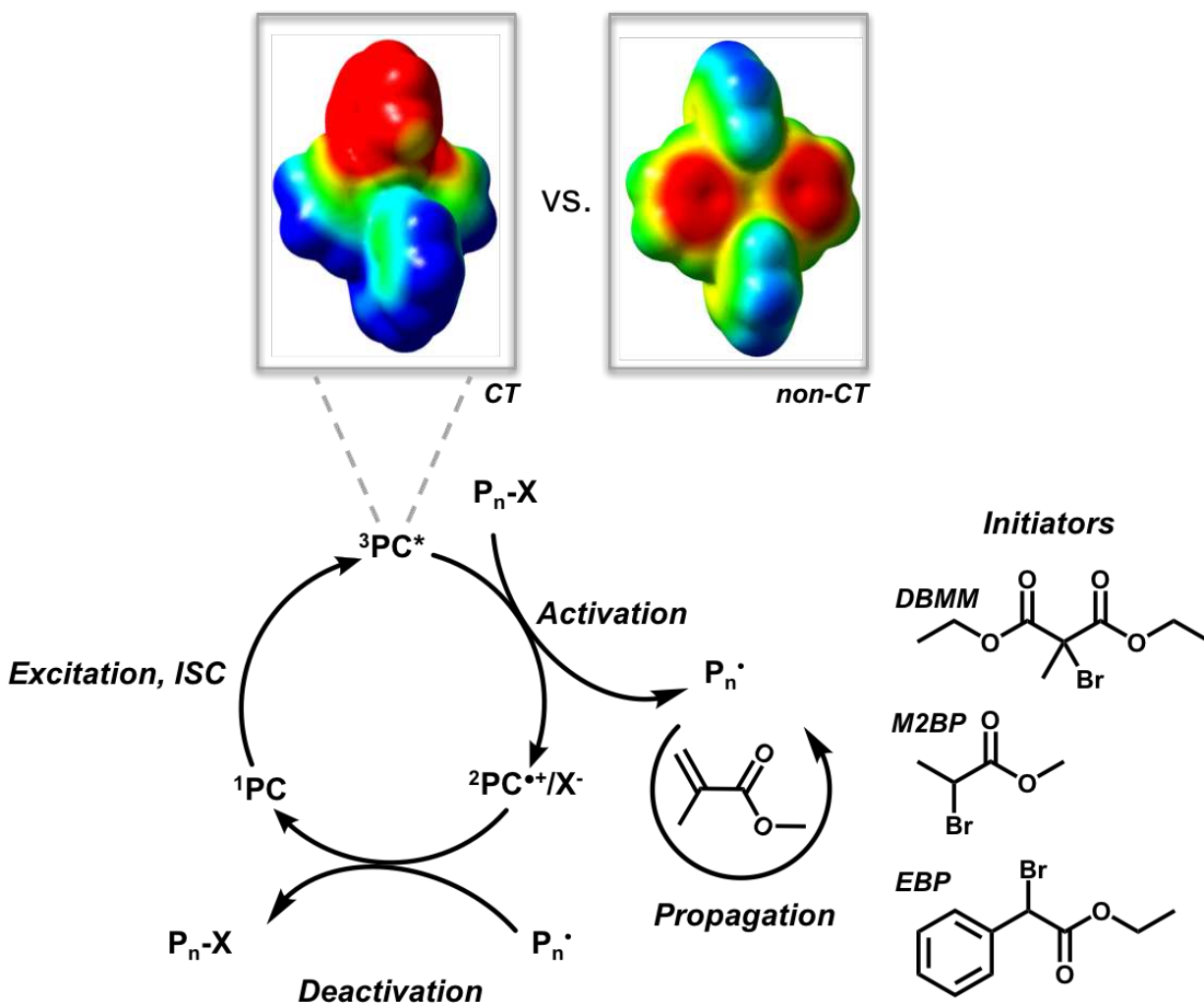


Figure 4.1. The proposed mechanism of O-ATRP, with computed electrostatic potential (ESP)-mapped electron density for the two different classifications of $^3\text{PC}^*$: charge transfer (CT) and non-charge transfer (bottom left). In the CT excited state, intramolecular electron transfer occurs from the phenazine core to the *N*-aryl substituent, while in the non-CT excited state, the electron

density of the promoted electron remains on the electron rich phenazine core (top). "Red" identifies the electron rich region while "blue" signifies the electron poor region. The different alkyl bromide initiators used in this study: DBMM, M2BP, and EBP (right).

Our interest has focused upon *N,N*-diaryl dihydrophenazine PCs, which can produce polymer products with low D (< 1.10) in an efficient manner, as evidenced by high initiator efficiencies (I^*).^{35,36} Furthermore, our recent work has revealed the importance of the PC to access an intramolecular charge transfer (CT) state for efficient catalyst performance. *N,N*-diaryl dihydrophenazines are strongly reducing organic PCs that operate under visible light irradiation, possessing similar excited state reduction potentials to *fac*-[Ir(ppy)₃]. The nature of the redox-active excited state species can be tuned by selection of the *N*-aryl substituents, which determines the excited state reduction potential and ability to access an intramolecular CT state. By installation of *N*-aryl groups with extended conjugation or electron-withdrawing groups (EWG), the PC's lowest energy excited states possess CT character, where the excited electron is intramolecularly transferred from the electron rich phenazine core of the PC (HOMO of the PC molecule) to the π^* orbital of the *N*-aryl substituent (LUMO of the PC molecule); HOMO = highest occupied molecular orbital, LUMO = lowest unoccupied molecular orbital. Conversely, use of electron donating groups (EDG) prevents access to this CT state, and both the HOMO and LUMO are localized on the central phenazine core. Herein, we report our continued investigation into the nature of the CT state of *N,N*-diaryl dihydrophenazines and the effect of the reaction conditions on catalyst performance. Facile syntheses of both CT and non-CT classifications of *N,N*-diaryl dihydrophenazines by *N*-aryl group selection allows the exploration of two key hypotheses: 1) CT

is a necessary process to achieve high PC performance, and 2) due to the ionic nature of a CT PC, reaction medium polarity plays a significant role in catalysis from CT vs. non-CT PCs.

Results and Discussion

To test these two hypotheses, four non-CT and five CT PCs were employed in the O-ATRP of MMA (Figure 4.2). Of the nine PCs, **3**, **4**, **8**, and **9** have not been previously employed in O-ATRP. The triplet energies (E_{triplet}) and excited state reduction potentials of ${}^3\text{PC}^*$ [$E^0({}^2\text{PC}^{*+}/{}^3\text{PC}^*)$], and the oxidation potential of ${}^2\text{PC}^{*+}$ [$E^0({}^2\text{PC}^{*+}/{}^1\text{PC})$] were evaluated with density functional theory (DFT) calculations and corroborated experimentally (See Experimental Section). DFT values in Figure 2 were computed at the improved M06/6-311+G(d,p)//M06/6-31+G(d,p) level of theory; previously reported values for PCs **1**, **2**, **5**, **6**, and **7** were computed at the M06/6-31+G(d,p) level of theory. The improved method resulted in $E^0({}^2\text{PC}^{*+}/{}^1\text{PC})$ predictions that are closer to experimental values. From these data, it can be determined that PCs **1-9** all have high triplet energies (< 2.5 eV), sufficiently reducing ${}^3\text{PC}^*$ states ($E^0({}^2\text{PC}^{*+}/{}^3\text{PC}^*) \sim -2$ V vs. SCE), and sufficiently oxidizing ${}^2\text{PC}^{*+}$ states ($E^0({}^2\text{PC}^{*+}/{}^1\text{PC}) \sim 0.1$ V vs. SCE) to operate a successful O-ATRP. What most strongly differentiates these catalysts is that the ${}^3\text{PC}^*$ state of PCs **1-4** fall under the non-CT classification, while the lowest energy ${}^3\text{PC}^*$ states of **5-9** are computed to be CT states. Our results indicate that PCs **5-9**, which possess CT excited states, show much better O-ATRP performance than the non-CT PCs **1-4**, and are more robust in carrying out O-ATRP across solvents of low and high polarities (*vide infra*).

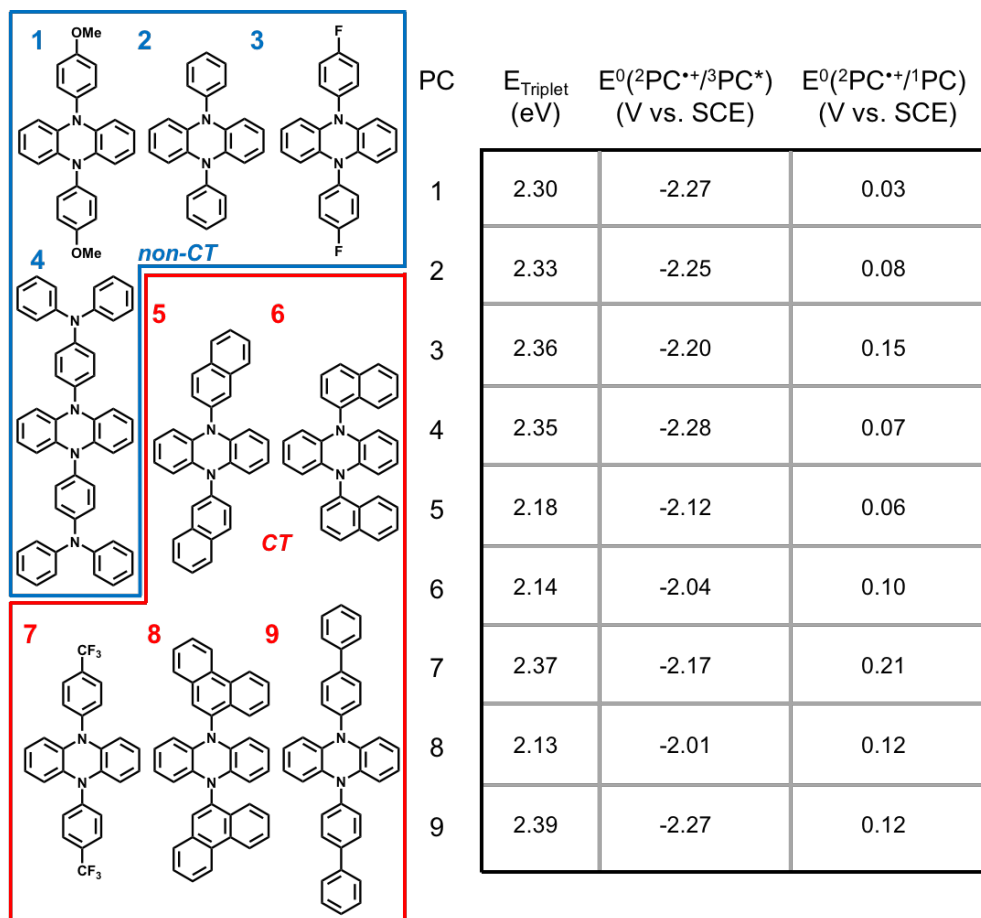


Figure 4.2. The PCs used in this study and their computed photophysical properties, calculated at the M06/6-311+G(d,p)//M06/6-31+G(d,p) level of theory

To visualize the presence of excited state CT character for the different PCs, the electrostatic potential (ESP)-mapped electron densities were generated for the ground state ^1PC and triplet excited state $^3\text{PC}^*$ (Figure 4.3). PCs 1-4 do not exhibit CT character in $^3\text{PC}^*$, as can be seen by the lack of dipole moment (μ) in $^3\text{PC}^*$ and no significant change of μ from ^1PC to $^3\text{PC}^*$. For PCs 5-9, significant polarization is observed in their $^3\text{PC}^*$ states as the presence of large μ , significant change of μ from ^1PC to $^3\text{PC}^*$, and localization of electron density (red) to one of the *N*-aryl substituents.

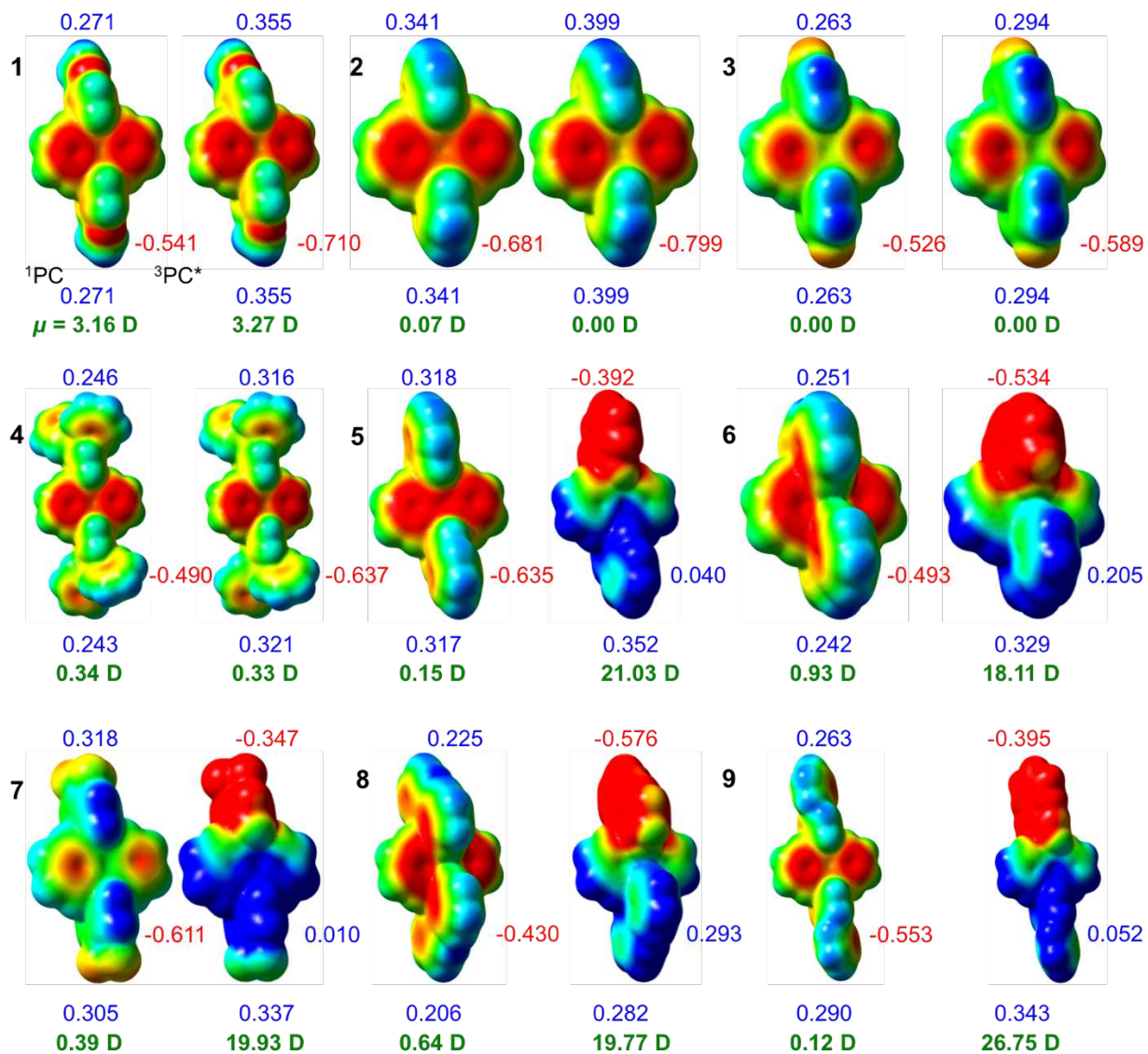


Figure 4.3. ESP-mapped electron density of the ground states (¹PC) and triplet (³PC*) excited states of *N,N*-diaryl dihydrophenazine PCs **1-9** used in this study. ESP-derived charges, in units of electron charge, of *N*-aryl substituents (top and bottom) and phenazine core (center) are displayed, along with dipole moments (μ) in units of Debye (D) shown as green text.

Initial screening of potential catalysts *via* DFT calculation of the character of the ³PC* states greatly accelerates the rate at which promising candidates can be identified, synthesized, and

used in O-ATRP. As examples, PCs **6** and **8** are predicted to have spatially separated singly occupied molecular orbitals (SOMO) in their triplet states (Figure 4.4E, F) and thus are expected to exhibit CT character in their lowest excited states; in contrast, PC **1**'s localized SOMO (Figure 4.4D) suggests that it possesses non-CT character in its lowest excited state.

The computed CT and non-CT nature of the PCs' excited states are corroborated experimentally by comparison of the absorption and emission spectra (Figure 4.4 A-C). For representative CT PCs **6** and **8**, a large Stokes shift and broad, featureless emission spectrum are features of a molecule in a CT state (Figure 4.4B, C).^{36,40} These characteristics are also observed for the other PCs possessing $^3\text{PC}^*$ states with CT character (see Supporting Information). In contrast, for non-CT PC **1** a small Stokes shift and narrow emission spectrum with defined features are observed (Figure 4.4A), as was also observed with the other non-CT PCs (see Experimental). Interestingly, PC **8** exhibits two emission peaks. A broad, featureless and red-shifted peak at ~ 650 nm was assigned as emission from the CT state. In addition, another blue-shifted peak at ~ 450 nm has rather sharp emission features similar to PC **1** and was attributed to emission from a non-CT local singlet state. The emission profile of PC **8** suggests that after initial photon absorption, PC **8**'s singlet excited state partitions into both the non-CT local state and a lower energy CT state.

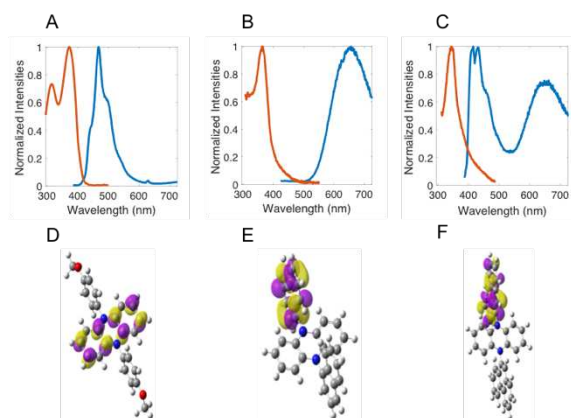


Figure 4.4. The overlaid absorption (red) and emission (blue) spectra for PCs **1** (A), **6** (B), and **8** (C). The high lying SOMOs of the triplet excited states of PCs **6** (D), **8** (E), and **1** (F) (bottom); SOMO = singly occupied molecular orbital.

To determine if CT is truly necessary for a successful O-ATRP, PCs **1-9** were employed for the polymerization of MMA with ethyl α -bromophenylacetate (EBP) initiator in *N,N*-dimethylacetamide (DMA) (Table 4.1). For non-CT PCs **1-4**, \bar{D} is consistently high (> 1.40), indicating a lower degree of control. Alternatively, for the CT PCs **5-9** the \bar{D} is significantly lower (< 1.30) and the I^* are improved as compared to their non-CT counterparts **1-4**. This indicates that CT PCs are superior in O-ATRP, and supports the hypothesis that CT PCs are efficient and superior at mediating this polymerization methodology.

Table 4.1. Polymerization Results for the O-ATRP of MMA in DMA.^a

Trial	PC	Conv. (%) ^b	M_n (kDa) ^c	M_w (kDa) ^c	\bar{D} (M_w/M_n) ^c	I^* (%) ^d
1	1	69.6	24.7	36.3	1.57	29.2
2	2	85.9	11.9	18.4	1.55	74.5
3	3	77.5	16.4	27.4	1.67	48.7
4	4	82.3	18.9	32.6	1.72	44.7
5	5	87.1	22.6	26.4	1.17	39.7
6	6	93.1	13.3	14.5	1.09	71.9
7	7	98.4	15.3	17.9	1.17	65.9
8	8	59.0	7.48	9.27	1.24	80.8
9	9	90.0	13.0	15.8	1.22	71.0

^aPolymerizations were performed with 1.00 mL MMA (9.35 mmol, 1000 eq), 16.4 μ L EBP (93.5 μ mol, 10 eq), 3.12-6.26 mg of PC (9.35 μ mol, 1 eq), 1.00 mL DMA, and irradiated by white LEDs for 8 h. Polymerization stoichiometry: [MMA]:[EBP]:[PC] 1000:10:1. ^b% Conversion measured by ¹H NMR. ^cMeasured using GPC-MALS. ^dInitiator efficiency (I^*) calculated from theo. M_n /exp. M_n .

With strong support for the general condition that ³PC* possess CT character as a necessary property for PCs to realize optimized O-ATRP, this defining classification was further explored in solvents of lower polarity. Previous results for the polymerization of MMA in a mixed DMA/THF solvent system indicated that operating in an overall lower solution polarity benefited the performance of CT PC **6**.³⁶ Based on these results, O-ATRP mediated by PCs **1** – **9** was performed in solvents of lower polarity than DMA, with otherwise identical conditions (Figure 4.5). Ethyl acetate, THF, dioxane, benzene, and hexanes were selected based on their value on the $E_T(30)$ scale of solvent polarity, defined as the molar electronic transition energy (E_T , kcal/mol) for a negatively solvatochromic charge transfer dye.⁴¹ Using this value, as opposed to the static dielectric constant (ϵ), accounts for the various effects of solvent on the reaction medium, as this value accounts for more possible medium effects, such as solute/solvent or solvent/solvent interactions.⁴² The selected solvents provide a wide range of polarities from 31.0 kcal/mol (hexanes) to 42.9 kcal/mol (DMA). CT PCs are polar in their photoexcited state and thus are affected by changes in the polarity of their surrounding environment^{43,44,45}, as evidenced by a large solvatochromic effect in their emission spectra.³⁶ Because of the CT character, the $E_T(30)$ value of the solvent may have an effect on PC performance in O-ATRP. Notably, PC **6** was previously shown to exhibit solvatochromic shifts in emission.

This observation suggests that the driving force to access the CT excited state is strong (as opposed to a local transition) that a polar solvent is not required for its formation, although polar solvents more significantly stabilize the CT state. As such, *N,N*-diaryl dihydrophenazines CT ³PC*s retain their CT character in solvents of varying polarities, although we questioned how this would affect their ability to mediate polymerizations over a wider window of solvent polarities.

Investigation of O-ATRP using PCs **1-9** in ethyl acetate, THF, dioxane, benzene, and hexanes, under otherwise identical conditions, revealed that all *N,N*-diaryl dihydrophenazines broadly perform moderately well in THF (Figure 4.5). However, all 4 non-CT PCs do not achieve high monomer conversions in the other solvents tested. The lowest \mathcal{D} for PCs **1-4** were obtained in THF, ranging from 1.24 to 1.35. For PCs **5-9**, higher monomer conversions are obtained in nearly all conditions, with the exception of PCs **5** and **9** in nonpolar hexanes. Excitingly, when ethyl acetate is used as the solvent, CT PCs **6-9** consistently produced polymer product of $\mathcal{D} \sim 1.10$. Evaluation of these data revealed polymerizations carried out in ethyl acetate for CT PCs produced polymer possessing a very low \mathcal{D} under standardized conditions. It is also noteworthy that ethyl acetate is considered a green solvent.^{46,47}

Photocatalyst	Hexanes	Benzene	Dioxane	Tetrahydrofuran	Ethyl Acetate
	$E_T(30) = 31.0$ (kcal mol ⁻¹)	$E_T(30) = 34.3$ (kcal mol ⁻¹)	$E_T(30) = 36.0$ (kcal mol ⁻¹)	$E_T(30) = 37.4$ (kcal mol ⁻¹)	$E_T(30) = 38.1$ (kcal mol ⁻¹)
non-Charge Transfer					
1 $\mu = 3.27$	Conv < 10 %	Conv < 10 %	Conv < 10 %	Conv: 34.5 % M_n : 7.61 M_w : 10.1 I^* : 46.4 % D : 1.32	Conv < 10 %
2 $\mu = 0.00$	Conv < 10 %	Conv < 10 %	Conv < 10 %	Conv: 38.3 % M_n : 7.68 M_w : 9.49 I^* : 51.1 % D : 1.24	Conv < 10 %
3 $\mu = 0.00$	Conv: 16.0 % M_n : 14.2 M_w : 21.1 I^* : 13.0 % D : 1.49	Conv: 13.0 % M_n : 5.8 M_w : 8.4 I^* : 26.7 % D : 1.45	Conv: 13.4 % M_n : 8.32 M_w : 9.23 I^* : 16.4 % D : 1.11	Conv: 33.2 % M_n : 5.31 M_w : 7.15 I^* : 64.0 % D : 1.35	Conv < 10 %
4 $\mu = 0.33$	Conv < 10 %	Conv < 10 %	Conv < 10 %	Conv: 32.2 % M_n : 6.13 M_w : 7.85 I^* : 53.8 % D : 1.28	Conv < 10 %
Charge Transfer					
5 $\mu = 21.03$	Conv < 10 %	Conv: 39.4 % M_n : 8.88 M_w : 9.32 I^* : 47.1 % D : 1.05	Conv: 30.8 % M_n : 6.58 M_w : 7.39 I^* : 47.9 % D : 1.12	Conv: 62.6 % M_n : 8.10 M_w : 8.90 I^* : 79.2 % D : 1.10	Conv: 18.9 % M_n : 6.49 M_w : 9.09 I^* : 29.8 % D : 1.40
6 $\mu = 18.11$	Conv: 15.8 % M_n : 5.28 M_w : 7.69 I^* : 30.7 % D : 1.46	Conv: 42.3 % M_n : 8.34 M_w : 8.73 I^* : 52.0 % D : 1.05	Conv: 39.4 % M_n : 8.87 M_w : 9.43 I^* : 45.5 % D : 1.06	Conv: 67.8 % M_n : 11.4 M_w : 11.9 I^* : 60.9 % D : 1.04	Conv: 25.5 % M_n : 6.30 M_w : 6.60 I^* : 41.5 % D : 1.05
7 $\mu = 19.93$	Conv: 17.0 % M_n : 4.30 M_w : 4.77 I^* : 40.5 % D : 1.11	Conv: 41.0 % M_n : 7.85 M_w : 8.40 I^* : 53.5 % D : 1.07	Conv: 26.4 % M_n : 6.09 M_w : 6.79 I^* : 44.4 % D : 1.11	Conv: 87.0 % M_n : 12.7 M_w : 14.4 I^* : 70.2 % D : 1.13	Conv: 26.5 % M_n : 5.81 M_w : 6.25 I^* : 49.8 % D : 1.08
8 $\mu = 19.77$	Conv: 61.4 % M_n : 8.90 M_w : 9.68 I^* : 71.7 % D : 1.09	Conv: 72.7 % M_n : 14.3 M_w : 15.0 I^* : 52.7 % D : 1.05	Conv: 40.8 % M_n : 6.34 M_w : 7.47 I^* : 65.9 % D : 1.18	Conv: 83.9 % M_n : 9.86 M_w : 10.6 I^* : 87.2 % D : 1.07	Conv: 62.4 % M_n : 10.9 M_w : 11.3 I^* : 59.6 % D : 1.04
9 $\mu = 26.75$	Conv: < 10 %	Conv: 14.0 % M_n : 6.61 M_w : 10.9 I^* : 21.7 % D : 1.65	Conv: 13.3 % M_n : 7.03 M_w : 7.96 I^* : 19.4 % D : 1.13	Conv: 64.0 % M_n : 10.7 M_w : 11.8 I^* : 61.3 % D : 1.10	Conv: 39.4 % M_n : 7.55 M_w : 7.93 I^* : 55.4 % D : 1.05

Figure 4.5. Polymerization data from O-ATRP using the 9 different PCs (vertical, μ = dipole moment of the ³PC*) in solvents with various $E_T(30)$, horizontal. All polymerizations were

conducted for 8 h, 1.00 mL solvent, 1.00 mL MMA (9.35 mmol, 1000 eq), 16.4 μ L EBP (93.5 μ mol, 10 eq), and 3.12-6.26 mg (9.35 μ mol, 1 eq) depending on the PC used.

As such, this solvent was chosen for further exploration with PCs possessing CT $^3\text{PC}^*$ states. First, the PCs were tested in ethyl acetate with different common O-ATRP initiators, methyl 2-bromopropionate (M2BP), diethyl 2-bromo-2-methylmalonate (DBMM), and methyl α -bromoisobutyrate (MBIB) (Table 4.2 and see Supporting Info). For PCs **5-9**, changing the initiator from ethyl α -bromophenylacetate (EBP) to methyl 2-bromopropionate (M2BP) or diethyl 2-bromo-2-methylmalonate (DBMM) allowed for the production of polymer products having remarkably low \bar{D} (< 1.10). Additionally, the I^* remained high, producing polymers of MW close to the theoretical value. These optimizations were successful in realizing closely similar outcomes for 5 different catalysts to produce polymers with low \bar{D} through achieving high I^* in the polymerization of MMA. Different ATRP catalysts commonly require selectively tuned experimental conditions to operate a controlled polymerization,⁴⁸ and these data represent the advantages and robustness of using *N,N*-diaryl dihydrophenazines capable of accessing CT in their lowest energy excited states, in contrast to the non-CT derivatives.

Table 4.2. Polymerization results of the O-ATRP of MMA using CT PCs in Ethyl Acetate.^a

Trial	PC	Initiator	Conv. (%) ^b	M_n (kDa) ^c	M_w (kDa) ^c	\bar{D} (M_w/M_n) ^c	I^* (%) ^d
10	5	M2BP	84.2	9.12	9.75	1.07	93.9
11	6	DBMM	69.3	8.44	8.72	1.03	84.2
12	6	M2BP	68.3	9.60	9.91	1.03	72.3
13	7	DBMM	77.8	8.57	9.57	1.12	93.0
14	7	M2BP	74.2	7.64	9.11	1.19	98.7
15	8	DBMM	77.2	9.47	9.79	1.03	83.6
16	8	M2BP	85.6	10.1	10.7	1.06	86.2
17	9	DBMM	76.9	9.44	10.0	1.06	83.6
18	9	M2BP	83.5	8.27	9.50	1.15	102.6

^aPolymerizations were performed with 1.00 mL MMA (9.35 mmol, 1000 eq), 16.4 μ L EBP (93.5 μ mol, 10 eq), 4.00-5.00 mg of PC (9.35 μ mol, 1 eq), 1.00 mL ethyl acetate, and irradiated by white LEDs for 20 h. Polymerization stoichiometry: [MMA]:[I]:[PC] 1000:10:1. ^b% Conversion from ¹H NMR. ^cMeasured using GPC-MALS. ^dInitiator efficiency (I^*) calculated from theo. M_n /exp. M_n .

A more detailed investigation of the performance of PCs **5-9** in ethyl acetate revealed that these PCs can consistently maintain control over the polymerization of MMA under nearly identical conditions. Time-point aliquots were taken during the course of polymerization and plots of M_n and \bar{D} as a function of monomer conversion were produced (Figure 4.6). For polymerization using PCs **5-9**, a linear increase in M_n was observed with monomer conversion, with consistently

low \bar{D} during the course of polymerization (< 1.20). The ability of these five catalysts to affect the linear growth of M_n as a function of monomer conversion while maintaining low \bar{D} supports the principle that for N,N -diaryl dihydrophenazines, the ability to access CT in the lowest excited states is a defining characteristic for high PC performance in O-ATRP. Further, these data reveal solution polarity has a stronger influence over the performance of non-CT versus CT PCs, as CT PCs can tolerate a wider range of solvent polarities and are more robust to varied experimental conditions. These experiments also revealed that ethyl acetate serves as an excellent solvent for O-ATRP catalyzed by CT dihydrophenazines, providing the most consistently low \bar{D} and high I^* for 5 different catalysts (PCs 5-9) under nearly identical experimental conditions.

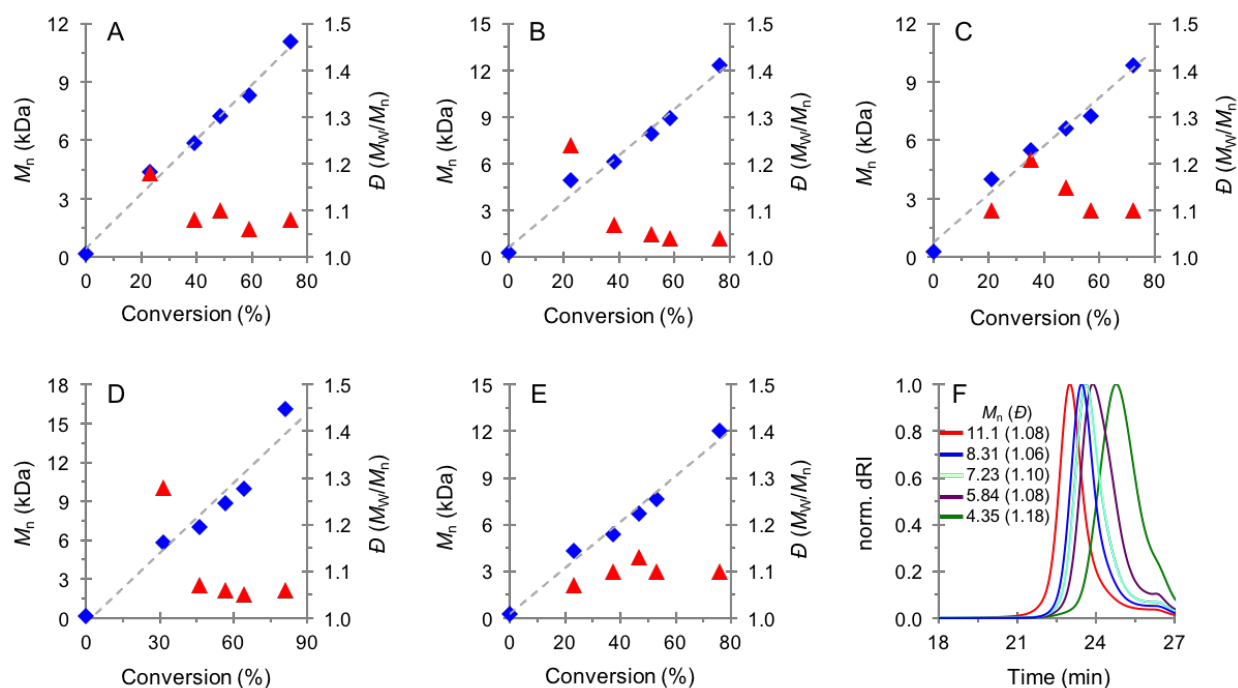


Figure 4.6. Plots of M_n (blue, diamonds) and \bar{D} (red, triangles) as a function of monomer conversion for PCs 5 (A), 6 (B), 7 (C), 8 (D), 9 (E), and the associated GPC traces for PC 5 (F). Conditions: 1.00 mL ethyl acetate, 1.00 mL MMA (9.35 mmol, 1000 eq), 10.4 μ L M2BP (93.5

μmol , 10 eq, PCs **5** and **8**) 17.9 μL DBMM (93.5 μmol , 10 eq, PCs **6,7**, and **9**), 4.00-5.00 mg PC (9.35 μmol , 1 eq, varies with PC).

These improved results in polymerization can be understood in context of the two main effects a solution of lower polarity is likely to provide: 1) a less stabilized CT state and thus a more reducing $^3\text{PC}^*$ for more efficient activation, and 2) formation of a strong $^2\text{PC}^{+\cdot}/\text{Br}^-$ ion pair for efficient deactivation. Given the good control over the O-ATRP reaction in ethyl acetate, we hypothesize that the effect of point 2 must be greater than the effect of point 1, that facile deactivation results in the synthesis of polymer with consistently low \bar{D} and high I^* .

Conclusions

Intramolecular charge transfer in the lowest energy excited state has been shown to be a key design principle for *N,N*-diaryl dihydrophenazines catalysts to achieve optimized performance in O-ATRP. By evaluating the performance of new PCs alongside previously explored candidates, the CT classification produces polymer product of very low \bar{D} (< 1.10) through achieving a high I^* , while the non-CT PCs typically produce polymers possessing a high \bar{D} (> 1.30) and achieve a low I^* . Additionally, changes in solvent polarity were found to affect CT and non-CT PCs differently, with CT PCs operating O-ATRP in a much wider solvent polarity window than their non-CT counterparts. Through screening the polymerizations in solvents of lower polarity, ethyl acetate was found to be a solvent in which five different CT PCs operated a highly controlled O-ATRP, as evidenced through the linear growth in M_n with monomer conversion, and low \bar{D} throughout polymerization.

Experimental

General Information

Reagents were purchased from Sigma-Aldrich. Monomers and solvents used in polymerizations: methyl methacrylate (MMA), dimethylacetamide (DMA), ethyl acetate (EtOAc), tetrahydrofuran (THF), dioxane, benzene, hexanes. DMA and MMA were dried over CaH_2 , purified by vacuum distillation, and degassed by three freeze-pump-thaw cycles or 20 minutes of N_2 sparging before storage and subsequent use in a N_2 glovebox. THF, dioxane, benzene, and hexanes were obtained from a Mbraun solvent system and used without further treatment. EtOAc used as received, in a SureSeal bottle. Monomers were stored at $-34\text{ }^\circ\text{C}$ in the glovebox freezer and allowed to warm to room temperature before use in polymerizations.

Alkyl halide initiators used in polymerizations: methyl 2-bromopropionate (M2BP), diethyl 2-bromo-2-methylmalonate (DBMM), and ethyl α -bromophenylacetate (EBP) were purified by vacuum distillation and degassed by three freeze-pump-thaw cycles before storage and subsequent use in a N_2 glovebox. Initiators were stored at $-34\text{ }^\circ\text{C}$ in the glovebox freezer and allowed to warm to room temperature before use in polymerizations.

The reagents used to synthesize the photocatalysts: 2-Dicyclohexylphosphino-2,6-diisopropoxybiphenyl (RuPhos) and Chloro-(2-Dicyclohexylphosphino-2,6-diisopropoxy-1,1-biphenyl) [2-(2-aminoethyl)phenyl] palladium(II) – methyl-t-butyl ether adduct (RuPhos precatalyst, 1st generation) were stored and used in N_2 glovebox. All other reagents were used as received from the supplier and used directly without further treatment.

Photoreactors were composed of white LEDs (16-inch strip, double-density white LEDs), purchased from Creative Lighting Solutions (item no. CL-FRS1210-5M-12V-WH), wrapped inside of a 400mL beaker lined with aluminum foil.

^1H , ^{13}C , and ^{19}F NMR spectroscopy were obtained from either a Varian INOVA 400 MHz, 500 MHz, or Bruker 300MHz spectrometer, as reported. Chemical shifts referenced to an internal solvent resonance as parts-per-million (ppm) relative to tetramethylsilane. Polymer molecular weights were obtained *via* gel permeation chromatography (GPC) coupled with multi-angle light scattering (MALS), using an Agilent HPLC fitted with one guard column and three PLgel 5 μm MIXED-C gel permeation columns, a Wyatt Technology TrEX differential refractometer, and a Wyatt Technology miniDAWN TREOS light scattering detector, using THF as the eluent at a flow rate of 1.0mL/min. Ultraviolet-visible spectroscopy (UV-Vis) was performed on an Agilent spectrophotometer using DMF or DMA as the solvent. Emission spectroscopy was performed on a SLM 8000C spectrofluorimeter using DMF or DMA as the solvent; samples sparged with argon for 15 minutes prior to data acquisition. Electrospray Ionization Mass Spectrometry (ESI-MS) and was performed at the University of Colorado-Boulder Central Analytical Mass Spectrometry Facility on a Waters Synapt G2 HDMS Qtof with MeCN as the solvent.

Procedures

Typical Polymerization Procedure

A 20 mL scintillation vial with a non-metal lined cap was charged with a small stirbar and PC **6** (~4.00 mg, 9.35 μmol , 1 eq), and transferred to a N_2 glovebox. Solvent (1.00 mL EtOAc), monomer (1.00 mL, 9.35 mmol, 1000 eq), and M2BP (10.4 μL , 93.5 μmol , 10 eq) were added sequentially *via* pipette for solvent and monomer, while initiator was added by a 25 μL Hamilton syringe. The vial was sealed and placed into the beaker (with white LEDs) and stirred for 22 hrs. To track the progression of the polymerization by % conversion, 0.1mL aliquots were removed *via* syringe and injected into a sealed vial containing 0.7 mL of CDCl_3 with 250 ppm butylated

hydroxytoluene (BHT) additive; at various timepoints. This timepoint sample was analyzed by ^1H NMR for % conversion, and then dried under reduced pressure to remove solvent and volatiles. This dried sample was re-dissolved in spectral grade THF for analysis of M_w , M_n , and D by GPC coupled with MALS.

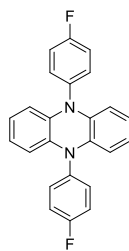
Control Experiments

Control experiments were reported in *Science* **352**, 1082-1086 (2016), and showed no controlled polymerization with the absence of any reaction components (*i.e.* light, catalyst, initiator), or in the presence of oxygen or TEMPO, as expected for a radical mechanism.

Catalyst Synthesis and Characterization

Syntheses for catalysts **1**, **2**, **5**, **6**, and **7** were previously described in *Science* **352**, 1082-1086 (2016).

5,10-di-*p*-fluorophenyl-5,10-dihydrophenazine (3):



*5,10-di-*p*-fluorophenyl-5,10-dihydrophenazine (3)* was synthesized using a modified literature procedure.¹ An oven-dried vacuum tube was charged with 5,10-dihydrophenazine (1.00 g, 5.50mmol, 1.00 eq.), *t*-BuONa (2.11 g, 22.0 mmol, 4.00 eq.), RuPhos (103 mg, 0.22 mmol, 0.04 eq.), RuPhos precatalyst (180 mg, 0.22 mmol, 0.04 eq.), 4-bromofluorobenzene (3.85 g, 22.0 mmol, 4.00 eq), and 11 mL dioxane. This flask was sealed under nitrogen and heated at 110 °C for 12 h. After cooling to room temperature, 200 mL CH_2Cl_2 and 200 mL H_2O was added to the

reaction flask, causing the product to precipitate. Filtration and washing with cold CH_2Cl_2 afforded the title compound as a light yellow powder (677 mg, 1.82 mmol, 33%). ^1H NMR (300 MHz, C_6D_6) δ 7.02 – 6.83 (m, 4H), 6.83 – 6.67 (m, 4H), 6.45 – 6.15 (m, 4H), 5.83 – 5.57 (m, 4H); ^{13}C NMR (75 MHz, C_6D_6) δ 162.3 (d, $^1J_{\text{C-F}} = 245$ Hz), 137.0, 136.3 (d, $^4J_{\text{C-F}} = 3$ Hz), 133.4, (d, $^3J_{\text{C-F}} = 8$ Hz), 121.6, 118.4 (d, $^2J_{\text{C-F}} = 23$ Hz), 113.1; ^{19}F NMR (282 MHz, C_6D_6) δ -112.84; HRMS (ESI): calcd. For $\text{C}_{24}\text{H}_{16}\text{F}_2\text{N}_2^+$ [M^+]: 370.1271. Found 370.1294.

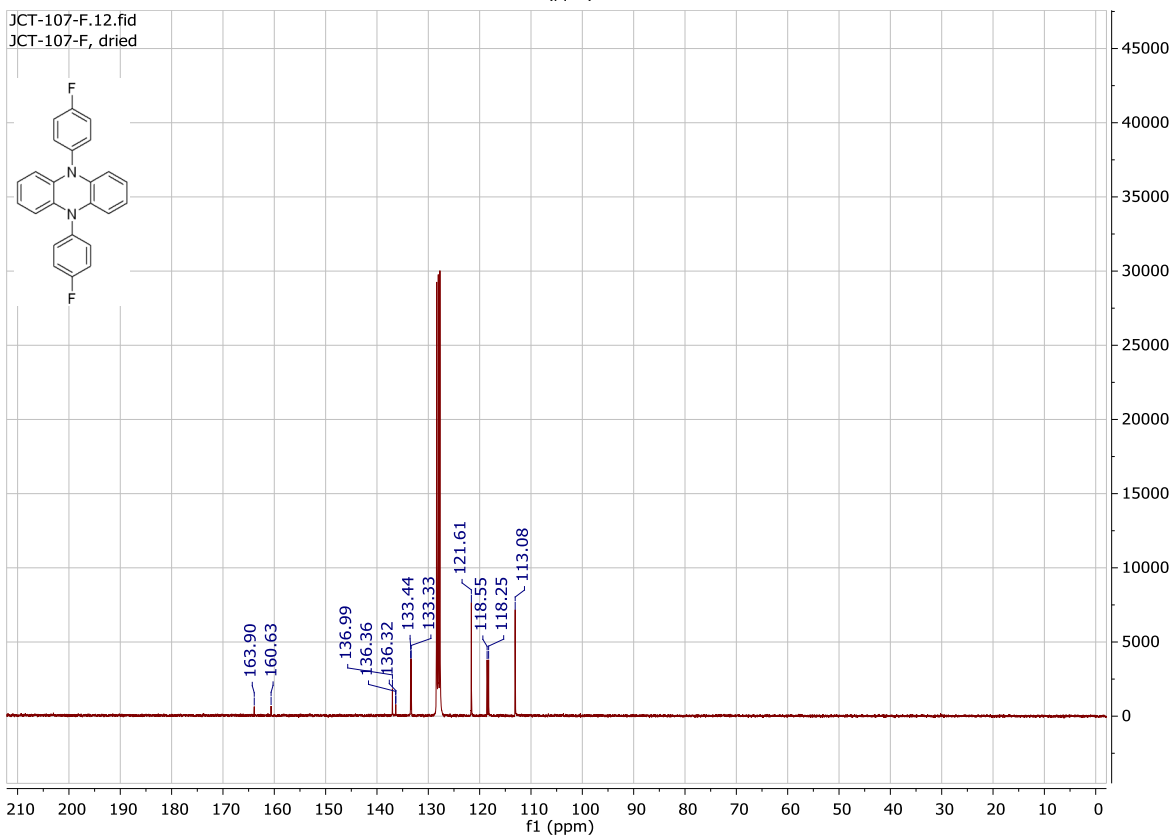
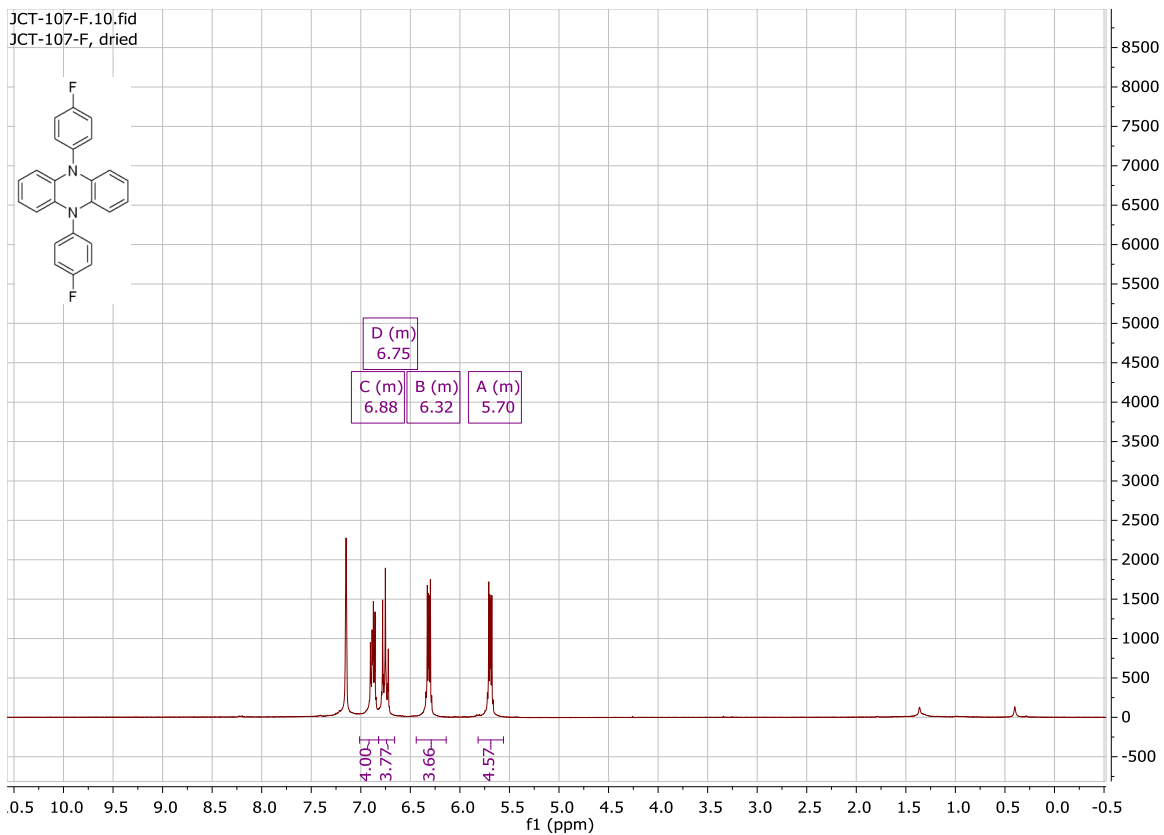


Figure 4.7 ^1H NMR (Top) and ^{13}C NMR (bottom) spectra for PC 3.

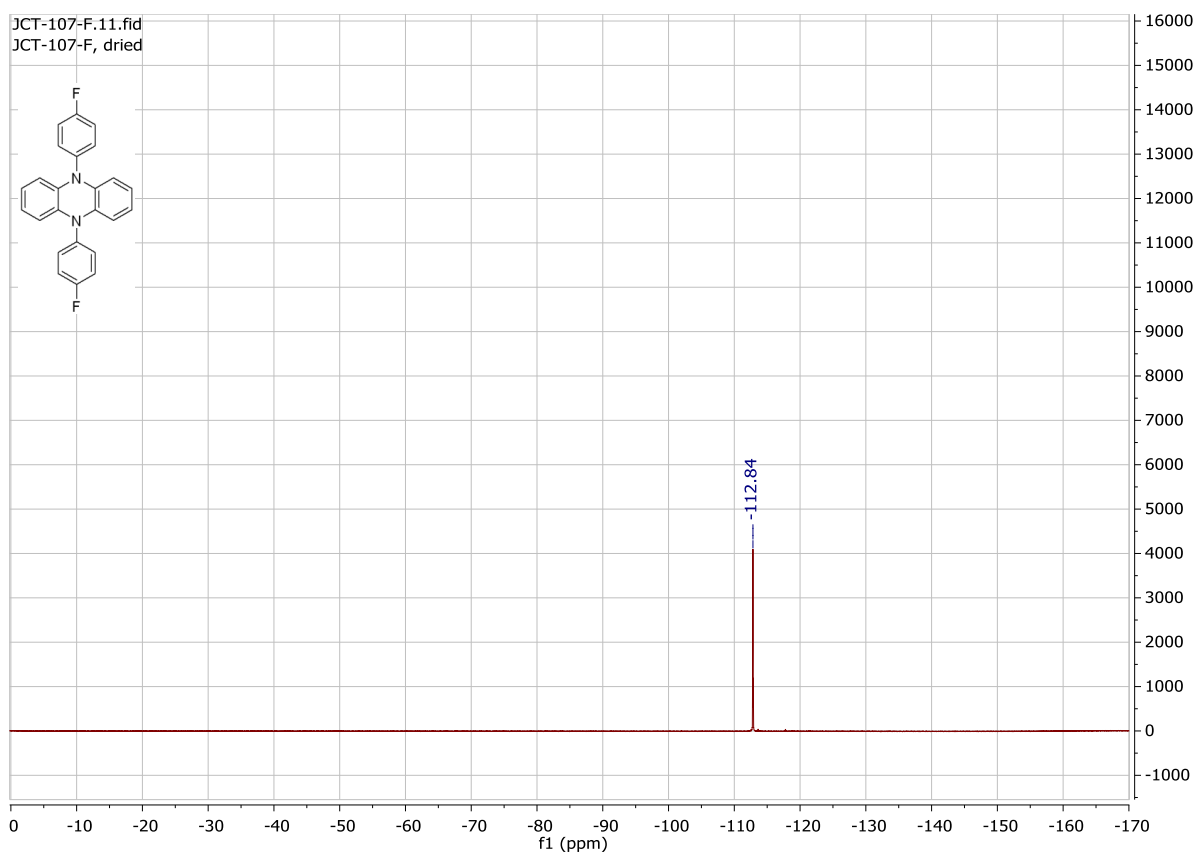
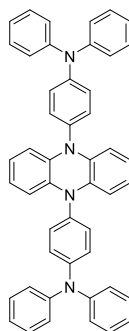


Figure 4.8 ^{19}F NMR of PC 3.

5,10-di-(p-diphenylaminophenyl)-5,10-dihydrophenazine (4):



5,10-di-(p-diphenylaminophenyl)-5,10-dihydrophenazine (4) was synthesized using a modified literature procedure.¹ An oven-dried vacuum tube was charged with 5,10-dihydrophenazine (728 mg, 4.00 mmol, 1.00 eq.), *t*-BuONa (1.54 g, 16.0 mmol, 4.00 eq.), RuPhos (75 mg, 0.16 mmol,

0.04 eq.), RuPhos precatalyst (131 mg, 0.16 mmol, 0.04 eq.), 4-bromotriphenylamine (5.16 g, 16.0 mmol, 4.00 eq), and 8 mL dioxane. This flask was sealed under nitrogen and heated at 110 °C for 12 h. After cooling to room temperature, 200 mL CH₂Cl₂ and 200 mL H₂O was added to the reaction flask, causing the product to precipitate. Filtration and washing with cold CH₂Cl₂ afforded the title compound as a light yellow powder (544 mg, 0.81 mmol, 20%). ¹H NMR (300 MHz, C₆D₆) δ 7.13 – 6.98 (m, 24H), 6.91 – 6.79 (m, 4H), 6.37 (dd, *J* = 5.9, 3.4 Hz, 4H), 6.04 (dd, *J* = 5.8, 3.4 Hz, 4H); ¹³C NMR (75 MHz, C₆D₆) δ 148.0, 147.9, 137.5, 134.1, 132.3, 129.8, 125.4, 125.3, 123.7, 121.5, 113.1. HRMS (ESI): calcd. For C₄₈H₃₆N₄⁺ [M⁺]: 668.2934. Found 668.2933.

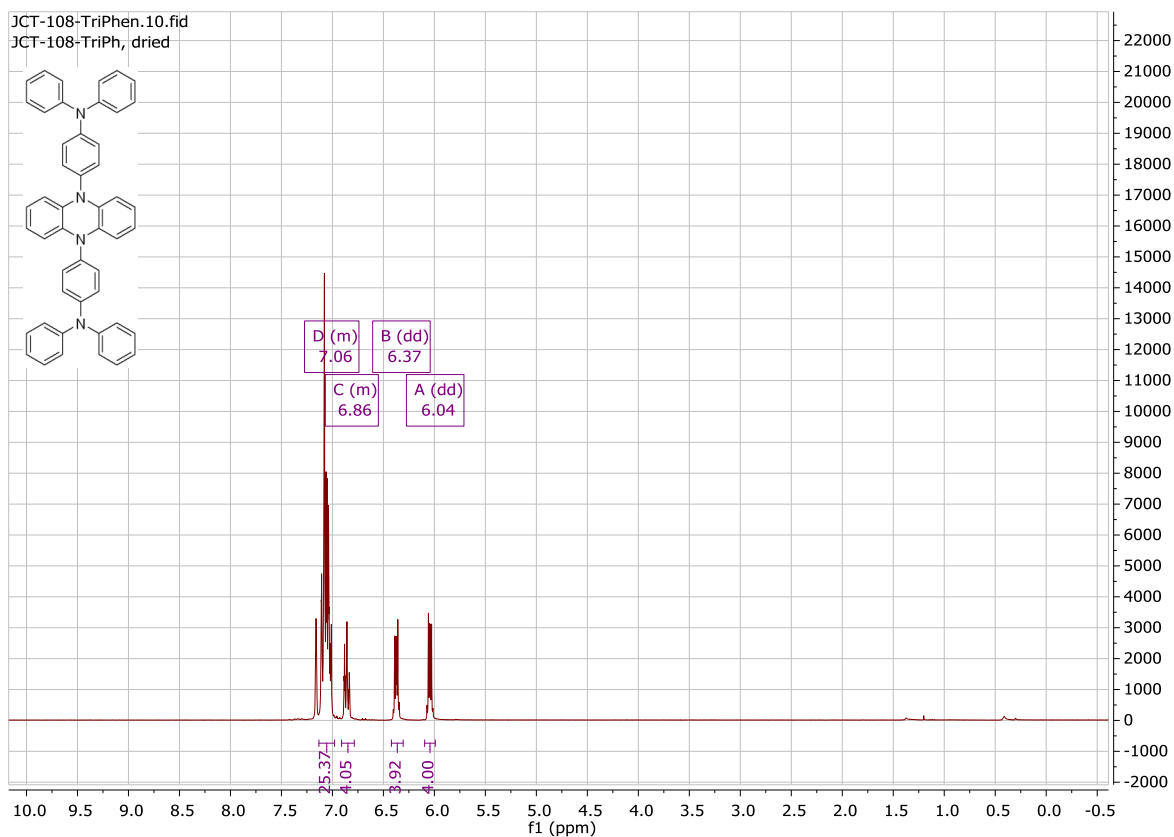


Figure 4.9 ¹H NMR spectra of PC 4.

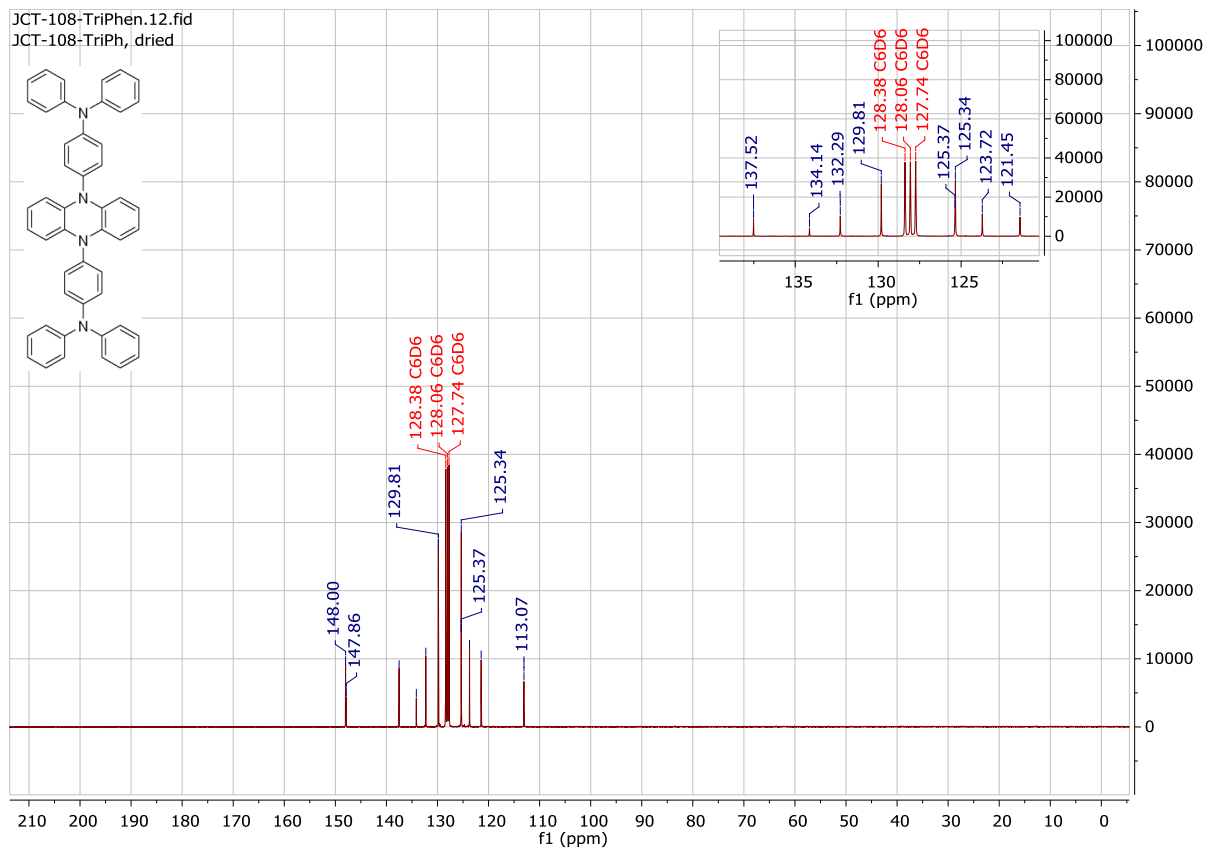
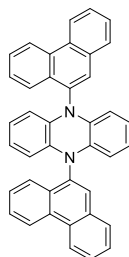


Figure 4.10 ^{13}C NMR spectra for PC 4.

5,10-di-9-phenanthryl-5,10-dihydrophenazine (8):



5,10-di-9-phenanthryl-5,10-dihydrophenazine (9) was synthesized using a modified literature procedure.¹ Under the N_2 atmosphere, a mixture of 5,10-dihydrophenazine (0.911 g, 5.0 mmol), 9-bromophenanthrene (5.14 g, 20.0 mmol), RuPhos (47 mg, 0.1 mmol), RuPhos precatalyst (82

mg, 0.1 mmol), *t*-BuONa (1.922 g, 20.0 mmol) and dioxane (10 mL) was heated at 110 °C for 2 d. The reaction mixture was cooled to rt and washed subsequently with methanol and acetone. The solid was recrystallized in benzene to give the product **9** as a yellow solid (82 mg, 3%). ¹H NMR (300 MHz, C₆D₆) δ 9.03 – 8.75 (m, 2H), 8.68 – 8.53 (m, 4H), 7.88 (d, *J* = 1.9 Hz, 2H), 7.74 – 7.63 (m, 2H), 7.56 – 7.42 (m, 8H), 6.15 (dd, *J* = 5.9, 3.4 Hz, 4H), 5.87 (ddd, *J* = 5.9, 4.2, 3.4 Hz, 4H); ¹³C NMR (126 MHz, C₆D₆) δ 132.9, 130.4, 129.0, 128.9, 127.9, 127.5, 127.4, 126.7, 123.6, 122.7, 124.7, 121.4, 113.1 (note: Due to the poor solubility and limited resolution of 2D NMR spectra, not all of the peaks of carbons are recognized); HRMS (ESI): calcd. For C₄₀H₂₆N₂⁺ [M⁺]: 534.2091. Found 534.2103.

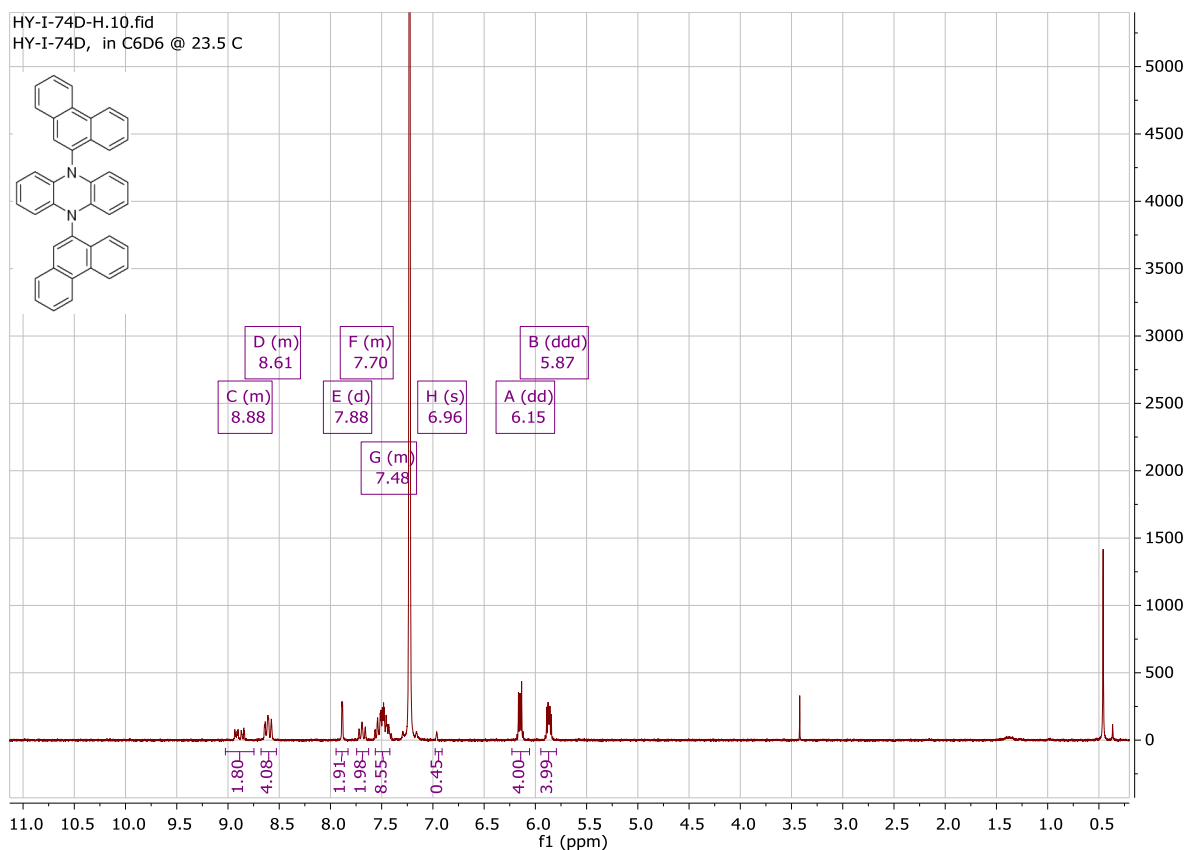


Figure 4.11 ¹H NMR spectra for PC **8**.

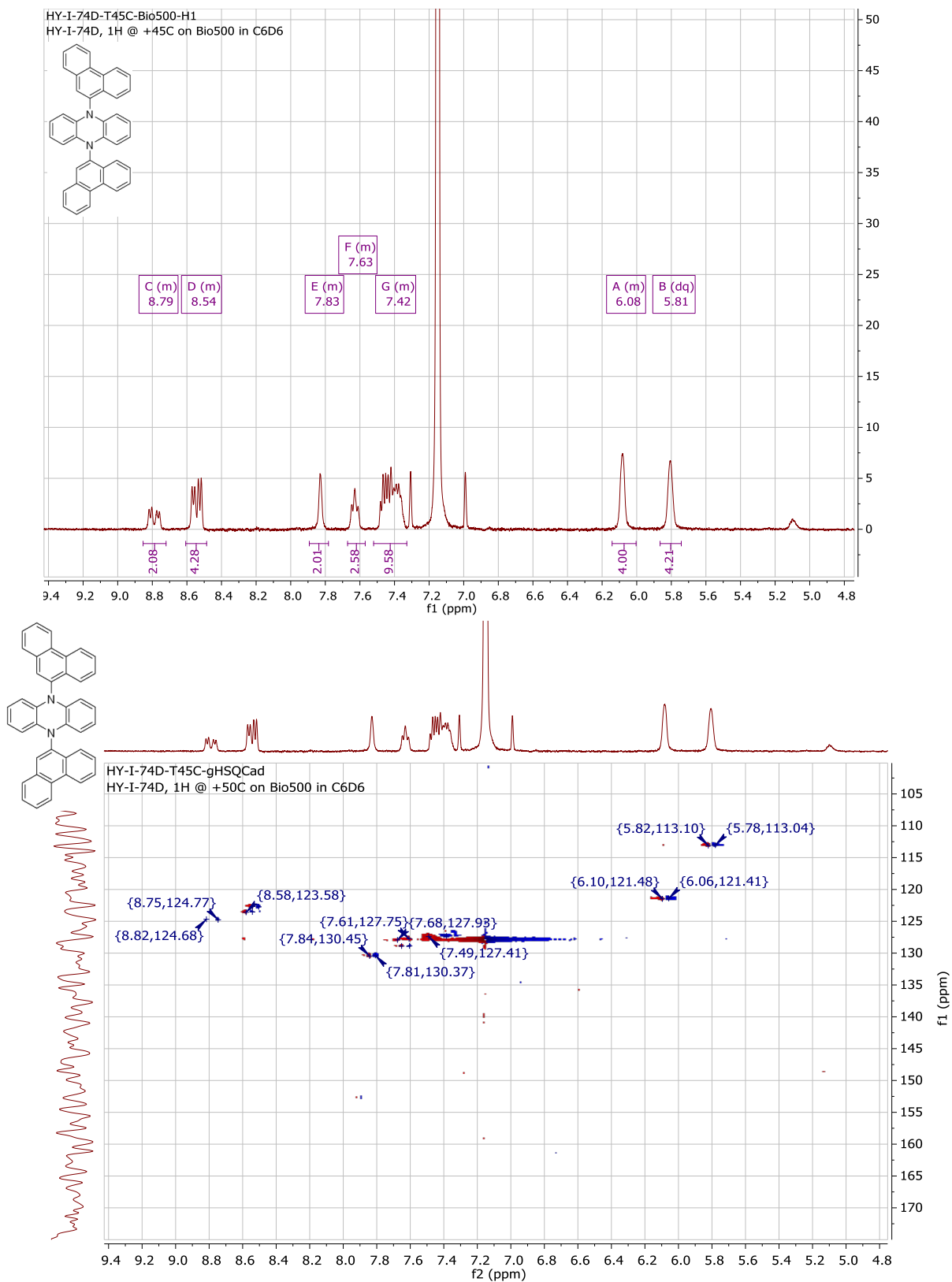


Figure 4.12 ^1H NMR (top) and HSQC (bottom) NMR for PC 8.

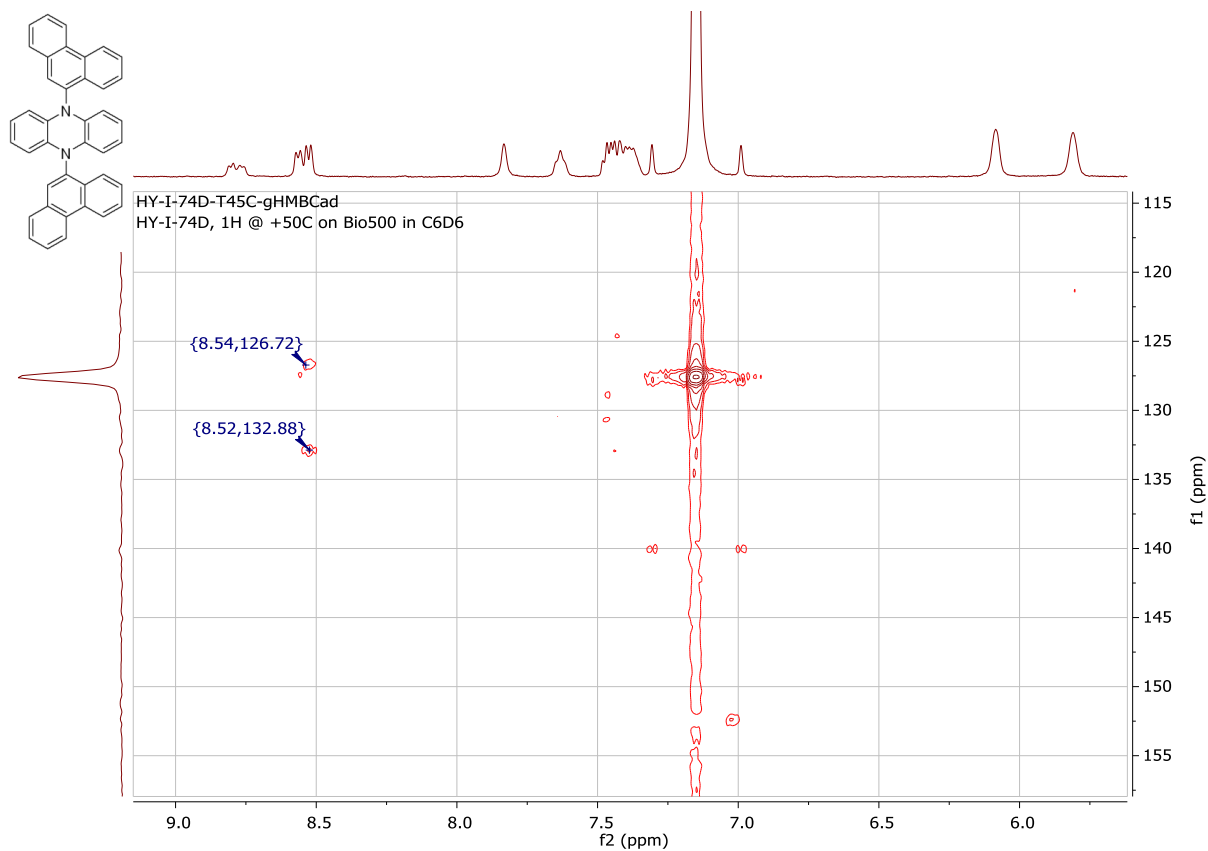
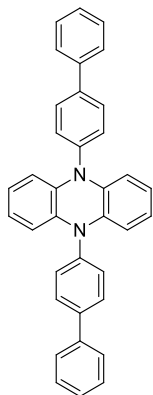


Figure 4.13 HMBC NMR for PC 8.

5,10-di([1,1'-biphenyl]-4-yl)-5,10-dihydrophenazine (9):



Chemical Formula: $C_{36}H_{26}N_2$
Molecular Weight: 486.61

5,10-di([1,1'-biphenyl]-4-yl)-5,10-dihydrophenazine (9) was synthesized using a modified literature procedure. Under a N_2 atmosphere, a mixture of 5,10-dihydrophenazine (1.67 g, 9.25

mmol), 4-bromobiphenyl (8.63 g, 37.02 mmol), Ruphos (0.173 g, 0.37 mmol), Ruphos pre-cat (.303 g, 0.37 mmol) and NaO^tBu (3.56 g, 37.02 mmol) and 20 mL anhydrous 1,4-Dioxane were heated at 110 C for 2 d. The reaction mixture was cooled to rt and washed sequentially with methanol and acetone. Similar recrystallization procedure to PC **8** to give the product as a yellow solid (2.50 g, 56 %). ¹H NMR (400 MHz Benzene-*d*₆) δ 7.51 – 7.44 (m, 4H), 7.44 – 7.37 (m, 4H), 7.25 – 7.15 (m, 8H), 7.09 – 7.08 (m, 2H), 6.30 (dd, *J* = 5.9, 3.4 Hz, 4H), 5.90 (dd, *J* = 5.9, 3.4 Hz, 4H). ¹³C NMR (101 MHz, Benzene-*d*₆) δ 141.71, 141.11, 140.70, 137.73, 130.49, 129.45, 128.24, 127.84, 121.99, 113.86. HR ESI⁺ MS: 486.2096 [M⁺]⁺

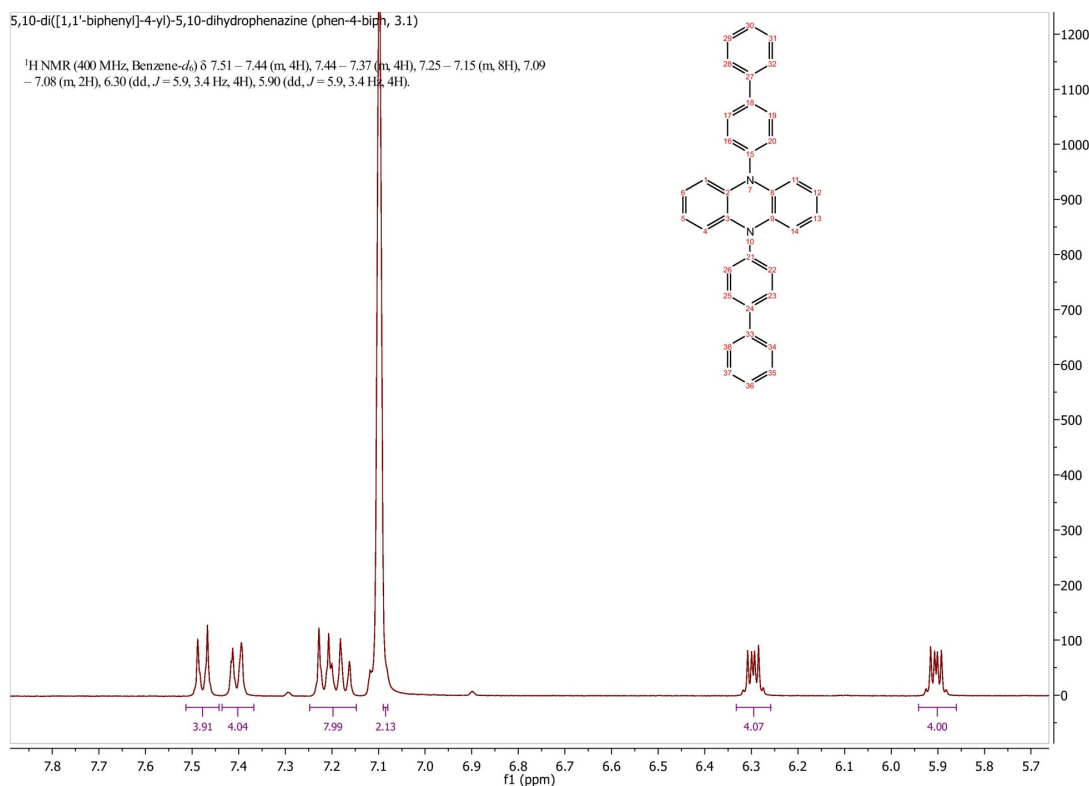


Figure 4.14 ¹H NMR spectra for PC **9**.

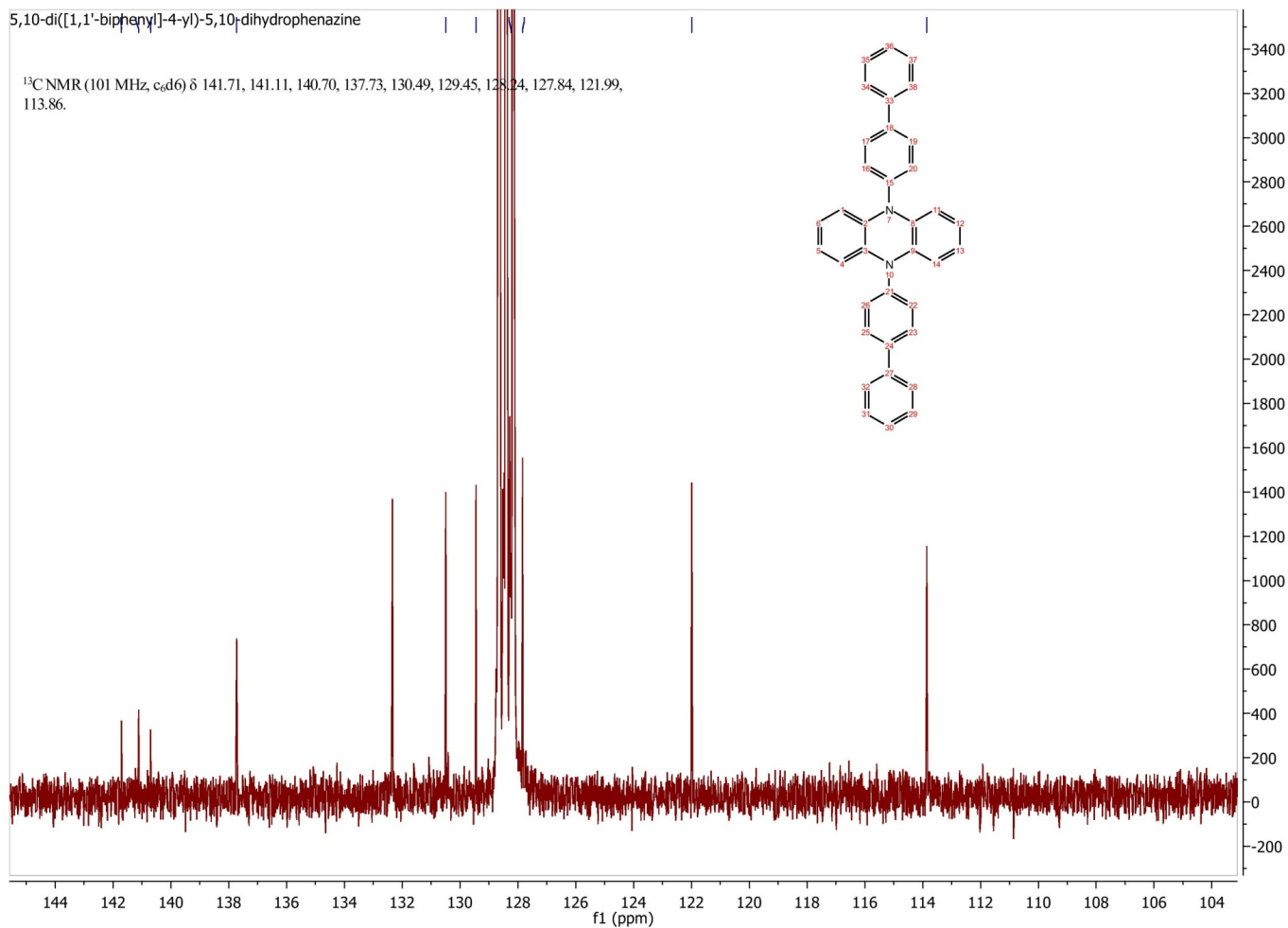
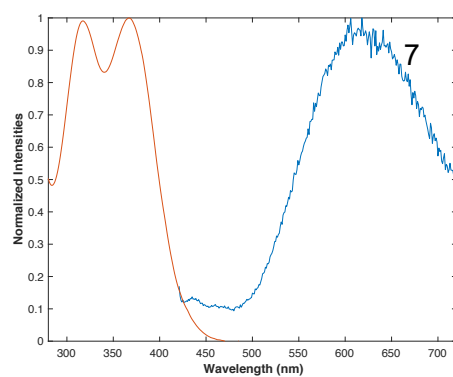
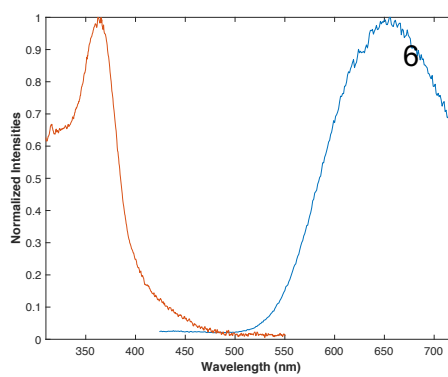
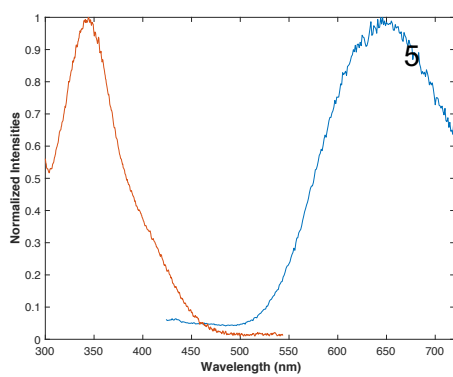
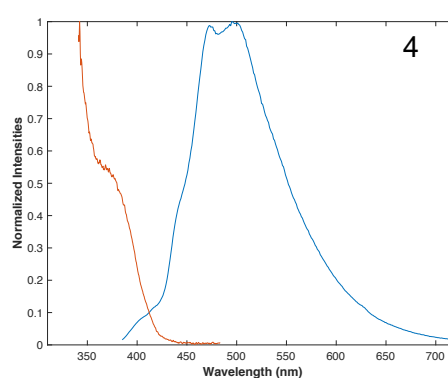
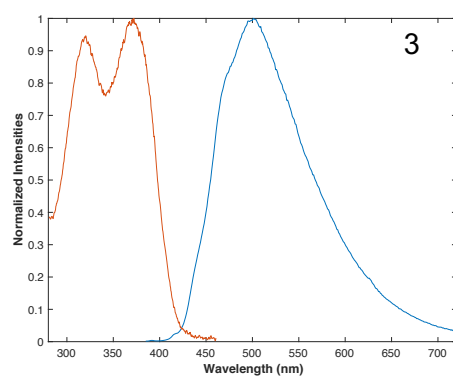
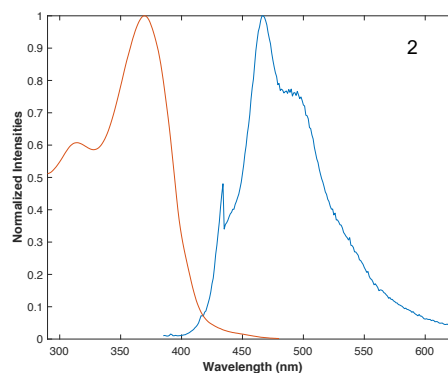
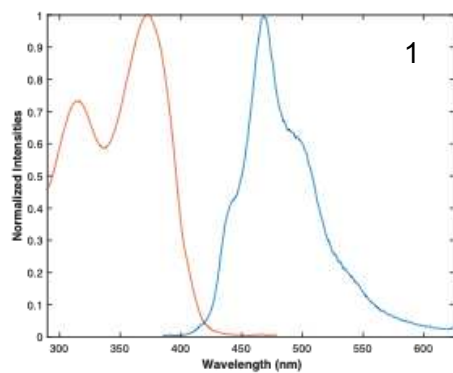


Figure 4.15 ^{13}C NMR spectra for PC 9.

Photophysical Characterization of Photocatalysts



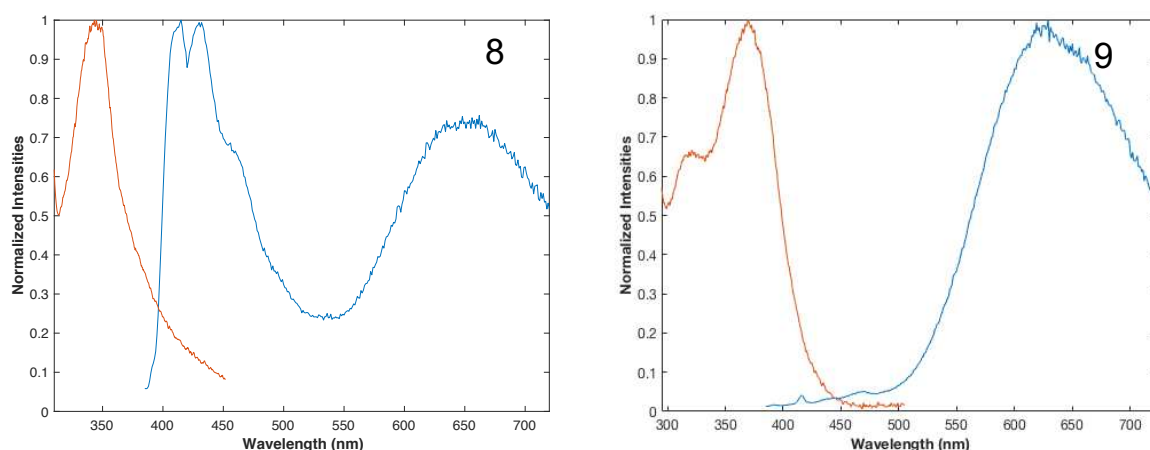


Figure 4.16. Overlaid UV-Vis (red) and emission (blue) spectra of photocatalysts **1-9**.

Computational Details

All calculations were performed using computational chemistry software package Gaussian 09 ver. D01.⁴⁹ We acknowledge the use of computational resource provided by XSEDE - Comet supercomputer.

Reduction Potentials Calculation

Standard reduction potentials (E^0) were calculated following previously reported procedures.^{50,51,52,53} A value of -100.5 kcal/mol was assumed for the reduction free energy of the standard hydrogen electrode (SHE). Thus, $E^0 = (-100.5 - \Delta G_{\text{red}})/23.06$ (V vs. SHE); for E^0 (${}^2\text{PC}^{*+}/{}^3\text{PC}^*$), $\Delta G_{\text{red}} = G({}^3\text{PC}^*) - G({}^2\text{PC}^{*+})$ while for E^0 (${}^2\text{PC}^{*+}/{}^1\text{PC}$), $\Delta G_{\text{red}} = G(\text{PC}) - G({}^2\text{PC}^{*+})$. To reference to the Saturated Calomel Electrode (SCE), E^0 (vs. SHE) is converted to E^0 (vs. SCE) using E^0 (vs. SCE) = E^0 (vs. SHE) - 0.24 V. Triplet energies (in eV) of PCs were obtained by $[G({}^3\text{PC}^*) - G(\text{PC})]$, in kcal/mol/23.06.

Geometries of ${}^3\text{PC}^*$, ${}^2\text{PC}^{*+}$, and ${}^1\text{PC}$ of PC 1-9 were optimized at unrestricted M06/6-31+G** level of theory in CPCM- H_2O solvent. Vibrational analysis to obtain zero point energy correction, thermal correction and entropy of all but PC 4 was conducted at the similar M06/6-31+G** level

of theory. Due to the extensive structure of PC 4, the vibrational analysis was conducted at M06/6-31G** level of theory with a smaller basis sets.

To obtain more accurate electronic energies, single point energy calculations were computed at the unrestricted M06/6-311+G** level of theory in CPCM-H₂O solvent using geometries optimized at unrestricted M06/6-31+G** level of theory. The triple zeta basis set (6-311+G**) generally improves the E⁰ (²PC^{•+}/¹PC) by ~0.1V relative to 6-31+G**, while the triplet energy is similar for these two basis sets.

Electrostatic Potential (ESP) Calculation

Converged ¹PC and ³PC* geometries of PC 1-9 were obtained using methods described above. Using these geometries, population analysis was performed using electrostatic potential (ESP)-derived charges with the CHELPG method⁵⁴ performed at the unrestricted M06/6-31G** level of theory in CPCM-DMA solvent. Total electron density of ¹PC and ³PC* were first plotted and then were mapped with ESP derived charges to show distribution of charges on the dihydrophenazine derivatives PC 1-9.

Coordinates of Molecular Structures

All coordinates are reported as XYZ Cartesian coordinates. Geometry optimizations were performed at uM06/6-31+G**/CPCM-H₂O level of theory. In parentheses are uM06/6-311+G**/CPCM-H₂O energies, computed at the geometries obtained from uM06/6-31+G**/CPCM-H₂O. Energies reported here are computed at 0 K (not ZPE and thermally corrected) and are stated in Hartrees units. Coordinates of PC 1, 2, 5, 6, and 7 geometries were previously reported in *Science* **352**, 1082-1086 (2016). The coordinates of the remaining PC 3, 4, 8, and 9 are reported here.

PC 3*Ground state (-1232.841731)*

C	0.69195	-3.65679	0.00005
C	1.38502	-2.44192	0.00004
C	0.70614	-1.22587	0.00003
C	-0.70614	-1.22587	0.00002
C	-1.38502	-2.44192	0.00002
C	-0.69196	-3.65679	0.00003
C	-0.70614	1.22587	-0.00003
C	0.70614	1.22587	-0.00002
C	1.38502	2.44192	-0.00002
H	2.47162	2.44655	-0.00001
C	0.69196	3.65679	-0.00004
C	-0.69195	3.65679	-0.00005
C	-1.38502	2.44192	-0.00004
H	1.25052	-4.58922	0.00006
H	2.47162	-2.44655	0.00005
H	-2.47162	-2.44655	0.00001
H	-1.25053	-4.58922	0.00004
H	1.25053	4.58922	-0.00004
H	-1.25052	4.58922	-0.00006
H	-2.47162	2.44655	-0.00005
N	-1.39364	0.00000	-0.00002
N	1.39364	0.00000	0.00001
C	-2.81908	0.00000	-0.00001
C	-3.51241	0.00001	1.20926
C	-3.51242	-0.00001	-1.20928
C	-4.90362	0.00001	1.21784
H	-2.95396	0.00002	2.14312
C	-4.90362	-0.00002	-1.21786
H	-2.95397	-0.00001	-2.14315
C	-5.56452	-0.00002	-0.00001
H	-5.47149	0.00002	2.14353
H	-5.47150	-0.00002	-2.14354
C	2.81908	0.00000	0.00001
C	3.51241	-0.00001	-1.20926
C	3.51242	0.00001	1.20928
C	4.90362	-0.00001	-1.21784
H	2.95396	-0.00002	-2.14312
C	4.90362	0.00002	1.21786
H	2.95397	0.00001	2.14315
C	5.56452	0.00002	0.00001
H	5.47149	-0.00002	-2.14353
H	5.47150	0.00002	2.14354

F	6.91320	-0.00002	0.00001
F	-6.91320	0.00002	-0.00000

Triplet excited state (-1232.751782)

C	0.71649	-3.64019	0.00004
C	1.40480	-2.44896	0.00003
C	0.72546	-1.21220	0.00002
C	-0.72545	-1.21220	0.00002
C	-1.40479	-2.44897	0.00003
C	-0.71647	-3.64019	0.00004
C	-0.72546	1.21220	-0.00002
C	0.72545	1.21220	-0.00002
C	1.40479	2.44897	-0.00003
H	2.49187	2.45612	-0.00003
C	0.71647	3.64019	-0.00004
C	-0.71649	3.64019	-0.00004
C	-1.40480	2.44896	-0.00003
H	1.26356	-4.57894	0.00004
H	2.49189	-2.45610	0.00002
H	-2.49187	-2.45612	0.00003
H	-1.26353	-4.57895	0.00005
H	1.26353	4.57895	-0.00005
H	-1.26356	4.57894	-0.00004
H	-2.49189	2.45610	-0.00002
N	-1.38693	-0.00001	0.00000
N	1.38693	0.00001	-0.00000
C	-2.82118	-0.00001	-0.00000
C	-3.50125	0.00000	1.21278
C	-3.50124	-0.00002	-1.21280
C	-4.89390	-0.00000	1.21913
H	-2.93933	0.00002	2.14414
C	-4.89389	-0.00003	-1.21915
H	-2.93932	-0.00002	-2.14415
C	-5.55293	-0.00003	-0.00001
H	-5.46240	0.00002	2.14412
H	-5.46239	-0.00002	-2.14414
C	2.82118	0.00001	0.00000
C	3.50125	-0.00000	-1.21278
C	3.50124	0.00002	1.21280
C	4.89390	0.00000	-1.21913
H	2.93934	-0.00002	-2.14414
C	4.89389	0.00003	1.21915
H	2.93932	0.00002	2.14415
C	5.55293	0.00003	0.00001
H	5.46240	-0.00002	-2.14412
H	5.46239	0.00002	2.14414

F	6.90100	-0.00003	0.00002
F	-6.90100	0.00003	-0.00002

Radical cation (-1232.671109)

C	0.70123	-3.62124	0.00002
C	1.39922	-2.43100	0.00001
C	0.70935	-1.20821	0.00002
C	-0.70935	-1.20821	0.00003
C	-1.39921	-2.43100	0.00003
C	-0.70121	-3.62124	0.00002
C	-0.70935	1.20821	-0.00003
C	0.70935	1.20821	-0.00003
C	1.39921	2.43100	-0.00003
H	2.48432	2.43473	-0.00002
C	0.70121	3.62124	-0.00002
C	-0.70123	3.62124	-0.00002
C	-1.39922	2.43100	-0.00002
H	1.24659	-4.56013	0.00000
H	2.48433	-2.43472	-0.00001
H	-2.48432	-2.43473	0.00002
H	-1.24656	-4.56014	0.00002
H	1.24656	4.56014	-0.00002
H	-1.24659	4.56014	-0.00001
H	-2.48433	2.43472	0.00000
N	-1.38527	-0.00001	0.00000
N	1.38527	0.00001	-0.00001
C	-2.82575	-0.00001	-0.00000
C	-3.50317	0.00003	1.21493
C	-3.50316	-0.00005	-1.21494
C	-4.89326	0.00003	1.21900
H	-2.94421	0.00007	2.14776
C	-4.89325	-0.00006	-1.21902
H	-2.94419	-0.00007	-2.14777
C	-5.55322	-0.00004	-0.00001
H	-5.46103	0.00007	2.14420
H	-5.46102	-0.00007	-2.14422
C	2.82575	0.00001	0.00000
C	3.50318	-0.00003	-1.21493
C	3.50316	0.00005	1.21494
C	4.89326	-0.00003	-1.21900
H	2.94421	-0.00007	-2.14776
C	4.89325	0.00006	1.21903
H	2.94419	0.00007	2.14776
C	5.55322	0.00004	0.00002
H	5.46104	-0.00007	-2.14419
H	5.46102	0.00007	2.14422

F	6.89726	-0.00003	0.00002
F	-6.89726	0.00003	-0.00002

PC 4

Ground state (-2068.719711)

C	-6.50906	0.04963	-0.99434
C	-5.18659	0.02563	-0.53957
C	-4.60909	1.14408	0.05654
C	-5.37493	2.32340	0.19079
C	-6.69141	2.33501	-0.26466
C	-7.26229	1.20272	-0.85457
C	-3.46294	3.44500	1.23300
C	-2.70024	2.26255	1.10833
C	-1.38544	2.25051	1.56846
H	-0.79990	1.33934	1.47755
C	-0.80987	3.38836	2.14309
C	-1.55583	4.54858	2.26065
C	-2.87867	4.57153	1.80692
H	-6.93201	-0.84077	-1.45271
H	-4.59727	-0.88096	-0.64950
H	-7.28198	3.24114	-0.15677
H	-8.29271	1.24103	-1.19860
H	0.21902	3.34903	2.49154
H	-1.12777	5.44465	2.70298
H	-3.46386	5.48243	1.90263
N	-4.79294	3.45773	0.78043
N	-3.28417	1.12558	0.52468
C	-5.56490	4.64973	0.91306
C	-6.32490	4.86649	2.06057
C	-5.56214	5.60296	-0.10280
C	-7.08198	6.02328	2.19122
H	-6.32950	4.11229	2.84562
C	-6.30456	6.76903	0.02846
H	-4.95911	5.42990	-0.99259
C	-7.07647	6.99109	1.17739
H	-7.68489	6.18301	3.08213
H	-6.28824	7.51823	-0.75967
C	-2.53754	-0.08806	0.46018
C	-1.68458	-0.33438	-0.61363
C	-2.65893	-1.03681	1.47330
C	-0.95203	-1.51243	-0.67249
H	-1.58371	0.41617	-1.39586
C	-1.94727	-2.22709	1.40914
H	-3.33352	-0.84297	2.30561
H	-0.27419	-1.69064	-1.50402

H	-2.06304	-2.97121	2.19371
C	-1.08153	-2.47900	0.33531
C	-8.49069	8.72974	0.18355
C	-8.43440	10.10769	-0.04987
C	-9.20799	7.91326	-0.69673
C	-9.09140	10.65886	-1.14516
H	-7.87475	10.74136	0.63535
C	-9.84849	8.46923	-1.79947
H	-9.26077	6.84236	-0.51116
C	-9.79734	9.84353	-2.02843
H	-9.04024	11.73183	-1.31488
H	-10.40396	7.82382	-2.47598
H	-10.30474	10.27585	-2.88713
C	-7.95298	8.80776	2.57066
C	-6.83200	8.96228	3.39358
C	-9.19202	9.29290	3.00225
C	-6.95521	9.57845	4.63441
H	-5.86593	8.59324	3.05503
C	-9.30392	9.92445	4.23673
H	-10.06506	9.17255	2.36400
C	-8.18947	10.06549	5.06235
H	-6.07620	9.68917	5.26505
H	-10.27323	10.29618	4.56092
H	-8.28219	10.55131	6.03039
C	0.11356	-4.28979	1.47036
C	0.80296	-3.53392	2.42362
C	-0.11270	-5.64947	1.70303
C	1.24720	-4.13035	3.59913
H	0.98537	-2.47726	2.23761
C	0.34935	-6.24381	2.87334
H	-0.65229	-6.23515	0.96137
C	1.02625	-5.48765	3.82898
H	1.78135	-3.53249	4.33390
H	0.16668	-7.30223	3.04405
H	1.38010	-5.95245	4.74576
C	-0.12757	-4.33273	-0.96372
C	1.11327	-4.92206	-1.23027
C	-1.14171	-4.40976	-1.92431
C	1.33090	-5.58000	-2.43645
H	1.90387	-4.86165	-0.48500
C	-0.91038	-5.05326	-3.13576
H	-2.11145	-3.96184	-1.71720
C	0.32416	-5.64548	-3.39834
H	2.30066	-6.03336	-2.62889
H	-1.70798	-5.10471	-3.87329
H	0.49944	-6.15336	-4.34332

N	-7.83502	8.17126	1.30986
N	-0.35101	-3.68153	0.27444

Triplet excited state (-2068.630246)

C	-6.52374	0.03855	-0.93784
C	-5.22010	-0.00146	-0.49881
C	-4.61570	1.12300	0.10178
C	-5.39198	2.34266	0.23779
C	-6.72869	2.35231	-0.21390
C	-7.29586	1.23701	-0.78659
C	-3.48546	3.44235	1.24904
C	-2.72041	2.21266	1.14482
C	-1.39477	2.19356	1.62816
H	-0.82159	1.27213	1.55900
C	-0.82038	3.31626	2.17875
C	-1.57176	4.53363	2.27053
C	-2.86986	4.57823	1.81569
H	-6.96448	-0.84186	-1.39786
H	-4.64029	-0.91409	-0.61294
H	-7.31543	3.26137	-0.10531
H	-8.32782	1.26975	-1.12530
H	0.20286	3.27579	2.54222
H	-1.12084	5.42402	2.70051
H	-3.43672	5.50305	1.89064
N	-4.79124	3.45109	0.80041
N	-3.31773	1.10681	0.57305
C	-5.55780	4.65684	0.92866
C	-6.29662	4.88134	2.08467
C	-5.56085	5.58519	-0.10569
C	-7.05313	6.04050	2.20482
H	-6.28902	4.13764	2.87920
C	-6.30305	6.75324	0.01887
H	-4.96948	5.39481	-0.99936
C	-7.06153	6.99123	1.17412
H	-7.64548	6.21282	3.10005
H	-6.29694	7.48969	-0.78093
C	-2.56610	-0.11197	0.48669
C	-1.72640	-0.33281	-0.59920
C	-2.67938	-1.06055	1.49637
C	-0.98611	-1.50631	-0.67215
H	-1.63984	0.42624	-1.37438
C	-1.95589	-2.24352	1.41647
H	-3.34798	-0.87458	2.33480
H	-0.31447	-1.67286	-1.51070
H	-2.05785	-2.99328	2.19706
C	-1.09733	-2.47912	0.33238

C	-8.47456	8.72247	0.16489
C	-8.41288	10.09842	-0.07742
C	-9.19629	7.90268	-0.70848
C	-9.06879	10.64492	-1.17579
H	-7.85002	10.73407	0.60335
C	-9.83552	8.45376	-1.81443
H	-9.25375	6.83336	-0.51510
C	-9.77879	9.82630	-2.05265
H	-9.01376	11.71650	-1.35281
H	-10.39455	7.80622	-2.48593
H	-10.28533	10.25477	-2.91378
C	-7.94664	8.81484	2.55284
C	-6.82683	8.99130	3.37251
C	-9.19165	9.28676	2.98104
C	-6.95703	9.61536	4.60871
H	-5.85621	8.63305	3.03538
C	-9.31085	9.92647	4.21073
H	-10.06324	9.14937	2.34420
C	-8.19750	10.08890	5.03383
H	-6.07908	9.74348	5.23747
H	-10.28461	10.28810	4.53298
H	-8.29588	10.58113	5.99805
C	0.11391	-4.28740	1.45235
C	0.80732	-3.53681	2.40657
C	-0.11283	-5.64792	1.67790
C	1.25469	-4.13957	3.57770
H	0.99009	-2.47942	2.22500
C	0.35236	-6.24874	2.84375
H	-0.65536	-6.22894	0.93468
C	1.03279	-5.49781	3.80101
H	1.79169	-3.54619	4.31399
H	0.16957	-7.30786	3.00975
H	1.38886	-5.96766	4.71434
C	-0.11708	-4.30861	-0.98283
C	1.13195	-4.88056	-1.24828
C	-1.12658	-4.39094	-1.94771
C	1.36257	-5.52646	-2.45866
H	1.91855	-4.81663	-0.49905
C	-0.88242	-5.02205	-3.16308
H	-2.10289	-3.95747	-1.74075
C	0.36057	-5.59666	-3.42507
H	2.33844	-5.96678	-2.65040
H	-1.67636	-5.07801	-3.90421
H	0.54585	-6.09516	-4.37314
N	-7.82120	8.17008	1.29613
N	-0.35450	-3.67194	0.26068

Cation radical (-2068.552152)

C	-6.54700	0.00738	-0.65045
C	-5.22490	-0.02640	-0.25646
C	-4.61499	1.12335	0.27035
C	-5.36899	2.31965	0.38862
C	-6.71358	2.33072	-0.01657
C	-7.29379	1.18823	-0.52862
C	-3.43896	3.44422	1.30258
C	-2.68679	2.24602	1.19066
C	-1.34486	2.23252	1.60391
H	-0.76963	1.31591	1.52191
C	-0.76328	3.37670	2.11078
C	-1.50564	4.56193	2.21757
C	-2.82657	4.59684	1.81961
H	-7.00634	-0.88909	-1.05622
H	-4.64882	-0.94142	-0.34975
H	-7.29269	3.24388	0.07533
H	-8.33436	1.20948	-0.83815
H	0.27531	3.35390	2.42676
H	-1.04391	5.46054	2.61581
H	-3.40043	5.51436	1.90181
N	-4.76299	3.45409	0.90012
N	-3.29154	1.11261	0.67616
C	-5.52696	4.67082	1.00436
C	-6.24099	4.93843	2.16709
C	-5.55595	5.55619	-0.06783
C	-7.00033	6.09581	2.25450
H	-6.21531	4.23109	2.99353
C	-6.30626	6.71845	0.02278
H	-4.98219	5.33739	-0.96627
C	-7.04713	7.00233	1.18243
H	-7.57266	6.29617	3.15635
H	-6.31937	7.41601	-0.81039
C	-2.53215	-0.10643	0.56615
C	-1.78425	-0.35119	-0.58081
C	-2.56113	-1.02874	1.60610
C	-1.05678	-1.52693	-0.68711
H	-1.76232	0.38632	-1.38056
C	-1.84535	-2.21110	1.49459
H	-3.15873	-0.82632	2.49268
H	-0.46014	-1.71184	-1.57640
H	-1.88477	-2.93905	2.30034
C	-1.08179	-2.47890	0.34615
C	-8.39985	8.74316	0.10410
C	-8.28662	10.11755	-0.12113

C	-9.10716	7.95013	-0.80406
C	-8.87386	10.69048	-1.24502
H	-7.73748	10.73095	0.59062
C	-9.67678	8.52670	-1.93467
H	-9.20705	6.88232	-0.61935
C	-9.56558	9.89821	-2.15957
H	-8.77992	11.76104	-1.41100
H	-10.22421	7.90132	-2.63588
H	-10.01788	10.34678	-3.04044
C	-8.04649	8.79958	2.51949
C	-6.97618	9.09645	3.36739
C	-9.34538	9.14970	2.89596
C	-7.20843	9.72479	4.58679
H	-5.96408	8.83408	3.06501
C	-9.56908	9.79259	4.10960
H	-10.17478	8.91687	2.23086
C	-8.50383	10.07896	4.96165
H	-6.36952	9.95249	5.24008
H	-10.58359	10.06165	4.39402
H	-8.68141	10.57636	5.91179
C	0.11962	-4.33393	1.40209
C	0.87807	-3.63819	2.34739
C	-0.15974	-5.68828	1.59983
C	1.33540	-4.28947	3.48828
H	1.10336	-2.58607	2.18365
C	0.31543	-6.33838	2.73476
H	-0.75013	-6.22529	0.85989
C	1.05898	-5.64182	3.68593
H	1.92238	-3.73969	4.22009
H	0.09264	-7.39258	2.88137
H	1.42276	-6.15005	4.57531
C	-0.14205	-4.28627	-1.02637
C	1.12087	-4.79302	-1.34555
C	-1.18901	-4.41631	-1.94327
C	1.33130	-5.41918	-2.57021
H	1.93243	-4.69448	-0.62718
C	-0.96691	-5.02737	-3.17313
H	-2.17616	-4.03664	-1.68732
C	0.29238	-5.53350	-3.49231
H	2.31797	-5.80969	-2.80816
H	-1.78795	-5.12118	-3.87990
H	0.46154	-6.01595	-4.45162
N	-7.81836	8.16695	1.26613
N	-0.35739	-3.67166	0.23648

PC 8

Ground state (-1648.604392)

C	-6.79368	-0.26032	0.20405
C	-5.41479	-0.21918	0.42623
C	-4.77321	0.97306	0.75444
C	-5.53381	2.15593	0.86306
C	-6.90721	2.10375	0.63432
C	-7.54027	0.90205	0.30674
C	-3.49262	3.42889	1.31583
C	-2.73117	2.24663	1.20315
C	-1.34426	2.31928	1.31664
H	-0.75598	1.40917	1.23239
C	-0.70037	3.53847	1.54267
C	-1.44840	4.69901	1.65342
C	-2.83961	4.63907	1.53813
H	-7.26617	-1.20607	-0.04848
H	-4.82868	-1.13139	0.34635
H	-7.49378	3.01521	0.71606
H	-8.61358	0.89230	0.13602
H	0.38282	3.56306	1.62801
H	-0.96774	5.65816	1.82808
H	-3.42715	5.54939	1.62605
N	-4.89469	3.35990	1.21414
N	-3.38685	1.01863	0.99285
C	-5.64693	4.57196	1.17883
C	-6.20529	5.04924	2.31928
C	-5.80719	5.26272	-0.07542
C	-6.97431	6.25477	2.32266
H	-6.06736	4.50268	3.25170
C	-6.56619	6.46400	-0.11151
C	-7.16332	6.97212	1.11179
C	-2.60021	-0.14272	0.73229
C	-2.16032	-0.40909	-0.61385
C	-2.26807	-0.96959	1.75529
C	-1.36873	-1.56212	-0.86762
C	-1.46661	-2.13379	1.54006
H	-2.61380	-0.73922	2.76252
C	-1.01092	-2.44231	0.23126
C	-6.70971	7.12026	-1.35267
C	-6.13476	6.61839	-2.50218
H	-6.26355	7.14542	-3.44428
C	-5.38554	5.43164	-2.45882
H	-4.93319	5.03857	-3.36579
C	-5.22636	4.76668	-1.26211
H	-4.64469	3.84714	-1.22583
H	-7.28371	8.04049	-1.41668
C	-2.50059	0.45240	-1.67834

H	-3.10306	1.33567	-1.47265
C	-0.95665	-1.80482	-2.19538
C	-1.30333	-0.95230	-3.22336
H	-0.97149	-1.16546	-4.23641
C	-2.08090	0.18798	-2.96436
H	-2.35108	0.85980	-3.77512
H	-0.35391	-2.67901	-2.42567
C	-7.54546	6.73126	3.52146
H	-7.38556	6.16310	4.43634
C	-8.28980	7.89099	3.53641
H	-8.72582	8.25186	4.46448
C	-8.48123	8.60572	2.34202
C	-7.93050	8.15521	1.15870
H	-8.09977	8.73276	0.25422
H	-9.06878	9.52053	2.34658
C	-1.12498	-2.97328	2.62126
H	-1.48559	-2.71501	3.61553
C	-0.35007	-4.09606	2.42540
H	-0.08990	-4.73661	3.26418
C	0.10343	-4.40798	1.13261
C	-0.22066	-3.59878	0.06184
H	0.14864	-3.86789	-0.92383
H	0.71530	-5.29205	0.97135

Triplet excited state (-1648.521324)

C	-6.79266	-0.26125	0.21382
C	-5.42572	-0.22813	0.39374
C	-4.77695	0.98684	0.67299
C	-5.54274	2.17681	0.77375
C	-6.93213	2.12335	0.57873
C	-7.54753	0.91892	0.30232
C	-3.52557	3.42364	1.23260
C	-2.77020	2.22765	1.12417
C	-1.37595	2.27600	1.29902
H	-0.81143	1.35242	1.21622
C	-0.74976	3.47466	1.56973
C	-1.49822	4.65775	1.66920
C	-2.86850	4.63464	1.50263
H	-7.28354	-1.20669	0.00206
H	-4.82340	-1.12924	0.32534
H	-7.51861	3.03439	0.64734
H	-8.62306	0.89042	0.15438
H	0.32759	3.49944	1.70415
H	-1.00216	5.60143	1.87696
H	-3.44517	5.55137	1.57861
N	-4.89866	3.37214	1.05098

N	-3.40425	1.03452	0.82953
C	-5.66144	4.59232	1.08497
C	-6.18679	5.01050	2.26185
C	-5.83647	5.32208	-0.13951
C	-6.94689	6.21819	2.32991
H	-6.02924	4.42421	3.16621
C	-6.58852	6.52816	-0.10353
C	-7.15433	6.98650	1.15356
C	-2.61503	-0.15373	0.62589
C	-2.16011	-0.44189	-0.67799
C	-2.29947	-0.94399	1.74730
C	-1.33671	-1.60615	-0.87427
C	-1.49104	-2.08452	1.58851
H	-2.67647	-0.66748	2.73185
C	-0.98920	-2.44386	0.28777
C	-6.75393	7.23569	-1.31271
C	-6.20901	6.77794	-2.49469
H	-6.35548	7.34490	-3.41037
C	-5.46818	5.58580	-2.51998
H	-5.04042	5.22772	-3.45262
C	-5.28513	4.87008	-1.35676
H	-4.70789	3.94695	-1.37532
H	-7.32235	8.16107	-1.32657
C	-2.47586	0.36551	-1.80772
H	-3.09742	1.25121	-1.67439
C	-0.89416	-1.89092	-2.16865
C	-1.21737	-1.08778	-3.26935
H	-0.85095	-1.34584	-4.26013
C	-2.01159	0.04400	-3.07362
H	-2.27244	0.68128	-3.91722
H	-0.27229	-2.76728	-2.34021
C	-7.48735	6.64664	3.56035
H	-7.31260	6.03936	4.44657
C	-8.21991	7.81074	3.63877
H	-8.63302	8.13685	4.58965
C	-8.43013	8.57622	2.47934
C	-7.90949	8.17257	1.26615
H	-8.09251	8.78899	0.39077
H	-9.00894	9.49474	2.53480
C	-1.14178	-2.91047	2.69678
H	-1.52345	-2.63757	3.68093
C	-0.34201	-4.02435	2.54565
H	-0.09238	-4.63228	3.41404
C	0.15043	-4.37410	1.27787
C	-0.18090	-3.58111	0.17875
H	0.21238	-3.86818	-0.79462

H	0.78274	-5.24952	1.15007
---	---------	----------	---------

Cation radical (-1648.432492)

C	-6.77201	-0.26141	0.19875
C	-5.40445	-0.22904	0.37750
C	-4.75907	0.98442	0.66294
C	-5.52452	2.17409	0.76671
C	-6.91479	2.11868	0.57822
C	-7.52898	0.91575	0.29805
C	-3.51014	3.43236	1.20912
C	-2.74420	2.24332	1.10228
C	-1.35008	2.30492	1.25919
H	-0.76129	1.39671	1.18020
C	-0.73345	3.51194	1.51546
C	-1.49133	4.68779	1.62068
C	-2.86204	4.65009	1.46971
H	-7.26004	-1.20632	-0.02035
H	-4.81841	-1.13968	0.30148
H	-7.50176	3.02841	0.65470
H	-8.60474	0.88527	0.15468
H	0.34515	3.54647	1.63446
H	-1.00182	5.63617	1.82064
H	-3.44851	5.55986	1.55093
N	-4.88325	3.37033	1.04035
N	-3.38616	1.04604	0.83266
C	-5.65367	4.58797	1.08238
C	-6.17064	4.99954	2.26518
C	-5.84103	5.31703	-0.14023
C	-6.93743	6.20223	2.34071
H	-6.00197	4.41287	3.16721
C	-6.59928	6.51887	-0.09520
C	-7.15894	6.97075	1.16699
C	-2.59496	-0.14399	0.64526
C	-2.12453	-0.44649	-0.67751
C	-2.30861	-0.92100	1.71779
C	-1.32720	-1.60975	-0.85613
C	-1.50618	-2.09329	1.56936
H	-2.68533	-0.64941	2.70309
C	-1.00834	-2.44734	0.28721
C	-6.77645	7.22877	-1.30119
C	-6.23740	6.77704	-2.48812
H	-6.39288	7.34595	-3.40104
C	-5.49121	5.58856	-2.52213
H	-5.06831	5.23511	-3.45869
C	-5.29626	4.87043	-1.36237
H	-4.71446	3.95026	-1.38872

H	-7.34928	8.15142	-1.30848
C	-2.43269	0.37398	-1.78276
H	-3.04289	1.26431	-1.64097
C	-0.87169	-1.90175	-2.15880
C	-1.18456	-1.08937	-3.22908
H	-0.81910	-1.34094	-4.22128
C	-1.97071	0.05854	-3.04207
H	-2.21554	0.69661	-3.88691
H	-0.26152	-2.78293	-2.33438
C	-7.47113	6.62478	3.57610
H	-7.28511	6.01751	4.45998
C	-8.21152	7.78330	3.66159
H	-8.61987	8.10511	4.61593
C	-8.43642	8.54855	2.50480
C	-7.92204	8.15086	1.28702
H	-8.11676	8.76700	0.41404
H	-9.02182	9.46248	2.56597
C	-1.20308	-2.89090	2.69256
H	-1.59604	-2.59466	3.66338
C	-0.42330	-4.01904	2.56333
H	-0.19057	-4.62848	3.43248
C	0.07207	-4.37675	1.29805
C	-0.21469	-3.60869	0.18724
H	0.18697	-3.91536	-0.77416
H	0.68850	-5.26559	1.19054

PC 9

Ground state (-1496.218247)

C	-6.66405	-0.04684	-0.69205
C	-5.33089	-0.07126	-0.27001
C	-4.72491	1.06215	0.26594
C	-5.47264	2.25525	0.37595
C	-6.79906	2.26794	-0.04910
C	-7.39815	1.12151	-0.58084
C	-3.50497	3.40326	1.27767
C	-2.75873	2.20879	1.17236
C	-1.41623	2.21087	1.54399
H	-0.84115	1.29179	1.46766
C	-0.79977	3.37315	2.01818
C	-1.53050	4.54454	2.11879
C	-2.87877	4.55509	1.74746
H	-7.11005	-0.94895	-1.10312
H	-4.75805	-0.99078	-0.35581
H	-7.37685	3.18438	0.03785
H	-8.43588	1.16066	-0.90187

H	0.24855	3.34371	2.30385
H	-1.07088	5.45910	2.48487
H	-3.44990	5.47600	1.82956
N	-4.86462	3.39788	0.92258
N	-3.39217	1.04264	0.71079
C	-5.61071	4.61145	1.00507
C	-6.32602	4.90911	2.16155
C	-5.62442	5.49810	-0.06953
C	-7.05145	6.09230	2.24350
H	-6.30082	4.21153	2.99668
C	-6.35044	6.67967	0.01598
H	-5.06778	5.24984	-0.97178
C	-7.07458	6.99754	1.17371
H	-7.58801	6.32837	3.16016
H	-6.37329	7.35507	-0.83680
C	-2.63014	-0.15678	0.58103
C	-1.90154	-0.39878	-0.58142
C	-2.60937	-1.08236	1.62056
C	-1.14952	-1.56139	-0.69835
H	-1.93345	0.32849	-1.39091
C	-1.85775	-2.24568	1.49912
H	-3.17826	-0.87740	2.52570
H	-0.59851	-1.75260	-1.61693
H	-1.82758	-2.95210	2.32617
C	-1.11326	-2.50283	0.33996
C	-0.30437	-3.73412	0.21718
C	0.94766	-3.70673	-0.41212
C	-0.76753	-4.95354	0.72851
C	1.71347	-4.86291	-0.52495
H	1.33668	-2.76491	-0.79522
C	-0.00277	-6.11058	0.61444
H	-1.74720	-5.00112	1.20081
C	1.24125	-6.06966	-0.01261
H	2.68701	-4.81848	-1.00761
H	-0.38401	-7.04915	1.01008
H	1.83978	-6.97315	-0.09984
C	-7.83891	8.25971	1.26538
C	-7.33825	9.44187	0.70374
C	-9.07766	8.30453	1.91922
C	-8.05294	10.63227	0.79339
H	-6.36701	9.43414	0.21235
C	-9.79330	9.49453	2.00854
H	-9.49588	7.39266	2.34193
C	-9.28361	10.66350	1.44654
H	-7.64257	11.54108	0.35933
H	-10.75672	9.50668	2.51285

H	-9.84264	11.59346	1.51649
---	----------	----------	---------

Triplet excited state (-1496.129186)

C	-6.48528	0.10824	-1.10194
C	-5.15202	0.08771	-0.74778
C	-4.54093	1.23732	-0.21860
C	-5.31127	2.41766	-0.05059
C	-6.66586	2.41809	-0.41875
C	-7.24415	1.27657	-0.93778
C	-3.36724	3.54899	0.82734
C	-2.60494	2.36402	0.65278
C	-1.24671	2.36058	1.01360
H	-0.67429	1.44833	0.87762
C	-0.66083	3.49726	1.53111
C	-1.41584	4.66692	1.70344
C	-2.75247	4.69394	1.35728
H	-6.94505	-0.78700	-1.51039
H	-4.55414	-0.81015	-0.87040
H	-7.25597	3.32058	-0.29431
H	-8.29297	1.28984	-1.21932
H	0.38962	3.48195	1.80629
H	-0.95270	5.56026	2.11228
H	-3.33277	5.60100	1.49357
N	-4.70620	3.54739	0.47416
N	-3.20343	1.22858	0.13650
C	-5.48892	4.74156	0.66080
C	-6.18899	4.91772	1.84866
C	-5.53844	5.69150	-0.35226
C	-6.95438	6.06445	2.01896
H	-6.12666	4.16327	2.63007
C	-6.30612	6.83529	-0.17086
H	-4.98713	5.52664	-1.27563
C	-7.02790	7.03854	1.01366
H	-7.48624	6.21467	2.95569
H	-6.36636	7.56890	-0.97148
C	-2.43314	0.02536	-0.02571
C	-1.72641	-0.21214	-1.22114
C	-2.39230	-0.93424	1.00444
C	-1.00517	-1.37484	-1.38012
H	-1.75682	0.53098	-2.01863
C	-1.66917	-2.09508	0.84294
H	-2.93969	-0.75065	1.92965
H	-0.47580	-1.51181	-2.32033
H	-1.66846	-2.80393	1.66747
C	-0.93375	-2.38665	-0.35939
C	-0.18717	-3.60249	-0.52964

C	0.53367	-3.90005	-1.72919
C	-0.10932	-4.60524	0.48766
C	1.24920	-5.07515	-1.88800
H	0.52792	-3.19338	-2.55625
C	0.61012	-5.77639	0.31699
H	-0.62638	-4.46062	1.43405
C	1.30703	-6.04093	-0.87189
H	1.77677	-5.24554	-2.82651
H	0.63194	-6.50258	1.12949
H	1.87095	-6.96166	-1.00132
C	-7.85315	8.25089	1.19659
C	-7.42116	9.49259	0.71293
C	-9.08822	8.18110	1.85451
C	-8.20109	10.63228	0.88313
H	-6.45434	9.57178	0.21903
C	-9.86949	9.32008	2.02212
H	-9.45289	7.22143	2.21643
C	-9.42867	10.54997	1.53758
H	-7.84457	11.58897	0.50884
H	-10.83013	9.24423	2.52604
H	-10.03904	11.44002	1.66886

Cation radical (-1496.049096)

C	-6.58426	0.08053	-0.98779
C	-5.24271	0.05462	-0.66569
C	-4.61333	1.20720	-0.16947
C	-5.36921	2.39682	-0.00288
C	-6.73211	2.40139	-0.33993
C	-7.33060	1.25682	-0.82550
C	-3.40061	3.53220	0.81582
C	-2.64473	2.34258	0.64925
C	-1.28181	2.33803	0.98625
H	-0.70196	1.42904	0.86367
C	-0.68331	3.48263	1.47174
C	-1.42964	4.65893	1.63397
C	-2.77121	4.68481	1.31193
H	-7.05898	-0.81822	-1.36987
H	-4.66830	-0.85700	-0.79419
H	-7.31194	3.31039	-0.21735
H	-8.38540	1.27285	-1.08250
H	0.37150	3.46663	1.72869
H	-0.95490	5.55772	2.01595
H	-3.34559	5.59646	1.44036
N	-4.74502	3.53059	0.48750
N	-3.26893	1.20880	0.15887
C	-5.51587	4.73589	0.66498

C	-6.19084	4.94023	1.86256
C	-5.57428	5.66583	-0.36571
C	-6.94028	6.09842	2.02508
H	-6.12122	4.20034	2.65705
C	-6.32629	6.82095	-0.19104
H	-5.04217	5.47819	-1.29592
C	-7.02222	7.05449	1.00323
H	-7.45206	6.27208	2.96887
H	-6.39388	7.53980	-1.00427
C	-2.49810	0.00350	-0.01867
C	-1.82318	-0.20081	-1.21628
C	-2.43965	-0.92646	1.01200
C	-1.07374	-1.35899	-1.37885
H	-1.89282	0.53912	-2.01074
C	-1.68765	-2.08157	0.83728
H	-2.97170	-0.73883	1.94225
H	-0.56195	-1.53261	-2.32265
H	-1.61997	-2.80042	1.65051
C	-0.99178	-2.31509	-0.35704
C	-0.18548	-3.54081	-0.53460
C	1.03704	-3.49725	-1.21780
C	-0.62415	-4.76893	-0.02326
C	1.79959	-4.64898	-1.38354
H	1.40685	-2.54808	-1.60147
C	0.13712	-5.92139	-0.19161
H	-1.58179	-4.82754	0.49093
C	1.35212	-5.86534	-0.87182
H	2.75030	-4.59418	-1.90849
H	-0.22432	-6.86767	0.20381
H	1.94754	-6.76562	-1.00212
C	-7.82847	8.28027	1.18073
C	-7.38983	9.50827	0.66907
C	-9.05095	8.23688	1.86401
C	-8.15104	10.66080	0.83727
H	-6.43227	9.56673	0.15473
C	-9.81344	9.38867	2.02961
H	-9.42079	7.28779	2.24785
C	-9.36598	10.60492	1.51763
H	-7.78962	11.60698	0.44162
H	-10.76412	9.33400	2.55464
H	-9.96135	11.50524	1.64781

References

- 1) Patten, T. E.; Xia, J.; Abernathy, T.; Matyjaszewski, K. *Science* **1996**, *272*, 866-868.
- 2) Moad, G.; Rizzardo, E.; Thang, S. H. *Acc. Chem. Res.* **2008**, *41*, 1133-1142.
- 3) Hawker, C. J.; Bosman, A. W.; Harth, E. *Chem. Rev.* **2001**, *101*, 3661-3688.
- 4) Su, J.; Liu, X.; Hu, J.; You, Q.; Cui, Y.; Chen, Y. *Polym. Int.* **2015**, *64*, 867-874.
- 5) Guillaneuf, Y.; Bertin, D.; Gimes, D.; Versace, D.-L.; Lalevee, J.; Fouassier, J.-P. *Macromolecules* **2010**, *43*, 2204-2212.
- 6) Moad, G.; Rizzardo, E.; Thang, S. H. *Aust. J. Chem.* **2005**, *58*, 379-410.
- 7) Xu, J.; Jung, K.; Atme, A.; Shanmugam, S.; Boyer, C. *J. Am. Chem. Soc.* **2014**, *136*, 5508-5519.
- 8) Shanmugam, S.; Xu, J.; Boyer, C. *J. Am. Chem. Soc.* **2015**, *137*, 9174-9185.
- 9) Xu, J.; Shanmugam, S.; Duong, H. T.; Boyer, C. *Polym. Chem.* **2015**, *6*, 5615-5624.
- 10) Niu, J.; Lunn, D. J.; Pusuluri, A.; Yoo, J. I.; O'Malley, M. A.; Mitragotri, S.; Soh, H. T.; Hawker, C. J. *Nature Chemistry* **2017**, DOI: 10.1038/NCHEM.2713.
- 11) David, G.; Boyer, C.; Tonnar, J.; Ameduri, B.; Lacroix-Desmazes, P.; Boutevin, B. *Chem. Rev.* **2006**, *106*, 3936-3962.
- 12) Ohtsuki, A.; Lei, L.; Tanishima, M.; Goto, A.; Kaji, H. *J. Am. Chem. Soc.* **2015**, *137*, 5610-5617.
- 13) Gaynor, S. G.; Wang, J.-S.; Matyjaszewski, K. *Macromolecules* **1995**, *28*, 8051-8056.
- 14) Matyjaszewski, K.; Tsarevsky, N. V. *J. Am. Chem. Soc.* **2014**, *136*, 6513-6533.
- 15) Chen, M.; Zhong, M.; Johnson, J. A. *Chem. Rev.* **2016**, *116*, 10167-10211.
- 16) Leibfarth, F. A.; Mattson, K. M.; Fors, B. P.; Collins, H. A.; Hawker, C. J. *Angew. Chem. Int. Ed.* **2013**, *52*, 199-210.

-
- 17) Wong, E. H. H.; Stenzel, M. H.; Junkers, T.; Barner-Kowollik, C. *J. Polym. Sci., Part A: Polym. Chem.* **2011**, *49*, 2118-2126.
 - 18) Adzima, B. J.; Tao, Y.; Kloxin, C. J.; DeForest, C. A.; Anseth, K. S.; Bowman, C. N. *Nature Chem.* **2011**, *3*, 256-259.
 - 19) Chen, M.; Gu, Y.; Singh, A.; Zhong, M.; Jordan, A. M.; Biswas, S.; Korley, L. T. J.; Balazs, A. C.; Johnson, J. A. *ACS Cent. Sci.* **2017**, DOI: 10.1021/acscentsci.6b00335.
 - 20) Fors, B. P.; Hawker, C. J. *Angew. Chem. Int. Ed.* **2012**, *51*, 8850-8853.
 - 21) Prier, C. K.; Rankic, D. A.; MacMillan, D. W. C. *Chem. Rev.* **2013**, *113*, 5322-5363.
 - 22) Nicewicz, D. A.; MacMillan, D. W. C. *Science* **2008**, *322*, 77-80.
 - 23) Abrahamsson, M.; Jager, M.; Osterman, T.; Eriksson, L.; Persson, P.; Becker, H.-C.; Johansson, O.; Hammarstrom, L. *J. Am. Chem. Soc.* **2006**, *128*, 12616-12617.
 - 24) Juris, A.; Balzani, V.; Barigelletti, S.; Campagna, P.; von Zelewsky, A. *Coord. Chem. Rev.* **1988**, *84*, 85-277.
 - 25) Kalyanasundaram, K. *Coord. Chem. Rev.* **1982**, *46*, 159-244.
 - 26) Parada, G. A.; Fredin, L. A.; Santoni, M.-P.; Jager, M.; Lomoth, R.; Hammarstrom, L.; Johansson, O.; Persson, P.; Ott, S. *Inorg. Chem.* **2013**, *52*, 5128-5137.
 - 27) Elliott, C. M.; Herschenhart, E. J. *J. Am. Chem. Soc.* **1982**, *104*, 7519-7526.
 - 28) Ydens, I.; Moins, S.; Botteman, F.; Degee, P.; Dubois, P. *e-Polymers* **2013**, *4*, 414-420.
 - 29) Miyake, G. M.; Theriot, J. C. *Macromolecules* **2014**, *47*, 8255-8261.
 - 30) Theriot, J. C.; Ryan, M. D.; French, T. A.; Pearson, R. M.; Miyake, G. M. *J. Vis. Exp.* **2016**, e53571-e53571.
 - 31) Treat, N. J.; Sprafke, H.; Kramer, J. W.; Clark, P. G.; Barton, B. E.; Read de Alaniz, J.; Fors, B. P.; Hawker, C. J. *J. Am. Chem. Soc.* **2014**, *136*, 16096-16101.

-
- 32) Pan, X.; Fang, C.; Fantin, M.; Malhotra, N.; So, W. Y.; Peteanu, L. A.; Isse, A. A.; Gennaro, A.; Matyjaszewski, K. *J. Am. Chem. Soc.* **2016**, *138*, 2411-2425.
- 33) Pan, X.; Lamson, M.; Yan, J.; Matyjaszewski, K. *ACS Macro Lett* **2015**, *4*, 192-196.
- 34) Matyjaszewski, K.; Dadashi-Silab, S. X.; Pan, X. *Chem. Eur. J.* **2017**, DOI: 10.1002/chem.201605574.
- 35) Theriot, J. C.; Lim, C.-H.; Yang, H.; Ryan, M. D.; Musgrave, C. B.; Miyake, G. M. *Science* **2016**, *352*, 1082-1086.
- 36) Lim, C.-H.; Ryan, M. D.; McCarthy, B. G.; Theriot, J. C.; Sartor, S. M.; Damrauer, N. H.; Musgrave, C. B.; Miyake, G. M. *J. Am. Chem. Soc.* **2017**, *139*, 348-355.
- 37) Pearson, R. M.; Lim, C.-H.; McCarthy, B. G.; Musgrave, C. B.; Miyake, G. M. *J. Am. Chem. Soc.* **2016**, *138*, 11399-11407.
- 38) Hunag, Z.; Gu, Y.; Liu, X.; Zhang, L.; Cheng, Z.; Zhu, X. *Macromol. Rapid Commun.* **2016**, DOI: 10.1002/marc.201600461.
- 39) Allushi, A.; Jockusch, S.; Yilmaz, G.; Yagci, Y. *Macromolecules* **2016**, *49*, 7785-7792.
- 40) Resch-Genger, U.; Grabolle, M.; Cavaliere-Jaricot, S.; Nitschke, R.; Nann, T. *Nature Methods* **2008**, *5* (9), 763-775.
- 41) Dimroth, K.; Reichardt, C.; Siepmann, T.; Bohlmann, F. *Liebigs Ann. Chem.* **1963**, *661*, 1-37.
- 42) Reichardt, C. *Chem. Rev.* **1994**, *94*, 2319-2358.
- 43) Frank, H. A.; Bautista, J. A.; Josue, J.; Pendon, Z.; Hiller, R. G.; Sharples, F. P.; Gosztola, D.; Wasielewski, M. R. *J. Phys. Chem. B* **2000**, *104*, 4569-4577.
- 44) Ragnoni, E.; Di Donato, M.; Iagatti, A.; Lapini, A.; Righini, R. *J. Phys. Chem. B* **2015**, *119*, 420-432.

-
- 45) Horng, M. L.; Dahl, K.; Jones II, G.; Maroncelli, M. *Chem. Phys. Lett.* **1999**, *315*, 363-370.
- 46) Prat, D.; Wells, A.; Hayler, J.; Sneddon, H.; McElroy, C. R.; Abou-Shehada, S.; Dunn, P. *J. Green Chem.* **2016**, *18*, 288-296.
- 47) Alfonsi, K.; Colberg, J.; Dunn, P. J.; Fevig, T.; Jennings, S.; Johnson, T. A.; Kleine, H. P.; Knight, C.; Nagy, M. A.; Perry, D. A.; Stefaniak, M. *Green Chem.* **2008**, *10*, 31-36.
- 48) Whitfield, R.; Anastasaki, A.; Nikolaou, V.; Jones, G. R.; Engelis, N. G.; Discekici, E. H.; Fleischmann, C.; Willenbacher, J.; Hawker, C. J.; Haddleton, D. M. *J. Am. Chem. Soc.* **2017**, *139*, 1003-1010.
- 49) Gaussian 09, R. D., Frisch, M. J.; Trucks, G. W.; Schlegel, H. B.; Scuseria, G. E.; Robb, M. A.; Cheeseman, J. R.; Scalmani, G.; Barone, V.; Mennucci, B.; Petersson, G. A.; Nakatsuji, H.; Caricato, M.; Li, X.; Hratchian, H. P.; Izmaylov, A. F.; Bloino, J.; Zheng, G.; Sonnenberg, J. L.; Hada, M.; Ehara, M.; Toyota, K.; Fukuda, R.; Hasegawa, J.; Ishida, M.; Nakajima, T.; Honda, Y.; Kitao, O.; Nakai, H.; Vreven, T.; Montgomery, J. A., Jr.; Peralta, J. E.; Ogliaro, F.; Bearpark, M.; Heyd, J. J.; Brothers, E.; Kudin, K. N.; Staroverov, V. N.; Kobayashi, R.; Normand, J.; Raghavachari, K.; Rendell, A.; Burant, J. C.; Iyengar, S. S.; Tomasi, J.; Cossi, M.; Rega, N.; Millam, J. M.; Klene, M.; Knox, J. E.; Cross, J. B.; Bakken, V.; Adamo, C.; Jaramillo, J.; Gomperts, R.; Stratmann, R. E.; Yazyev, O.; Austin, A. J.; Cammi, R.; Pomelli, C.; Ochterski, J. W.; Martin, R. L.; Morokuma, K.; Zakrzewski, V. G.; Voth, G. A.; Salvador, P.; Dannenberg, J. J.; Dapprich, S.; Daniels, A. D.; Farkas, Ö.; Foresman, J. B.; Ortiz, J. V.; Cioslowski, J.; Fox, D. J. Gaussian, Inc., Wallingford CT, 2009.
- 50) He, H.; Zapol, P.; Curtiss, L. A. *J. Phys. Chem. C* **2010**, *114*, 21474.
- 51) Tossell, J. A. *Comp. Theor. Chem.* **2011**, *977*, 123.

-
- 52) Winget, P.; Cramer, C. J.; Truhlar, D. G. *Theor. Chem. Acc.* **2004**, *112*, 217.
- 53) Zhao, Y.; Truhlar, D. *Theor. Chem. Acc.* **2008**, *120*, 215.
- 54) Spackman, M. A. *J. Comput. Chem.* **1996**, *17*, 1.

Chapter 5

Impact of Light Intensity on Control in Photoinduced Organocatalyzed Atom Transfer

Radical Polymerization

Overview

Organic photoredox catalysts have been shown to operate organocatalyzed atom transfer radical polymerizations (O-ATRP) using visible light as the driving force. In this work, the effect of light intensity from white LEDs was evaluated as an influential factor in control over the polymerization and the production of well-defined polymers. We posit the irradiation conditions control the concentrations of various catalyst states necessary to mediate a controlled radical polymerization. Systematic dimming of white LEDs allowed for consideration of the role of light intensity on the polymerization performance. The general effects of decreased irradiation intensity in photoinduced O-ATRP were investigated through comparing two different organic photoredox catalysts, perylene and an *N*-aryl phenoxazine. Previous computational efforts have investigated catalyst photophysical and electrochemical characteristics, but the broad and complex effects of varied irradiation intensity as an experimental variable on the mechanism of O-ATRP have not been explored. This work revealed that perylene requires more stringent irradiation conditions to achieve controlled polymer molecular weight growth and produce polymers with molecular weight dispersities < 1.50 . In contrast, the *N*-aryl phenoxazine is more robust, operating under significantly diminished irradiation intensity. This characteristic is significant, as the discovery of highly robust catalysts is necessary to allow for the adoption of O-ATRP in a wide scope of conditions, including those which necessitate low-light intensity irradiation.

Introduction

Controlled radical polymerization (CRP) methodologies have enabled the construction of well-defined and precise polymeric materials by providing synthetic approaches that produce polymers with well-defined molecular weight (MW), dispersity (D) and composition.^{1,2,3,4,5} Organocatalyzed atom transfer radical polymerization (O-ATRP) has recently emerged as a methodology to produce well-defined polymers without the use of metal catalysts. Since initial reports that perylene⁶ and phenyl phenothiazine⁷ could operate O-ATRP, more organic photoredox catalysts (PCs) have been introduced, including several diaryl dihydrophenazine,^{8,9} carbazole,¹⁰ phenoxazine,¹¹ anthracene/pyrene,¹² and other phenothiazine^{13,14,15,16} derivatives. A proposed mechanism of O-ATRP proceeds through an oxidative quenching pathway which consists of four main processes: 1) photoexcitation of the ground state PC to a singlet excited state ($^1\text{PC}^*$), followed by intersystem crossing to a triplet excited state ($^3\text{PC}^*$);^{8,17} 2) direct reduction of an alkyl halide initiator or polymer chain end by $^3\text{PC}^*$, generating an active radical for polymerization propagation and formation of a radical cation/halide anion “deactivator” complex ($^2\text{PC}^{+\cdot}/\text{X}^-$); 3) polymer MW growth *via* polymerization propagation; and 4) oxidation of the active radical by $^2\text{PC}^{+\cdot}/\text{X}^-$ to reversibly deactivate the polymerization and regenerate PC (Figure 5.1).

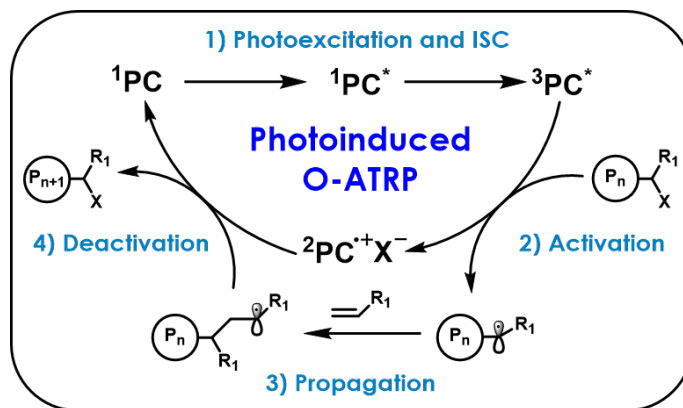


Figure 5.1. Proposed oxidative quenching cycle for O-ATRP mediated by photoredox catalysts.

Maintaining a low radical concentration by favoring dormant polymer chains through an efficient radical deactivation process is critical for CRPs to produce well-defined polymers. Minimizing bimolecular termination pathways allows for the synthesis of polymers with predictable MW and low \bar{D} through a controlled polymerization, achieving a linear increase in polymer MW with monomer conversion. In an ideal polymerization, no exogenous additives would be necessary for the system to be controlled, but in practice CRPs can be greatly improved by the addition of deactivating species or reagents that re-generate active catalysts.^{18,19} For example, a strategy to maintain a low radical concentration in copper ATRP is the addition of excess or exclusively^{20,21} deactivator in the form of Cu(II) salts at the beginning of the polymerization.²² Further, if excess Cu(II) species are not added, it is proposed that a steady-state Cu(II) concentration must be met before control over the system can be realized.²³ This approach influences the activation vs. deactivation equilibrium to favor dormant polymer chains by increasing the concentration of the deactivating species that regenerates Cu(I) and the halide capped polymer. If this condition is not met, deviation of the polymer MW from the theoretical values can be observed as a consequence of poor deactivation.²⁴ For O-ATRP, this translates to the requirement for a sufficient buildup of ${}^2\text{PC}^{+}/\text{Br}^{-}$ to be met to enable control over the polymerization. Holistically, the oxidizing power of this deactivator complex is also of importance, as the efficiency of deactivation is a function of both the concentration and reactivity of ${}^2\text{PC}^{+}/\text{Br}^{-}$.

In the O-ATRP mechanism, we hypothesize ${}^3\text{PC}^*$ is the predominant species responsible for reduction of the alkyl bromide and activation of the propagating radical for polymerization due

to the longer excited state lifetime of the triplet state relative to the singlet state.²⁵ Thereafter, the resulting ${}^2\text{PC}^{*\text{+}}\text{Br}^-$ ion pair must be sufficiently oxidizing to deactivate the propagating radical and realize a CRP. Furthermore, as is the case in all CRPs, the rate of deactivation (k_{deact}) must be equal to or greater than the rate of activation (k_{act}) to minimize undesirable termination pathways.²⁶ An idealized scenario to realize this balance of rates would involve the oxidized PC, ${}^2\text{PC}^{*\text{+}}\text{Br}^-$, remaining associated with the same polymer chain after activating the radical, and rapidly deactivating the same radical. However, the ion pair can likely diffuse away from the neutral propagating radical and potentially deactivate other radicals in solution. Such diffusion between deactivating species and propagating radicals in CRPs has been experimentally confirmed through cross-over studies in both polymerizations and model small molecule systems.^{27,28,29,30} As such, a critical concentration of the deactivating species is required to achieve control over the polymerization, which can either be added at the onset of the polymerization or generated through the activation step.^{31,32} In photoredox mediated ATRP, the ${}^2\text{PC}^{*\text{+}}\text{Br}^-$ deactivator is produced through the alkyl bromide reduction, which is dictated by the reduction potential and $[\text{}^3\text{PC}^*]$. In turn, $[\text{}^3\text{PC}^*]$ is influenced by a combination of the light intensity, initial PC loading, and the triplet quantum yield of the PC. In short, the $[\text{}^2\text{PC}^{*\text{+}}\text{Br}^-]$, through controlling intensity of irradiation, in concert with the photophysical and thermodynamic properties of the photocatalyst, must be optimized for k_{deact} to be sufficiently large to realize a controlled process through efficient deactivation.

The two PCs used in this study into the effects of light intensity on the control over O-ATRP, perylene (PC **1**) and an *N*-aryl phenoxazine (PC **2**), represent a comparison between an early example of an organic photoredox catalyst⁶ and a more successful PC designed to be highly reducing and absorptive under visible irradiation,¹¹ respectively. In regard to polymerization

performance, PC **1** typically achieved low initiator efficiency (I^*), while PC **2** commonly achieved nearly quantitative I^* while producing polymers with low dispersity ($D < 1.3$). By evaluating PCs **1** and **2** directly under previously employed conditions, which have demonstrated different levels of success in the polymerization of methacrylate monomers, the impact of the light source on the control over O-ATRP can be evaluated more completely. This reaction parameter has not been systematically explored for O-ATRP systems, even though the photoexcitation event adds a rich level of complexity to the polymerization mechanism. For photoinduced O-ATRP, the photoexcitation process controls the efficiency of activation directly, and the efficiency of deactivation indirectly. The characteristics of absorption ($PC \rightarrow PC^*$), quantum yield, excited-state lifetime, and reduction potential of $^3PC^*$ are major factors in the efficiency of the polymerization catalytic cycle. Modulating the irradiation intensity influences the concentration of $^3PC^*$ in solution and the rate of initiation, with decreased light intensity lowering the rate of initiation. As such, the concentration of $^2PC^{+}/Br^{-}$ is decreased under lower irradiation, as this complex is generated through activation.³³ Herein, the influence of light intensity and PC concentration are investigated as factors that affect the performance of O-ATRP by its modulation of $[^3PC^*]$, using PCs **1** and **2** as catalysts for the polymerization of methyl methacrylate (MMA).

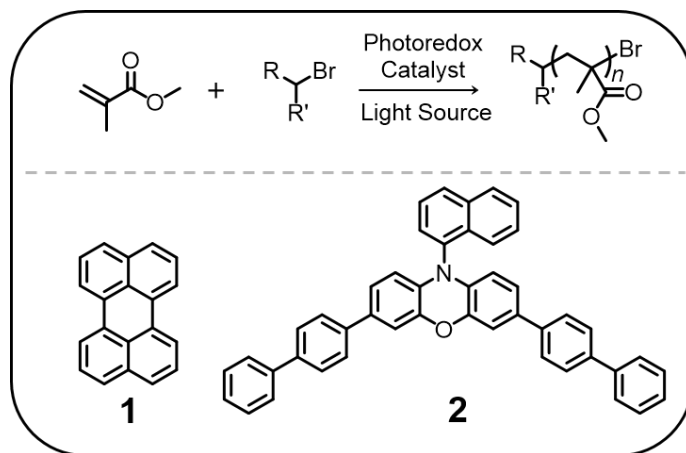


Figure 5.2. General reaction scheme for the O-ATRP of methyl methacrylate (Top). Structures of the two organic photoredox catalysts used in this study (Bottom).

Results and Discussion

Previous work with perylene demonstrated the feasibility of O-ATRP but did not achieve the control over the polymerization that is expected from ATRP. The photophysical properties of perylene are well studied and potentially provide insight into the poor performance of PC **1** as a PC for O-ATRP. The excited state reduction potential of ³PC* was computed to be -0.78 V (vs SCE) at the uM06/6-311+Gdp//uM06/6-31+Gdp level, the details of which have been previously reported.⁸ This value is similar to the activated alkyl bromide initiators^{34,35} commonly employed in ATRP and thus just strong enough of a reductant for their activation; Marcus theory explains that a stronger reducing ³PC* (compared to the alkyl halide), will provide a more favorable electron transfer.^{36,37} Additionally, the quantum yield for fluorescence of perylene is ~0.98 with $\tau = 4.9$ ns,^{38,39,40,41} which is most likely not sufficiently long for efficient bimolecular electron transfer and reduction of the alkyl bromide. Typically, excited state lifetimes exceeding 10 ns are required for productive electron transfer processes.⁴² The combination of the excited state reduction potential

of $^3\text{PC}^*$ of perylene, just strong enough for the reduction of an alkyl bromide ATRP initiator, and the inefficient formation of $^3\text{PC}^*$ could impact the activation efficiency of the alkyl bromide, yielding a low concentration of $^2\text{PC}^{+\cdot}\text{Br}^-$.

In contrast, phenoxazines are much stronger reductants in their photoexcited triplet states ($E^{0*} \sim -2.0$ V vs. SCE) and such classes of molecules are known to access long-lived $^3\text{PC}^*$ more efficiently.^{38,39,40} Under otherwise similar reaction conditions, the visible light absorbing PC **2** produced polymer product with \bar{D} as low as 1.13 and quantitative I^* , as compared to perylene which synthesized polymers with \bar{D} as low as 1.39, and $I^* < 50\%$ for a variety of experimental conditions. As such, we questioned if the poor control over the previously reported visible light induced O-ATRP using perylene as the PC could be attributed to poor irradiation conditions or simply that perylene is a poor catalyst for O-ATRP.

We reasoned that increasing the concentration of $^3\text{PC}^*$ in the polymerization reaction would enhance the activation step, increase the concentration of $^2\text{PC}^{+\cdot}\text{Br}^-$, and thus the efficiency of deactivation, improving control over the polymerization. The concentration of PC^* can be increased through increasing the catalyst loading and/or modulating the irradiation intensity. Under irradiation by white LEDs, polymerizations were performed with catalyst loadings of 0.1 mol% or 0.4 mol% (Table 5.1). Increasing the [**1**] decreased the \bar{D} from 1.82 to 1.38 for the polymerization of MMA (Runs 1 and 2). A general increase in the I^* is observed as well, with most trials $\sim 40\%$, representing a significant improvement for this system over previously reported results.⁶

Table 5.1. Results of the O-ATRP of MMA Mediated by PC **1** with Varied PC Concentrations and Irradiation Intensities.^a

Run No.	$h\nu$ (Intensity) ^a	[I]:[PC] ^b	Time (h)	Conversion (%) ^c	M_w (kDa) ^d	M_n (kDa) ^d	\bar{D} (M_w/M_n) ^d	I^* (%) ^e
1	100%	10:1	6	50.4	21.6	11.9	1.82	43.6
2	100%	10:4	6	49.4	19.4	14.0	1.38	36.1
3	100%	10:6	6	56.2	18.8	13.9	1.36	41.6
4	100%	10:10	6	47.3	16.7	11.8	1.42	41.2
5	50%	10:4	6	41.5	14.6	10.1	1.44	41.9
6	25%	10:4	6	42.6	16.5	12.6	1.31	34.6
7	5%	10:4	6	25.6	34.6	15.1	2.29	17.3

^aSee Supporting Information for details, polymerizations performed with 1.0 mL of MMA (1.87 M). ^bMolar ratio of initiator ([I]) to photocatalyst ([PC]). ^cMeasured by ¹H NMR. ^dMeasured by GPC coupled with light scattering. ^e I^* = theoretical number average MW/ experimentally measured number average MW *100.

By increasing the amount of catalyst from 0.1 mol% to 0.4 mol%, the \bar{D} of the resulting polymer greatly decreased (from 1.82 to 1.38) while I^* was similar (43.6 % vs 36.1 %). Further increasing the catalyst loading did not lead to significant enhancement, with the 0.6 mol% and 1 mol% trials resulting in less controlled M_n growth than for 0.4 mol%, as evidenced by plots of M_n as a function of monomer conversion, with linear growth the key characteristic to define a polymerization as “controlled” (Runs 3 and 4, Figure 5.13). As such, 0.4 mol% was chosen as the catalyst loading to systematically explore the effect of light intensity on the degree of control over the polymerization, performed with relative irradiation intensities of 100%, 50%, 25%, or 5%, by use of a LED dimmer (Table 5.1, Runs 5-7, Figures 5.9-5.12). By lowering the relative intensity

of irradiation from 100% to 50%, 25%, or 5%, the \bar{D} increases from 1.38 to 1.44, 1.69, and 2.29, respectively. From these results, it is clear that the light intensity has a significant impact on the control over the polymerization.

Investigating the polymerization of MMA and the growth in polymer MW in more detail, for the 100% relative intensity trial a linear increase in the M_n as a function of monomer conversion is observed (Figure 5.3A). The linear M_n growth as a function of monomer conversion had yet to be demonstrated for a perylene-mediated O-ATRP. The y-intercept of the trendline for M_n vs. monomer conversion in Figure 5.3A is ~ 4 kDa, deviating from the ideal value of 0.24 kDa, the mass of the alkyl bromide initiator. The y-intercept can be used to judge the efficiency at which a system achieves control in early periods of polymerization, with values closer to the mass of the initiator indicating more controlled and predictable MW growth. The 4 kDa y-intercept of this plot when using PC 1 suggests that there is an initial period of uncontrolled polymer growth at low monomer conversion. Additionally, a non-linear growth in M_n vs. monomer conversion holds mechanistic implications. This uncontrolled MW growth in early periods of polymerization is indicative of slow deactivation^{31,32,43} due to a low $[^2\text{PC}^+\text{Br}]$ during the early stages of polymerization. The polymerization irradiated at 50% relative intensity also resulted in a linear increase in polymer MW, however the \bar{D} is high for the early period of polymerization (Figure 5.3B). This trend in \bar{D} supports the hypothesis that decreasing the intensity of light decreases the efficiency of deactivation. Lowering the light intensity to 25% further results in an increase in \bar{D} and a loss of controlled growth in M_n for the early period of polymerization (Figure 5.3C), as evidenced by the non-linear growth in polymer MW. As the relative light intensity is lowered to 5%, control over the MW growth is lost, and polymer with high dispersity ($\bar{D} > 2.0$) is obtained because of a complete loss of control over the polymerization. A possible explanation for the

improvement in the performance of PC **1** in this study can be attributed to the increased concentration of excited state photocatalyst achieved through the combination of higher catalyst loading and increased irradiation intensity, as compared to the previous report.⁶

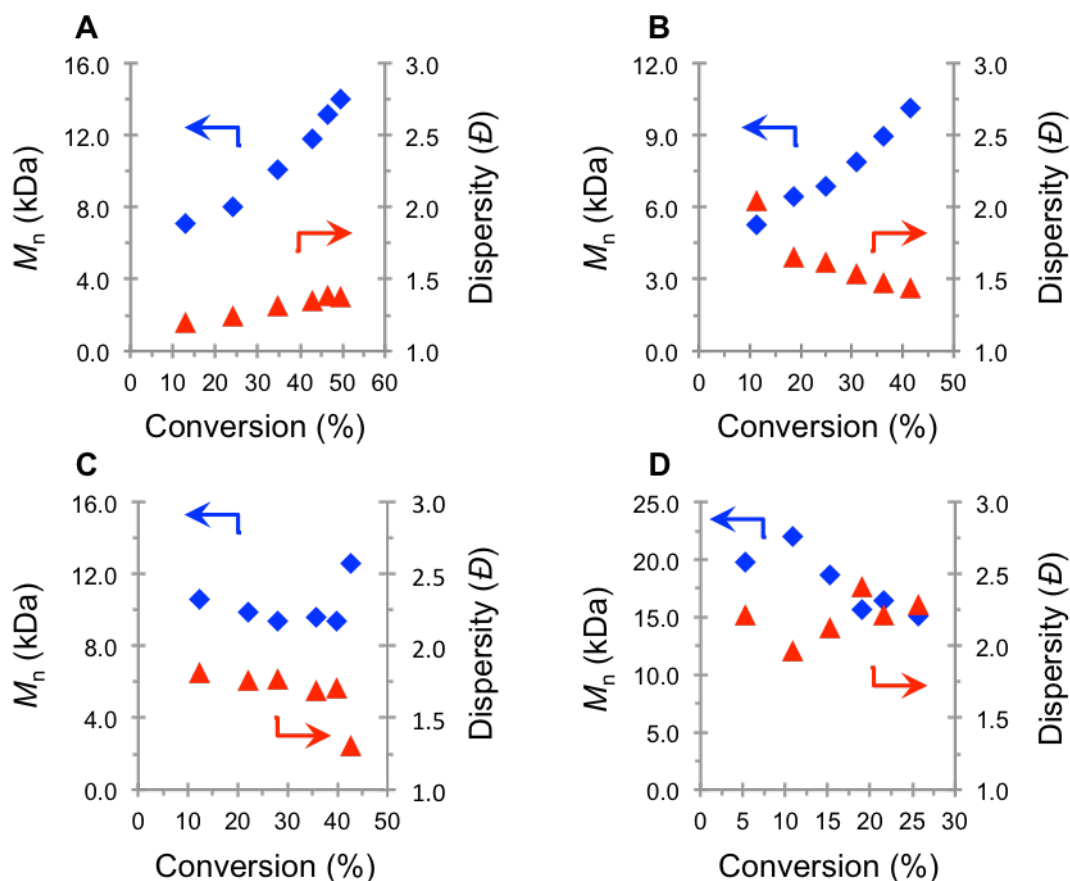


Figure 5.3. Plots of M_n (blue, \blacklozenge) and \bar{D} (red, \blacktriangle) as a function of monomer conversion irradiated with 100% (A), 50% (B), 25% (C), and 5% (D) relative irradiation intensity for the polymerization of MMA using PC **1**.

The kinetics of the polymerizations were also greatly affected by the relative intensity, with the rates of polymerization roughly correlating to the intensity of irradiation and decreasing with

lower light intensities (Figure 5.4). However, the rate of polymerization for the 25% intensity trial exceeded that of the 50% intensity trial, presumably a consequence of the loss of control over the polymerization, which agrees with the non-linear trend in MW growth (Figure 5.3C). As this was a surprising result, the polymerization under these conditions was repeated five times, and the averaged data plotted with error bars (Figure S9). Together, these features imply that there is sufficient irradiation to activate radicals, although not sufficient reaction conditions to produce an acceptable $[^2\text{PC}^+\text{Br}^-]$ to enable a CRP. The rate of polymerization using 5% intensity was the lowest level evaluated, and control over the polymerization is entirely lost under these conditions. It is conceivable that 5% intensity is too low for a high concentration of either PC* or active radical in solution, resulting in both lower rate of polymerization and loss of control. These data support the hypothesis that improvement in control over the polymerization mediated by PC **1** can be realized by increasing the intensity of irradiation. Further, by systematically decreasing the intensity, the loss in control over the polymerization can be related to the concentration of key species in solution.

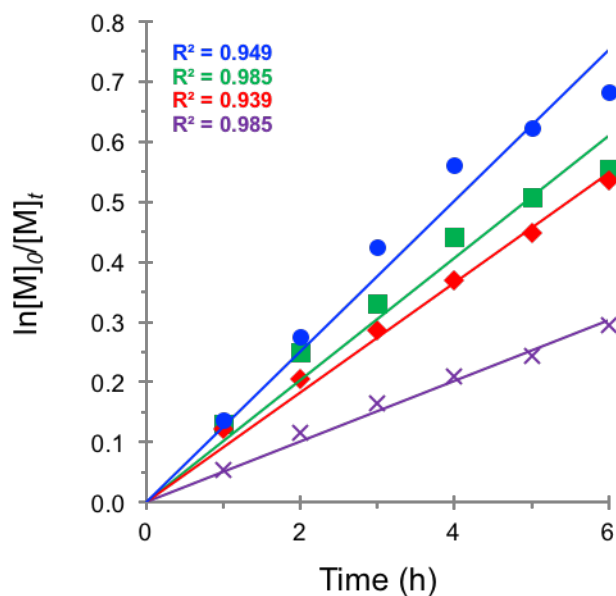


Figure 5.4. First order kinetic plot of the O-ATRP of MMA using PC **1**, irradiated at 100% (blue, ●), 50% (red, ◆), 25% (green, ■), and 5% (violet, ×) relative irradiation intensity.

To further examine the trends observed for PC **1**, the effects of varied light intensity when employing PC **2** were studied to investigate the activity of a PC that previously demonstrated superior performance in O-ATRP. PC **2** consistently produced polymer products with relatively low D (<1.30), and predictable M_n in a highly efficient manner ($I^*s > 90\%$).¹¹ In comparing the PCs, both PC **1** and PC **2** have high molar extinction coefficients ($>20,000$ L/mol*cm) and absorption profiles in the visible region,⁴⁴ but differ in other photophysical characteristics. The more reducing triplet excited state reduction potential of PC **2** vs **1** (-1.93 V vs. -0.78 V, respectively) likely results in a more efficient reduction of the alkyl bromide.

Table 5.2. Results of the O-ATRP of MMA Mediated by PC **2** with Varied PC Concentrations and Irradiation Intensities.^a

Run No.	$h\nu$ (Intensity) ^a	[I]:[PC] ^b	Time (h)	Conversion (%) ^c	M_w (kDa) ^d	M_n (kDa) ^d	\bar{D} (M_w/M_n) ^d	I^* (%) ^e
8	100%	10:0.1	6	83.3	14.4	10.2	1.42	84.1
9	100%	10:0.5	6	88.6	12.9	10.3	1.25	87.7
10	100%	10:1	6	83.9	10.7	8.9	1.20	96.3
11	100%	10:2	6	75.9	10.3	8.5	1.22	91.6
12	50%	10:1	6	60.6	9.3	7.8	1.20	80.1
13	25%	10:1	6	39.9	5.8	7.5	1.28	69.7
14	5%	10:1	6	16.2	9.7	5.4	1.80	31.0

^aSee Supporting Information for details, polymerizations performed with 1.0 mL of MMA (4.67 M). ^bMolar ratio of initiator ([I]) to photocatalyst ([PC]). ^cMeasured by ¹H NMR. ^dMeasured by GPC coupled with light scattering. ^e I^* = theoretical number average MW/ experimentally measured number average MW *100.

Overall, PC **2** is robust to broad changes in experimental conditions, as shown by maintaining a controlled O-ATRP in a wide range of irradiation intensities (100% - 25%) and catalyst concentrations (0.01 mol% - 0.2 mol%). The catalyst loading of PC **2** could be significantly lowered and still effectively catalyze O-ATRP (Table 5.2). At 0.05 and 0.01 mol%, low \bar{D} and $I^* > 80\%$ are obtained, indicating maintained control over the polymerization across an order of magnitude of catalyst loading (Runs 8-11). Increasing the amount of PC **2** to 0.2 mol% also provides successful results ($I^* = 91.6\%$ and $\bar{D} = 1.22$), although 0.2 mol% is beyond the solubility for this catalyst and the polymerization becomes heterogeneous in PC. A number of

general trends are observed for polymerizations mediated by PC **2** under the different irradiation conditions. By decreasing the intensity of irradiation from 100% to 5%, a significant decrease in I^* is observed from 96.3% to 31.0%. This lower I^* is accompanied by an increase in D from 1.20 to 1.80 (Table 2, Runs 12-14). Maintaining a controlled O-ATRP in a wide range of irradiation intensities (100%-25%) and catalyst concentrations (0.01 mol% - 0.2 mol%) makes PC **2** an attractive candidate for future applications of O-ATRP.

PC **2** exhibits a much wider window for successful performance in O-ATRP under altered irradiation conditions (Figure 5.5). For O-ATRP mediated by PC **2**, M_n growth is present from 100%, 50%, and 25% relative irradiation intensity (Figure 5.5A-C). Unlike PC **1**, the polymer M_n increases with monomer conversion for the 25% irradiation trial, although not in a completely linear fashion. When lowered to 5% relative intensity, there is a loss in control, as evidenced by a non-linear growth in M_n with monomer conversion, and high dispersity ($D > 2.0$) (Figure 5.5D). Additionally, lower light intensity leads to lower rates of polymerization, and the first order kinetic plots for the four different intensity trials remained linear, even at 5% relative intensity (Figure 5.6). Further, the degree of control does not significantly differ for polymerization in a photoreactor cooled by a fan (33°C) and not cooled (50°C) (Figure S8). These kinetic and MW data prove that the highly performing PC **2** can mediate a successful O-ATRP across broad irradiation intensities.

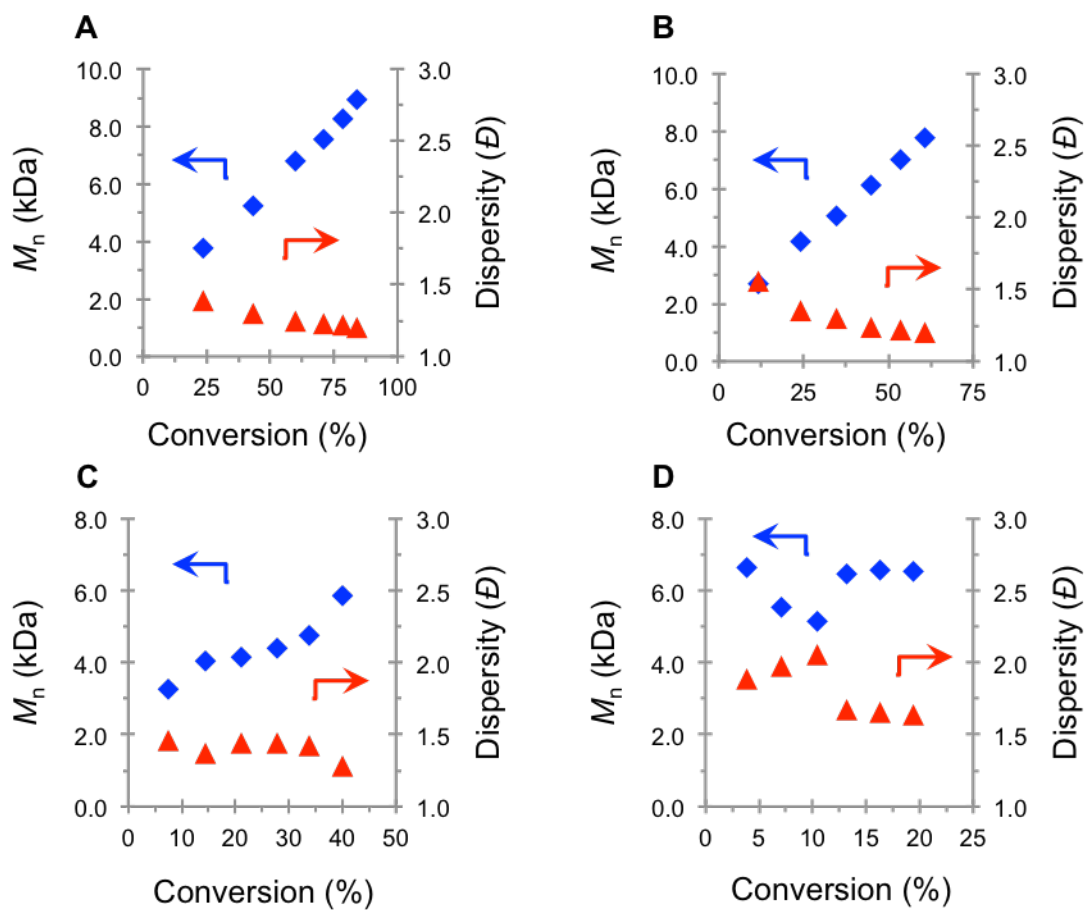


Figure 5.5. Plots of M_n (Blue, \blacklozenge) and \bar{D} (Red, \blacktriangle) as a function of monomer conversion at 100% (A), 50% (B), 25% (C), and 5% (D) relative irradiation intensity for the polymerization of MMA mediated by PC 2.

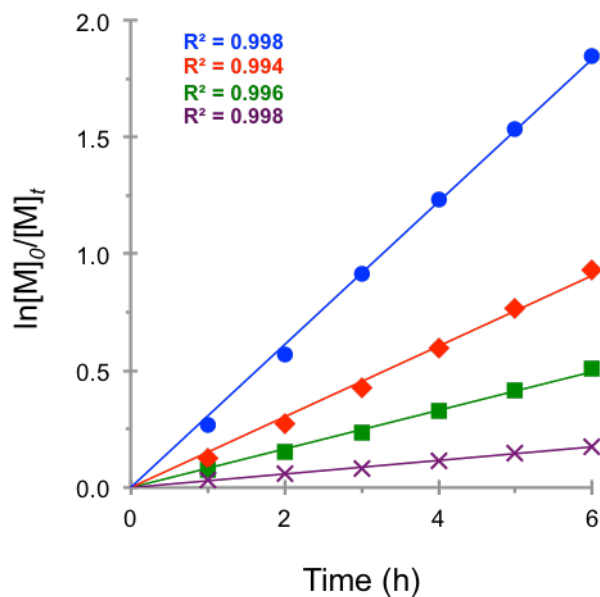


Figure 5.6. First order kinetic plot for the polymerization of MMA using PC 2 at 100% (blue, ●), 50% (red, ◆), 25% (green, ■), 5% (violet, ×) relative irradiation intensities.

Conclusions

Light intensity has been shown to have a significant effect on the degree of control achieved for photoinduced O-ATRP. Through exploring the effect of decreased irradiation intensity on multiple polymerization metrics, changes in experimental conditions were connected to concentrations of key catalyst states and their ability to successfully operate O-ATRP. Deeper understanding of the role that light intensity plays in the modulation of excited state catalyst concentrations allowed for the realization of conditions in which perylene catalyzed a controlled and linear growth in polymer molecular weight as a function of monomer conversion.

Additionally, by maintaining growth in polymer MW with monomer conversion and linear first order kinetics under significantly decreased irradiation intensity, the *N*-aryl phenoxazine catalyst proved to be robust to broad experimental conditions, highlighting its potential for success in a variety of future applications where low catalyst loading or low intensity irradiation are necessary.

Experimental

Materials & Methods

Materials:

Perylene (>98% purity) was purchased from TCI America and used as received. All other reagents were purchased from Sigma-Aldrich. 3,7-bis(4-biphenyl) 1-naphthalene-10-phenoxazine was synthesized according to a previously reported procedure.⁴⁵ Dimethylacetamide (DMA) and methyl methacrylate (MMA), were dried over calcium hydride for 24 hours, filtered, and purified *via* vacuum distillation followed by three freeze-pump thaw cycles at -78°C then stored in a N₂ glovebox. Ethyl α -bromophenylacetate (EBP) and diethyl 2-bromo-2-methylmalonate (DBMM) were purified *via* vacuum distillation followed by three freeze-pump thaw cycles at -78 °C, then stored in a N₂ glovebox.

General Polymerization Procedure For Perylene:

In a N₂ glovebox, a 20 mL scintillation vial was charged with a stir bar, perylene (9.5 mg, 0.037mmol, 4.0 eq.), and 4.00 mL of DMA. Then, MMA (1.00 mL, 9.35 mmol, 1000 eq.) was pipetted into the vial followed by EBP (16.4 μ L, 0.0935 mmol, 10 eq.). The vial was sealed with a plastic lined cap and placed into the photo reactor shown in Figure S1 with the indicated level of

light intensity, as controlled by the LED dimmer. The temperature in the beaker with un-dimmed LEDs was approximately 50°C.

General Polymerization Procedure For 3,7-Bis(4-biphenyl) 1-naphthalene-10-phenoxazine:

In a N₂ glovebox, a 20 mL scintillation vial equipped with stir bar was added phenoxazine catalyst (5.7 mg, 0.00935 mmol, 1 eq.) and 1.00 mL of DMA. Once the catalyst was fully dissolved, MMA (1.00 mL, 9.35 mmol, 1000 eq.) was pipetted into the vial followed by DBMM (17.9 μL, 0.0938 mmol, 10 eq.). The vial was then sealed with a plastic lined cap and quickly placed into the photo reactor shown in figure S1 with the indicated level of light intensity, as controlled by the LED dimmer. The temperature in the beaker with un-dimmed LEDs was approximately 50°C.

Time Point Collection for Kinetic Analysis:

A 0.10 mL sample was taken from the polymerization reaction vial in an oxygen free environment and injected into a vial with 0.6 mL of CDCl₃ and 25 ppm butylated hydroxytoluene (BHT). This solution was then used directly for analysis. Nuclear magnetic resonance (NMR) spectra were recorded on a Varian 300 MHz instrument. Monomer conversions were determined by integrating the methyl ester protons of the monomer at ~3.50-3.55 ppm against polymer methyl ester protons at ~3.30-3.45 ppm.

Molecular Weight Characterization:

After collecting NMR spectra, the sample was transferred into a 20 mL scintillation vial and the volatiles were removed. The resulting solid polymer was dissolved in 1 mL of HPLC grade THF and passed through a syringe filter before analysis *via* gel permeation chromatography (GPC)

coupled with multi-angle light scattering (MALS), using an Agilent HPLC fitted with one guard column, three PLgel 5 μm MIXED-C gel permeation columns, a Wyatt Technology TrEX differential refractometer, and a Wyatt Technology miniDAWN TREOS light scattering detector, using THF as the eluent at a flow rate of 1.0 mL/min.

Measurement of LED Emission

The emission spectrum of the white LEDs was measured with an Ocean Optics ADC1000 spectrometer. Light from the LEDs was attenuated as needed by use of a continuously variable neutral density filter to prevent saturation of the detector. Emission was measured at the seven different light intensities. The light was guided into the spectrometer with a fiber-optic cable. Data from the seven different measurements were processed with a home-built LabView program, and the spectra overlaid.

Photoreactor Setup: A 45 cm strip of double-density white LEDs purchased from Creative Lighting Solutions (item no. CL-FRS120-5M-12V-WH) was wrapped around the inside of a 400mL Pyrex beaker with a diameter of ~ 2.5 inches (Figure S1). The LED strip was powered by a 12VDC power Supply – 2.1A Commercial, 25W Power Supply by Creative Lighting Solutions LLC. A Dragonpad 12V12A inline mini LED dimmer control for single color LED strip lights with 7 dimmer settings was installed between the power supply and LED strips. The outside of the beaker was wrapped in aluminum foil. In this study the LEDs were dimmed from 100% to 50%, 25%, and 5% relative intensities (Figure 5.8).



Figure 5.7 A picture of the photoreactor used for O-ATRP, constructed from a 400mL beaker lined with 45 cm of white LEDs.



Figure 5.8. Picture of the relative light intensities used in this study, controlled by an LED dimmer. From left to right: 100%, 50%, 25%, 5% relative light intensity.

Measuring Light Intensity

To quantify the relative intensity of light emitted from the dimmed LEDs, lux readings were recorded by centering an LED lined beaker on the aperture of an integrating sphere diffuse reflectance accessory (Internal DRA-2500) equipped with a Amprobe LM-200 LED light meter with silicon photodiode and filter directed at the opening on the opposite side (Figure 5.9). The system was sealed to prevent light pollution from the surroundings. Measurement of the output from the various dimmer settings was repeated 10 times and the observed lux was averaged, with a standard deviation of $\pm 0.22\%$. The readings were plotted against intensity to calibrate our system (Figure 5.10).

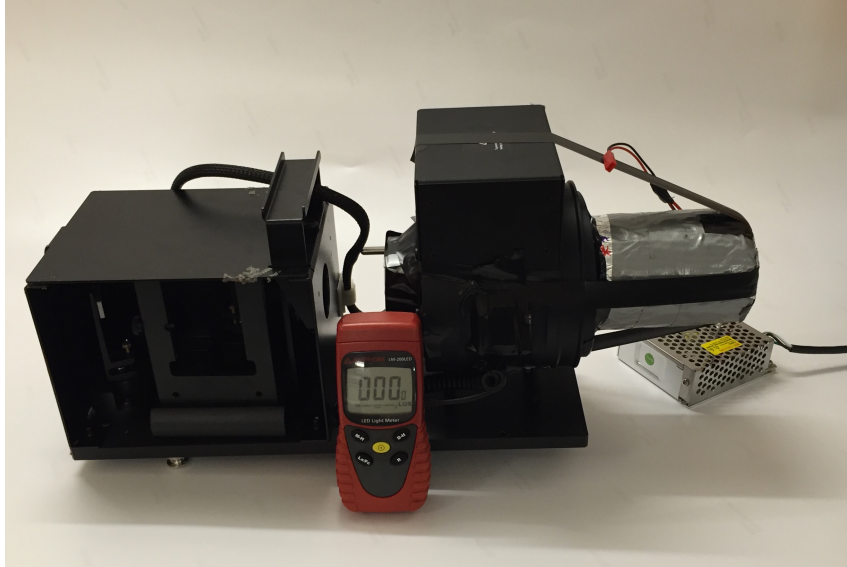


Figure 5.9 The set up used to measure lux at each dimmer setting, using an Amprobe LM-200 LED light meter and an integrating sphere diffuse reflectance accessory. The sealed system is shown, with no observed light pollution from the surroundings.

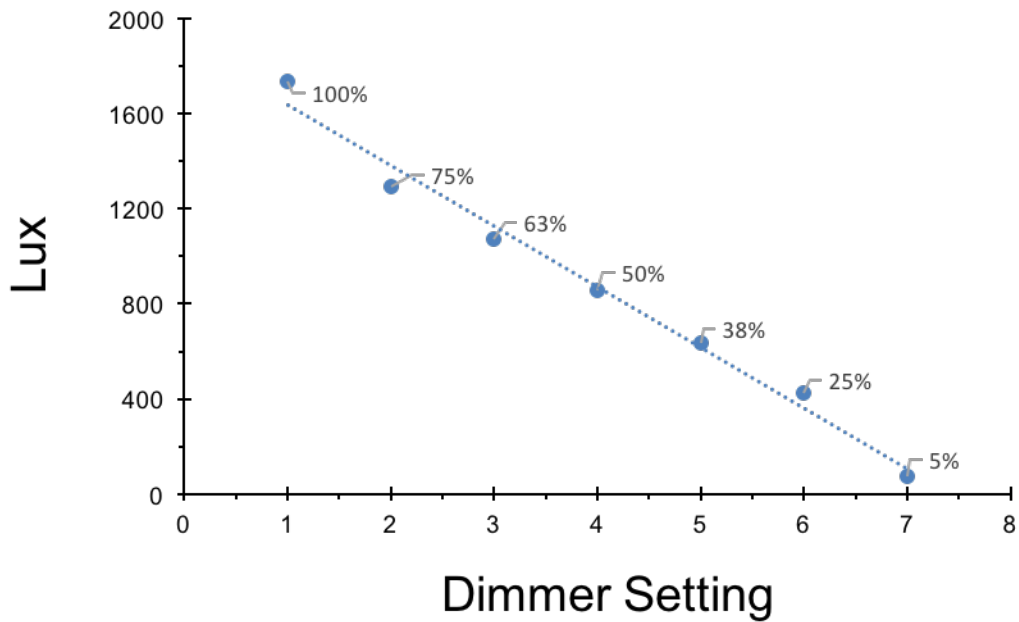


Figure 5.10 Plot of Lux as a function of dimmer setting, measured using the set up in Figure S3.

The relative percent intensity reported as data point labels.

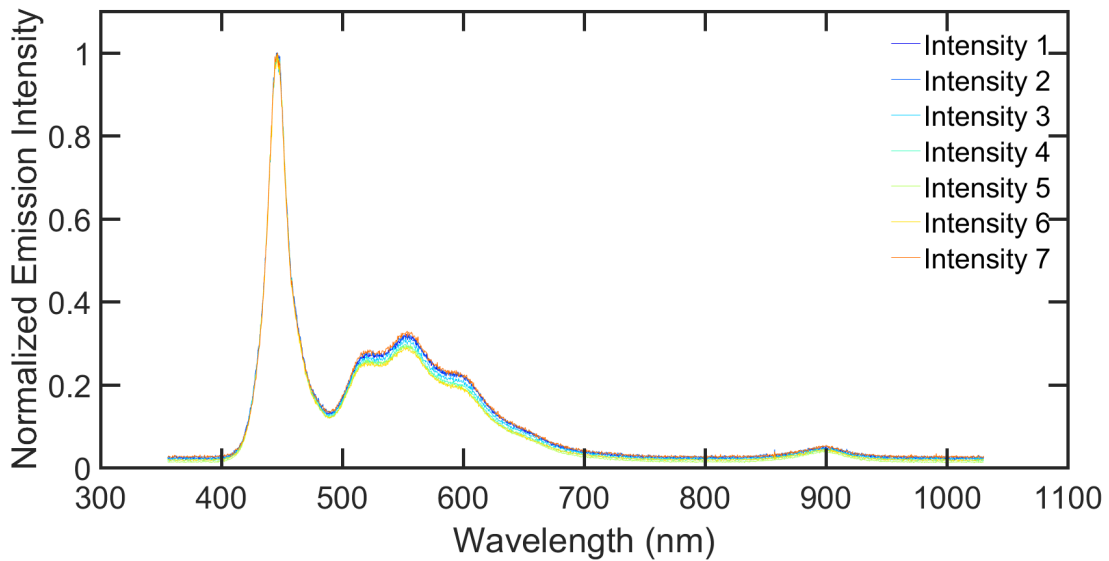


Figure 5.11. Overlaid plots of the normalized LED emission spectra at 7 different dimming settings.

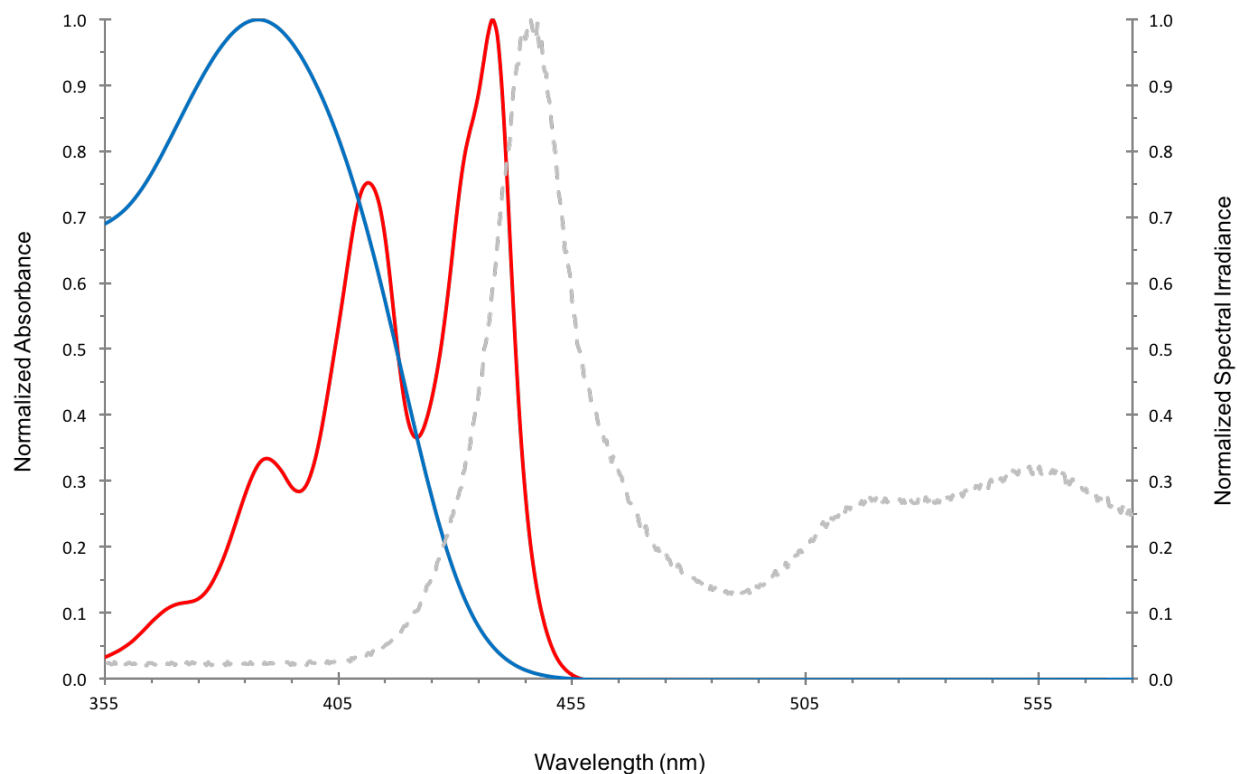


Figure 5.12. Overlaid normalized absorbance plots for PC 1 (red, $\epsilon = 37,961 \text{ M}^{-1}\text{cm}^{-1}$ @ 436 nm) and PC 2 (blue, $\epsilon = 26,635 \text{ M}^{-1}\text{cm}^{-1}$ @ 388 nm), and the normalized spectral irradiance of the white LED without dimming (gray).

Supplementary Polymerization Data

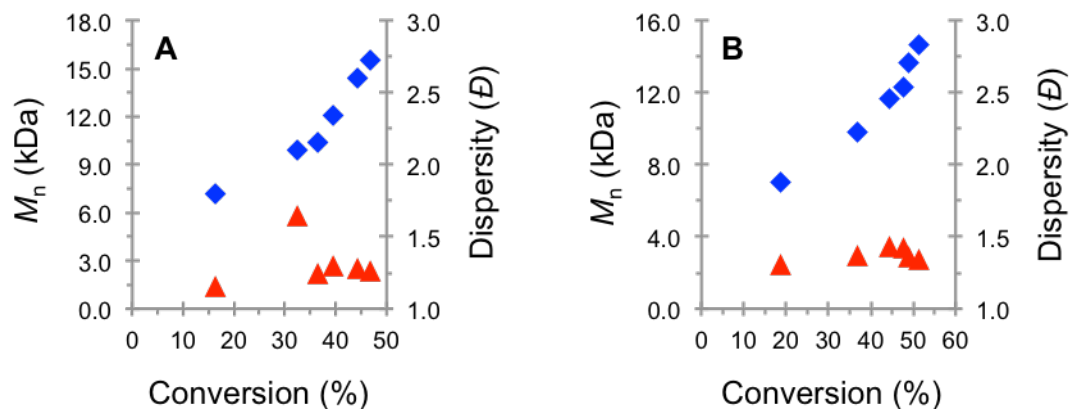


Figure 5.13 Plots of molecular weight (M_n , blue) and dispersity (D , red) as a function of monomer conversion for the polymerization of MMA (1000 eq, 1.00 mL, 9.35 mmol, 1.87 M) catalyzed by PC 1 (10 eq, 23.6 mg, 93.5 μ mol (A), 6 eq, 14.2 mg, 56.1 μ mol (B)) at ratios of 1000:10:10 (A) and 1000:10:6 (B) (monomer:initiator:PC) using EBP initiator (10 eq, 16.4 μ L, 93.5 μ mol).

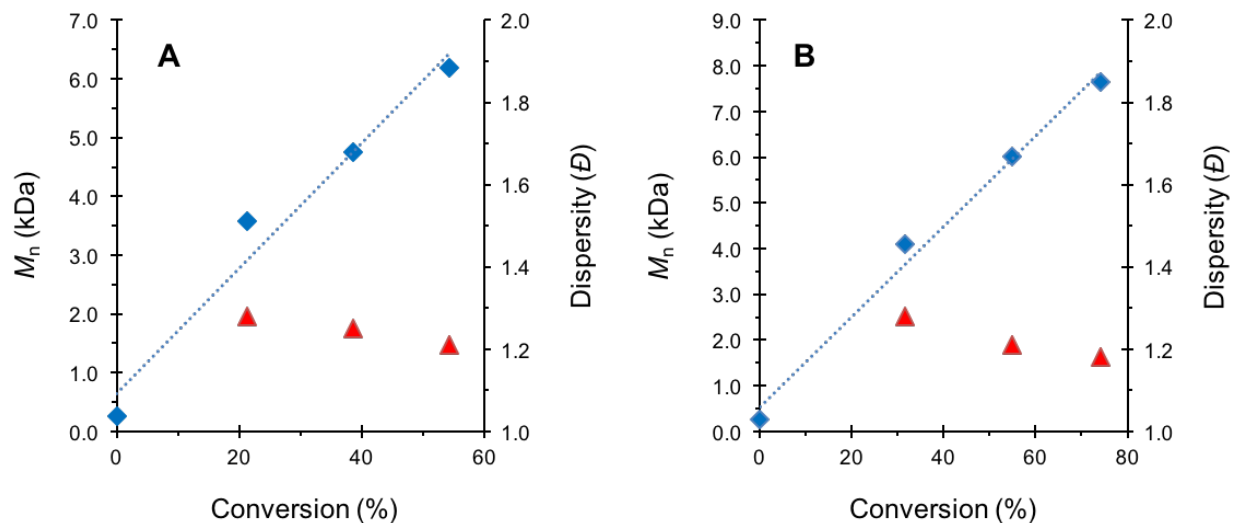


Figure 5.14 Plots of molecular weight (M_n , blue) and dispersity (D , red) as a function of monomer conversion for the polymerization of MMA (1000 eq, 1.00 mL, 9.35 mmol, 4.67 M) mediated by PC 2 (1 eq, 5.70 mg, 93.5 μ mol (A), 10 eq, 23.6 mg, 93.5 μ mol (B)) at ratios of 1000:10:10 (A) and 1000:10:6 (B) (monomer:initiator:PC) using EBP initiator (10 eq, 16.4 μ L, 93.5 μ mol).

mg, 9.35 μmol), using DBMM initiator (17.9 μL , 0.0938 mmol, 10 eq), cooled by a fan (A) and not cooled (B).

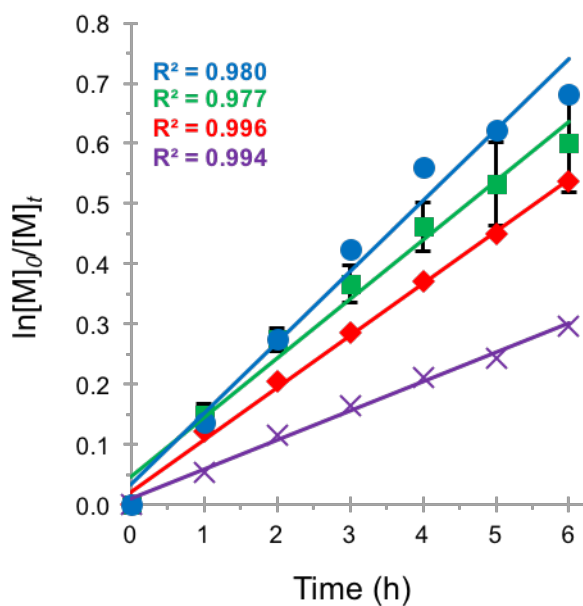
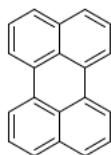


Figure 5.15. First order kinetic plot of the O-ATRP of MMA using PC 1, irradiated at 100% (blue), 50% (red), 25% (green), and 5% (violet) relative irradiation intensity, with data for the 25% trial repeated 5 times.

Computational Details:

Computed at uM06/6-311+Gdp//uM06/6-31+Gdp; V vs. SCE Reference. Details previously reported.⁴⁶



$$E^{0*} (\text{PC}^{\bullet+}/^3\text{PC}^*) = -0.78\text{V vs. SCE}$$

$$E_{\text{ox}} (\text{PC}^{\bullet+}/\text{PC}) = 0.57\text{V vs. SCE}$$

$$E_{\text{Triplet}} = 1.35\text{V}$$

References

- 1) Pan, X.; Tasdelen, M. A.; Laun, J.; Junkers, T.; Yagci, Y.; Matyjaszewski, K. *Prog. Polym. Sci.* **2016**, *62*, 73-125.
- 2) Chen, M.; Zhong, M.; Johnson, J. A. *Chem. Rev.* **2016**, *116* (17), 10167-10211.
- 3) Matyjaszewski, K.; Tsarevsky, N. V. *J. Am. Chem. Soc.* **2014**, *136* (18), 6513-6533.
- 4) Braunecker, W. A.; Matyjaszewski, K. *Prog. Polym. Sci.* **2007**, *32*, 93-146.
- 5) Kamigaito, M.; Ando, T.; Sawamoto, M. *Chem. Rev.* **2001**, *101* (12), 3689-3746.
- 6) Miyake, G. M.; Theriot, J. C. *Macromolecules* **2014**, *47* (23), 8255-8261.
- 7) Treat, N. J.; Sprafke, H.; Kramer, J. W.; Clark, P. G.; Barton, B. E.; de Alaniz, J. R.; Fors, B. P.; Hawker, C. J. *J. Am. Chem. Soc.* **2014**, *136* (45), 16096-16101.
- 8) Theriot, J. C.; Lim, C.-H.; Yang, H.; Ryan, M. D.; Musgrave, C. B.; Miyake. *Science* **2016**, *352*, 1082-1086.
- 9) Lim, C.-H., Ryan, M. D., McCarthy, B. G., Theriot, J. C., Sartor, S. M., Damrauer, N. H., Musgrave, C. B., Miyake, G. M. *J. Am. Chem. Soc.* **2016**, DOI: 10.1021/jacs.6b11022.

-
- 10) Huang, Z.; Gu, Y.; Liu, X.; Zhang, L.; Cheng, Z.; Zhu, X. *Macromol. Rapid Commun.* **2016**, DOI:10.1002/marc.201600461.
 - 11) Pearson, R. M.; Lim, C.-H.; McCarthy, B. G.; Musgrave, C. B.; Miyake, G. M. *J. Am. Chem. Soc.* **2016**, *138* (35), 11399-11407.
 - 12) Allushi, A.; Jockusch, S.; Yilmaz, G.; Yagci, Y. *Macromolecules* **2016**, *49*, 7785-7792.
 - 13) Pan, X.; Fang, C.; Fantin, M.; Malhotra, N.; So, W. Y.; Peteanu, L. A.; Isse, A. A.; Gennaro, A.; Matyjaszewski, K. *J. Am. Chem. Soc.* **2016**, *138* (7), 2411-2425.
 - 14) Pan, X.; Lamson, M.; Yan, J.; Matyjaszewski, K. *ACS Macro Lett.* **2015**, *4* (2), 192-196.
 - 15) Dadashi-Silab, S.; Pan, X.; Matyjaszewski, K. *Chem. Eur. J.* 10.1002/chem.201605574.
 - 16) Yan, J.; Pan, X.; Schmitt, M.; Wang, Z.; Bockstaller, M. R.; Matyjaszewski, K. *ACS Macro Lett.* **2016**, *5*, 661-665.
 - 17) Jockusch, S.; Yagci, Y. *Polym. Chem.* **2016**, *7*, 6039-6043.
 - 18) Williams, V. A.; Ribelli, T. G.; Chmielarz, P.; Park, S.; Matyjaszewski, K. *J. Am. Chem. Soc.* **2015**, *137* (4), 1428-1431.
 - 19) Jakubowski, W.; Matyjaszewski, K. *Angew. Chem. Int. Ed.* **2006**, *45*, 4482-4486.
 - 20) Wang, J.-S.; Matyjaszewski, K. *Macromolecules* **1995**, *28* (22), 7572-7573.
 - 21) Xia, J.; Matyjaszewski, K. *Macromolecules* **1997**, *30* (25), 7692-7696.
 - 22) Min, K.; Gao, H.; Matyjaszewski, K. *J. Am. Chem. Soc.* **2005**, *127* (11), 3825-2830.
 - 23) Matyjaszewski, K.; Patten, T. E.; Xia, J. *J. Am. Chem. Soc.* **1997**, *119* (4), 674-680.
 - 24) Matyjaszewski, K.; Nakagawa, Y.; Jasieczek, C. B. *Macromolecules* **1998**, *31*, 1535-1541.
 - 25) Arias-Rotondo, D. M.; McCusker, J. K. *Chem. Soc. Rev.* **2016**, *45*, 5803-5820.
 - 26) Matyjaszewski, K.; Paik, H. J.; Zhou, P.; Diamanti, S. *Macromolecules* **2001**, *34*, 5125-5131.

-
- 27) Wessely, I.; Mugnaini, V.; Bihlmeier, A.; Jeschke, G.; Brase, S.; Tsotsalas, M. *RSC Adv.* **2016**, *6*, 55715-55719.
- 28) Yamaguchi, G.; Higaki, Y.; Otsuka, H.; Takahara, A. *Macromolecules* **2005**, *38*, 6316-6320.
- 29) Turro, N. J.; Lem, G.; Zavarine, I. S. *Macromolecules* **2000**, *33*, 9782-9785.
- 30) Hawker, C. J.; Barclay, G. G.; Dao, J. *J. Am. Chem. Soc.* **1996**, *118* (46), 11467-11471.
- 31) Lacroix-Desmazes, P.; Lutz, J.-F.; Chauvin, F.; Severac, R.; Boutevin, B. *Macromolecules* **2001**, *34* (26), 8866-8871.
- 32) Veregin, R. P. N.; Odell, P. G.; Michalak, L. M.; Georges, M. K. *Macromolecules* **1996**, *29* (8), 2746-2754.
- 33) Lalevee, J.; Morlet-Savary, F.; Dietlin, C.; Graff, B.; Fouassier, J.-P. *Molecules* **2014**, *19*, 15026-15041.
- 34) Roth, H. G.; Romero, N. A.; Nicewicz, D. A. *Synlett* **2016**, *27*, 714-723.
- 35) Isse, A. A.; Lin, C. Y.; Coote, M. L.; Gennaro, A. *J. Phys. Chem. B* **2011**, *115*, 678-684.
- 36) Saveant, J.-M. *J. Am. Chem. Soc.* **1992**, *114* (26), 10595-10602.
- 37) Ebersson, L. *Acta Chem. Scand. B* **1982**, *36* (8), 533-543.
- 38) Gomez, M. L.; Montejano, H. A.; Previtali, C. M. *J. Photochem. Photobiol. A: Chem.* **2008**, *197*, 18-24.
- 39) Goldschmidt, C. R.; Ottolenghi, M. *J. Phys. Chem.* **1971**, *75* (25), 3894-3897.
- 40) Dreeskamp, H.; Koch, E.; Zander, M. *Chem. Phys. Lett.* **1975**, *31* (2), 251-253.
- 41) Turro, N. J.; Ramamurthy, V.; Scaiano, J. C. *Modern Molecular Photochemistry of Organic Molecules*; University Science Books: Sausalito, 2010.
- 42) Kavarnos, G. J.; Turro, N. J. *Chem. Rev.* **1986**, *86*, 401-449.

-
- 43) Chauvin, F.; Dufils, P.-E.; Gigmes, D.; Guillaneuf, Y.; Marque, S. R. A.; Tordo, P.; Bertin, D. *Macromolecules* **2006**, *39* (16), 5238-5250.
- 44) George, C.; Streckowski, R. S.; Kleffmann, J.; Stemmler, K.; Ammann, M. *Faraday Discuss.* **2005**, *130*, 195-210.
- 45) Pearson, R. M.; Lim, C.-H.; McCarthy, B. G.; Musgrave, C. B.; Miyake, G. M. *J. Am. Chem. Soc.* **2016**, *128*, 11399-11407.
- 46) Theriot, J. C.; Lim, C.-H.; Yang, H.; Ryan, M. D.; Musgrave, C. B.; Miyake, G. M. *Science* **2016**, *352*, 1082-1086.

Chapter 6

Summary

The work in this dissertation developed *N,N*-Diaryl Dihydrophenazines as visible light absorbing, highly reducing organic photoredox catalysts (PCs) for organocatalyzed atom transfer radical polymerization (O-ATRP). This catalyst family was shown to produce methacrylic polymers of very low dispersity in a highly efficient polymerization process, rivaling traditional metal-catalyzed atom transfer radical polymerization. In depth investigation of the photophysical characteristics led to the discovery of improved catalysts, optimized polymerization conditions, and set the stage for successful application in small molecule reactions.

Since the first report of the *N,N*-Diaryl Dihydrophenazines in 2016, our group has further developed the class of *N*-Aryl Phenoxazine^{1,2} and *N*-Aryl Acridine photocatalysts,³ which access a wider range of electrochemical properties. In synthesizing diverse sets of catalysts capable of operating O-ATRP, new reactivity has been enabled, including the controlled polymerization of more challenging monomers, synthesis of complex polymeric architectures⁴ and extension to pharmaceutically relevant small molecule transformations.⁵ Rigorous understanding of the structure-photophysical property-polymerization performance relationship has led to a new class of core-modified phenazine PCs capable of operating at < 50 ppm concentrations (Figure 6.1).⁶

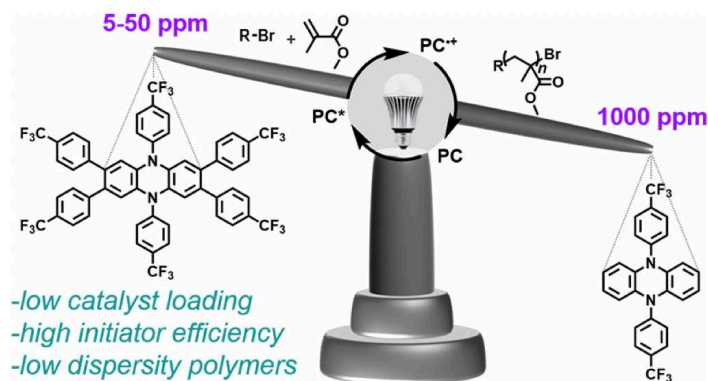


Figure 6.1. Development of new phenazine photoredox catalysts capable of operating controlled O-ATRP at low catalyst loadings.

The future is bright for organic photocatalysis, with the 2-naphthyl phenazine catalyst (5,10-Di(2-Naphthyl)-5,10-dihydrophenazine) now available through Millipore Sigma, which will hopefully lead to increased impact in both the polymer chemistry and organic chemistry communities (Figure 6.2).

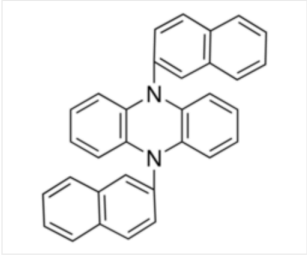
901112 Sigma-Aldrich

5,10-Di(2-Naphthyl)-5,10-dihydrophenazine

≥97%

Synonym: Miyake polymerization organophotoredox catalyst, PhenN_2Naph

CAS Number 1934269-97-2 | Empirical Formula (Hill Notation) C₃₂H₂₂N₂ | Molecular Weight 434.53 |



◆ SDS

SKU-Pack Size	Availability	Price (USD)	Quantity
901112-100MG	✔ Only 6 left in stock (more on the way) - FROM	109.00	0 ★ ⓘ

[Bulk orders?](#) ADD TO CART

Figure 6.2. Picture of the sales page for 5,10-Di(2-Naphthyl)-5,10-dihydrophenazine catalyst.

References

- 1) Pearson, R. M.; Lim, C.-H.; McCarthy, B. G.; Musgrave, C. B.; Miyake, G. M. *J. Am. Chem. Soc.* **2016**, *138*, 11399-11407.
- 2) McCarthy, B. G.; Pearson, R. M.; Lim, C.-H.; Sartor, S. M.; Damrauer, N. H.; Miyake, G. M. *J. Am. Chem. Soc.* **2018**, *140*, 5088-5101.
- 3) Buss, B.; Miyake, G. M. **2019** *In Preparation*.
- 4) Ramsey, B. L.; Beck, L. R.; Miyake, G. M. *Polym. Chem.* **2018**, *9*, 1658-1665.
- 5) Du, Y.; Pearson, R. M.; Lim, C.-H.; Sartor, S. M.; Ryan, M. D.; Yang, H.; Damrauer, N. H.; Miyake, G. M. *Chemistry - A European Journal* **2017**, *23*, 10962-10968.
- 6) Cole, J. P.; Federico, C. R.; Lim, C.-H.; Miyake, G. M. *Macromolecules* **2019**, *52*, 747-754.

Appendix I

List of Publications by Matthew D. Ryan

- 1) Ryan, M. D.; Pearson, R. M.; Miyake, G. M. "Organocatalyzed Controlled Radical Polymerizations," In *Organic Catalysis for Polymerisation*; Dove, A., Sardon, H., Naumann, S., Eds.; RSC Polymer Chemistry Series, 2018, Ch 13, pp 584-606.

- 2) Ryan, M. D.; Theriot, J. C.; Lim, C.-H.; Yang, H.; Lockwood, A. G.; Garrison, N. G.; Lincoln, S. R.; Musgrave, C. B.; Miyake, G. M. "Solvent Effects on the Intramolecular Charge Transfer Character of *N,N*-Diaryl Dihydrophenazine Catalysts for Organocatalyzed Atom Transfer Radical Polymerization," *J. Polym. Sci. Part A: Polym. Chem.* **2017**, *55*, 3017-3027.

- 3) Du, Y.; Pearson, R. M.; Lim, C.-H.; Sartor, S. M.; Ryan, M. D.; Yang, H.; Damrauer, N. H.; Miyake, G. M. "Strongly Reducing, Visible-Light Organic Photoredox Catalysts as Sustainable Alternatives to Precious Metals," *Chemistry - A European Journal* **2017**, *23*, 10962-10968.

- 4) Ryan, M. D.; Pearson, R. M.; French, T. A.; Miyake, G. M. "Impact of Light Intensity on Control in Photoinduced Organocatalyzed Atom Transfer Radical Polymerization," *Macromolecules* **2017**, *50*, 4616-4622.

- 5) Lim, C.-H.; Ryan, M. D.; McCarthy, B. G.; Theriot, J. C.; Sartor, S. M.; Damrauer, N. H.; Musgrave, C. B.; Miyake, G. M. "Intramolecular Charge Transfer and Ion Pairing in *N,N*-Diaryl Dihydrophenazine Photoredox Catalysts for Efficient Organocatalyzed atom Transfer Radical Polymerization," *J. Am. Chem. Soc.* **2017**, *139*, 348-355.

6) Theriot, J. C.; Lim, C.-H.; Yang, H.; Ryan, M. D.; Musgrave, C. B.; Miyake, G. M. “Organocatalyzed Atom Transfer Radical Polymerization Driven by Visible Light,” *Science* **2016**, 352, 1082-1086.

7) Theriot, J. C.; Ryan, M. D.; French, T. A.; Pearson, R. M.; Miyake, G. M. “Atom Transfer Radical Polymerization of Functionalized Vinyl Monomers using Perylene as a Visible Light Photocatalyst,” *Journal of Visualized Experiments* **2016**, e53571.